Dynamic Simulation of Human Heat Transfer and Thermal Comfort

by Dusan FIALA

A thesis submitted in partial fulfilment
of the requirements of De Montfort University
for the degree of Doctor of Philosophy

June 1998

Institute of Energy
and Sustainable Development
DE MONTFORT UNIVERSITY LEICESTER

and

Joseph-von-Egle Institut
für angewandte Forschung
FH STUTTGART - HOCHSCHULE FÜR TECHNIK

Abstract

A mathematical model predicting human thermal responses and the associated thermal sensations in steady state and transient conditions has been developed. The dynamic model of the human thermoregulatory system predicts body temperatures, regulatory responses, and components of the environmental heat loss in cold stress, cool, neutral, warm and hot stress conditions. The incorporated comfort model predicting the Dynamic Thermal Sensation (DTS) and the predicted percentage of dissatisfied (PPD) is based on physiological effects, and extends the predictability of (dis)comfort from mild, steady state environments to non-moderate climates, transient conditions, and from low activity levels up to levels of 10 met.

The passive system of the model - a multi-segmental, multi-layered representation of the human body with spatial subdivisions - accounts for phenomena of human heat transfer within the body (blood circulation, heat-generation, -conduction, and -accumulation) and at its surface (convection, long wave radiation, solar irradiation, skin moisture-evaporation, -diffusion, and -accumulation). Other effects, such as the non-uniform thermal and evaporative resistance of clothing ensembles and the change in the effective radiant body area with posture are also considered.

The active system model, simulates the responses of the human thermoregulatory system, ie. cutaneous vasomotion, sweat liquid excretion and increases in metabolism by shivering thermogenesis. Statistical analyses of data obtained from experiments covering a wide range of boundary conditions and different types of exposure revealed skin and head-core temperature, and the rate of change of skin temperature to be the governing afferent signals of these regulatory defense mechanisms. A non-linear active system was obtained by considering human thermoregulatory behaviour over a wide range of environmental and internal conditions. The complete model was validated extensively using various independent experiments and showed good agreement of predicted body temperatures as well as regulatory responses with measured data. When sweating in the cold, however, discrepancies arose between simulation and experiment which were found to be associated with the specific method of skin temperature measurement.

A thermal comfort model was developed which is based on physiological effects as indicators of human thermal feelings. Extensive comfort-experiments were used to derive a statistically founded model. Regression analyses revealed skin temperature, head-core temperature, and the rate of change of skin temperature to be the responsible thermophysiological variables which govern the overall dynamic sensation of temperature. The comfort model was validated against independent experimental data and showed good general agreement with sensation votes of sedentary and working subjects exposed to various steady and transient conditions.

Contents

Nomenclature

English Symbols	Description	Units[1)]
A	area	[m^2] [cm^2]
a	distribution or weighting coefficient	[-]
act	activity level	[met][2)]
b	regression coefficient(s)	
B	coefficient(s) modifying the classic *tanh*-function	[-]
B_X	parameter of arterial blood temperature arising from h_X	
C	heat loss by convection	[W]
c	heat capacitance	[J $kg^{-1}K^{-1}$] [kJ $kg^{-1}K^{-1}$]
Cc	coefficient of the blood pool temperature column of the major coefficient matrix	
Lc	coefficient of the blood pool temperature line of the major coefficient matrix	[W K^{-1}]
$CplC$	coupling coefficient of the major coefficient matrix	[W K^{-1}]
Cs	cutaneous vasoconstriction	[-]
Dl	cutaneous vasodilatation	[W K^{-1}]
DTS	dynamic thermal sensation	[-]
E	heat loss by evaporation	[W]
ET^*	ASHRAE effective temperature	[°C]
f_{cl}	overall clothing surface area factor	[-]
f_{cl}^*	local surface area factor of a garment	[-]
f_{eff}	effective radiant area of the body	[-]
f_{sk}	function of skin temperature in *DTS*	[-]
g	functions associated with the effect of core temperature on *DTS*	[-]
h	surface heat transfer coefficient	[W $m^{-2}K^{-1}$]
h_x	counter-current heat exchange coefficient	[W K^{-1}]
H	internal whole body workload	[W]
i_{cl}	overall moisture permeability index	[-]

1) Standard SI units, eg. W=Watts, Pa=Pascal, etc. Where alternative units are stated, the first are SI, others were adopted in some places to improve the clarity of presentation. Where this occurs the alternative units used are restated in the text.

2) 1 met = 58.2 W m^{-2} [5].

	from the skin to the clothing surface	
i^*_{cl}	local, garment oriented, equivalent to i_{cl}	[-]
I_{cl}	overall intrinsic clothing thermal insulation	[$m^2 K W^{-1}$]
	from the skin to the clothing surface	[clo][1)]
I^*_{cl}	local, garment oriented, equivalent to I_{cl}	[$m^2 K W^{-1}$]
		[clo]
k	conductivity	[$W m^{-1} K^{-1}$]
L	Lewis constant (air: 0.0165)	[$K Pa^{-1}$]
m	mass	[kg] [g]
M	whole body metabolism	[W]
MRT	mean radiant temperature	[°C]
p	water vapour pressure	[Pa]
P	level of statistical significance	[-]
PMV	predicted mean vote	[-]
PPD	predicted percentage of dissatisfied	[%]
q	heat flux density	[$W m^{-2}$]
q_m	metabolic rate	[$W m^{-3}$]
Q	heat flux	[W]
r_i	radius	[m] [cm]
r	simple-linear correlation coefficient	[-]
R	multi-linear correlation coefficient	[-]
R_E	moisture permeability resistance	[$m^2 Pa W^{-1}$]
rh	relative humidity	[-] [%]
s	short wave irradiation	[$W m^{-2}$]
s, sd	standard deviation	
SBF	skin blood flow	[$m^3 s^{-1}$]
		[$l min^{-1}$]
Sh	shivering	[W]
Sw	sweating	[$kg s^{-1}$]
		[$g min^{-1}$]
t	time	[s] [min] [h]
T	temperature	[°C]
T^*	absolute temperature	[K]
U^*_{cl}	local, garment oriented, clothing heat transfer coefficient including surface coefficients of the dry heat loss to the environment	[$W m^{-2} K^{-1}$]

1) 1 clo = 0.155 $m^2 K W^{-1}$ [5].

$U^{*}_{E,cl}$	local, garment oriented, clothing evaporation coefficient from the skin to the ambient air	[W m^{-2}Pa^{-1}]
TS	thermal sensation	[-]
TSV	thermal sensation vote	[-]
V	volume	[m^3] [l] [cm^3]
w	perfusion rate	[s^{-1}] [ml s^{-1}cm^{-3}]
w_{sk}	skin wettedness	[-] [%]
W_L	weight loss	[kg s^{-1}] [g min^{-1}]
x	independent variable	
y, Y	function	
z	function weighting temporal changes in *DTS*	[-]

Greek Symbols	**Description**	**Units**
α	short wave absorptivity	[-]
β	energy equivalent of the blood perfusion rate	[W m^{-3}K^{-1}]
β'	volume weighted energy equivalent β	[W K^{-1}]
Δ	difference	
η	mechanical efficiency of the human body	[-]
ε	long wave emissivity	[-]
γ, δ, ζ	time independent coefficients arising from the numerical (Crank-Nicolson) formulation of the bioheat equation	
κ	dimesionless geometry factor of an isothermal core domain of a body element	[-]
λ	heat of vaporization	[J kg^{-1}] [kJ kg^{-1}]
μ	proportionality factor	[K^{-1}]
ρ	density	[kg m^{-3}]
σ	Stefan-Boltzmann constant (=5.67*10^{-8})	[W m^{-2}K^{-4}]
Σ	sum	
τ_+, τ_-	function of positive/negative rates of change of the mean skin temperature in *DTS*	[-]
ϕ	function of core temperature in *DTS*	[-]
Ψ	view factor	[-]

ψ	function collecting dynamic components of *DTS*	[-]
Ω	linear operator	
φ	angle of a body element sector	[deg]

Subscripts and superscripts

-	last node next to an interface between two inhomogeneous tissue shells
+	first node next to an interface between two inhomogeneous tissue shells
0	sign of the thermal neutrality
a	air
acc	accumulation
bas	sign for a basal value
bd	body
bl	blood
bla	arterial blood
blp	central blood pool
blv	venous blood
C	convection
cl	clothing
CN	Crank-Nicolson
dp	dew point
Du	*Dubois*
E	evaporation
eff	effective
ex	expired
Ex	explicit
exp	experimental
f	fabric
frc	forced
g, G	globe
hy	hypothalamus
ifc	interface
i	running number
Im	implicit
,m	sign for a mean value

mix	mixed
msc	muscle
n	total number
nat	natural
o	sign for the operative temperature
oe	oesophageal
osk	outer skin node
r	node number (Numerical Methods)
R	long wave radiation
re	rectal
rsp	respiration
sat	saturated
set	setpoint
sf	surface
sh	shivering
sk	skin
sR	short wave radiation
sr	surrounding
sw	sweating
t	time step number
ty	tympanic
w	work
W	wall
x	sign of the counter-current heat exchange

Acronyms

ASHRAE	American Society of Heating, Refrigerating and Air-Conditioning Engineers
BAT	Brown adipose tissue
CNS	Central nervous system
DIN	Deutsche Industrie Norm
HVAC	Heating Ventilating and Air Conditioning
ISO	International Organisation for Standardization
KSU	Kansas State University
NST	Non-shivering thermogenesis

1 INTRODUCTION

1.1 Background

Computer simulation has become a popular technique for the analysis of complex physical problems being an attractive alternative to expensive experimental trials and destructive tests. This new technology has enabled the cost-effective development of optimum solutions in mechanical- and electrical engineering, thermodynamics, acoustics, etc. In architecture and environmental design, dynamic simulation programs predict the time varying thermal behaviour of whole buildings including heating demands, cooling loads, and solar gains. Computational fluid dynamics (CFD) codes are capable of simulating indoor climates in a detailed manner, predicting local air velocities, temperature patterns, etc.

In numerous disciplines of science and technology aspects of human heat transfer and/or thermal comfort play an important role. Expansion of scientific efforts in hostile environments, and the tightening of industrial health and safety standards are two areas of importance. Research into human performance, tolerance limits, thermal acceptability and comfort has applications in the car and aerospace industry, in textile engineering, meteorology, medicine, and for military applications.

Many problems associated with thermal comfort occur daily in artificial environments. Thermally uncomfortable indoor climates cause restrictions in the usability and functionality of spaces, and reduce occupants' performance in the work place. Inadequate conditioning of office rooms may provoke sickness of the employees accompanied by a loss of productivity to the company. The main purpose of the heating and air conditioning industry is, therefore, to create hygienic and thermally comfortable spaces for the users. Increasing efforts towards the rational use of energy in buildings, and the use of solar energy in buildings (solar architecture) are another reason to seek methods which allow an adequate evaluation of human thermal effects and comfort under the complex conditions met in practice.

The basis upon which thermal comfort and discomfort is currently assessed is the

Fanger model which is incorporated in a European standard. The validity of this model is restricted to uniform, *moderate, steady state* climatic conditions (no solar radiation), and levels of activity ≤3 met. This theory is based on 'physical' consideration rather than on 'physiological' principles of thermal comfort. Typical characteristics of the human thermal behaviour, eg. changes in body temperatures and regulatory reactions in thermally non-neutral conditions, are neglected.

Indoors, outdoors and in other special situations, man is, however, exposed to a variety of different thermal conditions which deviate from mild steady states. Transient changes in ambient temperatures (or any other climatic parameter), activity level, and/or clothing are conditions which prevail in daily life. In addition, inhomogeneous environments may arise, for example, due to asymmetric radiant fields (eg. near a cold window), direct solar radiation, or vertical air temperature and velocity gradients. Disturbances from mild climates toward both cold and hot conditions represent another field of complexity which is associated with changes in the bodily heat content and adjustments of the human thermoregulatory system.

To handle adequately with the complex thermal influences to which man is exposed, the specific behaviour of the human thermal system needs to be considered. Within the body, metabolic heat is produced. This heat is distributed over body regions by blood circulation and is carried by conduction to the body surface, where, insulated by clothing, heat is lost to the surrounding by convection, radiation, and evaporation. The heat capacitance of the body is a factor which affects the dynamic behaviour of the human thermal system under transient conditions. The amount of environmental heat loss is varied by changes in the effective insulation of the body shell due to thermoregulatory adjustments of skin blood flow. In addition, the heat production of the body may be increased and sweating may occur to regulate body temperature in the cold and in the heat, respectively. The geometric shape of the human body is a further characteristic which exerts an influence upon human heat transfer. In hot conditions, for example, there is an increased transfer of bodily heat by blood flow to extremities which offer an additional area for heat loss to the environment by evaporation of regulatory sweating.

Mathematical modelling of the human thermal system goes back 60 years. In the past three decades several multi-segmental models of human thermoregulation have been developed and have been valuable tools for contributing to a deeper understanding of regulatory processes. In these models, the human organism is separated into two interacting systems of thermoregulation: the controlling *active system* and the controlled *passive system*. The passive system simulates the physical human body and the heat transfer phenomena occurring in it and at its surface. The active system is simulated by means of cybernetic models predicting regulatory responses of the central nervous system, ie. the increase in heat production by shivering, changes in blood flows by vasomotor reactions, and sweating.

Despite the need to consider aspects of man's human thermal behaviour in different disciplines, mathematical models of human thermoregulation have not yet found widespread use. Reasons for this may include: lack of input data; poor modelling of the heat exchange with the environment; lack of ready-to-use program files or a limited range of applicability. Other reasons might arise from the fact that active systems have often been postulated using a limited number of experiments and test-subjects, and that model authors have used their own experiments to calibrate their models.

In addition to studies of thermoregulatory processes, dynamic models predicting the human thermal behaviour open doors for the 'first principles' research into the area of thermal comfort. The physiological nature of thermal comfort especially during exercise and in transient conditions is not yet well understood. Efforts to extend the predictability of the comfort sensation from mild environmental conditions to situations where regulatory responses govern the thermal state of the body and where changes in the body heat content occur are also associated with research on physiological effects. A multi-segmental model of human thermoregulation can be a valuable strategy into the area of *local* (dis)comfort in arbitrary asymmetric conditions, and physiological mechanisms involved in the thermal comfort adaptation.

1.2 Aims & Objectives

The aim of the research work was to create a computer simulation model which predicts human thermal behaviour and thermal sensation responses for a variety of different circumstances including transient conditions, and conditions where regulatory adjustments and changes in the body's heat content occur. Furthermore, the model should enable thermal influences on man to be evaluated for different exercise intensities and allow components of the environmental heat exchange to be predicted for complex, ie. inhomogeneous, boundary conditions.

The individual objectives were as follows.

A. To review the literature concerning:

(i) principles of biological thermoreception, temperature regulation, and perception of thermal comfort and its physiological basis to explore the problem and to devise routes to possible solutions;
(ii) existing mathematical models of human thermoregulation and the data needed to model the human body;
(iii) independent physiological experiments in which human thermal and thermoregulatory responses were measured to provide a database for developing the active system and to validate the complete model of human thermoregulation;
(iv) thermal comfort experiments to develop a statistically founded comfort model and to validate the model using independent experiments.

The results of the literature review have been described in several 'Interim Reports' produced during different stages of the project. A list of these reports is given in the Bibliography. The physiological basis of thermoregulation and thermal comfort is summerized in chapter 2. Experimental results and data related to modelling are introduced as appropriate throughout the thesis.

B. To develop a model of the passive system including:

(i) modelling of the human body by using collected body data obtained from literature;
(ii) modelling of heat transfer in living tissues;
(iii) location and direction dependent modelling of components of the environmental heat exchange, ie. surface convection, short and long wave radiation, skin evaporation, and respiration;
(iv) the development of appropriate numerical techniques to solve the complex problem of human heat transfer;
(v) validation of the numerical formulation using appropriate analytical solutions.

The passive system model is developed in chapter 3.

C. To develop a cybernetic model of the human thermoregulatory system (*active system*). This work involved:

(i) analysing experimental results and simulated data to what the thermal variables (afferent signals) of the body are and which are not involved in regulatory processes;
(ii) modelling individual thermoregulatory responses using the appropriate afferent signals; ie. to develop control equations for sweating, shivering, and cutaneous vasomotion (ie. constriction and dilatation) with respect to a wide range of boundary conditions and different types of exposure.

The development of the active system model is described in chapter 4.

D. To verify and to validate the complete model of human thermoregulation (see chap. 4), ie. to evaluate the steady and the transient behaviour of the model with respect to skin temperatures, body core temperatures and thermoregulatory responses:

(i) in cold and severe cold environments;
(ii) in moderate environments;

(iii) in warm and hot environments; and

(iv) during exercise.

E. To develop a 'first principles' model of thermal comfort (chap. 5):

(i) by analysing simulated and experimentally obtained results to investigate the physiological principles of thermal comfort and discomfort;

(ii) by modelling the sensation of temperature in moderate and non-moderate steady state environments;

(iii) by modelling the thermal sensation during exercise; and

(iv) by modelling thermal sensation in transient conditions.

(v) Finally, the complete comfort model was validated using independent experimental results for stationary and transient climatic conditions and for different activity levels.

2 PHYSIOLOGICAL BASIS OF THERMOREGULATION AND THERMAL COMFORT

2.1 Thermal Regulation in Humans

Homeothermic organisms are able to regulate their internal temperature so that it remains fairly constant over a wide range of environmental conditions. According to Encyclopeadia Britannica quoted by Hensel [88] *"homeothermy is defined as a pattern of temperature regulation in which... core temperature is maintained within arbitrary limits of ±2K despite much larger variations in ambient temperature"*. Body core temperature is kept constant against heat loss to the environment by internal heat production [83] and by means of appropriate counter measures taken by the thermoregulatory system [57].

Heat is produced by metabolism coming ultimately from the oxidation of food with carbohydrates, fats, and proteins as the major energy-carrying constituents. The body processes necessary for life require - even in the absence of conscious muscular activity - a minimum essential heat generation termed the basal metabolic rate. It is measured on a resting, awake, fasting subject. The basal metabolism of adult humans varies a little between the sexes and tends to decrease with age [36] (about 2% per decade [6]). Fluctuation of the basal metabolic rate may occur in homeotherms due to seasonal acclimation, induced by the effect of hormones on cells in response to changes in ambient temperature and/or to changes in the length of daylight. In human beings, however, there seems to be no clear effect of acclimatory changes on the basal metabolic rate [125].

During physical activities, body heat production increases in proportion to exercise intensity [6]. A part of the internal heat production is converted into external mechanical power [205] [46]. Training can improve the efficiency η of working by reduction of unnecessary effort. A maximum external work of about 20% of the actual metabolic rate (ie. η=0.2) can be reached by human subjects [205]. However, for most activities the mechanical efficiency is very small, near zero [46]. Metabolism during exercise is often treated in terms of activity level units (measured in met) as the ratio

between the body heat produced at that activity and the average metabolism when seated, defined as 58.2 W/m^2 [6], ie. one met. The met-values for various typical activities are tabulated in the standard literature [5] [94].

Exposures to cold stimulate a shift in the level of the metabolic activity. The capacity to raise heat production extends the range of environment conditions over which homeothermy can be sustained. There are three kinds of action by which the metabolic rate of human beings can be increased in response to cold boundary conditions [19].

- Non-shivering thermogenesis (NST) which is a rapid increase in heat production in brown adipose tissue (BAT) without shivering. NST occurs in neonates. Newborn human babies, however, soon loss their BAT and so the ability for NST. In adults NTS does not play a major role [88].

- An increase in cold-motivated voluntary exercise, ie. an elevation of the activity level.

- Cold-adaptive shifts in metabolism by shivering (ie. contraction of the muscle fibres) as a response of the human thermoregulatory system.

The effect of warm and hot ambient temperatures on metabolic rate is not straightforward, since behavioural responses overlap physiological reactions. Nevertheless, there is an increase in metabolic rate of about 12% both for resting and exercising subjects as observed experimentally [26] (quoted in [125]) when the ambient temperature rose from 29 to 38°C.

Heat exchange with the environment is controlled by regulatory changes to the skin blood flow (vasomotion) and the latent heat loss (sweating). In addition to these autonomic thermoregulatory adjustments, man is able to correct disturbances of the bodily thermal state by *behavioural thermoregulation*. In addition to the cold-motivated increases in activity level noted above, behavioural action might include eg. changes in clothing insulation, changes in body posture, and seeking shade.

Biological temperature regulation is made possible by specific central and peripheral nervous structures that continuously detect the organism's thermal state. Detailed information exists about peripheral thermosensors (for a review see eg. [88]). The current knowledge on central thermoreception is, however, rather fragmentary being based largely on animal experiments.

2.2 Thermoreceptors

Cutaneous thermoreceptors are defined as endings of nerve fibres (diameter between 1-4 µm [116]) which are excited by thermal (but not mechanical) stimuli [88]. The average depth beneath the skin surface is about 0.2 mm for cold, and about 0.5 mm for warm, receptors [88]. Single cold and warm thermoreceptors innervate about 1 mm^2 of skin area [97]. Cold receptors seem to be more densely distributed in the skin than warm receptors [84]. Both sorts of sensor are distributed inhomogeneously over the body surface resulting in the regionally different thermal sensitivity of the human skin [138]. Formulae for estimating the mean skin temperature - as an important measure of the overall physiological thermal strain at the bodies periphery - from a sample of local temperature probes need to reflect this asymmetry (and the contribution of the local skin area) in the overall mean value. Different approaches for estimating the mean skin temperature were compared eg. by Mitchell et al. [133]. The effect of local stimulus area was investigated by Stevens et al. [174]. Weighting coefficients for local area and local sensitivity during skin *warming* turn out to be virtually the same as coefficients weighting local area and local sensitivity during skin *cooling* [35] (with the exception of the forehead [138]). The average coefficients for calculating the mean skin temperature which apply with sufficient accuracy to a wide range of environmental conditions are listed in appx. B.1, ***Tab.B.1***.

Cutaneous thermoreceptors operate in the non-painful temperature range [86]. The threshold for hot-induced pain in man is about 46°C [6]. There is no well defined limit for pain elicited by cold stimuli. Local application of cold thermodes to the palm of human subjects indicated a threshold temperature for pain of less than 22°C [16] but also significantly lower values of 5 - 7°C were observed [6].

Cutaneous receptors respond by periodic electrical impulses (or bursts of impulses) [88] of about 50 mV constant amplitude [125]. They have a static discharge frequency at constant skin temperature and show a dynamic overshoot in frequency during temporal changes in skin temperature, the first time derivative, dT_{sk}/dt (see ***Fig.2.1***). There seems to be no indication of the presence of a second time-derivative component in the response [181]. Similarly, the hypothesis that spatial temperature gradients, ie. heat fluxes, are a stimulus for these transducers has not been verified by experiments [85] [186].

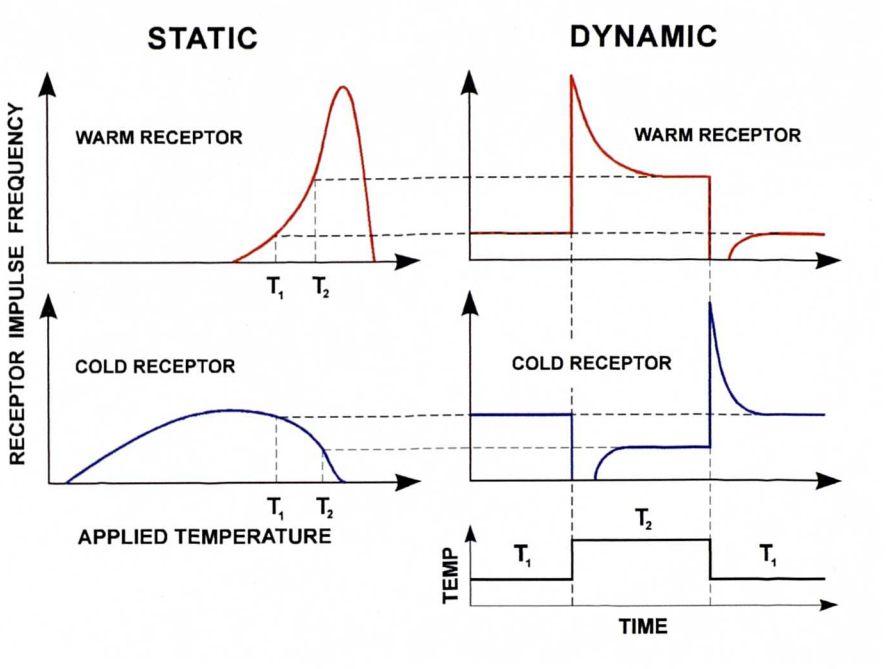

Fig.2.1

Static and dynamic responses of warm and cold cutaneous thermoreceptors as elicited during two constant levels of skin temperature and during sudden changes in skin temperature. Redrawn from [88].

The static impulse frequency of cutaneous receptors rises with temperature, reaches a maximum and falls again at higher temperatures [88]. The temperature range of static activity appears to be between -5°C and 43°C with a maximum firing rate at a skin temperature of about 25°C in cold receptors. Warm receptors exhibit a static discharge that begins in the range above 30°C and terminates before reaching 50°C. The static maximum frequency appears to be between 40 and 45°C [105] and is considerably higher than for cold receptors. The shift of the two bell-shaped discharge curves along the temperature axis causes a reciprocal activity behaviour between

cold and warm receptors in their "operational range": the decrease in activity of a sensor type is associated with an increase in activity of the other sensor type as the temperature of the skin changes (***Fig.2.1***). In terms of cybernetics, this opposing behaviour is capable of creating *set-point*s [19]; a concept which have found application in various engineered systems.

The reciprocal activity of cold and warm cutaneous sensors is also seen in their dynamic behaviour [181]. Cold receptors respond with an transient overshoot in discharge frequency when suddenly cooling the skin, and with a transient inhibition [181] on sudden warming. The opposite dynamic behaviour occurs in warm receptors [88] (***Fig.2.1***). Cutaneous receptors have been shown to be very sensitive to temporal changes in skin temperature [181]. However, there is a question concerning the extent to which the central nervous system utilizes such a high acuity for eliciting thermoregulatory actions [181].

Cold and warm populations of thermosensitive structures are also present in the body core [19]. Thermosensitive neurons are concentrated in the preoptic-anterior hypothalamic region [88]. Their presence has been demonstrated indirectly by eliciting appropriate regulatory and behavioural activity by local heating and cooling of this brain region in mammals [18] (in [88]). Also, attempts to directly measure the firing patterns of central neurons in this body region have been successful [139] [140]. Thermosensors have also been discovered in other core tissues such as the midbrain, medulla oblongata, and spinal cord. Even locations outside the central nervous system such as in blood vessels, abdominal cavity, etc. have been shown to be excited by thermal stimuli (for refs. see [88]). The role of these thermosensitive body sites in central thermoregulation, however, is unknown [19]. Nevertheless, the evidence of their existence may be important when developing theoretical models on thermoregulation.

2.3 Interpretation of Thermal Signals

Information from cutaneous and internal thermoreceptors is processed into conscious

sensations of temperature and into autonomic thermoregulatory responses. A central role in the processing of thermal signals is ascribed to the posterior hypothalamus [88]. The mechanisms of sensory processing in the afferent thermal pathways are, however, insufficiently understood.

The effect of individual body temperatures on thermoregulatory effectors has been proved by animal experiments involving the artificial stimulation of corresponding thermosensitive sites. The principal thermal and thermoregulatory behaviour of human subjects under *natural conditions* (where individual body temperatures were not separately controlled) has been described by Gagge et al. for sedentary [57] and exercising subjects [58] and is shown in ***Fig.2.2***.

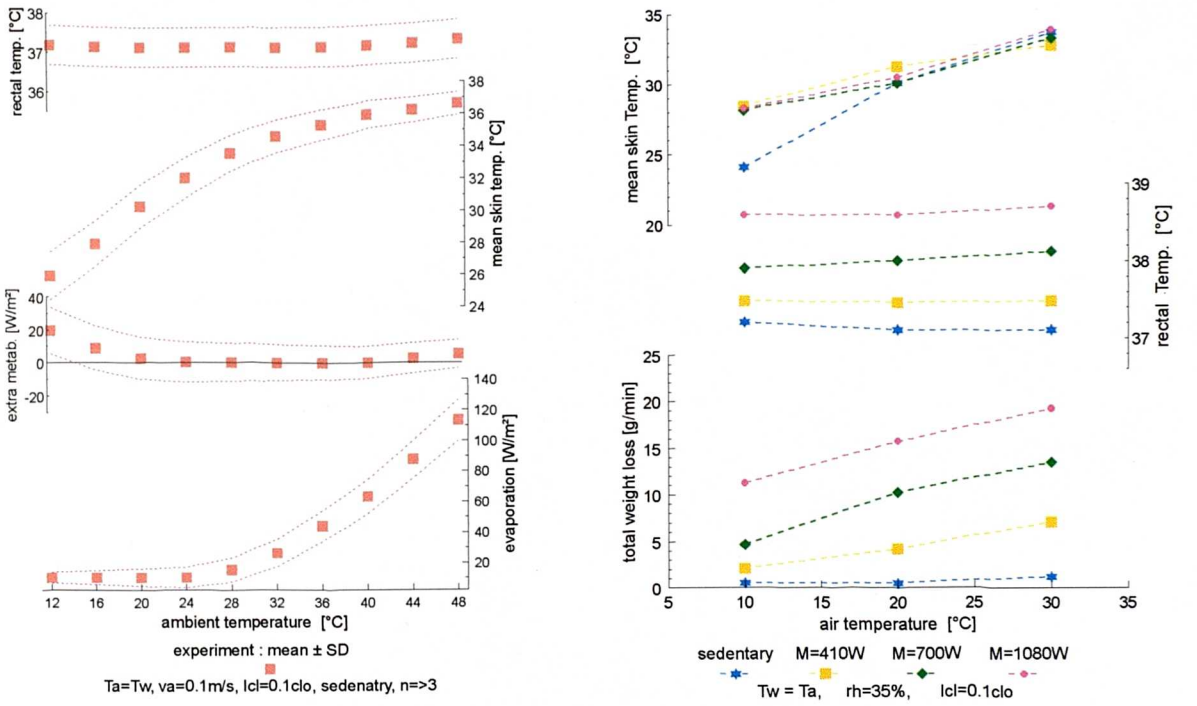

Fig.2.2

Skin temperature, body core temperature (rectum) and regulatory responses as measured [57] [75] over a wide range of environmental conditions for sedentary activity (left), and for three widely dispersed levels of exercise intensity and ambient temperature of 10, 20, and 30°C [58] (right).

Locally warming a mammalian anterior hypothalamus was found to increase skin blood flow (vasodilatation) and to induce sweating. Vasodilatation occurred even though a fall in body core temperature accompanied this regulatory reaction [1]. Hy-

pothalamic cooling in conscious mammals elicited a decrease in skin blood flow (vasoconstriction), and shivering even in hot environments. Vasoconstriction continued to take place despite a simultaneous general rise in body core temperature as a result of this response [1] (refs. [88]).

In human experiments cutaneous receptors were found to play a major role in the temperature regulation. They produce both positive and negative afferent signals into the human central thermal integrator for sweating [120] [137] [41] [11] and cutaneous vasomotion [21] [162] [195] [156]. The (integral, ie. mean) skin temperature turned out to be the trigger and the governing variable of shivering [156] [11] [183] [184] and vasoconstriction [185] in the cold. Although the involvement of positive afferent signals from the skin (ie. 'warm' skin temperatures) in thermoregulation against hot conditions has been questioned [11], various experiments have revealed that skin temperature may induce the onset of the whole-body sweating despite the body core temperature not being elevated [109] [110] [120] [137]. In comparison a weak effect of 'warm' skin temperature has been suggested from the (little) experimental data for the vasodilatation response [208]. On the other hand, there is evidence that whole-body vasodilatation may be trigged by an increase in skin temperature alone [120] [137] [207] [163] (in animals: [107] quoted in [88]).

In addition to the role of the (mean) skin temperature in central thermoregulation skin temperature has a further, local effect. Local skin temperature was found to modify the local sweating rate in the presence of a constant central nervous system drive [23] [137] [203]. The influence of skin temperature has also been observed on the response of local skin blood flow [42] [192]. Local vasodilatation was observed to be triggered by high local skin temperature even if there was no central drive for whole-body dilatation [99].

There is some evidence for a dynamic component in human thermoregulatory behaviour. Sweating can temporarily be inhibited by negative rates of change of skin temperature [203] [137]. Positive rates, however, do not seem to have any effect on sweating [137] [207]. Negative rates of change in skin temperature also influence the shivering response [81] [184].

Experimental results have been used to establish control equations for shivering [183] [184] [180] [81] and sweating [137] [178] [207]. Attempts have also been made to describe vasomotor reflexes in quantitative terms. However, in place of the overall skin blood flow, which is not directly measurable, forearm blood flow (which is not always reliable [88]) has often been analysed [207] [208]. Thermoregulatory effectors of the human central nervous system (central drive) turned out be multiple functions of temperature signals from the body core and the body periphery. Assuming a *proportional* system, *additive* connections between the mean skin temperature $T_{sk,m}$ and any internal temperature T_c (rectal, oesophageal, or tympanic) have been established [137] [178] [207] [184] [183] [180]. Others have developed relationships involving the product of $T_{sk,m}$ and T_c [176] [81]. The effect of local skin temperature on local sweating was mathematically described by Nadel et al. [137]. Similar expressions have also been assumed by others for skin blood flow [176].

2.4 Thermal Comfort

The cause of *conscious* actions to control the bodies thermal state appears to be the sensation of thermal (dis)comfort [57]. According to ASHRAE's definition, thermal comfort is "*that condition of mind which expresses satisfaction with the thermal environment*" [5]. Benzinger [11] defined thermal comfort more objectively as: "*... the absence of punitive impulses from both* (ie. cutaneous and hypothalamic) *receptor fields*". Only reclining resting subjects can reach this state of *ideal* comfort when exposed (unclothed) to an ambient temperature of T_a= 30°C [11] [57]. Under these thermoneutral conditions no regulatory adjustments occur. According to Benzinger [11], at higher activity levels a state of *mixed* comfort can be reached when internally born 'warnings of hot' (due to elevated central temperature) are balanced by 'warnings of cold' from cutaneous thermoreceptors. For a steady state, the physiological conditions of general thermal comfort (at low activity levels) have been described [76] as follows:

- internal body temperature 36.6 to 37.1°C,
- mean skin temperature 33 to 34.5°C for man and 32.5 to 35°C for women,

- local skin temperature is variable over the body but generally between 32 and 35.5°C,
- temperature regulation is completely accomplished by vasomotor control of blood flow to the skin (no sweating/shivering present).

Most applied work on thermal comfort has dealt with comfort and temperature sensation in direct relation to environmental conditions. Under steady states subjects' sensory estimates have been related to ambient temperatures (the relative effect of air and radiant temperature [129]), humidity [159], and air velocity [160]. Additional parameters such as the peak-to-peak variation and the fluctuation rate of the air temperature [161] have also been used to describe human perceptual responses under specific transient conditions (for a review see [89]).

According to Gagge [62], the physiological correlation of thermal (dis)comfort is a composite of: (i) signals evoking thermal sensation associated with skin temperature; and (ii) signals arising from autonomic thermoregulatory activities associated with both skin and central temperature. In contrast to perception of thermal comfort (TC) which is commonly attributed to the general thermal and regulatory state of the body, temperature sensation (TS) seems to depend mainly on the activity of cutaneous thermoreceptors [87] [57] [148]. Hence, TC appears to refer to the subjective state of the observer [87] that can be described using verbal scales for (dis)comfort[1)], (un)pleasantness[2)] [57] or perhaps the Bedford scale[3)] [9] (in [125]) which also contains evaluative terms. TS is a rational experience [87] which is directed towards an objective world and which can be characterized using terms in the ASHRAE-scale[4)] [5]. In many cases, however, the perception of TC and TS correlate with each other [57] [125].

Cold discomfort has been found to be governed by skin temperature [57] [66] [76], and warm discomfort has been related to skin temperature [57] [148] [67] [62]. Re-

---

1) *Comfortable - Slightly uncomfortable - Uncomfortable - Very uncomfortable*

2) *Pleasant - Indifferent - Slightly unpleasant - Unpleasant*

3) *Much too cool - Too cool - Comf. cool - Comfortable - Comf. warm - Too warm - Much too warm*

4) *Cold - Cool - Slightly cool - Neutral - Slightly warm - Warm - Hot*

ports of warm discomfort due to elevated skin temperature have been made even though no appreciable increase in body core temperature occurred [57]. In contrast, Benzinger suggested that warm-discomfort is originated exclusively from the warm hypothalamic receptors [11].

Skin wettedness - defined [60] as the ratio between the *actual* overall evaporative skin heat loss and its maximum (which occurs when the partial vapour pressure at the skin reaches the saturated value) - has been shown to be a good indicator for warm discomfort (for a review see [15]). A better correlation was obtained, however, when skin temperature was considered as a variable of warm discomfort in addition to skin wettedness [15]. Other approaches have treated thermal comfort in terms of the palm conductance [179], or heart rate [62]. However, all these relationships seem to apply only to steady state conditions and the physiological basis of transient comfort is not yet well understood. Investigations of comfort and temperature sensation under environmental transients [57] [67] have shown that both body temperatures and thermoregulatory responses (including skin wettedness) lag considerably behind dynamic sensory estimates. There are indications that the rate of change of skin temperature might be an important signal for the transient sensation of comfort and temperature [38]. However, further research on transient comfort is required [51].

As for the thermoregulatory responses, there are local effects in the perception of comfort and temperature. Local discomfort can be perceived due to inhomogeneous environmental conditions such as asymmetric radiant fields [130] [4] [49] [65], draughts [50] [48] [117], and vertical air temperature gradients [152] [206]. The mechanisms which evoke the perception of general and local (dis)comfort are different. A study was conducted [55] to show whether comfort models which predict overall comfort responses can be modified to predict local (dis)comfort. It was found that neither the overall heat-loss of the body (when calculated using ISO 7730 [94]) in conditions which cause local discomfort (due to draught [47]), nor the modification of the overall bodily heat loss (by the partial contribution of the increased local heat-loss due to draught) could reproduce the corresponding comfort sensations observed experimentally.

The physiological mechanisms governing local perceptive responses were found to be associated with (local) cutaneous thermoreception [87]. Overall perceptive responses reflect an integration of thermal afferents from various sites of the human skin. However, this integration is not unlimited. If the local temperature of the skin deviates too far from the mean skin temperature, local discomfort can be experienced in this area. Local thermal sensation has been found to be governed by skin temperature irrespective of the general thermal state of the body [135] [16]. In contrast, local (dis)comfort also appears to be highly dependent on the state of general comfort [95] (whereas local stimuli do not noticeably influence the perception of general comfort [95]). The dependence of local discomfort on the state of general comfort is the so called *alliesthesia*-effect discovered by Cabanac [24].

2.5 Summary

Biological temperature regulation is made possible by specific nervous structures that continuously detect the human being's thermal state at the bodies periphery and in the body core. The actual temperature (static component) and the rate of change in temperature (dynamic component) have been identified as the physical variables which provoke changes in the electrical activity of thermoreceptors. The hypothesis that heat flux is a stimulus for thermoreceptors has not found experimental verification. The responsibility of individual afferent signals and the involvement of different thermosensitive sites in thermoregulation is discussed in more detail in chap. 4 (see also [53]).

Information from core and peripheral (cutaneous) thermoreceptors is processed into thermoregulatory reactions. Thereby, cutaneous sensors produce positive and/or negative afferent signals into the human central thermal integrator for sweating, cutaneous vasomotion, and shivering. In addition to the central nervous system drive, skin temperature has a local, autonomic effect on sweating and skin blood flow. The body core temperature appears to exert a profound influence upon regulatory responses against heat. Diverse multiple relationships are presented in the literature to describe the individual regulatory effectors. The cybernetics of thermoregulation, ie.

the various aspects of modelling the active system, are discussed together with corresponding literature in chap. 4 (see also [56]).

The physiological correlation of thermal comfort and temperature sensation is a composite of signals which are associated with both skin and central temperature. Cold discomfort depends on skin temperature. In warm subjects discomfort has been related to skin temperature, core temperature, variables of thermoregulatory reactions (eg. skin wettedness, superficial palm conductance) and combinations of them. However, all these relationships seem to be limited to situations where subjects do not perform exercise and to steady-state conditions. Investigations of comfort and temperature sensation under environmental transients have shown that both body temperatures and thermoregulatory responses lag considerably behind the dynamic sensory estimates. There are indications that the rate of change of skin temperature might be an important signal for the transient sensation of comfort and temperature. The physiological correlations of thermal sensation within a wide range of environmental conditions, during exercise and in transient conditions, is discussed in chapter 5.

3 MODELLING THE PASSIVE SYSTEM

3.1 Introduction

Thermal modelling of the passive system is based on the physical laws for heat transfer occurring within the human body and at its surface. Within the body, metabolic heat is produced. This heat is distributed over body regions by conduction and convection (blood circulation). At the body surface heat is lost inhomogeneously to the surroundings by convection, radiation, and evaporation. In addition, some heat is lost by respiration.

Mathematical modelling of the human thermal system started with attempts to calculate system properties on the basis of a very general heat balance. Two-node models [60] [7] [91] simulated the human passive system using lumped data for the human body and employing overall heat balances for the body core (including metabolic heat production) and the body shell (including environmental heat losses). The two compartments were thermally coupled by the heat flux arising from the temperature difference between the core and the shell. The body shell had a variable resistance controlled by regulatory devices. The most well known two-node model - the Pierce-model [60] - was adopted by ASHRAE and used to calculate standardized environmental temperatures such as the standard operative humid temperature, T_{soh}. The model has been subject to further improvements and refinements [91].

Multi-segmental models [177] [69] [200] [132] [176] [201] simulate the human passive system in more detail. All thermally important body elements are incorporated, so the impact of the body's geometry on heat transfer can be accounted for. Instead of lumped data, locally variable thermal and physiological properties of tissue materials are used to construct the human body.

Stolwijk [177] modelled the human body as a spherical head element with cylindrical elements for the trunk, arms, legs, hands and feet. Each of these segments were lumped into four concentric, annular tissue-nodes: core, muscle, fat, and skin.

Detailed passive system models were formulated by Wissler [200] [201] and Werner [197]. The model of Wissler consisted of sixteen cylindrical elements which were subdivided into concentric tissue shells. The nodal energy balances included also heat transfer to the capillaries, and to major veins. However, the required specific input data into the system have not been published, probably due to the difficulty of obtaining them from direct measurements [200]. The model of Werner was developed for use with large computers. Werner gave up the idealized cylindrical symmetry of body elements in favour of a three-dimensional digital representation of the human body with individual organs. The focus of the model seemed to be a detailed analysis of temperature profiles *within* the human body for medical purposes rather than the exploration of climatic influences on man.

Gordon [69] comprehensively surveyed literature and presented the required data on the anatomy of the human body, thermophysical properties and basal physiological values of individual tissue materials. Gordon embellished the Stolwijk model by introducing elements for the neck, face and forehead to the head segment to allow improved modelling of respiratory losses and (according to Gordon) for their importance in temperature regulation. These (usually unclothed) body sites appeared to be of specific importance also in the perception of (local) thermal comfort [117]. The trunk was further subdivided into an abdomen and a thorax-segment to permit a separate modelling of the lung region. Body elements were divided distinctly into individual tissue layers. Gordon's research on the body's thermophysical properties has found application in diverse models and formed a basis for developing the passive system model presented in this thesis.

Whilst there is a comprehensive data base on anatomical, thermophysical, and basal physiological properties, efforts are required to improve the passive system to model the heat exchange between the human body and the environment in more detail. Poor modelling of environmental heat exchange reduces the universality and the practical applicability of models.

To be of practical value, a model of human heat transfer and thermal comfort must run on readily available computers with reliability and produce results reasonably

quickly. A fast, accurate and stable numerical method of solving the complex equations describing the passive system has to be therefore developed.

3.2 Body Construction

The passive system of the model was developed by using thermophysical and basal physiological properties of tissue materials from literature [29] [69] [197]. The humanoid was formulated to represent an *average* man (body weight 73.5kg, body fat 14 wt-%, *Dubois*-area of 1.9m^2, basal metabolism 87W, basal evaporation from the skin of 18 W, and basal cardiac output 4.9 l min^{-1}, see also ***Tab.A.2***). The body was idealized as 15 spherical or cylindrical body elements: head, face, neck, shoulders, arms, hands, thorax, abdomen, legs, and feet. The use of lumped data (eg. if body elements are divided into a core and a shell) is prone to errors during temperature transients, and was avoided. In accordance with former studies [69], a division was therefore made whenever a significant change of body tissue properties occurs. As a result, the present multi-layer model consists of annular concentric tissue layers and uses seven different tissue materials: brain, lung, bone, muscle, viscera, fat, and skin. Each of these is subdivided into one or more tissue nodes (see ***Tab.A.1***).

In accordance with the work of Weinbaum and Jiji [193], the skin was modelled as two layers with distinctly different physiological properties: the inner skin and the outer skin. The inner skin is about 1mm thick and simulates the cutaneous plexus - a region in which metabolic heat is generated and blood is perfused. The outer layer of skin is of similar thickness, but contains neither heat sources nor any thermally significant blood vessels. This superficial cutaneous layer plays a role when modelling evaporative heat losses through the skin. It contains sweat glands and simulates the vapour barrier for moisture diffusion through the skin.

Asymmetric removal of bodily heat is often experienced in practice. It may be due to inhomogeneous ambient conditions, eg. by solar irradiation, cold surfaces, draught effects, non-uniform clothing, or due to physiological effects on the skin such as local differences in evaporative heat losses, etc. Except for the face and shoulders, each

body element was, therefore, subdivided spatially into sectors. Most of the body elements were divided into three sectors: anterior, posterior and inferior (see ***Tab.A.1***). Anterior and posterior segments permit the treatment of lateral environmental asymmetries. Inferior segments account for body sides which are 'hidden' by other body parts (eg. sector *c* in ***Fig.3.1***) and thus have reduced radiant heat exchange with the environment.

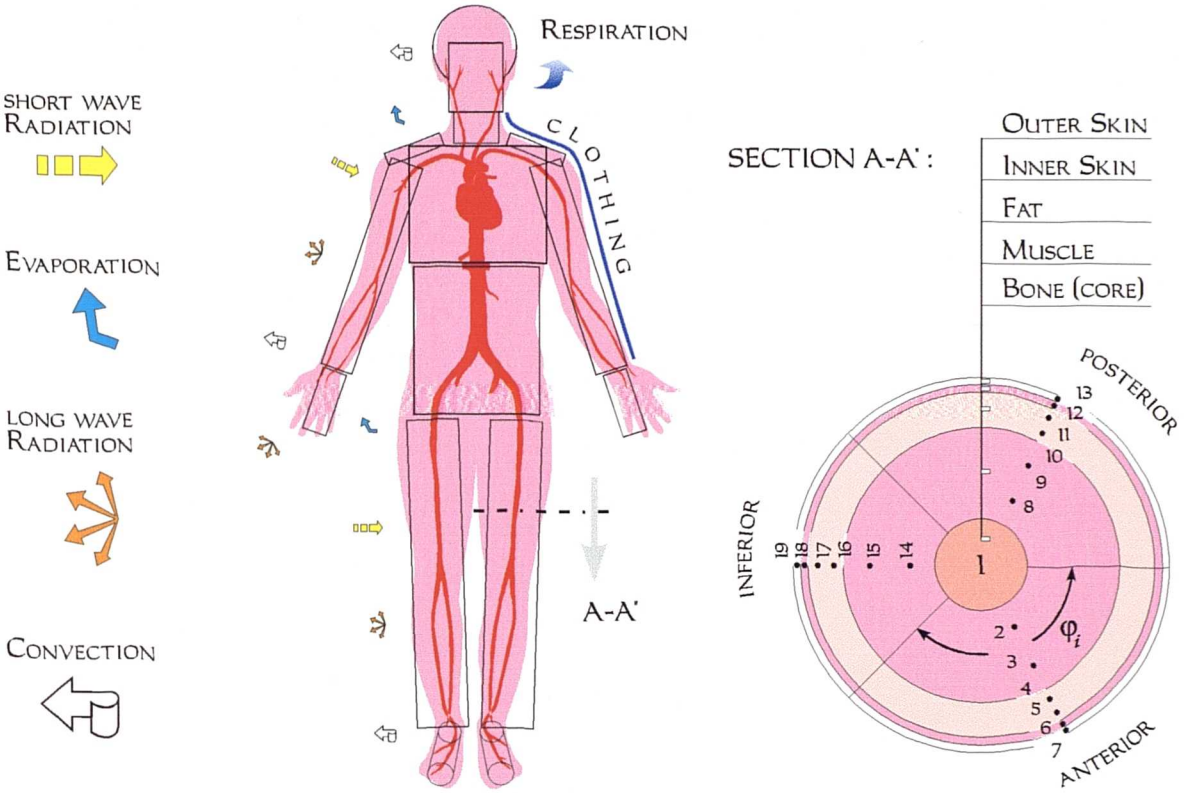

Fig.3.1

A schematic diagram of the passive system.

The sectors were coupled thermally by introducing a core element around the cylinder axis (see ***Fig.3.1***) or the midpoint of the sphere. In the model, except for the head, the radius of the core was defined to be identical to the radius of the innermost tissue material layer in each body element. In extremities, for instance, the radius of this domain is identical to the radius of the bone. However, the brain which has an outer radius of r=8.6 cm, (***Tab.A.1***) was given a core of radius 4cm.

3.3 Heat Transfer within the Tissue

The heat transport mechanisms occurring in the living tissue have been formulated by Pennes [153] in the so-called *bioheat equation*. This differential equation describes the heat dissipation in a homogeneous, infinite tissue volume:

$$k\left(\frac{\partial^2 T}{\partial r^2}+\frac{\omega}{r}\frac{\partial T}{\partial r}\right)+q_m+\rho_{bl}w_{bl}c_{bl}\left(T_{bla}-T\right)=\rho c\frac{\partial T}{\partial t} \qquad (3.1)$$

According to eq. (3.1), from left to right, the radial heat flow from warmer to colder tissue regions (heat conduction term, where k is the tissue conductance [$W m^{-1}K^{-1}$], T tissue temperature [°C], r radius [m], ω a geometry factor [ ]: ω=1 for polar coordinates and ω=2 for spherical coordinates (head)), is overlaid by metabolism q_m [$W m^{-3}$], and blood perfusion (heat convection term, where ρ_{bl} density of blood [$kg m^{-3}$], w_{bl} blood perfusion rate [$m^3 s^{-1} m^{-3}$], c_{bl} heat capacitance of blood [$J kg^{-1}K^{-1}$]), T_{bla} arterial blood temperature [°C]). This combined effect is balanced by the storage of heat within the tissue mass (right-hand side of eq. (3.1), where ρ is tissue density [$kg m^{-3}$], c tissue heat capacitance [$J kg^{-1}K^{-1}$], t time [s]).

The bioheat equation was applied to all tissue nodes using the appropriate material constants k, ρ, c, the basal heat generation term q_m, and basal blood perfusion rate w_{bl} for each tissue layer (***Tab.A.1***). It should be noted that the magnitudes of the physiological variables q_m and w_{bl} are affected by responses of the active system and are described in chapter 4. The arterial blood temperature T_{bla} in eq. (3.1) arises from the actual overall thermal state of the body, and is obtained by simulating the human blood circulatory system.

3.3.1 Heat Conduction

The heat conduction term in eq. (3.1) considers only temperature variations in the radial direction, whereby ω=1 stands for polar coordinates and ω=2 for spherical coordinates (head). Angular heat flows were also neglected in the present model even though the body elements were divided into sectors and environmental asymmetries are considered. There were two reasons for this simplification. Firstly, at the periphery (ie. predominantly in the skin) although significant angular temperature gradients may occur due to asymmetric boundary conditions, the total amount of the heat conducted angularly from one skin sector to another is negligible compared with the total amount of heat transferred radially through a sector band. This is because peripheral sectors have large shell-areas compared with the small interface-areas between adjacent skin sectors. Secondly, ambient influences are insignificant in internal tissue layers where heat dissipation is dominated by metabolism and by blood circulation [153] [171] [172]. Therefore, inhomogeneities of q_m and w_{bl} between individual organs of the abdominal viscera [197], for instance, which can hardly be considered by symmetrical geometry models, govern local temperature profiles within the body and swamp the effect of environmental asymmetries.

3.3.2 Metabolism

In the model, the metabolic heat production of a finite tissue volume is treated as a sum of the basal value $q_{m,bas,0}$ and the additional heat Δq_m which may be produced by local autonomic thermoregulation, while exercising and/or shivering:

$$q_m = q_{m,bas,0} + \Delta q_m \tag{3.2}$$

The basal metabolic rates of individual tissue materials $q_{m,bas,0}$ were obtained from literature [69] [197] [29] and are listed in ***Tab.A.1***. In thermal neutrality (T_a=30°C, for a detailed specification see ***Tab.A.3***), where no regulation occurs, the overall basal

metabolism $M_{bas,0}=\int q_{m,bas,0}\ dV$ of the passive system results in a value of 87W; which agrees with the (standardized) whole-body metabolism of a reclining average man according to ASHRAE Standards 55 [5] and ISO 7730 [94].

In muscles, the extra heat Δq_m may contain three components, ie. changes in the basal metabolism, $\Delta q_{m,bas}$, and additional metabolism by shivering and working, $q_{m,sh}$ and $q_{m,w}$, respectively:

$$\Delta q_m = \Delta q_{m,bas} + q_{m,sh} + q_{m,w} \tag{3.3}$$

The change in the basal metabolism $\Delta q_{m,bas}$ is the difference between the actual basal rate and the basal rate corresponding to neutral thermal conditions. It appears also in non-muscular tissues where $q_{m,bas,0}$ is present and where the tissue temperature differs from its setpoint T_0. This local regulation arises from the so called Q_{10}-effect with a sensitivity coefficient of 2 [197] which reflects the dependence of biochemical reactions on local tissue temperature T:

$$\Delta q_{m,bas} = q_{m,bas,0} \cdot \left[2^{(T-T_0)/10} - 1 \right] \tag{3.4}$$

The shivering term $q_{m,shiv}$ in eq. (3.3) is a portion of the overall regulatory response elicited by the active system (see chap. 4). The $q_{m,w}$-term can be written as:

$$q_{m,w} = \frac{\partial (a_{m,w} H)}{\partial V_{msc}} \tag{3.5}$$

where $a_{m,w}$ (see ***Tab.A.1***) is a coefficient distributing the overall extra metabolism due to exercise over body elements, V_{msc} is the corresponding body-element muscle volume, and H is the internal whole body workload. The values of $a_{m,w}$ for standing activities were obtained from Stolwijk [177]. The present model uses other estimates of $a_{m,w}$ for sedentary activities because the extra metabolism shifts from the muscles of the legs to the musculature of the trunk and arms when seated. The workload H in

eq. (3.5) represents that part of the overall *extra* energy which is produced by muscular activity but which does not appear as external work. It is obtained as the *difference* between the actual overall heat generation rate remaining in the body and the basal metabolism $M_{bas,0}$:

$$H = act \frac{M_{bas,0}}{act_{bas}} (1-\eta) - M_{bas,0} \tag{3.6}$$

The calculation of the actual metabolic rate utilizes the activity level units *act* (measured in met) as related to its basal value of act_{bas}=0.8 met. The *act*-units - used as (time-dependent) input-variables to the model - are commonly known and can easily be obtained by the users from standard literature (eg. [5] [6] [94]).

The bracked term $(1-\eta)$ in eq. (3.6) represents that fraction of the overall metabolic heat actually produced which remains for warming the body, ie. which is not converted into external mechanical power. The human mechanical efficiency η is not constant in reality, but rises with increasing activity levels. In the present model, the following formula for η was developed by means of regression analysis from measurements of Wyndham et al. [205]:

$$\eta = 0.2 \cdot \tanh\left\{ b_1 \cdot act + b_0 \right\} \tag{3.7}$$

The regression coefficients were b_1 = 0.39 ± 0.13 met^{-1} and b_0 = -0.60 ± 0.28 with a correlation coefficient of r=0.86. This equation reflects the behaviour of the human work efficiency during normal activities (eg. stepping, or cycling [205]). At low activity levels (act<1.6met), where man works most inefficiently, η is close to zero, at higher activity levels (ca. 1.6<act<5.0 met) η rises almost linearly with increasing activity level. At high activity levels η begins to approach a theoretical maximum of about 0.2, ie. about 20% of the whole body metabolism is transferred into external work.

3.3.3 Blood Circulation

Blood circulation is of vital importance for the dissipation of heat within the human body. The dissipation effect was examined by simulations using the present model without blood circulation: the core temperature of the brain, which has a high metabolic rate (***Tab.A.1***), exceeded 73°C, when the passive system was exposed to steady neutral ambient temperatures of 30°C.

In the present model, the human blood circulatory system was simulated as three main components: 1) the central blood pool, 2) counter-current heat exchanges and 3) pathways to individual tissue nodes. Body elements are supplied with warm blood from the central pool by the major arteries. However, before perfusing the tissues of the extremities and shoulders, the blood is cooled by heat lost to the counter-current blood streams in the adjacent veins. The arterial blood exchanges heat by convection in the capillary beds according to the bioheat equation (3.1). The venous blood then collects in the major veins and is rewarmed by heat from the adjacent arteries as it flows back to the central blood pool. It mixes with blood from other elements to produce the new central blood pool temperature.

The blood perfusion term of the bioheat equation (3.1) is based on *Fick's* first principle, assuming that heat is exchanged with the tissue in the capillary bed and that no heat storage occurs in the blood stream. The blood perfusion term has been critically discussed in the literature [30] [202] [182] and has been subjected to various improvements [171] [31] [43] [102]. Also, alternative models of microvascular structures have been developed [193] [96] [194]. However, the traditional blood perfusion term seems preferable in whole body models. It is simple and produces an accuracy which is comparable [28] with more detailed models which require comprehensive data on the vascular architecture of tissues.

The simulation of the counter-current heat exchange (*CCX*) was introduced into the model in an attempt to obtain a more realistic distribution of the arterial blood temperature T_{bla}, instead of assuming a constant arterial blood temperature for all body elements equal to the temperature of the central blood pool T_{blp}. A number of models

of the CCX between pairs of adjacent vessels exist in the literature (for a review see eg. Eberhart [43]) but these are seldom incorporated into whole body models.

Assuming mass-continuity in blood vessels, the decrease in the temperature of the blood in the arteries of an element T_{blp}-T_{bla} corresponds to the increase in temperature $T_{blv,X}$ - T_{blv} of the blood in the veins of the same body element after *CCX* :

$$\rho_{bl} c_{bl} \int w_{bl}\, dV \,(T_{blp} - T_{bla}) \;=\; \rho_{bl} c_{bl} \int w_{bl}\, dV \,(T_{blv,X} - T_{blv}) \tag{3.8}$$

Here, $\int w_{bl}\, dV$ represents the blood flow in the veins as the volume-integral of capillary blood flows w_{bl} over the body element. The blood temperatures after undergoing *CCX*, T_{bla} and $T_{blv,X}$ are the two unknowns in eq. (3.8). In order to obtain an element's arterial blood temperature T_{bla} in eq. (3.8) the net heat exchange between adjacent vessels Q_x was defined using the equation of Gordon [69]:

$$Q_x \;=\; h_x \,(T_{bla} - T_{blv}) \tag{3.9}$$

where h_x is the corresponding counter-current heat exchange coefficient and T_{blv} is the venous blood temperature before *CCX*. The arterial blood temperature T_{bla} of a body element is then obtained by substituting the right-hand side of eq. (3.8) by the right-hand side of eq. (3.9) and rearranging:

$$T_{bla} \;=\; \frac{\rho_{bl} c_{bl} \int w_{bl} dV \cdot T_{blp} + h_x \cdot T_{blv}}{\rho_{bl} c_{bl} \int w_{bl} dV + h_x} \tag{3.10}$$

The computation of the central blood pool temperature T_{blp} utilized a special calculation process (see section 3.5). Since the bioheat equation assumes that capillary blood reaches an equilibrium with the surrounding tissue, T_{blv} of a body element in

eq. (3.10) is obtained as follows:

$$T_{blv} = \frac{\int w_{bl} T \, dV}{\int w_{bl} \, dV} \tag{3.11}$$

The heat-exchange coefficients h_x between adjacent arteries and veins in eq. (3.10), are zero for central body elements [69] (ie. no counter-current heat exchange). Few reliable data on h_x of extremities exist in literature. Therefore, h_x of extremities and of shoulders were estimated by a trial and error procedure in which the coefficients were adjusted to obtain agreement between local skin temperatures as predicted and measured. For legs, feet, arms and hands h_x were obtained from measurements by Mayer et al. [117] and Nielsen et al. [143]. An experiment of Budd et al. [22], provided data for the shoulders. The individual coefficients h_x are listed in ***Tab.A.1***.

In thermal neutrality, tissues are supplied at basal perfusion rates $w_{bl,0}$ (see ***Tab.A.1***). In non-neutral conditions or when working, the blood flows, w_{bl} in eq. (3.1), vary with changes in regional metabolic rates, q_m. Experimental results [164] indicate a linear relationship between w_{bl} and q_m. Instead of dealing with blood perfusion rates w_{bl}, the present model considers directly their energy equivalent $\beta = \rho_{bl} c_{bl} w_{bl}$ [$W m^{-3} K^{-1}$]. The increased demand for oxygen is therefore accounted for by calculating the change in the gain factor $\Delta\beta = \rho_{bl} c_{bl} \Delta w_{bl}$ as a functions of the change in metabolism Δq_m using a proportionality constant μ_{bl}=0.932 [K^{-1}] which was obtained from Stolwijk [177]:

$$\Delta\beta = \mu_{bl} \cdot \Delta q_m \tag{3.12}$$

Utilizing $\Delta\beta$ the blood perfusion term in eq. (3.1) becomes:

$$\beta \, (T_{bla} - T) \quad \text{where} \quad \beta = \beta_0 + \Delta\beta \quad \text{and} \quad \beta_0 = \rho_{bl} c_{bl} w_{bl,0}$$

The very variable blood perfusion rates in the cutaneous plexus arise from man's temperature regulation mechanisms and are considered in chapter 4.

3.4 Heat Exchange with the Environment (Boundary Conditions)

At the body surface, heat is exchanged by convection with the ambient air q_c, by radiation with surrounding surfaces q_r, by irradiation from high-temperature sources q_{sR}, and by evaporation of moisture from the skin q_e. The rate of heat exchange varies over the body and is affected by the clothing ensemble worn. Hence, in the model, heat balances were established for each skin sector of each body element as boundary conditions to eq. (3.1). In general, the net heat flux q_{sk} passing the surface of a peripheral sector is equivalent to the sum of individual heat exchanges:

$$q_{sk} = q_c + q_r - q_{sR} + q_e \tag{3.16}$$

The elements of this equation are considered in detail in following sections.

3.4.1 Convection

The convective heat exchange q_c between a skin sector of surface temperature T_{sf} and ambient air of temperature T_a was modelled by considering both natural and forced convection using *combined*-convection coefficients $h_{c,mix}$ [W m^{-2}K^{-1}]:

$$q_c = h_{c,mix} \cdot (T_{sf} - T_a) \tag{3.17}$$

In the present model, the convection coefficients $h_{c,mix}$ are a function of the location on the body, the temperature difference between the surface and the air, and the effective air speed $v_{a,eff}$:

$$h_{c,mix} = \sqrt{a_{nat}\sqrt{T_{sf} - T_a} + a_{frc}\, v_{a,eff} + a_{mix}} \tag{3.18}$$

The basis for $h_{c,mix}$ are the experiments of Wang [189] [190] [191] who measured

local convective heat losses on a heated full-scale manikin with a realistic skin temperature distribution for both natural and forced convection. Coefficients a_{nat}, a_{frc}, a_{mix} (see ***Tab.A.1***) were obtained by means of regression analysis in which Wang's results were modified and transformed into expressions more appropriate for computer simulation as shown by eq. (3.17). To check the reliability of the convective heat exchange model the overall, ie. the mean convection coefficient of the whole human body, $h_{c,m}$ [W m^{-2}K^{-1}], was obtained by integrating the local convective heat losses $q_c = h_{c,mix}\,(T_{sk}-T_a)$ over the (naked) body surface A_{Du}:

$$h_{c,m} = \frac{\int q_c \, dA_{sk}}{A_{Du}\,(T_{sk,m}-T_a)} \qquad (3.19)$$

Here, $T_{sk,m}$ is the *area*-weighted mean skin temperature.

The overall coefficient was computed both for conditions of natural convection ($v_{a,eff}$< 0.05 m s^{-1}) and for forced convection. ***Fig.3.2*** compares the simulation results for the free convection with data of Fanger [45], Bach [8], and data quoted by McIntyre [125], ie. coefficients for a 2-m high cylinder obtained from Birkebak [17] and coefficients obtained by Rapp [155] which are recommended (by McIntyre) for sedentary people.

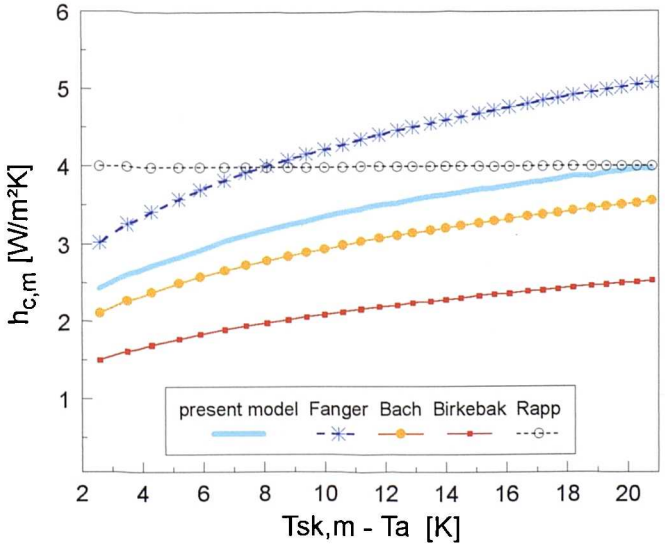

Fig.3.2

Overall convective heat transfer coefficient $h_{c,m}$ for natural convection.

Simulated forced convection coefficients were compared with formulae used by Fanger [45], Bach [8], Colin et al. [34], and Nishi [146] and are illustrated in ***Fig.3.3***. As apparent from ***Fig.3.3*** the model's overall coefficient for forced convection correlates better with results of more recent literature [8] indicating higher values (see also [27] [117]) when compared with earlier investigations.

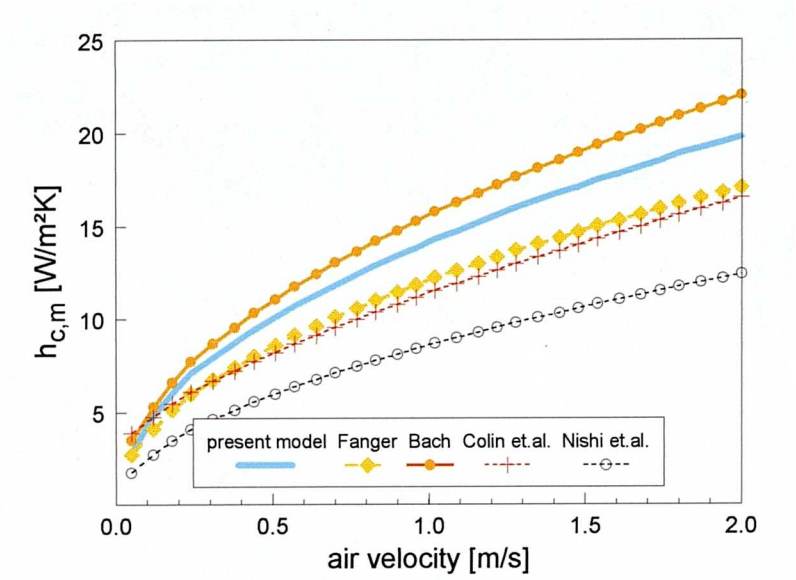

Fig.3.3

Overall convective heat transfer coefficient $h_{c,m}$ for forced convection.

The effective air velocity $v_{a,eff}$ in eq. (3.17) is a composite of the local room air speed and the relative air speed due to body motion. Earlier investigations on walking subjects [146] suggested an increase in $h_{c,m}$ with increasing body movement. More recent experiments [27], however, have illustrated constant or even decreasing h_c-coefficients during walking. Similarly, simulations using the present model did not show evidence of functional dependency of the convective heat loss on the activity level. Obviously, h_c is affected by the type of activity rather then by its level. Hence, instead of introducing a fixed relationship between h_c and the activity level which could produce systematic errors in predictions, users of the model should modify appropriately the input variable $v_{a,eff}$, if detailed information on h_c for a specific task is available.

3.4.2 Radiation

The exchange of heat by long wave radiation q_r is usually of similar importance in the heat balance of the human body as the heat exchange by convection.

In asymmetric environments q_r of a body element sector represents the sum of the partial heat exchanges between this sector and the surrounding structures (walls, windows, etc.) which may have different surface temperatures. Thus, the exact simulation of q_r requires the computation of view factors (which describe the influence of geometry on the radiative heat exchange) between the surface sectors of the body and each surface segment of the surrounding. Unfortunately, calculation of the view factors between the curved surfaces of the body and surrounding structures is very computer intensive. Hence, the concept of average temperatures for the surrounding structures was adopted. In the model either $T_{sr,m}$ - the mean temperature of the surrounding surfaces - or mean radiant temperature (*MRT*) can be used. Each of these will differ from one body sector to another and they may vary with time. The value of $T_{sr,m}$ is defined as the temperature of a fictitious uniform envelope 'seen' by a sector which causes the same radiative heat exchange with the sector as the actual asymmetric enclosure. *MRT* is defined similarly but it refers to a fictitious uniform *black* envelope. Employing $T_{sr,m}$, and rearranging the Stefan-Bolzmann law by introducing the (local) radiative heat exchange coefficient h_r [$W m^{-2} K^{-1}$], the energy exchange is calculated by:

$$q_r = h_r \cdot (T_{sf} - T_{sr,m}) \tag{3.20}$$

where

$$h_r = \sigma \, \varepsilon_{sf} \, \varepsilon_{sr} \, \Psi_{sf\text{-}sr} \left(T_{sf}^{*2} + T_{sr,m}^{*2}\right) \left(T_{sf}^{*} + T_{sr,m}^{*}\right) \tag{3.21}$$

and σ=5.67·10^{-8} $W m^{-2} K^{-4}$ is the Stefan-Bolzmann constant, ε_{sf} and $\varepsilon_{sr,m}$ are the emission coefficients of the body surface sector considered and of the surrounding, respectively, $\Psi_{sf\text{-}sr}$ is the corresponding view factor, T_{sf}^{*} and $T_{sr,m}^{*}$ are the absolute temperatures [K] of the body surface sector and of the surrounding surfaces 'seen' by

the body sector.

The longwave emissivity of the body segments ε_{sf} depends on the covering material. The values for skin and hair in ***Tab.A.1*** were obtained from [6] and [69]. Clothing usually has a value close to 0.95 [45]. The emissivity of the surroundings which is an input variable into the model is typically ε_{sr}= 0.93 in indoor spaces. Note, that if *MRT* is used in place of $T_{sr,m}$, ε_{sr} has to be set to unity.

The concept of using mean surrounding temperatures $T_{sr,m}$ makes it possible to introduce the view factors $\psi_{sf\text{-}sr}$ between sectors and the surroundings 'seen' by them. The view factors $\psi_{sf\text{-}sr}$ of the cylindrical and spherical body elements (***Tab.A.1***) were calculated - for each sector separately - by a specially developed finite-element program [52]. They vary from 0.1 to unity depending on the degree to which individual skin sectors are 'hidden' by other body parts. View factors are given for postures with stretched limbs (reclining, standing activities) and for the seated position ($1.0 \leq act < 1.2$ met) which is characterized by a decreased body radiation-area. As a check on the reliability of the view factors the *effective radiant area ratio* of the (nude) body $f_{eff} = \int \Psi_{sf\text{-}sr}\, dA_{sk} / A_{Du}$ was computed. The resultant whole body values of f_{eff}=0.80 for the standing position and f_{eff}=0.74 for the seated position are somewhat higher than provided eg. by Fanger [45], but they are in excellent agreement with results of recent, more detailed investigations [92].

The mean surrounding temperatures are provided together with other environmental variables in a, so called, climate-input-file. For inhomogeneous environments, $T_{sr,m}$ should be given separately for the half of the room infront of the person (to be applied to the anterior sectors of the body elements) and the half behind the person (for posterior sectors). However, sometimes, it might be useful to determine $T_{sr,m}$ for additional directions. For example, $T_{sr,m}$ would be calculated separately for the upper part of the room when investigating the radiative effects of heating/cooling ceilings which may cause occupants to perceive local discomfort to the head and shoulders.

While the *MRT* of a halfroom can be measured directly, the corresponding $T_{sr,m}$ must

be calculated from measurements of individual surface temperatures. A simple approach to calculate $T_{sr,m}$ is to weight the surface temperatures $T_{sr,i}$ by the corresponding surface areas $A_{sr,i}$:

$$T_{sr,m} = \frac{\sum_{i=1}^{n} T_{sr,i} A_{sr,i}}{\sum_{i=1}^{n} A_{sr,i}} \tag{3.22}$$

A more detailed method is to consider the effect of the bodies location in the room using the view factors $\psi_{bd\text{-}sr,i}$:

$$T_{sr,m} = \sqrt[4]{\sum_{i=1}^{n} \Psi_{bd\text{-}sr,i} \cdot T_{sr,i}^{*4}} - 273.15 \tag{3.23}$$

The overall view factors $\Psi_{bd\text{-}sr,i}$ between the body and wall-segments have been measured experimentally by means of photographic projection techniques for both standing and sitting postures [45] and can either be taken from graphs or calculated using appropriate algorithms [25].

The irradiation of the body by high temperature sources (sun, fireplaces, etc.) was also considered in the formulation of the passive system. The short wave radiation intensity and its direction is a characteristic of the environment and is provided, together with other environmental variables in the climate-input-file. The amount of heat q_{sR} absorbed at a sector surface is taken into account in the heat balance of superficial body element sectors by the term:

$$q_{sR} = \alpha_{sf} \Psi_{sf\text{-}sr} s \tag{3.24}$$

where α_{sf} is the surface absorption coefficient and depends on the colour of the covering material, s is the radiant intensity, and $\Psi_{sf\text{-}sr}$ is the view factor between the sector and the surrounding envelope (see ***Tab.A.1***).

3.4.3 Clothing Insulation

Because clothing plays an important role in the behavioural thermoregulation of human beings efforts were made to model garments in some detail. Unfortunately, standard literature provides only *overall* clothing parameters, ie. the intrinsic clothing insulation I_{cl}, the clothing area factor f_{cl} and the moisture permeability index i_{cl} (for exact definitions see eg. [121]). These do not reflect the real insulating properties of the garments but provide characteristics of a uniform (imaginary) clothing layer covering the entire body. Therefore, a simple computer model was developed which uses the present passive system and re-simulates the experimental procedures for measuring the overall insulation characteristics of garments undertaken by McCullough et al. [121] [122]. The program computes the required real insulation values I^*_{cl}, f^*_{cl}, and i^*_{cl} of trousers, shirts, underwear, socks, etc. from measured uniform-layer data I_{cl}, f_{cl}, i_{cl} for these garments and the evaporative resistance of the fabric R_{Ef}. These local values include the insulation effect provided by any layer of air trapped between the skin and the fabric. A database on clothing parameters was created which is used to compose clothing ensembles in the present multisegmental model.

The local sensible effective heat transfer coefficient U_{cl}^* [W m^{-2}K^{-1}] of an i-layered clothing ensemble worn on a body element sector is computed in the model as:

$$U_{cl}^* = \frac{1}{\sum_{i=1}^{m} (I_{cl}^*)_i + \frac{1}{f_{cl}^* (h_{c,mix} + h_r)}} \qquad (3.25)$$

where $I_{cl,i}^*$ [W m^{-2}K^{-1}] is the 'local' heat resistance of i-th clothing layer, f_{cl}^* the 'local' clothing area factor of the outer clothing-layer, and $h_{c,mix}$ and h_r are the actual local coefficients for convection and radiation, respectively.

The corresponding evaporative coefficient $U_{E,cl}^*$ [W m^{-2}Pa^{-1}] is obtained using the

local values i^*_{cl}, $I_{cl}{}^*$ of individual clothing layers applied to the body sector, $f_{cl}{}^*$ of the outer clothing layer, the local convection coefficient $h_{c,mix}$, and the *Lewis* constant L_a for air (see eg. [125]):

$$U^*_{E,cl} = \frac{L_a}{\sum_{j=1}^{m}\left(\frac{I^*_{cl}}{i^*_{cl}}\right)_j + \frac{1}{f^*_{cl}\cdot h_{c,mix}}} \tag{3.26}$$

As a check on the validity of the new clothing model, the overall insulation I_{cl} of clothing ensembles and of individual garments was computed using a similar procedure to that which was employed for obtaining the overall convection coefficient $h_{c,m}$. However, $\int q_c dA_{sk}$, A_{Du} and T_a in eq. (3.18) were replaced by the integral of the local heat fluxes through the clothing $\int q_{cl}\, dA_{cl}$, the overall surface area A_{cl} of the clothed body, and the corresponding mean surface temperature $T_{cl,m}$, respectively. The comparisons with results of experiments on clothed subjects (see also chaps. 4 and 5) showed good agreement with published data. For instance, simulating the thermal comfort experiment of Olesen et al. [150], in which the subjects wore the so called 'KSU-uniform', I_{cl}=0.6clo, i_{cl}=0.34, the overall insulation was predicted to be I_{cl}=0.59 clo and i_{cl}=0.34.

3.4.4 Evaporation

The present skin evaporation model ensures heat and mass transfer balances at each skin sector of each body element. The latent energy transport from a skin sector of area A_{sk} is given by:

$$U^*_{E,cl}\,(p_{sk}-p_a) = \lambda_{H_2O}\frac{dm_{sw}}{A_{sk}\,dt} + \frac{p_{osk,sat}-p_{sk}}{R_{E,sk}} \tag{3.27}$$

The left-hand side of eq. (3.26) represents the net energy transfer as driven by the evaporative potential between skin and air where p_{sk} is the water vapour pressure *at* the skin surface, p_a is the vapour pressure of the ambient air, and $U^*_{E,cl}$ is the resultant evaporation coefficient of garments covering the sector.

The first right-hand term of eq. (3.26) considers the evaporation of sweat from the skin surface, whereby λ_{H_2O}=2256 kJ kg^{-1} is the heat of vaporisation of water, and dm_{sw}/dt is the rate of sweat production over A_{sk} as elicited by the active system (chap. 4).

The last term of eq. (3.26) describes the heat transport by moisture diffusion through the skin where $p_{osk,sat}$ is the saturated vapour pressure *within* the outer skin layer of the body sector considered. In this superficial cutaneous layer, where sweat glands are located, moisture is always present. Hence, the vapour pressure at this location is set to its saturated value $p_{osk,sat}$ depending on tissue temperature of the outer skin, T_{osk} [125]:

$$p_{osk,sat} = 100 \times \exp\left[18.965 - \frac{4030}{T_{osk}+235}\right] \tag{3.28}$$

The model uses a skin moisture permeability equal to $1/R_{E,sk}$=0.003 Wm^{-2}Pa^{-1} which is also the published value [45]. Simulations using the present model showed that this value produces the model's basal skin wettedness of w_{sk}=0.06 which is a basic property of the human skin [6].

The net skin evaporation of a body sector arises from the actual vapour pressure p_{sk} [Pa] at the skin surface. This quantity is calculated using a rearranged eq. (3.26):

$$p_{sk} = \frac{\lambda_{H_2O}\frac{dm_{sw}}{A_{sk}\,dt} + \frac{p_{r,sat}-p_{sk}}{R_{E,sk}} + U^*_{E,cl}\,p_a}{U_{E,cl} + \frac{1}{R_{E,sk}}} \tag{3.29}$$

The present evaporation model accounts for the storage of sweat liquid at the skin surface as described by Jones [101]. Moisture is accumulated when p_{sk}, as computed by eq. (3.28), exceeds the saturated vapour pressure $p_{sk,sat}$ which is calculated from T_{sk} using an equation similar to eq. (3.27). The rate of moisture storage dm_{acc}/dt [kg s^{-1}] is then equivalent to the rate of moisture production dm_{sw}/dt minus the rate of moisture evaporation:

$$\frac{dm_{acc}}{dt} = \frac{dm_{sw}}{dt} - \frac{U^{*}_{E,cl}\,(p_{sk,sat}-p_a)}{\lambda_{H_2O}}\,A_{sk} \qquad (3.30)$$

According to the experimental results of Berglund [12], quoted by Jones [101], the maximum amount of sweat liquid on the skin is limited to about m_{acc}/A_{sk}=35 g m^{-2}. Quantities exceeding this threshold run off and are not considered in the model.

3.4.5 Respiratory Heat Losses

Most heat is lost through the body surface; however, heat exchange with the environment also occurs by respiration. The model for respiratory heat loss was obtained from the work of Fanger [45] taking into account the loss by evaporation and convection. The latent heat exchange is calculated from the pulmonary ventilation as a function of the whole body metabolism, $\int q_m dV$, latent heat of vaporisation of water, and the difference between humidity ratio of the expired and inspired air which depends on the ambient air temperature, T_a, and the partial vapour pressure of the ambient air, p_a:

$$E_{rsp} = 4.373 \cdot \int q_m dV \left(0.028 - 6.5\cdot10^{-5} T_a - 4.91\cdot10^{-6} p_a \right) \qquad (3.31)$$

Since the enthalpy of the expired air still depends to a certain degree upon the con-

dition of the inspired air, E_{rsp} appears as a function of T_a and p_a allowing E_{rsp} to be calculated for a wide range of ambient conditions.

The dry heat loss of respiration due to the temperature difference between expired and inspired air can be expressed as a function of the pulmonary ventilation rate, and the temperature and vapour pressure of the ambient air, T_a and p_a, respectively:

$$C_{rsp} = 1.948 \cdot 10^{-3} \cdot \int q_m dV \left(32.6 - 0.066 \cdot T_a - 1.96 \cdot 10^{-4} p_a \right) \qquad (3.32)$$

The total respiratory heat loss $E_{rsp} + C_{rsp}$ was distributed over body elements of the pulmonary tract: the lung, and the muscle layers of the face and of the neck. The distribution coefficients a_{rsp} were derived from the work of Scherer and Hanna [166]. This approach recognizes that inspired air is mainly conditioned in the nasal cavity where it reaches about 60% of its final enthalpy deep in the lung. By considering also the rewarming of the nasal region by expiration, the following distribution percentage was obtained: 25% in the outer face muscles, 20% in the inner face muscles, 25% in the muscle band of the neck, and 30% in the lung. These heat losses appear in the nodal heat balances for these tissues as the volume derivative in the heat generation term q_m in eq. (3.1):

$$q_m = q_{m,bas,0} + \Delta q_m - \frac{\partial \left[a_{rsp} (E_{rsp} + C_{rsp}) \right]}{\partial V} \qquad (3.33)$$

3.5 Numerical Methods

In the model, each sector of each tissue shell was divided into nodes. These were unequally spaced in the radial direction being closer together in the outer regions where temperature gradients are generally the steepest and where, therefore, the largest numerical errors could occur [71]. The number of nodes per tissue shell n can be chosen arbitrarily in the model, it is only limited by the capacity of the computer memory. The current nodal configuration is shown in ***Tab.A.1***.

The *finite-difference scheme* was used to discretize equation (3.1). The partial derivatives with radius were approximated by the *central* difference method which provides improved (ie. second order) accuracy, compared with the first order of the *forward* or *backward* difference methods (see eg. [170]). The partial derivative for the temporal change was approximated using a *hybrid* scheme, the *Crank-Nicolson* method, which also has a second order of accuracy. This method remains unconditionally stable, so the model can tolerate time-steps of variable length. This means the model can be more easily integrated with other dynamic simulation programs (eg. of the building or vehicle environment). The *Crank-Nicolson* method ($\Omega_{CN}\, T_r$) is constituted by averaging the *explicit* ($\Omega_{Ex} T_r$) and the *implicit* ($\Omega_{Im} T_r$) methods which have been defined for the current time-step *(t)* and the 'future' time-step *(t+1)*, respectively:

$$\Omega_{CN} T_r^{(t)} = \frac{1}{2}\left(\Omega_{Ex} T_r^{(t)} + \Omega_{Im} T_r^{(t+1)}\right) \tag{3.34}$$

When applied to the eq. (3.1) the explicit and the implicit numerical expressions for the node r of a cylinder yield:

$$\Omega_{Ex} T_r^{(t)}: \quad \rho_r c_r \frac{T_r^{(t+1)} - T_r^{(t)}}{\Delta t} = k_r \left(\frac{T_{r+1}^{(t)} + T_{r-1}^{(t)} - 2T_r^{(t)}}{\Delta r^2} + \frac{T_{r+1}^{(t)} - T_{r-1}^{(t)}}{2r\Delta r} \right) + q_{m,r}^{(t)} + \beta_r^{(t)} \left(T_{bla}^{(t)} - T_r^{(t)}\right)$$

$$\Omega_{Im} T_r^{(t+1)}: \quad \rho_r c_r \frac{T_r^{(t+1)} - T_r^{(t)}}{\Delta t} = k_r \left(\frac{T_{r+1}^{(t+1)} + T_{r-1}^{(t+1)} - 2T_r^{(t+1)}}{\Delta r^2} + \frac{T_{r+1}^{(t+1)} - T_{r-1}^{(t+1)}}{2r\Delta r} \right) + q_{m,r}^{(t+1)} + \beta_r^{(t+1)} \left(T_{bla}^{(t+1)} - T_r^{(t+1)}\right) \tag{3.35}$$

By applying eq. (3.33) and separating the 'future' temperature terms one obtains commonly:

$$(\gamma_r - 1)\, T_{r-1}^{(t+1)} + \left(\frac{\zeta_r}{\Delta t} + 2 + \delta_r \beta_r^{(t+1)}\right) T_r^{(t+1)} - (1+\gamma_r)\, T_{r+1}^{(t+1)} - \delta_r\, \beta_r^{(t+1)}\, T_{bla}^{(t+1)}$$

$$=$$

$$(1-\gamma_r)\, T_{r-1}^{(t)} + \left(\frac{\zeta_r}{\Delta t} - 2 - \delta_r \beta_r^{(t)}\right) T_r^{(t)} + (1+\gamma_r)\, T_{r+1}^{(t)} + \delta_r (q_{m,r}^{(t+1)} + q_{m,r}^{(t)}) + \delta_r \beta_r^{(t)}\, T_{bla}^{(t)} \tag{3.36}$$

where

$$\gamma_{r\,(cyl.)} = \frac{\Delta r}{2r} \qquad \gamma_{r\,(sph.)} = \frac{\Delta r}{r} \qquad \delta_r = \frac{\Delta r^2}{k_r} \qquad \zeta_r = 2\Delta r^2 \frac{\rho_r c_r}{k_r}$$

The time step Δt approximates the differential dt, and β_r represents a time-dependent factor for the nodal blood flow rate (see above).

This particular numerical formulation of the bioheat equation has universal applicability. It is valid for heat transfer both in cylindrical and spherical coordinates (with $\gamma_{r\,(sphere)} = 2\,\gamma_{r\,(cyl.)}$) and the steady-state expression (used for computing setpoint-temperatures in the model) arises by dropping the 'transient' coefficient $\zeta_r/\Delta t$ and removing all temperature terms on the current (right-hand)-side:

$$(\gamma_r - 1)\, T_{r-1} + (2 + \delta_r \beta_r)\, T_r - (\gamma_r + 1)\, T_{r+1} - \delta_r \beta_r T_{bla} = \delta_r q_{m,r} \tag{3.38}$$

The accuracy of the FD-method depends on the formulation of the boundary conditions. Usually, temperature nodes are located at interfaces and the corresponding heat fluxes are calculated assuming a plane geometry of the interfaces. This method, however, may cause errors in transient conditions [167]. To avoid this, the last node of a homogeneous tissue layer was attached to an additional imaginary node with the same thermophysical tissue properties. Similarly, an additional fictitious node was placed before the first node of the next homogeneous tissue layer. The boundary

condition was then satisfied by equating both the interface temperatures and the heat fluxes between pairs of regular and imaginary nodes of the neighbouring material layers [167] (see also appx. A.2.1). Hereby, the impact of the geometry on the heat dissipation in cylinders and spheres was modelled. In cylindrical coordinates the interface temperature T_{ifc} depends on the interface radius r_{ifc} and the temperatures of the adjacent (regular or fictitious) nodes T_- (corresponding to the radius $r_-= r_{ifc}-\Delta r/2$) and T_+ (corresponding to the radius $r_+= r_{ifc}+\Delta r/2$):

$$T_{ifc} = \frac{\ln\left(\frac{r_{ifc}}{r_{ifc}+\Delta r/2}\right)}{\ln\left(\frac{r_{ifc}-\Delta r/2}{r_{ifc}+\Delta r/2}\right)} T_- - \frac{\ln\left(\frac{r_{ifc}}{r_{ifc}-\Delta r/2}\right)}{\ln\left(\frac{r_{ifc}-\Delta r/2}{r_{ifc}+\Delta r/2}\right)} T_+ \tag{3.39}$$

The corresponding heat flux q_{ifc} can be written as:

$$q_{ifc} = \frac{k_r\,(T_- - T_+)}{\ln\left(\frac{r_{ifc}+\Delta r/2}{r_{ifc}-\Delta r/2}\right)} \tag{3.40}$$

Similarly, T_{ifc} and q_{ifc} in a spherical element (head) are given by:

$$T_{ifc} = \frac{r_{ifc}+\Delta r}{2\Delta r} T_+ - \frac{r_{ifc}-\Delta r}{2\Delta r} T_- + \frac{T_- - T_+}{\frac{r_{ifc}}{r-\Delta r} - \frac{r_{ifc}}{r+\Delta r}} \tag{3.41}$$

$$q_{ifc} = \frac{k_r\,(T_- - T_+)}{\frac{r_{ifc}^2}{r_{ifc}-\Delta r/2} - \frac{r_{ifc}^2}{r_{ifc}+\Delta r/2}} \tag{3.42}$$

The boundary condition in the core of each body element was formulated by establishing an isothermal 'core' element around the cylinder axis or the midpoint of the sphere (see also appx. A.2.2). As an example, ***Fig.3.1*** shows this domain for a leg (node-no.1). Since there is no temperature gradient with depth in these isothermal domains the *heat storage element method* had to be applied substituting the conduc-

tion term in eq. (3.1) by heat fluxes $q_{ifc,i}$ passing the interface between the core and the adjacent tissue sectors:

$$\rho_1 c_1 \frac{dT_1}{dt} = q_{m,1} + \beta_1 (T_{bla} - T_1) - \frac{\kappa}{\pi r_1} \sum_{i=1}^{sectors} \varphi_i \, q_{ifc,i} \qquad (3.43)$$

In eq. (3.42), the symbol φ_i is the angle of sector *i* (see ***Fig.3.1*** for φ_i of the anterior leg), and arises - together with the factor $\kappa/\pi r_1$ - from relating the interface area of the *i*-th sector to the core volume. The parameter κ depends on the geometry and is κ=1 for cylinders and κ=3/2 for spheres. The conductive heat fluxes $q_{ifc,i}$ are obtained by eqs. (3.39) and (3.41) for cylinders and spheres, respectively. The *Crank-Nicolson* scheme was also used to discretize eq. (3.42).

The conductive heat flux at the surface of a skin sector q_{sk}, ie. the heat flux calculated between the last skin node and the adjacent imaginary node (see also appx. A.2.3), was calculated from eqs. (3.39) and (3.41). It is balanced by the sum of the dry heat loss through the clothing, the evaporative heat loss from the skin:

$$q_{sk} = U^*_{cl} \, (T_{sk} - T_o) + U^*_{E,cl} \, (p_{sk} - p_a) \qquad (3.44)$$

where the operative environmental temperature T_o [°C] was formulated to integrate the influences of convection ($h_{c,mix} T_a$), the temperature radiation ($h_r T_{sr,m}$) and short wave radiation ($\psi_{sf\text{-}sr} \, \alpha_{sf} \, s$) absorbed by a body sector surface:

$$T_o = \frac{h_{c,mix} T_a + h_R T_{sr,m} - \psi_{sf\text{-}sr} \alpha_{sf} \, s}{h_{c,mix} + h_R} \qquad (3.45)$$

The sensible heat transfer coefficient, U^*_{cl}, incorporates three heat transport mechanisms: conduction through clothing, surface convection, and long wave radiation to surrounding surfaces. Because of the way eq. (3.24) for U^*_{cl} and eq. (3.25) for the evaporative coefficient ($U^*_{E,cl}$) are formulated, eq. (3.43) is valid even when no garments cover the skin. The resultant partial water vapour pressure acting on the skin,

ie. p_{sk} in eq. (3.43), is calculated by eq. (3.28).

To obtain the heat dissipation of the whole body, eq. (3.35) is applied to all the tissue nodes of the passive system, and is coupled by boundary conditions at the interfaces. The resulting set of linear equations is solved at each time of an exposure for the boundary conditions at the skin surfaces (eq. (3.43)) and the regulatory responses of the active system (see chap. 4).

The generated equation set contains both time-*in*dependent coefficients and time-dependent coefficients. The time independent constants γ_r, δ_r, ζ_r in eq. (3.35), which describe geometry and thermophysical material properties, have only to be computed once. These terms, taken from the left-hand side of eq. (3.35), are:

$$(\gamma_r - 1)T_{r-1}^{(t+1)} + \left(\frac{\zeta_r}{\Delta t} + 2\right)T_r^{(t+1)} - (1 + \gamma_r)T_{r+1}^{(t+1)} \qquad (3.46)$$

They were arranged to form the tri-diagonal conduction matrices which are a characteristic of the finite difference method. The pattern for the leg of the body (see ***Fig.3.1***) is shown in ***Fig.3.4***. The off-diagonal terms reflect the coupling role of the core element.

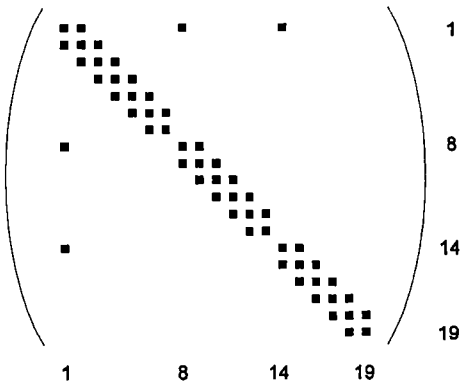

Fig.3.4

The pattern of the conduction coefficient matrix of the leg body element.

The two terms on the left-hand side of eq. (3.35), containing the coefficient $\beta_r^{(t+1)}$, formed *'blood matrices'* for each body element. Because the coefficients of a blood matrix change with time they had to be determined for each time-step and each step of any iteration procedure simulating the active system.

A direct solution for calculating the arterial blood temperatures was developed. This produces numerically exact results and is considerably quicker than popular (eg. [69]) but less accurate and computationally expensive *iteration*-techniques. The solution was obtained by substituting elements' T_{bla} in eq. (3.35) with the numerical equivalent of eq. (3.10) in which T_{blv} and the integrals had been replaced by eq. (3.11), and the corresponding sums, respectively:

$$T_{bla} = \frac{T_{blp} \sum_{r}^{nodes} \beta_r V_r}{h_x + \sum_{r}^{nodes} \beta_r V_r} + \frac{h_x \sum_{r}^{nodes} T_r \beta_r V_r \Big/ \sum_{r}^{nodes} \beta_r V_r}{h_x + \sum_{r}^{nodes} \beta_r V_r} \qquad (3.47)$$

The *blood coefficient matrix* of a body element is constituted by collecting the blood flow terms on the left hand sides of the model equations (3.35), but excluding the T_{blp}-term. Expression (3.47) shows a simplified blood coefficient matrix (the *(t+1)*-index was dropped) for a body element when it would consist of four-nodes :

$$\begin{pmatrix} \delta_1\beta_1 + B_x\beta_1^2 & B_x\beta_1\beta_2 & B_x\beta_1\beta_3 & B_x\beta_1\beta_4 \\ B_x\beta_2\beta_1 & \delta_2\beta_2 + B_x\beta_2^2 & B_x\beta_2\beta_3 & B_x\beta_2\beta_4 \\ B_x\beta_3\beta_1 & B_x\beta_3\beta_2 & \delta_3\beta_3 + B_x\beta_3^2 & B_x\beta_3\beta_4 \\ B_x\beta_4\beta_1 & B_x\beta_4\beta_2 & B_x\beta_4\beta_3 & \delta_4\beta_4 + B_x\beta_4^2 \end{pmatrix} \qquad (3.48)$$

where

$$B_X = \frac{-h_x \delta_r V_r \Big/ \sum_r^{noaes} \beta_r V_r}{h_x + \sum_r^{nodes} \beta_r V_r}$$

In central body elements where h_x is zero (see ***Tab.A.1***) the blood coefficient matrix of the 4-node element would reduce to :

$$\begin{pmatrix} \delta_1\beta_1 & 0 & 0 & 0 \\ 0 & \delta_2\beta_2 & 0 & 0 \\ 0 & 0 & \delta_3\beta_3 & 0 \\ 0 & 0 & 0 & \delta_4\beta_4 \end{pmatrix} \tag{3.50}$$

Because the central blood pool temperature T_{blp} appears (as a further unknown) in eq. (3.46) for all the nodal heat balances an extra equation was needed which balances the heat content of pool's inlet and outlet. The equilibrium blood pool temperature resulted in an expression similar to eq. (3.11), however, the product of elements' venous blood temperatures after *CCX*, $T_{blv,X}$, and the corresponding blood flow rates as well as the local perfusion rates w_{bl} were integrated over the whole body. In the final equation (3.50), T_{blp} is a function of *all* the nodal tissue temperatures and underlines the coupling effect of blood circulation in the heat dissipation of the passive system:

$$T_{blp} = \frac{\sum_n^{elem.} \left\{ \frac{\sum_r^{nodes} \beta_{n,r} V_{n,r}}{h_{x_n} + \sum_r^{nodes} \beta_{n,r} V_{n,r}} \times \sum_r^{nodes} \beta_{n,r} V_{n,r} T_{n,r} \right\}}{\sum_n^{elem.} \left\{ \left(\sum_r^{nodes} \beta_{n,r} V_{n,r} \right)^2 \Big/ \left(h_{x_n} + \sum_r^{nodes} \beta_{n,r} V_{n,r} \right) \right\}} \tag{3.51}$$

Eq. (3.50) completed the set of equations that formed the main matrix of the whole body. The coefficients of the main coefficient matrix, ***Fig.3.5***, were generated by adding the time-independent *conduction* submatrices and the corresponding time-dependent *blood* submatrices.

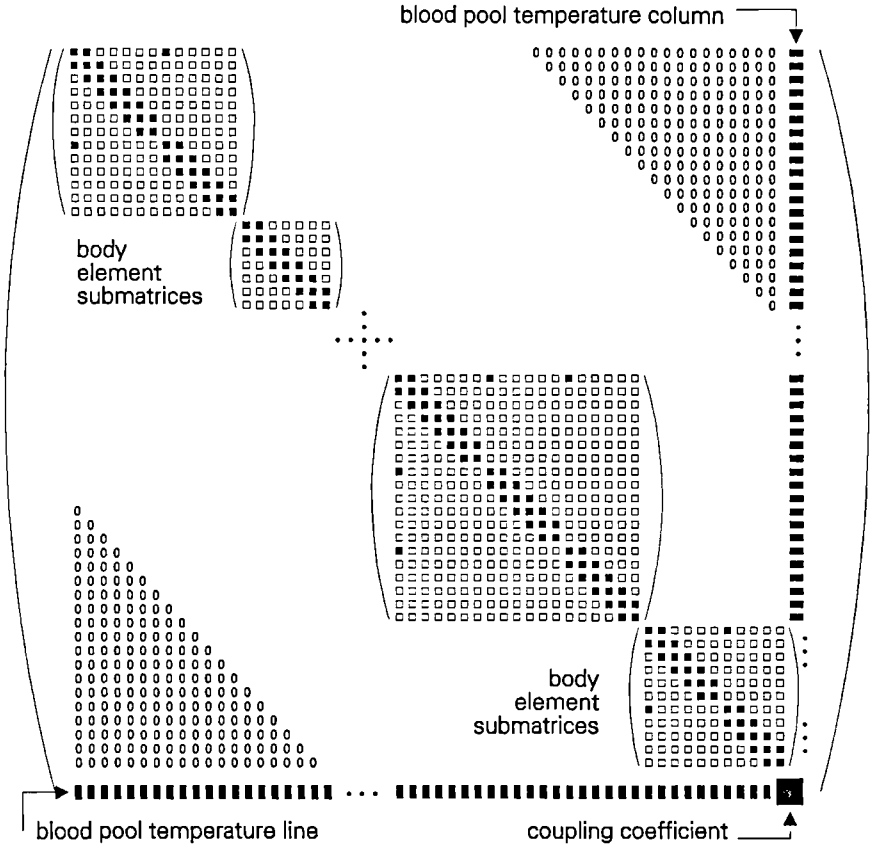

Fig.3.5

The structure of the final whole-body coefficient matrix.

The coefficients of the blood pool temperature line in ***Fig.3.5*** arise from eq. (3.50) and are:

$$Lc_{n,r} = \frac{\sum_{r}^{nodes} \beta_{n,r} V_{n,r}}{h_{x_n} + \sum_{r}^{nodes} \beta_{n,r} V_{n,r}} \times \beta_{n,r} V_{n,r} \qquad (3.52)$$

The coefficients of the blood pool temperature column $Cc_{n,r}$ were generated from eqs. (3.35) (with eq. (3.46)) and result in $Cc_{n,r} = - Lc_{n,r}\delta_{n,r} / V_{n,r}$.

The so called *coupling coefficient* which plays a role in the solution procedure was obtained from eq. (3.50):

$$CplC = \sum_{n}^{elem.} \left\{ \frac{\left(\sum_{r}^{nodes} \beta_{n,r} \right)^2}{h_{x_n} + \sum_{r}^{nodes} \beta_{n,r}} \right\} \tag{3.53}$$

A quick solver was developed for the matrix system which works very efficiently because only the non-zero cells are considered (see appx. A.3). The solver reduced the computer time by about 75% when compared with a traditional *Gaussian algorithm*, and the demand for computer memory was reduced by about 90%.

3.6 Verification and Validation

The passive system model was verified using available analytical solutions for homogeneous cylinders and spheres. The objects had the same geometrical and nodal configuration as the body elements of the passive system. Of most concern was the accuracy of the predicted temperatures, but the correct formulation of the boundary conditions was also examined. Tests were performed for a variety of thermal conditions in which the passive system was exposed to cold air. Because of producing steep temperature gradients in the tissues, these conditions reveal computational errors better than warm-air or hot-air exposures [70].

Analytical solutions for conduction in cylinders (appx. A.4.1) and spheres [54], as well as for conduction superimposed by internal heat generation [73] (appx. A.4.2), and a steady state solution for the bioheat equation in spheres (appx. A.4.3) were employed to verify the model in steady-state conditions. These tests indicated that the model predicts steady state tissue temperatures to an accuracy which is typically less than 0.02K mean error.

The performance of the model in transient conditions was of special interest. An analytical solution for transient heat conduction (without heat generation and fluid perfusion) in spheres derived by Gröber et al. [73] (see appx. A.4.5) was compared with the predictions of the model for the head-sphere made of brain tissue (for cylinders see appx. A.4.4). At t=0, the head, which had an initially homogeneous temperature of T_{init}=37°C, was exposed to ambient temperatures of T_a=0°C. Since there was no internal heat source, the head sphere continuously cooled down. Good agreement with Gröber's solution was obtained for all temperatures in the sphere as shown in ***Fig.3.6*** for three nodes (core, periphery, and a node inbetween). An error analysis of all nodal temperatures and times indicated a mean error of $|\Delta T|$ = 0.19 K with the largest deviations arising in the node next to the core, $|\Delta T|$=0.45K (core: $|\Delta T|$= 0.15K), and the smallest errors occurring at the periphery, $|\Delta T|$=0.04K. Simulations with a time step of 60s did not significantly increase the accuracy for the given nodal configuration (see ***Tab.A.1***). The numerical scheme employed provided reasonable accuracies for both polar and spherical coordinates (mean error of $|\Delta T|$

<0.5K) even for time steps (Δt) of 1hr.

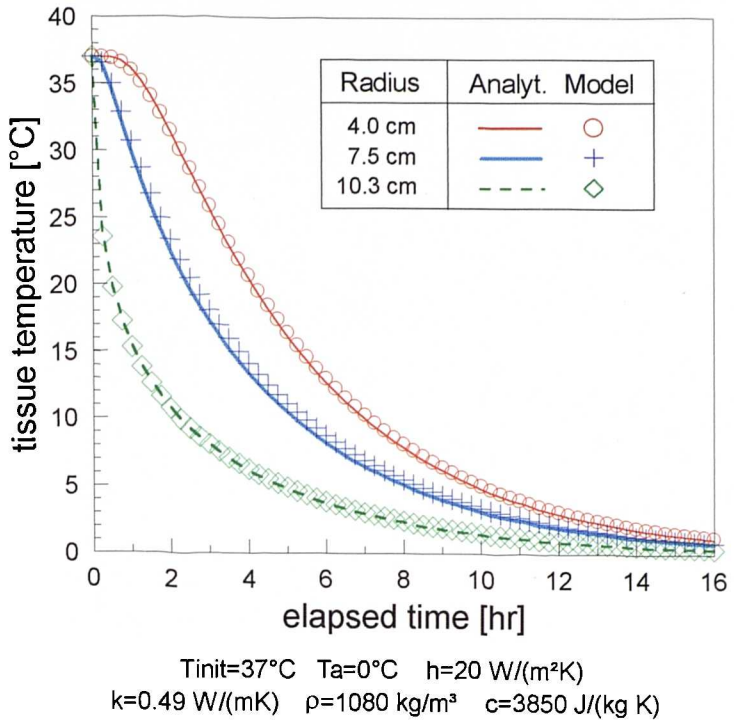

Fig.3.6

Comparison of predicted head-sphere temperatures with exact, analytically derived values for conductive cooling using a time-step of 5 minutes.

In another severe test of the model, the calculated temperature within a homogeneous cylinder of muscle tissue was compared with an analytical solution of the bioheat equation derived, according to Eberhart [43], by Mitchell et al. [134] (appx. A.4.6). The cylinder is initially in thermal equilibrium with the environment at $T_{init}=T_a$= 0°C. At t=0, the cylinder is suddenly supplied with a constant rate of blood flow (w_{bl} =0.001ml cm^{-3} s^{-1}, T_{bla}=37°C) and source of metabolic heat (q_m=600 W m^{-3}). The temperature of the cylinder therefore rises quickly before converging asymptotically to the final steady value. The predicted temperatures for three nodes in the cylinder, the core, the periphery and a node between them, are compared with the analytically derived values in ***Fig.3.7***. The mean error for all temperatures at Δt=5min was |ΔT| =0.04 ± 0.11K. The reverse error behaviour to the previous example was observed: larger deviations from the exact values occurred at the surface (|ΔT|=0.11K), and the lower mean errors occurred in the core (|ΔT|=0.04K).

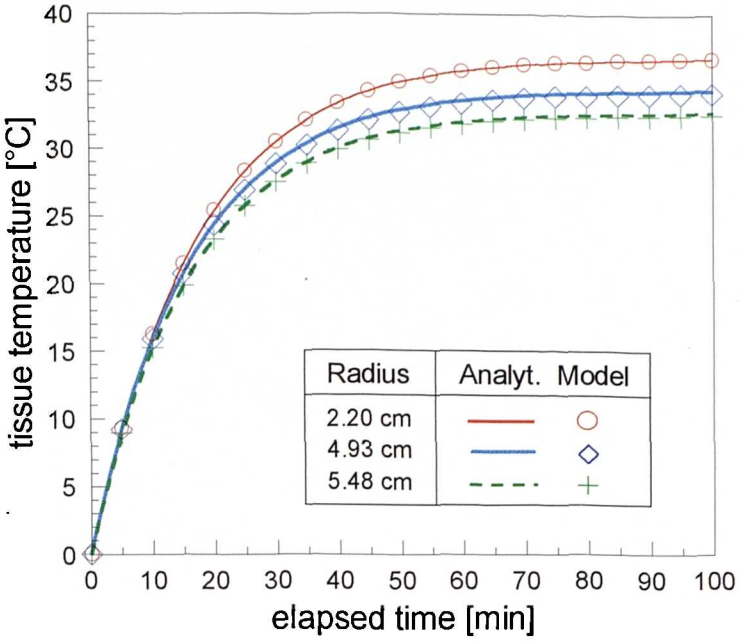

Fig.3.7

Comparison of predicted muscle tissue temperatures in a leg-cylinder with exact analytically derived values after the sudden supply of blood and metabolic heat. The prediction time step was 5 minutes.

The effect of time-step length was investigated using the previous test but with a higher blood perfusion rate (w_{bl}=0.005 ml cm^{-3}s^{-1}) to ensure an even more rapid heating of the cylinder (reaching ca. 95% of the steady state value after 10min). The simulation was undertaken with a time step of 10 min, and the predictions were compared with the exact solution (***Fig.3.8***). There was an initial 'overshoot' of the predicted temperature in the outermost cylinder node, but the temperature 'oscillations' were strongly damped and the predicted values quickly approached the analytical solution. This demonstrates the stability of the model even for disproportionally large time-steps.

Finally, the temperature distribution within -, and at the surface of - the whole passive system was calculated for conditions of *'thermal neutrality'* of T_a=30°C [11] (for a detailed specification see ***Tab.A.3***). The simulation of the non-regulated, reclining and unclothed human body provided a mean skin temperature of $T_{sk,m}$=34.4°C, and

a head core temperature (*hypothalamus*) of T_{hy}=37.0°C, values which agree with published data of $T_{sk,m}$=34.4°C [11] and tympanic temperature of T_{ty}=37.0°C [45] for reclining subjects exposed to thermoneutral conditions. Some further simulation results of this steady state exposure are listed in ***Tab.A.4***.

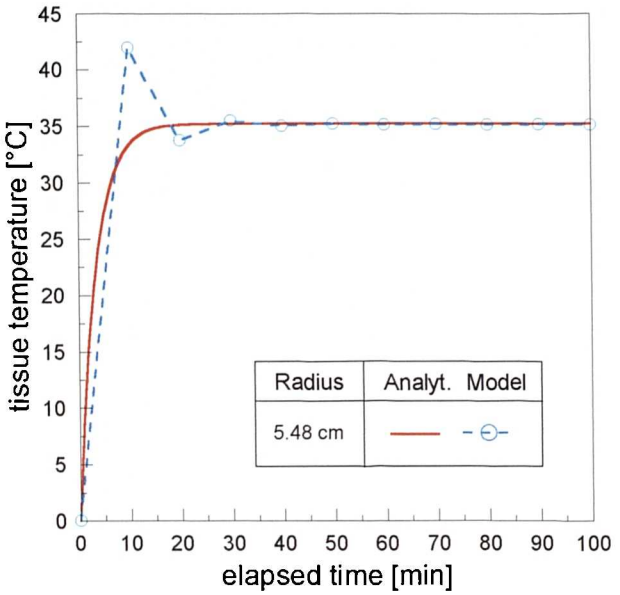

Fig.3.8

Comparison of predicted muscle tissue temperatures in a leg-cylinder with exact analytically derived values following the instantaneous introduction of a high blood flow and metabolic heat. The prediction time step was 10 minutes.

4 MODELLING THE ACTIVE SYSTEM

4.1 Introduction

Man maintains his internal temperature at a fairly constant value by four essential responses. Peripheral vasomotion, via suppression (*vasoconstriction*) and elevation (*vasodilatation*) of the skin blood flow, is activated to regulate internal temperature in moderate environments. These cardiovascular responses govern the transfer of heat from the body core to body surface (where it is lost to the environment). Skin blood flow is subject to considerable variability, varying from almost complete suppression (in extremities) to about an eleven-fold local increase of the basal value [164]. In cold conditions, vasoconstriction is accompanied by *shivering* thermogenesis in adult humans. A maximum of about a 5-fold elevation of the basal metabolic heat production [81] can be induced by the muscular tension while shivering. In hot conditions, vasodilatation is accompanied by the excretion of sweat which evaporates reaching an effective maximum cooling power over 7-times greater then the basal metabolism [6].

It is now well recognized that the human thermoregulatory system is a multiple input system which integrates thermal stimuli from different sites of the body allowing the organism to respond in a balanced way to concurrent signals. There is experimental evidence for various thermosensitive sites such as the skin, the brain stem, and other deep tissue receptors (see chap. 2).

One of the most well known cybernetic models of human thermoregulation (ie. the active system) was created by Stolwijk [177]. His feedback control system has been the source of motivation for various refinements and improvements [69] [198] [106] and for further development [201]. The basic principles of Stolwijk's active system were also adopted in the present model. The passive system suffers thermal disturbances at different body sites and these are represented as *error*-signals (see sec. 4.3.1). Positive error-signals, ie. positive disturbances from the thermoneutral state of the body, where no regulation occurs, represent warm receptors. Negative error-signals represent cold receptors. These local afferent signals are integrated in the 'regulatory centre' which transmits appropriate commands to the effector system. These commands are translated into the overall regulatory actions which are distribu-

ted over the body and may be weighted via autonomic local regulation (chap. 2).

Stolwijk and others [106] [132] based their models on temperature as the controlled physical variable. In contrast, Gordon [69] postulated a *calorimetrically* oriented active system to simulate the transient regulatory behaviour in severe cold (T_a=5°C). He used the heat flux through the skin as an important afferent signal. Unfortunately, because of the way that models of the active system have been formulated they have not provided evidence from which the responsibility of different afferent signals can be deduced. This is because modellers often employed postulative methods of selecting afferent signals into the regulatory centre. Nevertheless, temperature-based active systems receive more experimental support (see also chap. 2). There are very few effects (for a summary see [69]) which give reason to suppose that energy content or flux could play a role in human thermoreception and -regulation.

The two most popular models of human thermoregulation (ie. the models of Stolwijk [177] and Gagge [61]) have been subjected to analysis by different authors [79] [114] [40]. They tested models using independent physiological experiments and found typical inconsistencies in the predictions; these are outlined here.

Generally, the considered models were found to be more suitable for simulating thermal human behaviour in warm environments rather than in cold environments. Both models (which provided similar trends of prediction) tended to underestimate the actual skin evaporation and the body core temperature, and to overpredict skin temperature. The magnitude of the error was found to be associated with the exercise intensity [40]. For high activity levels the actual skin evaporation was less accurate. The empirical *linear* control equations for sweating and skin blood flow were supposed to be the source of error. In cold environments the models overpredicted skin temperature and underestimated (in parts considerably) core temperature [79] [114]. Also the temporal trends of predicted internal temperatures were incorrect (see ***Fig.4.16***).

The aim of the present study is to formulate a representative model of human thermal and thermoregulatory behaviour (of a *healthy, unacclimatized* subject) for a wide

range of environmental and internal conditions. Computer aided regression analysis has to be utilized to explore the role of individual afferent signals in regulatory reactions and to formulate a statistically founded active system model. The afferent signal analysis also allows signals to be investigated which are difficult, or impossible, to be measured experimentally.

Another aim of the model development is to obtain improved predictions of the body core temperature. In transient conditions, for instance, it shows a specific temporal behaviour which can significantly differ from temporal patterns of temperature found at the body's periphery. Internal temperature is one of the most important thermal characteristics of the human body. It represents an important criterion for health and safety limits and for tolerable exposure times [119]. Internal temperature is also an important quantity for obtaining thermal comfort [11].

Reliable prediction of body core temperatures presumes adequate modelling of the peripheral vasomotion. This is because there is a strong link between cutaneous vasomotor responses and internal temperature even in mild environments. For example, without vasoconstriction, the predicted body core temperature, T_{re}, of a seminude, reclining subject would reach 35°C after about 2 hours of exposure to a moderate environment of T_a=25°C (using the passive system model simulation described in chap. 3). In contrast, in a well regulated body the rectal temperature is maintained to within ±0.4K (simulation using the complete model) for the same set of conditions.

There are several problems with modelling vasomotor responses [164] but the main difficulty is associated with the lack of appropriate experimental data. Usually, experiments on human thermoregulation (including experiments involved in this study) did not provide any information on the total skin blood flow (*SBF*) - it is not directly measurable. Experiments in which regional (eg. forearm) blood flows were measured are rare, and, in any case, regional quantities give only a rough estimate of the *overall SBF* [88]. For these reasons, modellers have had to deal with simplifying assumptions and/or hypothetical treatments. Attempts to deal with vasomotor responses in terms of the average skin conductance as an index of the overall *SBF* [61] [177] have been seriously questioned [164] as a source of numerous errors. This is

because this approach is based on a simple, steady state calculation of heat flux from the body 'core' to the body 'shell'.

In the absence of appropriate experimental data on *SBF*, a new method has to be assessed which enables models of vasomotor responses to be developed. These models must reliably predict body core temperature for a wide range of different thermal circumstances.

4.2 Methods of Model Development

Numerous thermophysiological experiments have been conducted to study human thermal responses to various boundary conditions. The idea of this project was to use a computer simulation model as a tool for re-evaluating these physiological experiments. Thereby, each individual experiment can be seen as one stone in a mosaic. Each piece of knowledge is useful for creating a more coherent picture of the nature and principles of human thermoregulation. The challenge is to formulate a cybernetic model of thermoregulation which behaves like human beings with respect to a *wide range* of ambient conditions and *different types* of exposure.

Literature was surveyed for *appropriate* physiological experiments, ie. air exposures with both detailed information on boundary conditions and reports on the necessary physiological variables. *Air exposures* are the primary area of the model's intended application. The experiments were chosen to cover a wide range of environmental conditions as well as a variety of different exposure types. Included were severe cold [156] [188] [209], cool and cold [75] [187] [188] [196], neutral [117] [175] [188], warm [59] [165] [177] [175] and hot [59] [75] [106] [175] exposures. The exposures included: quasi-steady states; various types of transient changes in ambient parameters; as well as internal heat stresses due to working [165] [177]. Transients with respect to environmental parameters included sudden [75] [106] [175] [196] and gradual [59] [117] changes in ambient temperatures and changes in the water vapour content of the air [59]. All the experiments used to develop the active system model are listed in ***Tab.4.1***.

type of exposure	author of exp. reference	Images in text	controlled variables		n	use made
			physiol.	environ.		
steady T_a of 28°C	Wagner et al. [188]	*Fig.B.49*	T_{sk},T_{re},O_2,CO_2	T_G,v_a,rh	37	regr. for Cs
steady T_a of 28°C	Stolwijk et al. [175]	*Fig.4.21*	T_{sk},T_{re},T_{ty},O_2,W_L	T_a,T_w,rh	3	regr. for Cs
gradual decrease in T_a from 30 to 25°C	Mayer et al. [117]	*Fig.B.52*	T_{sk}	T_a,T_w,v_a	53	coeff. a_{cs}
step changes in T_a: 29-22-29°C	Hardy et al. [75]	*Fig.B.47*	T_{sk},T_{re},T_{ty},O_2,W_L	T_G, rh	3	regr. for Cs
steady T_a of 20°C	Wagner et al. [188]	*Fig.B.48*	T_{sk},T_{re},O_2,CO_2	T_G,v_a,rh	37	regr. for Cs, Sh
steady T_a of 20°C	Vogelaere et al. [187]	*Fig.B.53*	T_{sk},T_{re},O_2,CO_2	T_G,v_a,rh	6	regr. for Cs, Sh
step changes in T_a : 28-18-28°C	Hardy et al. [75]	*Fig.4.20*	T_{sk},T_{re},T_{ty},O_2,W_L	T_G, rh	3	regr. for Cs
steady T_a of 17.7°C	Hardy et al. [75]	*Fig.B.51*	T_{sk},T_{re},T_{ty},O_2,W_L	T_G, rh	3	regr. for Cs
steady T_a of 15°C	Wagner et al. [188]	*Fig.4.19*	T_{sk},T_{re},O_2,CO_2	T_G,v_a,rh	37	regr. for Cs, Sh
steady T_a of 13°C	Hardy et al. [75]	*Fig.4.18*	T_{sk},T_{re},T_{ty},O_2,W_L	T_G, rh	3	regr. for Cs, Sh
step change in T_a: 12-28°C	Werner et al. [196]	*Fig.B.46*	T_{sk},T_{oe},T_{ty},O_2,CO_2	T_a, rh	3	regr. for Sh
steady T_a of 10°C	Wagner et al. [188]	*Fig.B.50*	T_{sk},T_{re},O_2,CO_2	T_G,v_a,rh	37	regr. for Cs, Sh coeff. bcs
step change into T_a=5°C	Raven et al. [156]	*Fig.4.17*	T_{sk},T_{re},O_2,CO_2	T_G,v_a,rh	11	regr. for Cs, Sh coeff. a_{cs}, a_{sh}
step change into T_a=5°C	Young et al. [209]	*Fig.4.16*	T_{sk},T_{re},O_2,CO_2	T_G,rh	7	regr. for Cs, Sh
work & rest at T_a=10°C	Saltin et al. [165]	*Fig.B.62*	T_{sk},T_{re},T_{oe},O_2,W_L	T_G,rh	1	regr. for Dl, Sw
transient work at T_a=20°C	Stolwijk et al. [177]	*Fig.B.61*	T_{sk},T_{re},W_L,O_2	T_G,v_a,rh	3	regr. for Dl, Sw
work & rest at T_a=20°C	Saltin et al. [165]	*Fig.B.59*	T_{sk},T_{re},T_{oe},O_2,W_L	T_G,rh	1	regr. for Dl, Sw
transient work at T_a=30°C	Stolwijk et al. [177]	*Fig.4.26*	T_{sk},T_{re},W_L,O_2	T_G,v_a,rh	3	regr. for Dl, Sw
work & rest at T_a=30°C	Saltin et al. [165]	*Fig.B.60*	T_{sk},T_{re},T_{oe},O_2,W_L	T_G,rh	1	regr. for Sw
step changes in T_a: 28-33-28°C	Stolwijk et al. [175]	*Fig.4.22*	T_{sk},T_{re},T_{ty},O_2,W_L	T_a,T_w,rh	3	regr. for Dl, Sw
transient changes in rel. hum. at T_a=36°C	Gagge et al. [59]	*Fig.B.54*	T_{sk},T_{re},W_L	T_a,T_{dp},T_r	6	regr. for Dl, Sw
step changes in T_a: 29-37-29°C	Stolwijk et al. [175]	*Fig.B.58*	T_{sk},T_{re},T_{ty},O_2,W_L	T_a,T_w,rh	3	regr. for Dl, Sw
step changes in T_a: 18-42-18°C	Hardy et al. [75]	*Fig.4.23*	T_{sk},T_{re},T_{ty},O_2,W_L	T_G, rh	3	regr. for Dl, Sw
linear increase in T_a: 29 to 44°C	Gagge et al. [59]	*Fig.B.55*	T_{sk},T_{re},W_L	T_a,T_{dp},T_r	5	regr. for Dl, Sw
step change into T_a=43°C	Konz et al. [106]	*Fig.B.56*	T_{sk},T_{re},W_L	T_a,T_r,v_a,rh	1	regr. for Dl, Sw
step changes in T_a: 28-42.5 28°C	Stolwijk et al. [175]	*Fig.B.57*	T_{sk},T_{re},T_{ty},O_2,W_L	T_a,T_w,rh	3	regr. for Dl, Sw
step changes in T_a: 28-48-28°C	Stolwijk et al. [175]	*Fig.4.24*	T_{sk},T_{re},T_{ty},O_2,W_L	T_a,T_w,rh	3	regr. for Dl, Sw

Tab.4.1

Experiments used to develop the active system model. Temperatures [°C]: skin T_{sk}, rectal T_{re}, oesophageal T_{oe}, tympanic T_{ty}, air T_a, globe T_G, mean radiant T_R, mean wall T_W, dew point T_{dp}. Evaporative weight loss W_L [g min]. Variables of metabolic heat generation: oxygen consumption O_2 [l min^{-1}], carbon dioxide release CO_2 [l min^{-1}]. Relative air motion v_a [m s^{-1}], relative humidity rh [%]. Number of subjects n. Regulatory responses: vasoconstriction Cs [-], vasodilatation Dl [W K^{-1}], shivering Sh [W], sweat rate Sw [g min^{-1}].

Transient exposures were found to be very instructive for the afferent signals analysis. In quasi-steady states, where no pronounced changes of regulatory responses with time occur it is always possible to find sets of arbitrary signals which correlate well with them. In rapid transients, however, the time-varying behaviour of the variables can give conclusive evidence as to the partial responsibilities of individual afferent signals and hence to the selection of appropriate sets of signals.

The required information on the boundary conditions was a complete set of the prevailing environmental parameters, ie. air temperature, mean surrounding surface or mean radiant temperature(s), air velocity, any information on the water vapour content of the ambient air, and information on subjects' activity and the clothing worn.

The necessary physiological variables were some form of body core temperature measurement and information on measurements of the regulatory behaviour, ie. the overall latent heat loss of the body in the hot (including the sweating-response) or the whole body metabolism in the cold (including the shivering-response). The internal temperature, ie. the rectal or the oesophageal temperature, was employed to understand the vasomotor responses. Tympanic temperatures, which may deviate considerably from internal body temperatures especially in the cold [112], were not accepted for this purpose. Optionally, experiments with information on the local skin temperatures [117] [156] [188] were employed to estimate, or to verify, the validity of the coefficients distributing individual efferent outputs over the body.

The calibration procedure consisted of re-simulating each individual experiment by 'exposing' the passive system described in chap. 3 to the experimental boundary conditions for the duration of the experiment. The heat dissipation of the body, the heat transfer through clothing, and the environmental and respiratory heat exchange could be computed using the passive system. At this stage of development, however, in place of a running active system, the overall regulatory responses obtained from measurements (see further below) were used as input data into the system for each time instant of a simulation run. Thereby, the overall CNS-responses of shivering (*Sh*), vasoconstriction (*Cs*), vasodilatation (*Dl*), and sweating (*Sw*) were distributed over muscle tissues (*Sh*) and over the skin surface (*Cs, Dl, Sw*) by the

coefficients a_{sh}, a_{cs}, a_{dl}, and a_{sw}, respectively, listed in ***Tab.B.1***.

The simulations of the bodily thermal state provided sequences of afferent signals which were considered to influence individual regulatory responses. Each overall response was then subjected to linear regression analysis to study correlations of individual afferent signals and to establish quantitative relationships between responses and afferent signals.

The calibration procedure distinguished between regulatory responses, which were directly obtained from measured data, and responses which could not be inferred directly from experimental recordings. The overall shivering response *Sh* and the overall sweat liquid production *Sw* were filtered out from experimental data. Vasomotor responses *Cs* and *Dl* were obtained indirectly from measurements on the body core temperature using a procedure described below.

The amount of metabolism generated by shivering was obtained for each time of an exposure from the experimentally determined whole body metabolism[1)]. The shivering response *Sh* [W] resulted from eliminating the extra metabolism attributed to the activity level performed in the experiment and the basal heat production of the passive system:

$$Sh = M_{\exp} - \left[H + \sum_i q_{m,bas,i} V_i \right] \qquad (4.1)$$

where M_{exp} [W] is the actual measured overall metabolic rate of the subjects, H [W] is the overall work load arising from the *met*-value of subjects' activity in the experiment. The data on *met* was obtained from standard-literature [6] [5] [94]. The overall *basal* metabolism of the passive system which depends to a certain extent on body temperatures due to the Q_{10}-effect was calculated for each time of an exposure

1) usually obtained from measurements of the O_2-consumption of the test-persons

by summing nodal densities of the actual basal metabolic rates, $q_{m,bas,i}$ [W m^{-3}] (see chap. 3.3.2), over the body volume V.

The response of sweating was filtered out for each time of an exposure from the experimental information on subjects' overall latent heat loss L_{exp} [W][1]. The overall evaporative heat loss due to sweating, E_{sw} [W], results when correcting L_{exp} for respiration and moisture diffusion through the skin:

$$E_{sw} = L_{\exp} - (E_{rsp} + E_{diff}) \tag{4.2}$$

where E_{rsp} [W] represents the model's *latent* heat loss by respiration (see chap. 3.4.5), and E_{diff} is the model's overall heat loss due to water vapour diffusion through the skin. Herein, E_{diff} is a sum of local diffusion rates, ie. the model's insensible latent heat loss-rates from skin sectors as driven by gradients of vapour pressure found in the skin:

$$E_{diff} = \sum_{i} \frac{\Delta p_{sk,i} \cdot A_{sk,i}}{R_{E,sk}} \tag{4.3}$$

where $\Delta p_{sk,i}$ [Pa] is the difference between the vapour pressure found within the i-th outer skin sector and the vapour pressure found at the skin surface, and $A_{sk,i}$ [m^2] and $1/R_{E,sk}$ [W m^{-2} Pa^{-1}] are the corresponding surface area and moisture permeability, respectively (see also section 3.4.4).

In order to obtain the CNS-effector signal for sweating the local effect of skin temperature had to be eliminated from E_{sw}. Experimental investigations [23] [137] revealed the local sweat evaporation to be a function of both the local portion $a_{sw,i}$ of the central drive $SWEAT$ [W] and the local autonomic regulation as a function of the

[1] obtained from measurements on the loss of body-weight

disturbance of the local skin temperature, $T_{sk,i}$, from its setpoint, $T_{sk,i,0}$ [177]. The overall quantity E_{sw} is a sum of the local influences:

$$E_{sw} = \sum_i a_{sw,i}\ SWEAT \times 2^{\frac{T_{sk,i} - T_{sk,i,0}}{10}} \tag{4.4}$$

The required resulting overall *Sw*-response [g min^{-1}] was obtained by equating eqs. (4.2) and (4.4), and converting *SWEAT* from energy flow units [W] (heat loss) to mass rate units (moisture mass production) using the heat of vaporisation of water, λ_{H_2O} [J kg^{-1}], and an equivalency number of $6 \bullet 10^4$ [g kg^{-1} s min^{-1}]:

$$Sw = \frac{\left(L_{\exp} - E_{rsp} - E_{diff}\right) \times 6 \cdot 10^4}{\lambda_{H_2O} \sum_i a_{sw,i} \times 2^{\frac{T_{sk,i} - T_{sk,i,0}}{10}}} \tag{4.5}$$

In the model, the *Sw*-response was treated in terms of mass rate units to account also for situations where the whole amount of the sweat liquid production cannot evaporate[1)].

Cutaneous blood flow is highly dependent on CNS-regulation. The basal *SBF* at thermal neutrality is reduced or elevated via separate [164] mechanisms of peripheral constriction and dilatation. In addition to CNS-control the local skin temperature affects the local amount of skin blood flow (see also chap. 2). Stolwijk [177] considered all these aspects for the local skin blood perfusion rate SBF_i, by adding the local portion $a_{dl,i}$ of the central drive for vasodilatation, $DILAT$, to the corresponding basal value $SBF_{0,i}$, entering the constrictive tone $STRIC$, weighted locally by $a_{str,i}$, as a divisor, and recognizing that SBF_i can be about doubled by a 10K-increase in local skin temperature (Q_{10}-effect):

---

1) Note, that the amount of sweat liquid evaporated depends on the degree of water vapour content at the skin and in the ambient air, the air velocity, and the evaporative resistance of the clothing worn. The sweat moisture which cannot evaporate will be accumulated, to certain degree, on the skin or it will run off (for more detail on modelling eveporative heat losses see chap. 3.4.4).

$$SBF_i = \frac{SBF_{0,i} + a_{dl,i}\, DILAT}{1 + a_{str,i}\, STRIC} \times 2^{\frac{T_{sk,i} - T_{sk,i,0}}{10}} \qquad (4.6)$$

In general, the Stolwijk formula was found to be sufficient for the purposes of the present study. However, in the model, instead of treating peripheral vasomotion in terms of flow rates, vasomotor responses were dealt with directly in terms of the energy-equivalent β' [W K^{-1}] of SBF [m^3 s^{-1}] (see also chap. 3):

$$\beta' = \rho_{bl}\, c_{bl}\, SBF \qquad (4.7)$$

where ρ_{bl} [kg m^{-3}] and c_{bl} [J kg^{-1}K^{-1}] are the density and heat capacitance of blood, respectively. Furthermore, Stolwijk's formula seems to incline to inconsistencies in the prediction of body core temperature in conditions where $DILAT$ and $STRIC$ appear simultaneously. Another modification of eq. (4.6) concerned, therefore, efforts to avoid these inconsistencies by introducing a coupling term $e^{-DI/50}$. The formula of skin blood flow used in the model yields then:

$$\beta'_i = \frac{\beta'_{0,i} + a_{dl,i}\, Dl}{1 + a_{cs,i}\, Cs \times e^{-Dl/50}} \times 2^{\frac{T_{sk,i} - T_{sk,i,0}}{10}} \qquad (4.8)$$

where $\beta'_{0,i}$ arises from $SBF_{0,i}$ (***Tab.A.1***) according to eq. (4.7), $a_{dl,i}$ and $a_{cs,i}$ are distribution coefficients listed in ***Tab.B.1***, and $T_{sk,i}$ and $T_{sk,i,0}$ are the actual and the setpoint surface temperature of the i-th skin sector. DI [W K^{-1}] and Cs [ ] represent the vasomotor responses for which control equations had to be derived by afferent signal analysis.

Because of its specific properties an exponential function was used to couple the effects of Cs and DI when they appear simultaneously. Usually, either the product $Cs \cdot e^{-DI/50}$ vanishes (in warm and hot environments, because $Cs \rightarrow 0$) or the term $e^{-DI/50}$

approaches unity (in cool and cold environments, because DI is small or zero) and does not affect β'_i, eq. (4.8). However, $e^{-DI'50}$ operates in a balancing way in situations where constriction (due to cold stress at the skin) would eliminate the effect of dilatation (induced by internal hot stress) because of the form of the Stolwijk formula. The coefficient in the exponent of the coupling term was adjusted to achieve coherent predictions of core temperature with respect to different activity levels. For this purpose a series of simulations were performed, in which the activity level and ambient temperature were varied as parameters, and the continuity of predicted body core temperatures was analysed. A value of 50 was about the optimum for obtaining a consistent, stable behaviour of the model for exercise intensities of up to 10 met in different climatic conditions.

An iteration routine was temporally introduced into the model of the passive system, using which either DI or Cs was automatically adjusted for each time step of a simulation run until agreement between reported and predicted internal temperatures was achieved. Predicted temperatures of either the abdomen core, or of the thorax core, were considered when the rectal or the oesophageal temperature was measured. Body core temperature as a characteristic of the bodily thermal state was chosen as a criterion for adjusting DI and Cs because of its close dependence on *SBF* [1]. Skin temperature appeared to be a less adequate quantity for this purpose. Although there is an effect of *SBF*, skin temperature is primarily determined by ambient conditions even if internal conditions vary [58].

The procedure employed the classic *bisection* iteration scheme for examining roots of a function $f(x)$. Thereby, the root x_0 is bracketed by setting a lower and an upper limit of x which produce the opposite signs for $f(x)$ (to ensure that x_0 is located between $x_{low}<x_0<x_{upp}$). With each iteration step the limits of x fall closer together (by appropriate shifting of either the upper or the lower limit) until x_0 is confined by the required range of accuracy. For more detail see eg. [154].

SBF was varied by adjusting either Cs or DI which represented the independent variable x of the procedure. The iteration was interrupted when the *difference* between

the predicted and measured body core temperature - as the dependent variable, ie. $f(x)$ - became smaller than the standard deviation of the temperature measurements, ie. typically 0.1K.

Since eq. (4.8) accepts a co-existence of Dl and Cs it was necessary to separate their influences in the procedure. This separation was realized by carefully sequencing the use of the measured data. At first, the Cs response was determined by re-simulating cool and cold air exposure experiments during which obviously no vasodilatation occurred, so Dl could be set to zero in eq. (4.8). After the control equation for Cs was established, Dl was modelled by re-simulating experiments of warm, hot and intermediary exposures utilizing the passive system with a running control system for Cs. This concept enabled the impact of Cs to be accounted for when both Cs and Dl occurred in intermediary conditions, ie. conditions in which subjects respond by hot stress reactions caused by internal heat production while working despite cold stress at the skin.

During the simulations, the overall CNS-responses obtained from experiments were distributed over the body by the coefficients a_{sh}, a_{cs}, a_{dl}, and a_{sw} listed in ***Tab.B.1***. The distribution coefficients for responses in the warmth, ie. a_{dl} and a_{sw}, were obtained from Stolwijk [177]. However, no reliable information on the distribution of responses to cold was found in the literature. The coefficients for shivering a_{sh} and constriction a_{cs} were estimated by a laborious trial and error procedure in which the coefficients were adjusted to obtain agreement between predicted and measured local skin temperatures. The a_{cs}-coefficients for the body elements of the head, trunk, and extremities were obtained by simulations of: moderate environment exposure experiments undertaken by Mayer (in which local skin temperatures were measured on more than n=50 subjects) [117]; and cold and severe-cold air-exposure experiments by Wagner (n=37) [188] and Raven (n=11) [156]. The latter were also used to determine the a_{sh}-coefficents. To ensure reliable final results, the whole procedure of simulating the complete set of experiments and performing afferent signal regression analyses was repeated for any change in either distribution coefficient.

4.3 Afferent Signal Analysis

4.3.1 Introduction

The aim of this part was to investigate the responsibilities of afferent signals to the human thermoregulatory behaviour and to establish quantitative relationships for effector outputs. Each experiment was studied individually, and responses were correlated with different individual afferent signals as well as sets of them by means of linear regression analysis.

The analysis used the brain core temperature as the afferent signal from the body core (hypothalamus temperature) T_{hy} [°C] (see chap. 2). The mean skin temperature $T_{sk,m}$ [°C] was taken as the *integral* punitive signal from the bodies periphery, obtained from:

$$T_{sk,m} = \sum_{i}^{elem.} \left(a_{sk,i} \sum_{j}^{sect.} \frac{A_{sk,ij}}{A_{sk,i}} T_{sk,ij} \right) \tag{4.9}$$

where $a_{sk,i}$ (see appx. ***Tab.B.1***) is a coefficient for the skin sensitivity of the i-th body element. These coefficients were obtained by averaging the skin sensitivities of body elements to cold and warm stimuli as reported by [138] and [35]. $A_{sk,i}$ [m^2] and $A_{sk,ij}$ [m^2] are the skin surface areas of the i-th body element as a whole and as the j-th lateral sector of $A_{sk,i}$, respectively. $T_{sk,ij}$ represents the corresponding local skin temperature.

In experiments (see chap. 2), the rate of change of cutaneous temperature was discovered to be another physical variable which causes changes in the electrical activity of nerve fibres and which affects the dynamic thermoregulatory responses. Thus, the rate of change of the mean skin temperature $dT_{sk,m}/dt$ [$K\,h^{-1}$] was included in the study as a further initiator of punitive signals.

Theoretical investigations using the simulation model also permitted signals to be considered which are difficult to investigate experimentally. Suggestions have been

made [82] that afferent signals attributed to muscle tissues could play a role in generating warm stress responses for working subjects. The temperature of exercising muscle groups can exceed the actual body core temperatures by more than 4K [82] and might influence the effector outputs. The other theoretically possible, but not experimentally verified, afferent signals might arise from the temperature gradient in the cutaneous layer, ie. the skin heat flux. Gordon [69] argued that cutaneous temperature receptors are located at different depths of the skin, and therefore, the CNS could interpret these signals as heat fluxes. These signals were considered as the volume-weighted mean muscle temperature $T_{msc,m}$ [°C], and the mean skin heat flux Q_{sk} [W], respectively. In the study, Q_{sk} was defined in a similar way to $T_{sk,m}$ by using a modified eq. (4.9) in which the temperatures were substituted by the corresponding heat fluxes $q_{sk,ij}$ [W m^{-2}].

The present active system model operates with the so called *error signals* (according to the concept of Stolwijk [177]) as measures of the heat strain on the body. An error signal Δx is generated as the difference between the actual state of a variable x and its setpoint x_0 :

$$\Delta x = x - x_0 \tag{4.10}$$

The setpoint values of local skin and muscle temperatures, skin heat fluxes, and the hypothalamus temperature arise from the *thermoneutral* state of the (nude) body when reclining in an environment of 30°C (see also chap. 3.6 and ***Tab.A.3***). In these conditions no thermoregulation occurs [11].

Each individual thermoregulatory response was investigated using simple linear and multiple linear regression analysis [74]. The simple linear analysis indicated which single signals are primarily responsible for a regulatory reaction in a given situation. It also revealed signals which have no effect on thermoregulatory reactions. The results are described by example using one or - if necessary - two typical experiments for each response. The behaviour of the linear regression models $f(x)$ is discussed using diagrams where $f(x)$ are plotted over time and are compared with sequences of measured data (see also appx. B.2). This form of presentation makes it possible

to plot and compare several regression curves in one diagram over the duration of an experiment.

The simple linear regression analysis provided a basis for selecting appropriate sets of signals for multiple linear regressions. Adequate multiple regression equations of the 26 different exposures were then subjected to a further, supra-experimental analysis as described in section 4.4.

4.3.2 Shivering

Shivering *Sh* as a response of the *CNS* was studied using exposures to ambient temperatures of 20°C [187] [188], 15°C [188], 13°C [75], 12°C [196], 10°C [188], and 5°C [156] [209]. The regressions for the shivering response were performed taking into account the shift of the threshold for shivering $b_{sh,0}$ from the thermoneutral conditions toward cold conditions:

$$Sh = \sum_{i=1}^{n} b_{sh,i}\,\Delta x_i + b_{sh,0} \qquad (4.11)$$

where Δx_i is the i-th error signal of a multi-linear relationship (for a simple linear regression n=1), $b_{sh,i}$ and $b_{sh,0}$ are the corresponding regression coefficients to be determined.

In the experiment of Young [209] the test-subjects underwent a sudden change in ambient temperatures from 28°C to 5°C and remained reclining for 90 minutes in this severe cold environment[1)]. This example illustrates a typical dynamic shivering pattern - an initial 'overshoot' of the metabolic rate as a response toward the rapid fall in ambient temperatures, followed by a moderate increase in shivering with time.

Simple linear regressions suggest that the integral temperature error signal from the

---

1) more information on the boundary conditions and related thermal reactions of the subjects are shown in ***Fig.4.16*** further below

skin $\Delta T_{sk,m}$ is likely to have a significant (P<0.001) influence on Sh during the post-initial phase of the exposure, ie. after 40 minutes (***Fig.4.1***). Both the magnitude and the shape of the regression line fitted the measured values well for this period (r=0.99). On the other hand, it can be seen that the peak in Sh at t=10 minutes cannot be explained by this afferent signal. Rather, the rate of change of the mean skin temperature $dT_{sk,m}/dt$ or the product $dT_{sk,m}/dt\ \Delta T_{sk,m}$ can explain the nature of this event since the time of the peak of $dT_{sk,m}/dt$ is coincident with the occurrence of the metabolic overshoot.

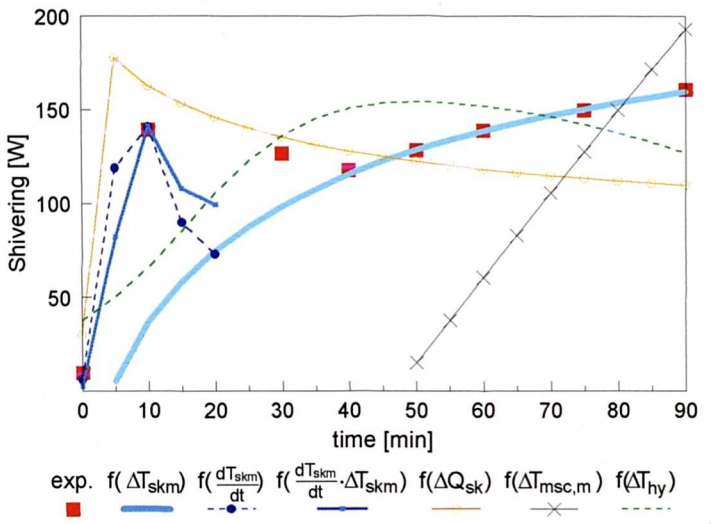

Fig.4.1

Curves of simple linear regressions to shivering during an exposure to T_a=5°C [209].

The error signal arising from the mean skin heat flux ΔQ_{sk} as another (theoretically) possible afferent signal did not provide sufficient explanation for the time of the occurrence of the peak shivering or for the change in metabolic rate after this peak. In contrast to $dT_{sk,m}/dt$ which - after reaching a peak - decreases with time, ΔQ_{sk} may level off at arbitrary values. Hence, ΔQ_{sk} appears to be inappropriate for describing the dynamic component of Sh in a multiple model.

The analysis also revealed that the mean muscle temperature error signal $\Delta T_{msc,m}$, as well as the hypothalamus temperature error signal ΔT_{hy}, as single afferent signals do not correlate with Sh.

Three regression curves were selected to demonstrate the results of the multi-linear regression analysis for the Young-experiment (***Fig.4.2***). The regression using temperature error signals from the skin and the hypothalamus confirmed the pronounced effect of the skin temperature in severe cold, and the result is very similar to the corresponding regression curve drawn in ***Fig.4.1***. The ΔT_{hy}-signal was found to play a subordinary role (affecting *Sh* at a significance level of P>0.1) in these conditions.

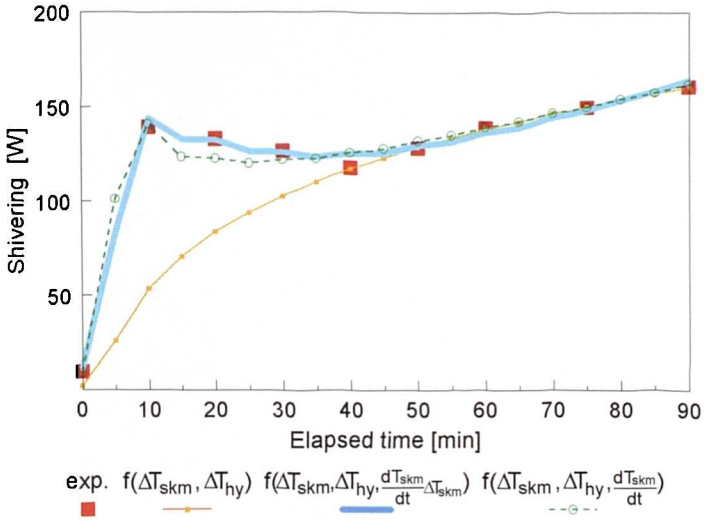

Fig.4.2

Curves of multi-linear regressions to shivering during an exposure to T_a 5°C [209].

Analysis of less severe cold air exposures where the effect of skin temperature is less dominant and where a decrease in the body core temperature in time was observed, indicated more clearly the sensitivity of *Sh* to ΔT_{hy}. Wagner et al. [188] exposed seminude, sedentary subjects to ambient temperatures of T_a=15°C (for detailed information see ***Fig.4.19***). The effect of ΔT_{hy} as an addition to the signal $\Delta T_{sk,m}$ is illustrated in ***Fig.4.3***

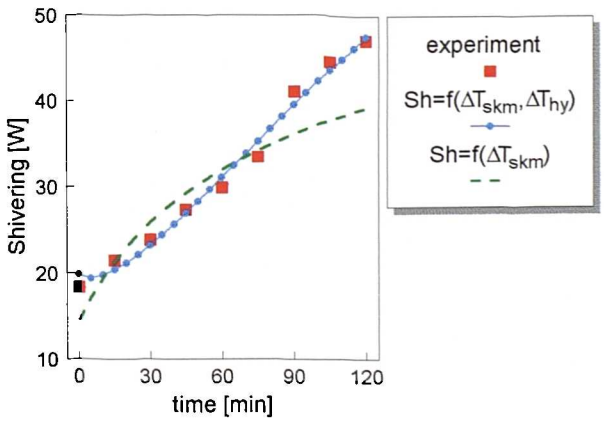

Fig.4.3

Temporal trends of linear regressions using $\Delta T_{sk,m}$, and $\Delta T_{sk.m}$ & $\Delta T_{sk,m}$, respectively, to shivering during an exposure to T_a 15°C [188].

(see also appx. B.2). The simple linear regression using $\Delta T_{sk,m}$ alone indicates a progressive decrease in the rate of change of metabolism. The opposite trend was observed in the experiment. The multiple regression analysis using $\Delta T_{sk,m}$ and ΔT_{hy} revealed the decrease in ΔT_{hy} to be responsible (P<0.001) for the experimentally observed trend.

As can be seen from ***Fig.4.2***, linear combinations of $\Delta T_{sk,m}$ and ΔT_{hy} with $dT_{sk,m}/dt$ and the product $\Delta T_{sk,m}\ dT_{sk,m}/dt$, respectively, provided good fits (R=0.96 and 0.99) to the measured data including the initial metabolic peak. The addition of further signals did not significantly improve the results of the regressions.

The use of other signals, in addition to $\Delta T_{sk,m}$ and ΔT_{hy}, produced less accurate predictions or - for modelling the Sh-response - inappropriate relationships. For instance, the regression equation combining $\Delta T_{sk,m}$ and ΔT_{hy} with $\Delta T_{msc,m}$ provided a *positive* regression coefficient for this variable. This indicates that $\Delta T_{msc,m}$ depends on Sh (ie. shivering warms muscles) but not vice versa.

4.3.3 Vasoconstriction

The vasoconstriction response Cs was analysed by re-simulating experiments of exposures to: quasi-neutral climates of 28°C [175] [188]; exposures to moderate ambient temperatures of 22°C [75], 20°C [187] [188], 18°C [75]; and to cold and severe cold ambient conditions of 17°C [75], 15°C [188], 10°C [188], and 5°C [156] [209].

In contrast to shivering (for which the onset is shifted toward cold using the constant $b_{sh,0}$ in the model) Cs remains active in moderate environments in which there are small disturbances from the state of thermal neutrality. Hence, the *absolute* regression coefficient for vasoconstriction, $b_{cs,0}$, was omitted in the regression equation:

$$CS = \sum_{i=1}^{n} b_{cs,i} \cdot \Delta x_i \qquad (4.12)$$

where Δx_i is the i-th error signal of a multi-linear relationship (for a simple linear regression n=1), and $b_{cs,i}$ is the corresponding coefficient to be determined by regression analysis.

The analysis of the Cs-response are discussed using an experiment by Hardy [75] who exposed seminude subjects to sudden changes in ambient temperatures of T_a = 28 - 18 - 28 °C (for more information see ***Fig.4.20***). As can be seen from ***Fig.4.4*** (for further examples see appx. B.2), the iteration scheme for estimating vasomotor responses described in section 4.2 predicted a trend for the Cs-response which correlated best with the $\Delta T_{sk,m}$-signal (r=-0.95). While a poor correlation (r=0.5) resulted for the ΔQ_{sk}-signal (also drawn in ***Fig.4.4***), Cs did not show a correlation with either ΔT_{hy} or with $\Delta T_{msc,m}$.

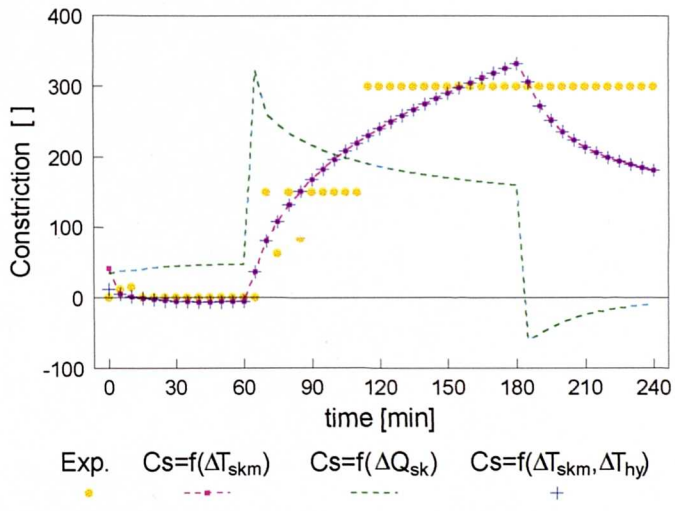

Fig.4.4

Curves of linear regressions to vasoconstriction during sudden changes in ambient temperature from T_a=28 to 18°C occurring at t 60 min, and from 18 to 28°C at t=180 min of the experiment [75].

The multiple regression (R=0.97) combining $\Delta T_{sk,m}$ and ΔT_{hy} error signals underlined the dominant effect of the skin temperature. At this point it might be interesting to note that the iteration method, which was based on adjusting body core temperatures, revealed a dependence of the vasoconstriction response on the skin temperature. So, two conclusions can be drawn from this observation. Firstly, that the actual dependence of the Cs-variable on the skin temperature was not concealed by the na-

ture of the iteration procedure, and secondly, from the physiological point of view, this result shows that the regulation of the body core temperature may be based on detecting the thermal state of bodies periphery.

The resolution of the *Cs*-response, did not allow for the proper multiple regression analysis of further afferent signals in addition to $\Delta T_{sk,m}$ and ΔT_{hy}. In particular, the role of the dT_{sk}/dt-signal (which was important for the shivering response, and which might also control vasoconstriction in some circumstances) could not be clearly defined using regression analysis. Furthermore, there were no effects which would justify the introduction of the $\Delta T_{msc,m}$-signal into the control equation of *Cs*.

4.3.4 Sweating

Linear regression analysis of measured and predicted data (see also appx. B.2) was used to investigate the sweating response: (i) during gradual changes between two levels of relative humidity of 40-80-40% at an ambient temperature of 35°C [59]; (ii) gradual changes of the operative temperature ET* (for definition see eg. [6]) from 28 to 43°C [59]; (iii) sudden temperature changes from cool to hot 18-42-18°C [75]; (iv) from neutral to warm 28-33-28°C; (v) from 29 to 37.5 and then 29°C [175], (vi) from neutral to hot 28-42.5-28°C [175]; (vii) from neutral to hot stress 28-48-28°C [175]; (viii) as well as an exposure to 43.3°C [106]. Sweating in intermediary conditions was studied using transient work at different levels of activity in ambient temperatures of 10°C, 20°C, and 30°C [165] [177].

Sweating was analysed using the following regression equation which allows *Sw* to respond to any change in bodily thermal state from neutral conditions (ie. $b_{sw,0} = 0$):

$$Sw = \sum_{i=1}^{n} b_{sw,i} \cdot \Delta x_i \qquad (4.13)$$

where Δx_i is the i-th error signal of a multi-linear relationship (for a simple linear reg-

ression n=1), and $b_{sw,i}$ is the corresponding regression coefficient to be determined.

The results of the linear regression analysis for a sudden exposure to ambients of 18-42-18°C [75] (for more information see ***Fig.4.23***) are shown in ***Fig.4.5***. As can be seen, sweating correlated best with skin temperature (ie. $\Delta T_{sk,m}$) as a single afferent signal (r=0.70) for these conditions. In particular, the final (quasi-static) sweating rate (~120-180 min.) was fitted well, whereas the transient phase of increasing Sw was slower in the experiment than the regression equation would predict. This might indicate a non-linear relationship between $\Delta T_{sk,m}$ and Sw.

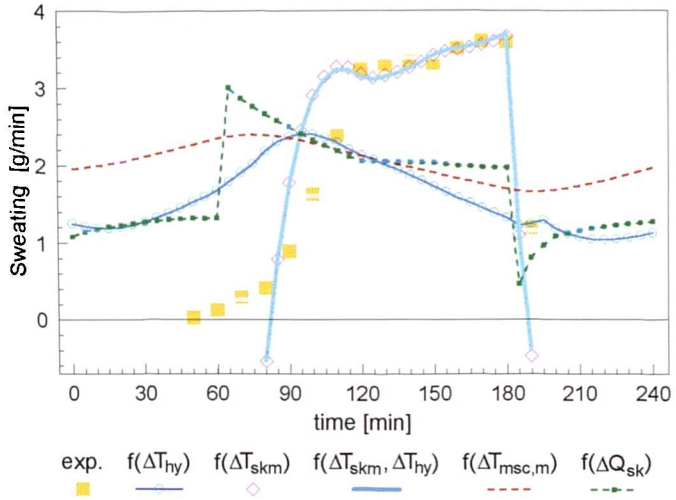

Fig.4.5

Curves of linear regressions to the sweating response during sudden changes in ambient temperature from T_a 18 to 42°C occurring at t 60 min, and from 42 to 18°C at t 180 min of the experiment [75].

The multiple-regression with the error signal from the hypothalamus ΔT_{hy} in addition to $\Delta T_{sk,m}$ did not notably improve the correlation (R=0.70). The imperceptible influence of body core temperature on Sw was a characteristic of all the hot-air exposures investigated.

Step changes into the hot environment revealed the unreliability of the skin heat flux as an input variable into the regulatory centre for sweating. The sudden increase in environmental temperatures produces a peak in the skin heat flux followed by a sub-

sequent fall in this variable. This pattern is quite different from the trend of the measured sweating response, see ***Fig.4.5***. The low value of the correlation coefficient, r=0.39, reflects the inappropriateness of this single afferent signal in modelling the Sw-response. Other afferent signals, ie. ΔT_{hy}, $\Delta T_{msc,m}$, also provided poor fits, and resulted in correlation coefficients of r=0.32 and r=0.14, respectively.

There is some reason to suppose that sweating may depend on temporal changes of the skin temperature $dT_{sk,m}/dt$, particularly when the rate is negative [137]. Some simulation results also indicated that this may be the case. However, there was no consistently close relationship between the measured and predicted sweat rates when using $dT_{sk,m}/dt$ and often (see 180-190 min. in ***Fig.4.5***) changes in $\Delta T_{sk,m}$ could sufficiently explain the transient suppression of sweating.

In cold environments sweating may occur while exercising due to 'internal' hot stresses. An example of the pattern of the sweat liquid production during a heavy work & recovery-sequence at ambient conditions of 10°C [165] is shown in ***Fig.4.6***. The subject worked at a high activity level for 30 min followed by a recovery period (for more information see ***Fig.4.25***).

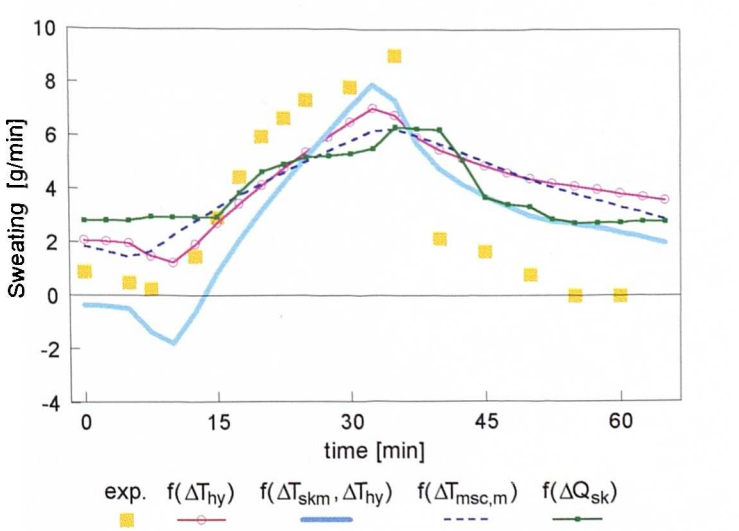

Fig.4.6

Curves of linear regressions to the sweating response during working at 9 met for 25 min in T_a=10°C [165]. The work period begins at t 10 min.

The simple-linear regression analysis revealed ΔT_{hy} to be the best single predictor of sweating for this type of exposure (r=0.74). The integral muscle temperature error signal, $\Delta T_{msc,m}$ (r=0.69) showed similar patterns to ΔT_{hy}. The integral heat flux signal through the skin, $\Delta q_{sk,m}$ also correlated well with this response (r=0.68) which contrasts with the regression results of hot-air exposures. This result may be misleading and simply be because $\Delta q_{sk,m}$ reflects the effect of sweat evaporating from the skin rather than $\Delta q_{sk,m}$ actually initiating the sweating. In contrast to hot-air exposures, sweating did not correlate well with $\Delta T_{sk,m}$ (r=-0.22) when taken as a single error signal.

Multi-linear regressions (see ***Tab.4.4***) with ΔT_{hy} and $\Delta T_{sk,m}$ as input variables into the regulatory centre, provided satisfactory correlations with respect to both environmental and internal heat stresses. The addition $\Delta T_{msc,m}$ as a further signal was generally found to be not significant (P>0.4) or did not provide plausible results, ie. negative regression coefficients for the $\Delta T_{msc,m}$-variable. Similar conclusions were drawn when the variable dT_{sk}/dt was used as an additional afferent signal to ΔT_{hy} and $\Delta T_{sk,m}$.

4.3.5 Vasodilatation

The overall vasodilatation response Dl was investigated using experiments designed to study sweating (see section 4.3.4).

Similarly to vasoconstriction, Cs, the Dl-response is active in moderate environments in which small disturbances from the state of thermal neutrality occur. Hence, the *absolute* regression coefficient for vasoconstriction, $b_{dl,0}$, was omitted in the regression equation:

$$Dl = \sum_{i=1}^{n} b_{dl,i} \cdot \Delta x_i \qquad (4.14)$$

where Δx_i is the i-th error signal of a multi-linear relationship (for a simple linear reg-

ression n=1), and $b_{dl,i}$ is the corresponding coefficient to be determined by regression analysis.

Typically, in exposures to warm and hot air, Dl correlated well with $\Delta T_{sk,m}$ as a single error signal. This is demonstrated in the analysis of exposures to step changes in ambient temperatures from T_a=28°C to 43°C and back [175] in ***Fig.4.7***, where r=0.76 (for more detail see ***Fig.B.57***). It can also be seen that dilatation was not simulated well by simple linear equations using the hypothalamus-temperature signal ΔT_{hy} or the skin heat flux signal $\Delta q_{sk,m}$. The regression equation using ΔT_{hy} as a single signal predicted a maximum value for Dl after terminating the hot air exposure when the subjects returned to a cool room. The regression equation using $\Delta q_{sk,m}$ as a single signal predicted a short-lasting peak in Dl while entering the hot environment with an immediate, sharp suppression in Dl toward zero. Both results conflict with observations based on experimental measurements.

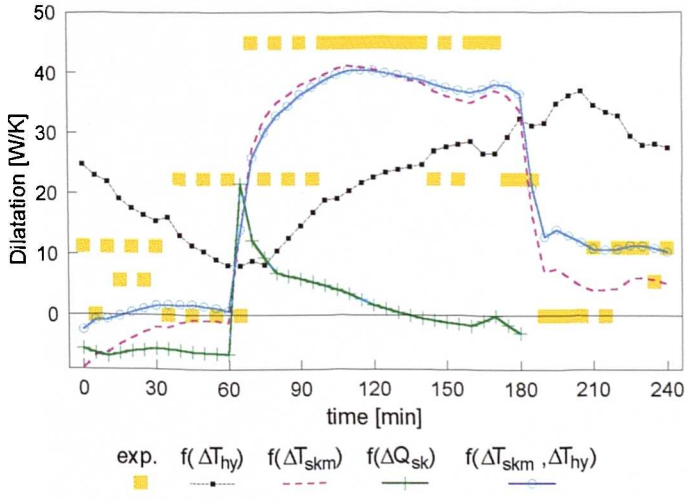

Fig.4.7

Curves of linear regressions from the vasodilatation response during sudden changes in ambient temperature from T_a 28 to 42.5°C occurring at t 60 min, and from 42.5 to 28°C at t 180 min of the experiment [175].

Multiple regression analysis utilizing $\Delta T_{sk,m}$ and ΔT_{hy} as independent variables underlined the dominant role of the skin temperature in hot air conditions. As for the sweating response, the minor changes in the body core temperature which occurred in hot ambients when subjects were not working, did not influence vasodilatation significantly (P>0.05). Furthermore, there were no characteristics of the vasomotor

behaviour in hot air which would justify the addition of the $dT_{sk,m}/dt$-signal, or other signals, in a multiple relationship for the peripheral dilatation Dl.

The Dl-response as evoked by internal heat stress in an environment of T_a=20°C [177] in which subjects performed transient work is shown in ***Fig.4.8*** (see also ***Fig.B.61***). Each exercise period was accompanied by increasing body core temperature, but - as apparent from ***Fig.4.8*** - Dl was significantly elevated only during the period of heavy work, ie. for t>150 min. The single regression analysis indicated that Dl correlated best with ΔT_{hy} as a single signal (r=0.78) or, alternatively, with the integral muscle temperature error signal, $\Delta T_{msc,m}$ (r=0.8) which showed similar patterns to ΔT_{hy}. In contrast, Dl did not correlate well with the $\Delta T_{sk,m}$-variable for this type of exposure (r=0.33). Moreover, the analysis provided a negative regression coefficient which is unrealistic since, obviously, rising dilatation is not induced by decreasing skin temperature. Similarly, the skin heat flux signal $\Delta q_{sk,m}$ was found to be an inappropriate afferent signal for Dl when evoked by internal heat stress (r=0.41). Moreover, a positive regression coefficient for this variable indicated that - from the physiological point of view - $\Delta q_{sk,m}$ does not represent an useful signal for modelling Dl.

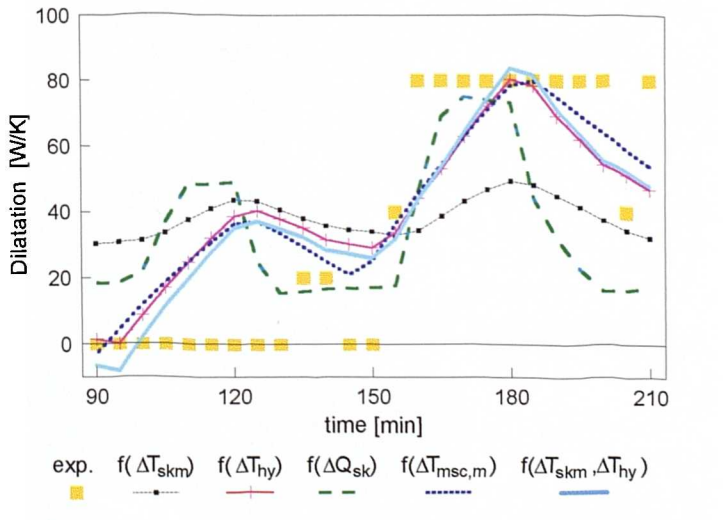

Fig.4.8

Curves of linear regressions to the sweating response during transient work in T_a 20°C [177]. The two exercise periods performed at act 5 met and act 8 met lasted for 30 min begining at t 90 min and t 150 min of the experiment, respectively.

Multi-linear regression with ΔT_{hy} and $\Delta T_{sk,m}$ as input variables (see also appx. B.2) indicated a dominant role for the ΔT_{hy}-signal ($P<10^{-5}$) and a insignificant effect from the $\Delta T_{sk,m}$-signal ($P>0.1$). The resolution of the DI-response, did not allow for the reliable multiple regression analysis of further afferent signals in addition to $\Delta T_{sk,m}$ and ΔT_{hy}. The addition of $\Delta T_{msc,m}$ provided no useful results, ie. negative regression coefficients. Also the role of the dT_{sk}/dt-signal could not be clearly defined using the multilinear regression analysis.

4.4 Supra-Experimental Analysis and Model Formulation

The afferent signal analysis indicated a temperature oriented thermoregulatory system for all the regulatory responses. A calorimetrically based active system, which uses skin heat fluxes as input variables into the regulatory centre, showed inconsistencies during the transient phase of responses to warmth as well as inappropriate regulatory actions in the cold. The skin temperature error signal $\Delta T_{sk,m}$ was shown to be an important input variable into the regulatory centre for responses against cold, ie. *Sh* and *Cs*. Furthermore, $\Delta T_{sk,m}$ was found to govern vasodilatation and sweating in warm environments where no significant changes in the body core temperature occur. The *Sw*- and the *Dl*-response, however, were usually best described using the temperature error signal from the head core, ΔT_{hy}, during conditions of internal hot stress.

Simulation of human thermoregulatory behaviour in complex thermal situations indicated that regulatory actions arise from multiple relationships of afferent signals from different body sites. Thereby, the combination of temperature-error signals from the periphery and from the core of the body, ie. $\Delta T_{sk,m}$ and ΔT_{hy} turned out to describe human thermoregulatory behaviour adequately for the whole range of boundary conditions and regulatory reactions studied. Regression analysis did not indicate the necessity of considering further temperature-error signals, such as the mean muscle temperature, $\Delta T_{msc,m}$, in addition to $T_{sk,m}$ and ΔT_{hy}. However, the afferent signal analysis revealed the rate of change of the mean skin temperature, $dT_{sk,m}/dt$, to be a further signal which influences the (dynamic) regulatory behaviour during rapid transients in addition to the 'static' signals $\Delta T_{sk,m}$ and ΔT_{hy}. The evidence of the dynamic effect of $dT_{sk,m}/dt$ was provided for the *Sh*-response. Using the linear regression analysis, however, no consistently close, clear effect of $dT_{sk,m}/dt$ could be defined for the *Sw*-, *Cs*-, or *Dl*-response.

In this section, the results of the multi-linear regression analyses using $\Delta T_{sk,m}$ and ΔT_{hy} (as obtained in individual experiments, see appx. B.2) are subjected to a supra-experimental analysis. The afferent signal analysis indicated that a set of linear

control equations can satisfactorily describe regulatory responses for a given experimental protocol. The equation coefficients, however, varied from one experiment to another. Therefore, the behaviour of the following multi-linear regression equations obtained for each individual experiment was examined over the whole range of ambient and internal conditions studied:

$$Sh = b_{sh,sk}\,\Delta T_{sk,m} + b_{sh,hy}\,\Delta T_{hy} + b_{sh,0} \quad [W]$$

$$Cs = b_{cs,sk}\,\Delta T_{sk,m} + b_{cs,hy}\,\Delta T_{hy} \quad [-]$$

$$Dl = b_{dl,sk}\,\Delta T_{sk,m} + b_{dl,hy}\,\Delta T_{hy} \quad [W\,K^{-1}]$$

$$Sw = b_{sw,sk}\,\Delta T_{sk,m} + b_{sw,hy}\,\Delta T_{hy} \quad [g\,min^{-1}]$$

The regression coefficients $b_{sh,sk}$ [W K^{-1}], $b_{sh,hy}$ [W K^{-1}], $b_{sh,0}$ [W], $b_{cs,sk}$ [K^{-1}], $b_{cs,hy}$ [K^{-1}], $b_{dl,sk}$ [W K^{-2}], $b_{dl,hy}$ [W K^{-2}], $b_{sw,sk}$ [g min^{-1}K^{-1}], and $b_{sw,hy}$ [g min^{-1}K^{-1}] were examined for their dependence on the temperature error signals from the periphery, $\Delta T_{sk,m}$, and from the head core, ΔT_{hy}. For this purpose, the time-averaged values of $\Delta T_{sk,m,t}$ and $\Delta T_{hy,t}$ were used to characterize the strain level achieved in each experiment. For transient exposures, the period of averaging was usually the last 30-60 minutes of an exposure in which quasi-steady state conditions were approached and the level of the bodily thermal strain could be defined.

The nine coefficients were found to fluctuate widely from one experiment to another. However, as can be seen from ***Fig.4.9*** to ***Fig.4.15***, the fluctuations were often not erratic, but obeyed changes in the bodily thermal state, ie. in either $\Delta T_{sk,m,t}$ or $\Delta T_{hy,t}$. When coefficients were found to be dependent of an afferent signal, they behaved in a fashion which was common to all responses: the coefficients had a lower and an upper limit with a (more or less) steep transition phase in between, in which the coefficients rose or fell approximately linearly before approaching the limits asymptotically. Such behaviour can mathematically be described using the following combined exponential equation:

$$y = \frac{e^{x} - e^{-x}}{e^{x} + e^{-x}}. \tag{4.15}$$

This is the classic *hyperbolic tangent (tanh)* of x which runs from $-1<y<1$ and is mirror-symmetrical with respect to the coordinate origin.

The use of this function for fitting the trend of the coefficients presumed the following modification:

$$y = B_1 \tanh[f(x)] + B_0 \tag{4.16}$$

where B_1 moves the asymptotes, so that $|y|_{max} \neq 1$, and B_0 shifts the function vertically along the y-axis. The coefficients b_1 and b_0 of the linear function $f(x)=b_1 x+b_0$ which fitted the regression coefficients in the transition phase were obtained by performing regression analysis to the linearized eq. (4.16):

$$v = artanh\left\{\frac{y - B_0}{B_1}\right\} = b_1 x + b_0. \tag{4.17}$$

The x-variable stands for any afferent signal used in the analysis, eg. either $\Delta T_{sk,m,t}$ or $\Delta T_{hy,t}$. Because eq. (4.16) is linearised for purposes of regression analysis the standard deviations s_y of the individual data-points were transformed into $s_v = s_y/(1-y^2)$ (see eg. [74]).

4.4.1 Shivering

The regression coefficients for the shivering response $b_{sh,sk}$, $b_{sh,hy}$, and $b_{sh,0}$ are given in ***Tab.4.2***. These were derived by multiple linear regressions for each experimental data set using the approach described in section 4.3.2. The coefficients $b_{sh,sk}$ are plotted against the temperature error signals from the skin $\Delta T_{sk,m,t}$ in ***Fig.4.9***. Filled symbols (with bars showing the standard deviations $s_{sh,sk}$[1)]) represent coefficients obtained from the multiple regressions with $\Delta T_{sk,m}$ and ΔT_{hy}. Empty symbols indicate coefficients of simple linear regressions. These were plotted to illustrate the general similarity of the coefficients obtained from multiple regression with the coefficients of the simple regressions.

experiment	ref.	$\Delta T_{sk,m,t}$	$\Delta T_{hy,t}$	$b_{sh,sk} \pm sd$	$b_{sh,hy} \pm sd$	$b_{sh,0} \pm sd$	*R*	Image
		[K]	[K]	[W K^{-1}]	[W K^{-1}]	[W]		
steady T_a of 20°C	Wagner et al [188]	-5.01	-0.39	-0.65 ± 0.37	-14.7 ± 5.8	0.0 ± 2.4	0.65	***Fig.B.1***
steady T_a of 20°C	Vogelaere et al [187]	-4.04	0.03	-0.54 ± 0.44	-30.7 ± 3.1	3.4 ± 1.1	0.95	***Fig.B.2***
steady T_a of 15°C	Wagner et al [188]	-7.05	-0.39	-2.47 ± 0.58	-42.2 ± 2.9	9.9 ± 1.1	0.99	***Fig.B.3***
steady T_a of 13°C	Hardy et al [75]	-8.17	-0.76	-13.5 ± 3.0	-1.6 ± 5.1	-76.8 ± 6.3	0.92	***Fig.B.4***
step change in T_a: 12-28°C	Werner et al [196]	-7.08	-0.08	-12.7 ± 1.9	-6.1 ± 11.0	-42.8 ± 17	0.81	***Fig.B.5***
steady T_a of 10°C	Wagner et al [188]	-8.91	-0.30	-12.0 ± 3.1	-37.3 ±12.6	-47.9 ± 2.2	0.99	***Fig.B.6***
step change into T_a=5°C	Raven et al [156]	-10.06	0.25	-19.1 ± 0.8	-52.0 ± 58	-39.3 ± 4.9	0.99	***Fig.B.7***
step change into T_a=5°C	Young et al [209]	-10.88	0.41	-18.8 ± 0.5	-35.3 ± 11	-34.2 ± 0.4	1.00	***Fig.B.8***

Tab.4.2

*Results of multi-linear regression analyses for the **Sh** [W] response using $\Delta T_{sk,m}$ and ΔT_{hy} as afferent signals. The corresponding regression coefficients $b_{sh,sk}$ and $b_{sh,hy}$, and the absolute coefficient $b_{sh,0}$ are provided with standard deviations **sd**. **R** is the multi-linear correlation coefficient of the regressions. The time-weighted averages of afferent signals from the skin and the head core, $\Delta T_{sk,m,t}$ and $\Delta T_{hy,t}$, characterize the strain level achieved in each experiments. The results of the regressions are presented graphically in appendix **B.2**.*

1) The two coefficients closest zero had standard deviations which were too small to be drawn.

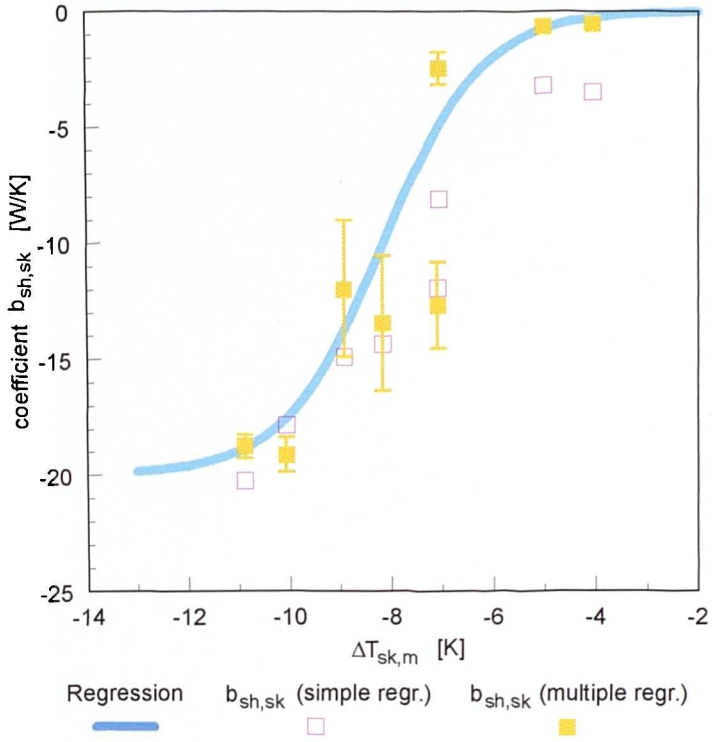

Fig.4.9

Dependency of the linear regression coefficients $b_{sh,sk}$ (± standard deviation), Tab.4.2, on the $\Delta T_{sk,m}$-signal.

It can be seen, that the $b_{sh,sk}$-coefficients show an evident decreasing trend with increasing cold stress at the skin. The lower limit of about $b_{sh,sk}$=-20 W K arose from experiments of 5°C as the most severe cold exposures studied where $\Delta T_{sk,m,l} \approx$-11K, ie. 11°C below the skin setpoint temperature, $T_{sk,m,0}$, of 34.4°C. Moderate exposures to ambient temperatures of T_a=20°C indicated an upper limit of $b_{sh,sk}$= 0 for $\Delta T_{sk,m} \rightarrow 0$. These limits correspond to coefficients of B_0=-10 and B_1=10 in eq. (4.16). The correlation analysis using eq. (4.17) for determining the function $f(x)$ provided regression coefficients of b_0=4.19 ±0.84 and b_1=0.51 ±0.11 with r=0.90. The following non-linear relationship can thus be written for the effect of $\Delta T_{sk,m}$ on Sh:

$$Sh = 10\left[\tanh\left(0.51\,\Delta T_{sk,m} + 4.19\right) - 1\right]\Delta T_{sk,m} \qquad (4.18)$$

No functional dependency on $\Delta T_{sk,m}$ or ΔT_{hy} was discovered either for the regression coefficients $b_{sh,hy}$ or for the absolute constants $b_{sh,0}$. The coefficients fluctuated errati-

cally over their mean values of $b_{sh,hy}$=-27.5±16.9 W K^{-1} and $b_{sh,0}$=-28.5±28.2 W K^{-1}.

The contribution of the $dT_{sk,m}/dt$-signal to the shivering 'overshoot' during rapidly decreasing skin temperature was studied by renewed simulations of the sudden cold exposure experiments [156] [209] using the passive system with the adopted *Sh*-controller based on $\Delta T_{sk,m}$ and ΔT_{hy} as afferent signals (ie. eq. (4.19) without the dynamic term). The temporal difference between the actual extra-metabolism obtained from experiments for each time and the corresponding predicted values were correlated with the product $\Delta T_{sk,m}\, dT_{sk,m}/dt$. As ***Fig.4.1*** and ***Fig.4.2*** demonstrated, $\Delta T_{sk,m}\, dT_{sk,m}/dt$ correlated better with the dynamic trend of *Sh* than the unweighted $dT_{sk,m}/dt$-signal which provided peaks of shorter duration. Also the isolated $dT_{sk,m}/dt$-signal appears inappropriate as it could elicit shivering at any pronounced temporal decrease in skin temperature even in warm environments. In contrast, the product $\Delta T_{sk,m}\, dT_{sk,m}/dt$ evokes shivering only when the actual level of skin temperature falls below its set-point, ie. for $\Delta T_{sk,m}$< 0. Hence, it seems that the actual skin temperature (causing a static discharge activity of cold cutaneous receptors), does modify the magnitude of the dynamic response of cold skin receptors. As a result of the correlation analysis, the coefficient was found to be $b_{sh,dyn}$=1.90±0.09 W h K^{-2} (r=0.89). With this dynamic term the control equation for shivering becomes:

$$\begin{aligned} Sh \;=\; & 10\left[\, tanh\left(0.51\,\Delta T_{sk,m} + 4.19\right) - 1\,\right]\Delta T_{sk,m} \;- \\ & - 27.5\,\Delta T_{hy} \;-\; 28.2 \;+\; 1.9\,\Delta T_{sk,m}\,\frac{dT_{sk,m}}{dt} \end{aligned} \qquad (4.19)$$

In practice, shivering will most often be elicited by punitive signals from the periphery of the body. In contrast (see further below), sweating is strongly affected by body core temperatures. Hence, in some extraordinary circumstances, this could result in a simultaneous occurrence of shivering and sweating which, however, is not observed in reality. In the model the *Sh*-effector is, therefore, switched off when sweating is predicted due to internal heat stresses. This precaution recognises the central object of thermoregulation, the appropriate maintenance of internal body temperatures.

Eq. (4.19) predicts an unlimited, linear increase in shivering for $\Delta T_{sk,m}$< -14K. In reality, however, there is an average upper limit for the regulatory increase in the bodily heat generation of some 300-380 W [77] [81]. Thus, the upper limit for Sh was set to Sh_{max}= **350** W in the model.

The overall response Sh, eq. (4.19), appears as an additional term in the heat generation equation of the i-th muscle node:

$$q_{m,i} = \Delta q_{m,bas,i} + q_{m,w,i} + q_{m,sh,i} \tag{4.20}$$

where: $q_{m,i}$ [W m^{-3}] is the actual nodal metabolism produced in i; $\Delta q_{m,bas,i}$ [W m^{-3}] the basal metabolism (including the Q_{10}-effect, see chap. 3), $q_{m,w,i}$ [W m^{-3}] is extra heat due to exercise; and $q_{m,sh,i}$ [W m^{-3}] is the nodal increase in metabolism by shivering. This is calculated by:

$$\Delta q_{m,sh,i} = a_{sh,j} \frac{Sh}{V_j} \tag{4.21}$$

where $a_{sh,j}$ is the shivering distribution coefficient of the j-th body element (***Tab.B.1***), and V_j [m^3] is the volume of the j-th body element.

The increased demand for oxygen while shivering is associated with increased blood circulation in muscles. Thereby, the change in blood flow $\Delta\beta'_i$ [W K] of the i-th muscle node is proportional to the change in metabolism [164] (see also chap. 3).

$$\Delta \beta'_i = 0.932\ q_{m,sh,i}\ V_i \tag{4.22}$$

4.4.2 Vasoconstriction

The results of multi-linear regressions employing the $\Delta T_{sk,m}$- and ΔT_{hy}-signal as described in section 4.3.3 are given for the constriction response *Cs* in ***Tab.4.3***.

experiment	ref.	$\Delta T_{sk,m,t}$ [K]	$\Delta T_{hy,t}$ [K]	$b_{cs,sk}$ ± *sd* [K^{-1}]	$b_{cs,hy}$ ± *sd* [K^{-1}]	*R*	Images
steady T_a of 28°C	Wagner et al [188]	-1.21	-0.25	-4.90 ± 2.21	-8.34 ± 10.6	0.38	***Fig.B.9***
steady T_a of 28°C	Stolwijk et al [175]	-0.47	0.27	-19.4 ± 5.0	-8.45 ± 8.83	0.46	***Fig.B.10***
step changes in T_a: 29-22-29°C	Hardy et al [75]	-2.67	0.10	-25.4 ± 2.3	11.0 ± 32.1	0.55	***Fig.B.11***
steady T_a of 20°C	Wagner et al [188]	-4.30	-0.22	-44.6 ± 7.0	-246 ± 120	0.70	***Fig.B.12***
steady T_a of 20°C	Vogelaere et al [187]	-4.14	-0.30	-25.8 ± 7.2	-192 ± 132	0.49	***Fig.B.13***
step changes in T_a: 28-18-28°C	Hardy et al [75]	-4.79	0.02	-58.1 ± 1.7	-77.5 ± 20.6	0.97	***Fig.B.14***
steady T_a of 17.7°C	Hardy et al [75]	-5.31	0.15	-64.7 ± 6.3	-90.3 ± 69.4	0.66	***Fig.B.15***
steady T_a of 15°C	Wagner et al [188]	-6.70	-0.48	-54.4 ± 6.0	-101 ± 119	0.64	***Fig.B.16***
steady T_a of 13°C	Hardy et al [75]	-8.06	-0.45	-69.3 ± 1.9	111 ± 42.2	0.69	***Fig.B.17***
steady T_a of 10°C	Wagner et al [188]	-8.88	-0.27	-62.2 ± 1.7	665 ± 73	0.92	***Fig.B.18***
step change into T_a=5°C	Raven et al [156]	-10.13	0.31	-67.2 ± 15.2	497 ± 413	0.91	***Fig.B.19***
step change into T_a=5°C	Young et al [209]	-9.68	0.29	-58.7 ± 33.4	392 ± 617	0.84	***Fig.B.20***

Tab.4.3

Results of multi-linear regression analyses for the ***Cs*** *response using $\Delta T_{sk,m}$ and ΔT_{hy} as afferent signals. The coresponding regression coefficients $b_{cs,sk}$ and $b_{cs,hy}$ are provided with standard deviations* ***sd****. **R** is the multi-linear correlation coefficient of the regressions. The time-weighted averages of afferent signals from the skin and the head core, $\Delta T_{sk,m,t}$ and $\Delta T_{hy,t}$, characterize the strain level achieved in each experiments. The results of the regressions are presented graphically in appendix **B.2**.*

It is apparent that the level of correlation is lower than was found for the *Sh*-response. This was because cutaneous blood streams (containing both *Cs*- and *Dl*-responses) are subject to considerable inter- and intra-individual variations to an extent not found in shivering. Furthermore - in contrast to *Sh* which is directly measured - *Cs* was obtained indirectly (from measurements on the body core temperature) and thus contains a source of uncertainty. The lowest correlation coefficients arose from exposures to moderate conditions. Obviously, in moderate conditions near the thermo-neutral point, where thermal punitive drives become small ($\Delta T_{sk,m} \rightarrow 0$), non-thermal and subjective variables gain increasing influence in the cutaneous blood flow.

In ***Fig.4.10***, the coefficients $b_{cs,sk}$ are plotted over the error signal from the skin $\Delta T_{sk\,m\,t} = T_{sk,m,t} - T_{sk,m,0}$. Filled symbols with (bars showing the corresponding standard deviations, $s_{bcs,sk}$) represent coefficients obtained from the multiple regressions with $\Delta T_{sk,m}$ and ΔT_{hy}. Empty symbols indicate coefficients from simple linear regressions.

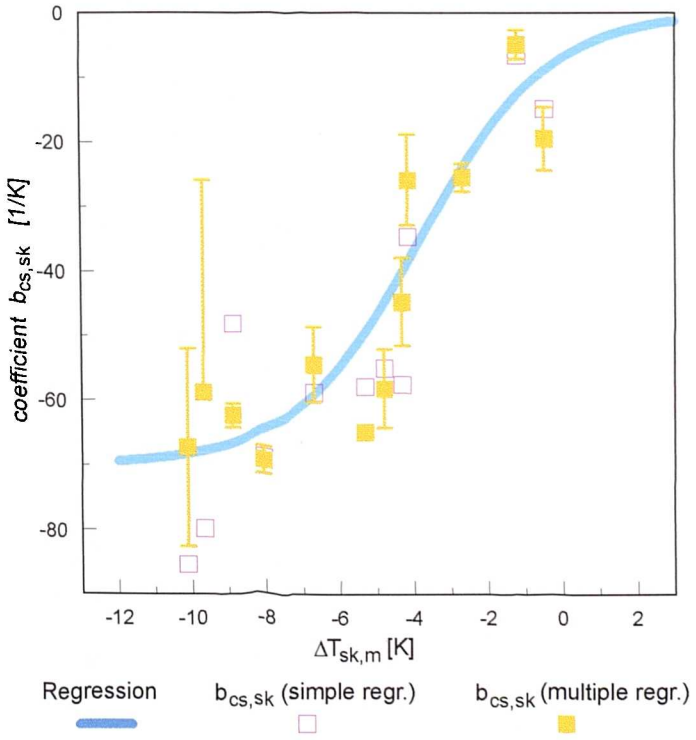

Fig.4.10

Dependency of the linear regression coefficients $b_{cs,sk}$ (± standard deviation), Tab.4.3, on the $\Delta T_{sk,m}$-signal.

The trend of the coefficients with changing $\Delta T_{sk,m}$ was fitted using eq. (4.16) with B_1= -B_0 = 35.0 K^{-1}. Regression analysis using eq. (4.17) showed a good correlation (r=0.87) for the linear function $f(x)$ of Cs providing coefficients b_0=1.11 ± 0.23 and b_1 = 0.29 ± 0.05. With these results the following relationship can be written for the effect of $\Delta T_{sk,m}$ on Cs:

$$Cs = 35\left[\tanh\left(0.29\,\Delta T_{sk,m} + 1.11\right) - 1\right]\Delta T_{sk,m} \qquad (4.23)$$

No functional relationship was discovered for the $b_{cs,hy}$-coefficient neither with respect to $\Delta T_{sk,m}$ nor ΔT_{hy}. The $b_{cs,hy}$ coefficients fluctuated widely over the average of $b_{cs,hy}$= -7.7 ±322.5 K^{-1} indicating a negligible effect for this variable on the response of Cs. Nevertheless, this signal was used in the model to account for some elevation of Cs by negative ΔT_{hy}-signals [1] (see also chap. 2).

A thorough analysis of experimental data revealed that a rise in the body core temperature occurs during sudden decreases in ambient temperature, eg. Hardy et al. [75], Raven et al. [156], Young [209] (see also ***Fig.4.28***). This is illustrated in ***Fig.4.11*** which shows the (relative) increase of the rectal temperature after entering a room with T_a=18°C from a neutral environment at T_a=28 °C [75]. A model which uses only the skin and head core temperatures as afferent signals for vasoconstriction (static Cs) did not reproduce this pattern. However, predictions reproduced the pattern of the body core temperature well when $dT_{sk,m}/dt$ (dynamic Cs) was introduced into the control equation for vasoconstriction.

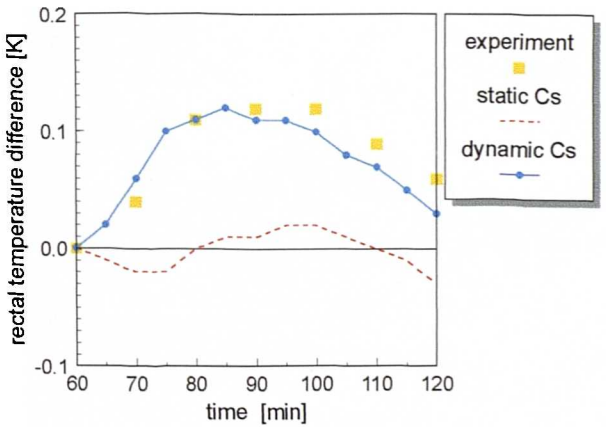

Fig.4.11

Temporal trend of rectal temperature after entering a cold space of T_a=18°C: (a) as measured [75] and (b) as predicted by the model using a control equation for constriction as either a multiple function of the $\Delta T_{sk,m}$- and ΔT_{hy}-signal, or as a function of the $\Delta T_{sk,m}$-, ΔT_{hy}-, and $dT_{sk,m}$ dt-signal.

The *Cs*-data obtained from the iteration procedure for adjusting *SBF* was not detailed enough to quantify the role of the $dT_{sk,m}/dt$-signal on the *Cs*-response by means of regression analysis. So, this effect had to be explored by a trial and error procedure. In this procedure, an additional term, similar to that used for the shivering response, was introduced into the control equation for *Cs*, consisting of the $dT_{sk,m}/dt$-signal weighted by $\Delta T_{sk,m}$ and a coefficient z_{dyn} to be adjusted. The procedure involved simulating transient exposures from neutral to ambient temperatures of 18°C, 22°C [75], and 5°C [209]. The measured and simulated rectal temperatures were compared 'by-eye' and a coefficient of z_{dyn}= 3.0 [h K^{-2}] obtained. With this dynamic extension, the final control equation for vasoconstriction was:

$$Cs = 35\left[\tanh\left(0.29\,\Delta T_{sk,m} + 1.11\right) - 1\right]\Delta T_{sk,m} - 7.7\,\Delta T_{hy} + 3.0\,\Delta T_{sk,m}\frac{dT_{sk,m}}{dt} \qquad (4.24)$$

Since no effect was observed for $dT_{sk,m}/dt > 0$ or for positive values of ΔT_{sk}, the dynamic term in eq. (4.24) was set to zero for either case in the model. The *Cs*-response appears in the equation of nodal skin blood flow β'_i [W K]:

$$\beta'_i = \frac{\beta'_{i,0} + a_{dl,i}\,Dl}{1 + a_{cs,i}\,Cs \times e^{-Dl/50}} \times 2^{\frac{T_{sk,i} - T_{sk,0,i}}{10}} \qquad (4.25)$$

In eq. (4.25), $\beta'_{0,i}$ [W K^{-1}] is the basal nodal skin blood flow, $a_{dl,i}$ and $a_{cs,i}$ are distribution coefficients of the *Dl*- and *Cs*-response (***Tab.B.1***), and $T_{sk,i}$ and $T_{sk,i,0}$ are the actual and the setpoint surface temperature of the *i*-th skin sector.

4.4.3 Sweating

The regression coefficients for the sweating response $b_{sw,sk}$ and $b_{sw,hy}$ obtained for each experimental data set, as described in section 4.3.4, are given in ***Tab.4.4***.

experiment	ref.	$\Delta T_{sk,m,t}$	$\Delta T_{hy,t}$	$b_{sw,sk} \pm sd$	$b_{sw,hy} \pm sd$	R	Images
		[K]	[K]	[g min^{-1}K^{-1}]	[g min^{-1}K^{-1}]		
step changes in T_a: 28-33-28°C	Stolwijk et al [175]	0.53	0.22	1.18 ± 0.15	1.67 ± 0.27	0.76	Fig.B.21
transient changes in rel. hum. at T_a=36°C	Gagge et al [59]	0.96	0.45	0.93 ± 0.56	7.23 ± 0.97	0.69	*Fig.B.22*
step changes in T_a: 29-37-29°C	Stolwijk et al [175]	1.12	0.21	1.38 ± 0.09	2.59 ± 0.35	0.94	*Fig.B.23*
step changes in T_a: 18-42-18°C	Hardy et al [75]	1.66	0.09	1.91 ± 0.05	0.19 ± 0.43	0.70	*Fig.B.24*
linear increase in T_a: 29 to 44°C	Gagge et al [59]	1.34	0.40	1.73 ± 0.24	7.08 ± 0.65	0.91	*Fig.B.25*
step change into T_a=43°C	Konz et al [106]	2.09	0.30	1.78 ± 0.06	0.03 ± 0.44	0.90	*Fig.B.26*
step changes in T_a: 28-42.5-28°C	Stolwijk et al [175]	1.80	0.32	1.69 ± 0.11	1.81 ± 0.45	0.93	*Fig.B.27*
step changes in T_a: 28-48-28°C	Stolwijk et al [175]	2.43	0.52	1.38 ± 0.12	2.23 ± 0.51	0.94	*Fig.B.28*
work & rest at T_a=10°C	Saltin et al [165]	-8.48	0.95	0.54 ± 0.17	9.30 ± 1.61	0.76	*Fig.B.29*
transient work at T_a=20°C	Stolwijk et al [177]	-6.30	0.80	0.43 ± 0.42	12.5 ± 3.15	0.70	*Fig.B.30*
work & rest at T_a=20°C	Saltin et al [165]	-5.03	1.37	0.69 ± 0.84	11.05 ± 3.07	0.83	*Fig.B.31*
transient work at T_a=30°C	Stolwijk et al [177]	-1.35	0.85	0.34 ± 0.44	8.84 ± 1.19	0.78	*Fig.B.32*
work & rest at T_a=30°C	Saltin et al [165]	-0.88	1.08	0.56 ± 1.15	10.93 ± 1.18	0.72	*Fig.B.33*

Tab.4.4

*Results of multi-linear regression analyses for the **Sw** [g min^{-1}] response using $\Delta T_{sk,m}$ and ΔT_{hy} as afferent signals. The corresponding regression coefficients $b_{sw,sk}$ and $b_{sw,hy}$ are provided with standard deviations **sd**. **R** is the multi-linear correlation coefficient of the regressions. The time-weighted averages of afferent signals from the skin and the head core, $\Delta T_{sk,m,t}$ and $\Delta T_{hy,t}$, characterize the strain level achieved in each experiment. The results of the regressions are presented graphically in appendix **B.2**.*

In general, good correlations were obtained for the *Sw*-response using a linear approach and $\Delta T_{sk,m}$ and ΔT_{hy} as afferent signals. Whereas the mean skin temperature had a more significant influence on sweating in hot environments, the head core

temperature signal became significant in evoking and governing the sweat moisture production due to internal heat stresses.

The coefficients $b_{sw,sk}$ are plotted against the average temperature error signals from the skin $\Delta T_{sk,m,t}$ in ***Fig.4.12***. Filled symbols (with bars showing the standard deviation $s_{bsw,sk}$) represent coefficients obtained from the multi-linear regressions with $\Delta T_{sk\,m}$ and ΔT_{hy}. Empty symbols indicate coefficients from simple linear regressions.

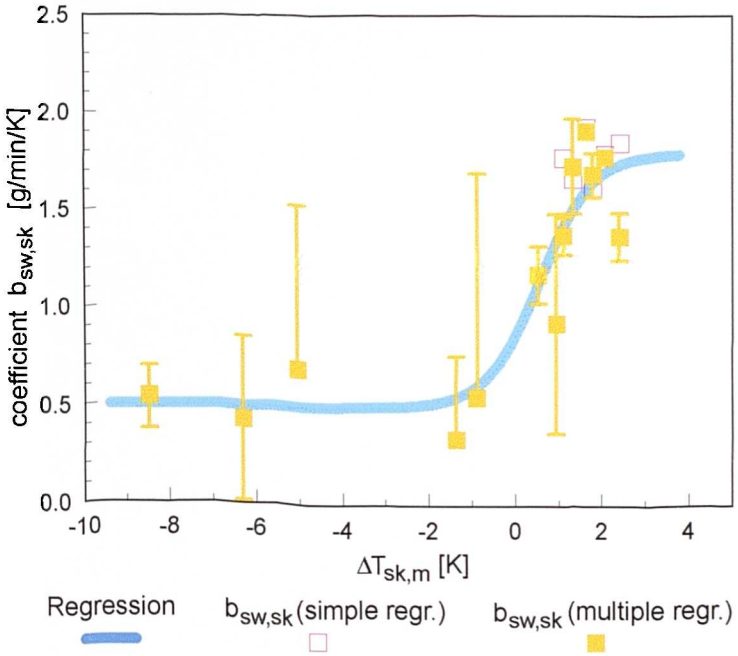

Fig.4.12

Dependency of the linear regression coefficients $b_{sw,sk}$ (± standard deviation), Tab.4.4, on the $\Delta T_{sk,m}$-signal.

As can be seen, elevating hot stress on the periphery of the body raised the relative contribution of the $\Delta T_{sk,m}$-variable. In hot environments (T_a>40°C), $b_{sw,sk}$ reached an average maximum level of about 1.4-1.9 g $min^{-1}K^{-1}$. In contrast, sweating during exercise in cool and cold environments was suppressed in proportion to the (negative) $\Delta T_{sk,m}$-signal via an average coefficient of about $b_{sw,sk}$= 0.5 g $min^{-1}K^{-1}$. These correspond to the limits of the regression curve in ***Fig.4.12*** by setting B_1=0.65 and B_0 = 1.15 in eq. (4.16).

The correlation analysis using eq. (4.17) for determining the function $f(x)$ of $b_{sw,sk}$ provided regression coefficients of b_0=-0.47 ±0.27 and b_1=0.82 ±0.26, with r=0.82. Thus, the following non-linear equation results for Sw and a wide range of $\Delta T_{sk,m}$-values:

$$Sw = \left[0.65 \tanh\left(0.82\, \Delta T_{sk,m} - 0.47 \right) + 1.15 \right] \Delta T_{sk,m} \qquad (4.26)$$

In contrast to regulatory defense mechanisms against cold, the regression coefficients of the hypothalamus error signal for sweating, $b_{sw,hy}$, were not erratic but showed a functional dependency on ΔT_{hy} when considering a wide range of boundary conditions, ***Fig.4.13***.

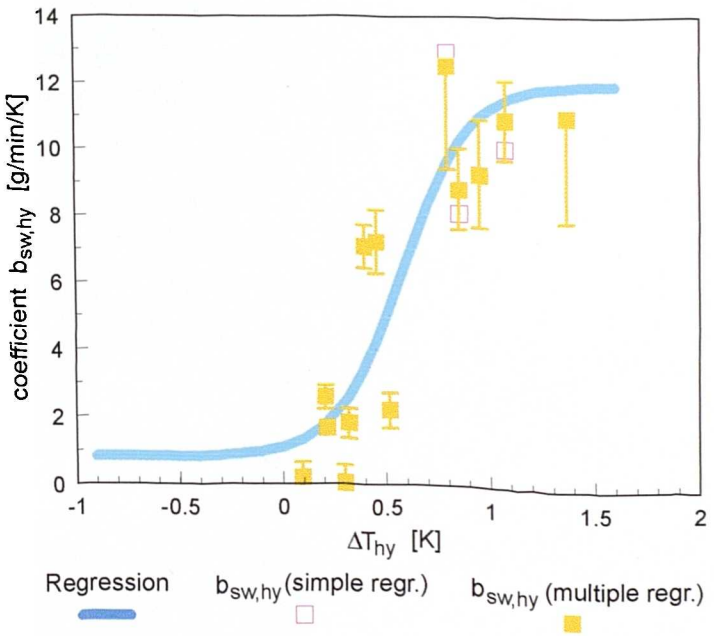

Fig.4.13

Dependency of the linear regression coefficients $b_{sw,hy}$ (± standard deviation), Tab.4.4, on the ΔT_{hy}-signal.

The typical pattern of a *tanh*-function characterized also the dependency of the $b_{sw,hy}$-coefficient on the integral afferent signal from the head core $\Delta T_{hy,t}$. The coefficients rose with the level of heat stress in the body core reaching on average a maximum of about $b_{sw,hy}$=12 g min^{-1}K^{-1} (for heavy exercise). The lower limit of the intended regression curve was established at about $b_{sw,hy}$= 0.8 g min^{-1}K^{-1}. A constant coef-

ficient $b_{sw,hy}$ >0 for negative error signals ΔT_{hy} was used to allow sweating to be suppressed by low hypothalamus temperatures [177].

Corresponding to the lower and upper limit of $b_{sw,hy}$ the fitting parameters in eq. (4.16) which were used to match the trend of $b_{sw,hy}$ were B_1=5.6 and B_0=6.4. Linear regression analysis to the $b_{sw,hy}$-data using eq. (4.17) provided coefficients of b_0=-1.83 ±0.70 and b_1=3.14 ±1.77 for the function $f(x)$, with r=0.75. With these results the dependency of the Sw-response on ΔT_{hy} yields:

$$Sw = \left[5.6\ tanh\left(3.14\,\Delta T_{hy} - 1.83\right) + 6.4\right]\Delta T_{hy} \tag{4.27}$$

The final control-equation for sweating in the present model is then:

$$\begin{aligned} Sw = {} & \left[0.65\ tanh\left(0.82\,\Delta T_{sk,m} - 0.47\right) + 1.15\right]\Delta T_{sk,m} + \\ & + \left[5.6\ tanh\left(3.14\,\Delta T_{hy} - 1.83\right) + 6.4\right]\Delta T_{hy} \end{aligned} \tag{4.28}$$

In the model, the sweat liquid production is limited to Sw_{max}= **30** g min^{-1} which seems to be the maximum rate of sweating for an average man [6]. The Sw-response is used to calculate the local sweat rate $dm_{sw,i}/dt$ [g min^{-1}] of the i-th skin sector:

$$\frac{dm_{sw,i}}{dt} = a_{sw,j}\,\frac{A_{sk,i}}{A_{sk,j}}\,Sw \times 2^{\frac{T_{sk,i} - T_{sk,i,0}}{10}} \tag{4.29}$$

where: $a_{sw,i}$ is the local portion of the central drive Sw [g min^{-1}] attributed to the j-th body element (see ***Tab.B.1***); $A_{sk,i}/A_{sk,j}$ is the skin area ratio between the i-th skin sector and the j-th body element; and $T_{sk,i}$ [°C] and $T_{sk,i,0}$ [°C] are the local skin temperature and the corresponding setpoint value, respectively. Not all local sweat excretion as calculated by eq. (4.29) must evaporate. A part of the sweat moisture overproduction may be accumulated at the skin surface and/or it may run off. The details depend on the physical boundary conditions (evaporative resistance of

clothing, air velocity, water vapour content of the ambient air). The physics of evaporation of $dm_{sw,i}/dt$ is treated by the passive system model, chap. 3.

4.4.4 Vasodilatation

The afferent signal analysis of the vasodilatation-response provided results similar to the sweating analysis: Dl depended on the integral temperature error signal from the skin in hot environments, and was governed by the hypothalamus temperature for internal hot stress. The coefficients of the multi-linear regressions with $\Delta T_{sk,m}$ and ΔT_{hy} obtained from individual experiments are shown in ***Tab.4.5***. The evaluation of regression data for seated subjects in warm and hot environments producing punitive signals from 'warm' cutaneous thermoreceptors, revealed increasing $b_{dl,sk}$-coefficients with rising $\Delta T_{sk,m}$-values, see ***Fig.4.14***. In contrast, $b_{dl,sk}$ fluctuated around zero for punitive signals from the skin due to cold cutaneous receptors, ie. for $\Delta T_{sk\,m} < 0$.

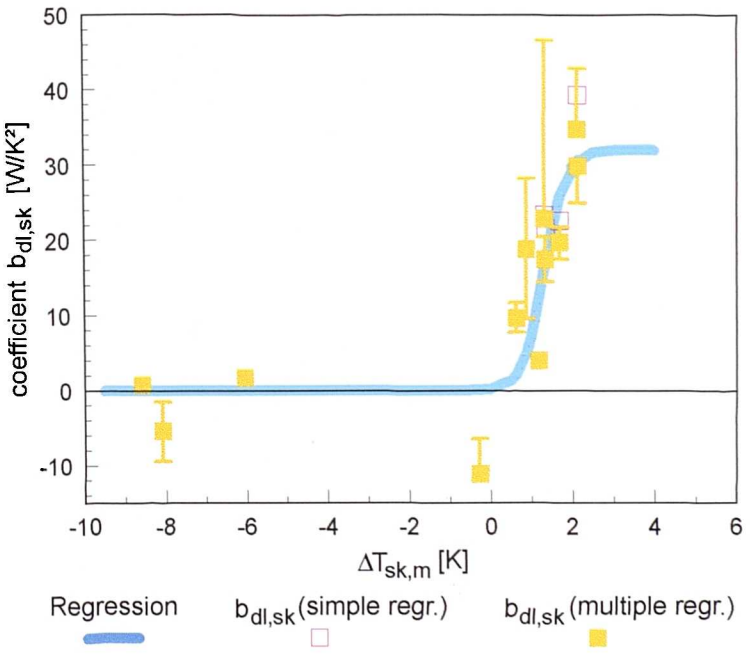

Fig.4.14

Dependency of the linear regression coefficients $b_{dl,sk}$ (± standard deviation), Tab.4.5, on the $\Delta T_{sk,m}$-signal.

experiment	ref.	$\Delta T_{sk,m,t}$ [K]	$\Delta T_{hy,t}$ [K]	$b_{dl,sk} \pm sd$ [W K^{-2}]	$b_{dl,hy} \pm sd$ [W K^{-2}]	R	Images
step changes in T_a: 28-33-28°C	Stolwijk et al [175]	0.63	0.22	9.69 ± 1.80	9.53 ± 3.58	0.58	***Fig.B.34***
transient changes in rel. hum. at T_a=36°C	Gagge et al [59]	1.32	0.73	22.9 ± 23.8	2.02 ± 45.01	0.44	***Fig.B.35***
step changes in T_a: 29-37-29°C	Stolwijk et al [175]	1.34	0.29	17.5 ± 2.9	16.2 ± 9.9	0.63	***Fig.B.36***
step changes in T_a: 18-42-18°C	Hardy et al [75]	1.19	0.14	3.99 ± 0.67	23.6 ± 4.2	0.76	***Fig.B.37***
linear increase in T_a: 29 to 44°C	Gagge et al [59]	0.88	0.51	18.8 ± 9.3	30.5 ± 18.0	0.71	***Fig.B.38***
step change into T_a=43°C	Konz et al [106]	2.12	0.28	34.8 ± 8.4	31.9 ± 54.8	0.53	***Fig.B.39***
step changes in T_a: 28-42.5-28°C	Stolwijk et al [175]	1.69	0.36	19.74 ± 2.09	14.3 ± 7.7	0.78	***Fig.B.40***
step changes in T_a: 28-48-28°C	Stolwijk et al [175]	2.14	0.82	29.9 ± 5.5	56.4 ± 12.2	0.89	***Fig.B.41***
work & rest at T_a=10°C	Saltin et al [165]	-8.58	0.55	0.79 ± 0.50	43.5 ± 6.7	0.74	***Fig.B.42***
transient work at T_a=20°C	Stolwijk et al [177]	-6.03	0.85	1.69 ± 1.03	58.7 ± 7.42	0.83	***Fig.B.43***
work & rest at T_a=20°C	Saltin et al [165]	-8.07	0.78	-5.4 ± 4.0	52.3 ± 40.2	0.42	***Fig.B.44***
transient work at T_a=30°C	Stolwijk et al [177]	-0.27	0.72	-11.2 ± 4.5	57.9 ± 12.2	0.58	***Fig.B.45***

Tab.4.5

*Results of multi-linear regression analyses for the **Dl** [W K^{-1}] response using $\Delta T_{sk,m}$ and ΔT_{hy} as afferent signals. The corresponding regression coefficients $b_{dl,sk}$ and $b_{dl,hy}$ are provided with standard deviations **sd**. **R** is the multi-linear correlation coefficient of the regressions. The time-weighted averages of afferent signals from the skin and the head core, $\Delta T_{sk,m,t}$ and $\Delta T_{hy,t}$, characterize the strain level achieved in each experiment. The results of the regressions are presented graphically in appendix **B.2**.*

Since negative coefficients are not useful from the physiological point of view, the lower asymptote of the function for $b_{dl,sk}$ was located at zero. Thus negative values of $\Delta T_{sk,m}$ do not influence the *Dl*-response in the model (in contrast to sweating, see above). The model's *SBF* is inhibited by cold skin temperatures exclusively by the vasoconstriction (*Cs*-)response.

The upper asymptote of the intended $b_{dl,sk}$-curve was set at 32 W K^{-2}. To correspond to the lower and upper limits of the $b_{dl,sk}$-function, the coefficients of eq. (4.16) were set to B_0=B_1=16. The regression curve plotted in ***Fig.4.14*** had a correlation coefficient of r=0.69 and provided regression coefficients of the $f(x)$-function, eq. (4.17), of b_1=1.92 ± 0.34 and b_0= -2.53 ± 0.66. The following function therefore describes the dependency of Dl on $\Delta T_{sk,m}$:

$$Dl = 16 \left[tanh\left(1.92\, \Delta T_{sk,m} - 2.53 \right) + 1 \right] \Delta T_{sk,m} \qquad (4.30)$$

The supra-experimental analysis indicated that the coefficient $b_{dl,hy}$ depends on the ΔT_{hy}-signal. Coefficients lower than 20 W K^{-2} were associated with hypothalamus temperatures not exceeding 37.5°C, whereas $b_{dl,hy}$-coefficients reaching nearly 60 W K^{-2} were obtained for head core temperatures in the range of 38°C. Therefore, the fitting function was chosen to run from zero to 60 W K^{-2}, ie. B_1=B_0=30 in eq. (4.16). The regression to the $f(x)$-function in eq. (4.17) provided coefficients of b_1 = 3.51 ± 0.59 and b_0= -1.48 ± 0.23, with r = 0.90. The regression function $Dl\,(\Delta T_{hy})$ plotted in ***Fig.4.15*** is:

$$Dl = 30 \left[tanh\left(3.51\, \Delta T_{hy} - 1.48 \right) + 1 \right] \Delta T_{hy} \qquad (4.31)$$

The final control equation for Dl collects the effect of $\Delta T_{sk,m}$ and ΔT_{hy}:

$$\begin{aligned} Dl = {} & 16 \left[tanh\left(1.92\, \Delta T_{sk,m} - 2.53 \right) + 1 \right] \Delta T_{sk,m} + \\ & + 30 \left[tanh\left(3.51\, \Delta T_{hy} - 1.48 \right) + 1 \right] \Delta T_{hy} \end{aligned} \qquad (4.32)$$

Equation (4.32) permits an unlimited rise in *SBF*. Literature [163], however, indicates the existence of an upper limit for overall *SBF* of about 8 l min^{-1} for resting subjects. Moreover, the magnitude of the vasodilator outflow appears to depend on the type and level of the activity performed [98].

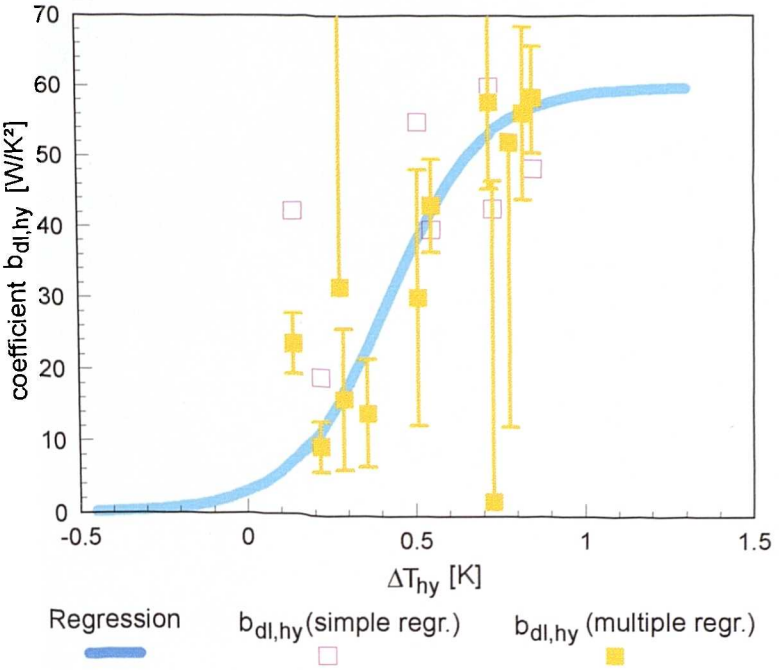

Fig.4.15

Dependency of the linear regression coefficients $b_{dl,hy}$ (± standard deviation), Tab.4.5, on the ΔT_{hy}-signal.

Rowell [164] summarised experimental data describing changes in the distribution of the cardiac output over body regions depending on exercise intensity. According to that survey, exercising in hot conditions showed reduced vasodilatation when compared with the *SBF* of 'resting' subjects in the same ambient conditions (43.3°C). The cutaneous vasodilator outflow was inhibited quasi-linearly as the muscle blood flows rose in proportion to the exercise intensity (see chap. 3, eq. 3.12), whereas the sum of the blood flow rates in the resting tissues (eg. viscera, brain) remained fairly constant throughout all activity levels.

The inhibition of the vasodilatation response whilst working in hot conditions was assumed to be associated with the restricted performance capacity of the human blood circulation system. During exercise, increases in the cardiac output are directed primarily to working muscle groups to accommodate the increased demand for oxygen. Less blood is then available for thermoregulation by peripheral vasodilatation [164].

The reduction of regulatory increases in *SBF* (ie. β'_{sk} in the model) as compiled by

Rowell, was related to the extra overall blood flow $\Delta\beta' = \beta' - \beta'_{bas}$ (due mainly to the extra blood flow into skeletal muscles during exercise). Linear regression to these data provided the following expression for the maximum overall skin blood flow $\beta_{sk,max} = 386.9 - 0.32\,\Delta\beta'$ [W K^{-1}] (with r=0.99). The constant of 386.9 W K^{-1} corresponds to a maximum *SBF* of about 6 l min^{-1}. Any overall skin blood flow, β'_{sk}, as computed using equations (4.8) and (4.32), which would exceed this threshold, is reduced to $\beta'_{sk,max}$. It should be noted that the reduction of *SBF* via $\beta'_{sk,max}$ also has the effect of restricting the exercise power of the model. The maximum activity level was defined to be at *act*=12met (corresponding to a cardiac output of 20 l min^{-1}) a value which, on average, reflects the (short-term) maximum possible activity level of human subjects. At these conditions the maximal overall skin blood flow $\beta'_{sk,max}$ becomes zero.

The overall *DI*-response is used to calculate the local skin blood flow of a skin sector as described by eq. (4.25) in section 4.4.2.

4.5 Testing the Complete Model

The complete model was tested using all the experiments used to develop the model (see also appendix B.3). It was interesting to see to what extent the new non-linear model (which has coefficients in the control-equations which do not exactly match the data in the individual experiments) can reproduce the thermal behaviour observed in the individual experiments. The validation of the model using additional experiments is discussed in section 4.6.

In the experiment of Young et al. [209] seven unacclimatized, seminude subjects reclined in a room at T_a=24°C before entering a cold room of T_a = 5°C in which they reclined for 90 minutes. The initial (t=0) sudden change in ambient temperature caused a rapid cooling of the skin which in turn induced a transient peak in the metabolic activity at t=10 min. A comparison of the predictions of the present model and the Stolwijk model with experimental data for these severe conditions are shown in *Fig.4.16*.

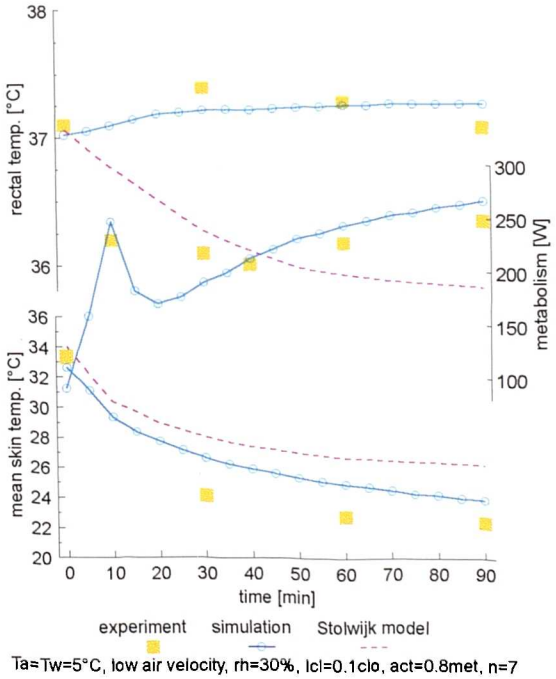

Fig.4.16

Exposure to severe cold of T_a 5°C investigated by Young et al. [209]. The experimental conditions and the number of subjects are noted in the legend.

The present model does not reproduce exactly that sharp fall in the mean skin

temperature. The measured value, however, was obtained as an average from only three body sites and it is questionable whether such an average is representative for the actual mean skin temperature.

The reverse pattern, ie. an increase with time, was observed for the body core temperature (rectum in this case). In contrast to the Stolwijk model (data obtained from [79]), the present model reproduced the increasing trend as a result of the combined effect of shivering and a sudden massive inhibition in *SBF*. Raven et al. [156] observed even higher rectal temperatures (see ***Fig.4.17***) for virtually the same environmental conditions. However, as Gordon [72] pointed out, rectal temperatures exceeding the 'neutral' level by nearly 1K might have been due to local effects so they may not reflect the average temperature of the body core.

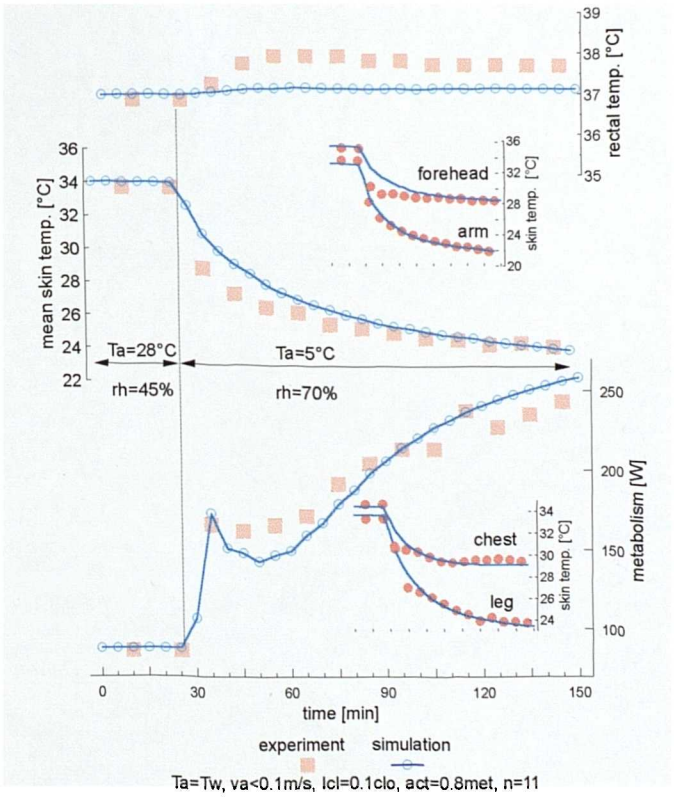

Fig.4.17

Exposure to an environment of T_a 5°C investigated by Raven et al. [156]. The experimental conditions and the number of subjects are noted in the legend.

As apparent from ***Fig.4.16*** and ***Fig.4.17***, good agreement between predicted and observed data was obtained for the shivering response in severe cold.

Nevertheless, the tests also revealed discrepancies which should be discussed here. The most crucial disagreement was with an experiment involving exposure to ambient temperatures of T_a=13°C which was conducted by Hardy et al. [75]. In that experiment, only a small increase in the metabolic heat production of about 40 W was recorded for the whole 4-hr-exposure (see ***Fig.4.18***). In contrast, the model predicted the onset of shivering after t=30 min. Then, the extra metabolism due to shivering continued to increase, because of both low skin and low body core temperatures, and reached a maximum of more then 100 W over base rate at the end of exposure. It is supposed that this discrepancy may reflect differences between the anthropho-metric properties assumed for the model's passive system (which was designed to represent an average subject with respect to the size of the body and body fat), and the subjects in the experiment (who had rather atypical body data). A similar argument can also explain the differences in both the predicted mean skin temperatures and the predicted rectal temperatures. The premature onset of shivering that was observed in ***Fig.4.18***, does not, however, seem be a basic characteristic for the model. Other experiments [188] show that people start to shiver at ambient temperatures higher than 13°C (see ***Fig.4.19***) and this is consistent with the model's predictions.

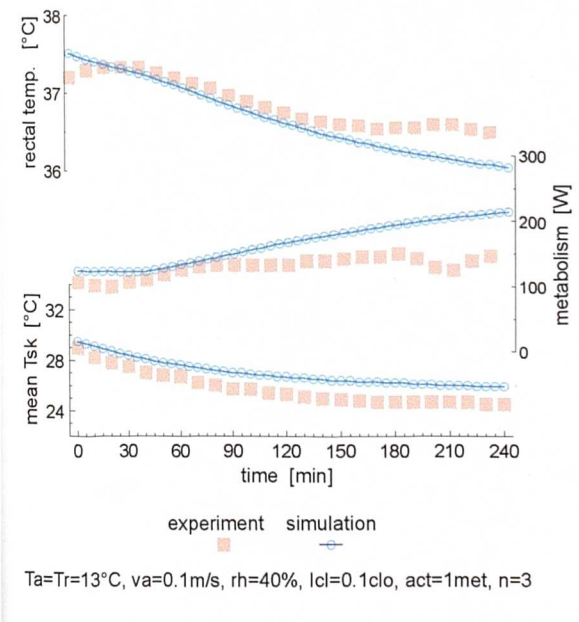

Fig.4.18

Exposure to an environment of T_a 13°C investigated by Hardy et al. [75]. The experimental conditions and the number of subjects are noted in the legend.

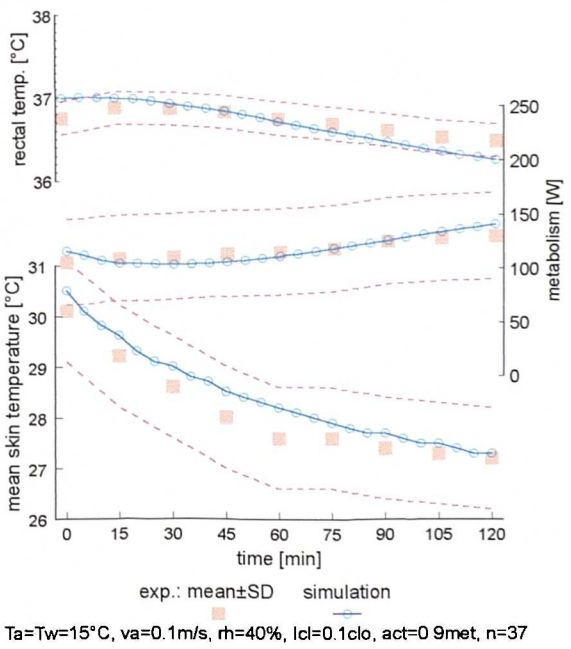

Fig.4.19

Exposure to an environment of T_a 15°C investigated by Wagner et al. [188]. The experimental conditions and the number of subjects are noted in the legend.

The predictions of the model due to ambient temperature changes from neutral (T_a=28 °C) to cold (T_a=22°C) and vice versa is illustrated in ***Fig.4.20*** (other results are shown in appendix B.3, ***Fig.B.47***). Good agreement with the measurements characterises these exposures. The predicted mean skin temperature did not differ from the measurements by more than 1K at any time. The subjects were the same as those which yielded the experimental data for ***Fig.4.18***; they had a slightly higher level of the body core temperature and a lower basal metabolism than the standardized value of the model, probably for the reasons noted above. Nevertheless, there was no increase in either the measured or predicted metabolic heat production during the cold exposure.

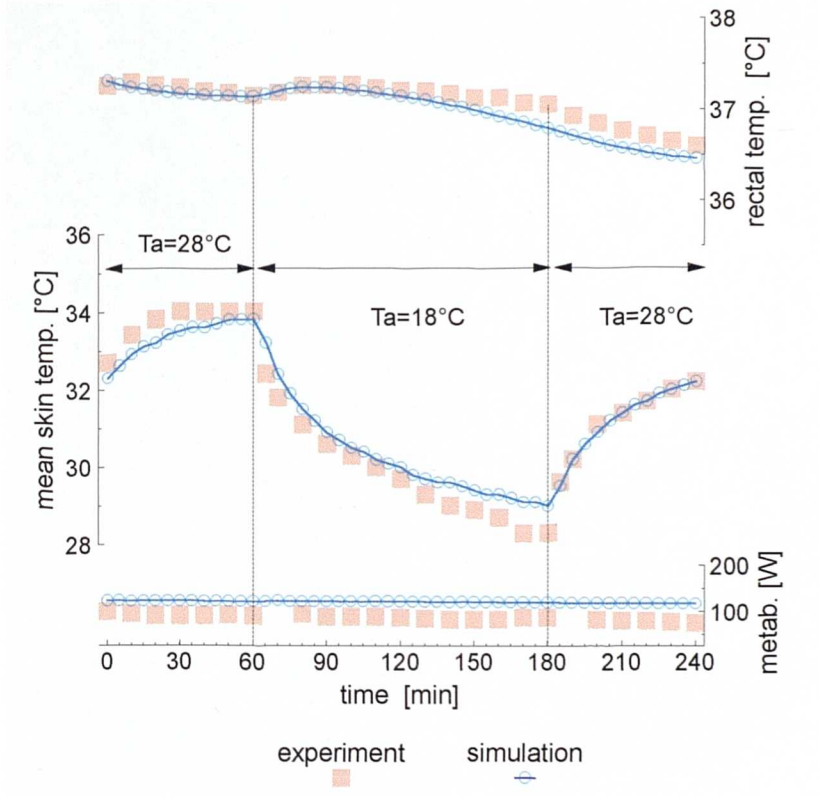

Ta=Tr, va=0.1m/s, rh=40%, Icl=0.1clo, act=1met, n=3

Fig.4.20

Exposure to sudden changes in ambient temperature of T_a 28-18-28°C investigated by Hardy et al. [75]. The experimental conditions and the number of subjects are noted in the legend.

The performance of the model in mild environmental conditions was tested using experiments by Stolwijk et al. [175] and Wagner et al. [188], as shown in ***Fig.4.21*** and ***Fig.B.49*** of appendix B.3. In these experiments there was neither shivering nor sweating (either as measured or as predicted). Except for the initial phase the model

reproduced the body core temperature to within 0.2 K (***Fig.4.21***). The deviations of the mean skin temperatures were always less than 1K.

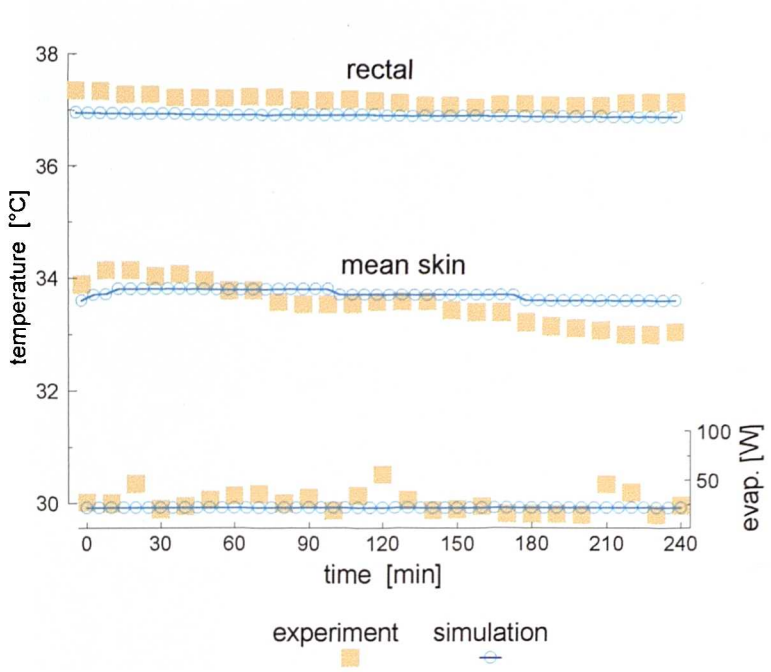

Ta=Tw =28°C, va=0.1m/s, rh=31%, act=1met, 0.1clo, n=3

Fig.4.21

Exposure to a mild environment of T_a 28°C investigated by Stolwijk et al. [175]. The experimental conditions and the number of subjects are noted in the legend.

The reliability of the non-linear dilatation- and sweating-model in hot conditions could possibly be analysed best using transient exposures to environments representing a wide range of hot stress conditions. Some predicted thermal behaviours are illustrated using experiments for warm ambients of 33°C [175], moderate heat of 42°C [75], and hot stress of 48°C [175] [57] in ***Fig.4.22*** - ***Fig.4.24***. Further examples for environmentally induced hot stress are provided in appendix B.3, ***Fig.B.54*** - ***Fig.B.58***. In all the experiments, the seminude subjects were seated. They moved at t=60 min from a thermally neutral or moderately cold room into another, warm or hot space and returned at t=180 min. This sort of experiment is useful to examine the predictive abilities of the model for a transient change into a hot environment as well as a rapid change back into a neutral or cool environment. Both types of change result in different thermal reactions not only at the body's periphery, as one could expect, but also at the body core. A step change into a hot environment is typically associated with an apparently paradoxical fall in the internal body temperature (best

shown in ***Fig.4.23***). This phenomenon, which was also reproduced by the model, is a result of cooling the vasodilated blood flow in the skin. During the warm and hot exposure the predicted and measured rectal temperature rose continuously indicating that steady states were not reached for any of the exposures even after two hours. The rise of body core temperature was stopped almost immediately after returning into the neutral ambient conditions (***Fig.4.22*** and ***Fig.4.24***) but it continued to rise when re-entering the cold space (***Fig.4.23***) due to cutaneous blood flow constriction. This abrupt inhibition of *SBF* reduced the heat flow from the body core to the body surface.

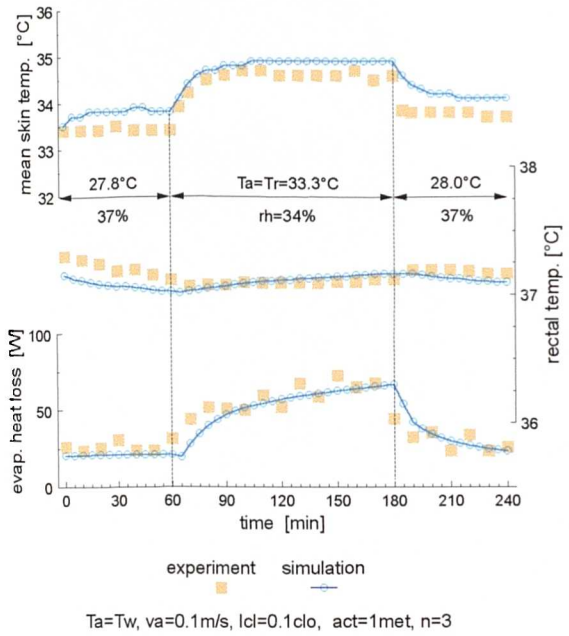

Fig.4.22

Sudden changes in ambient temperature from a neutral- into a warm environment of T_a 33°C and back again investigated by Stolwijk et al. [175]. The experimental conditions and the number of subjects are noted in the legend.

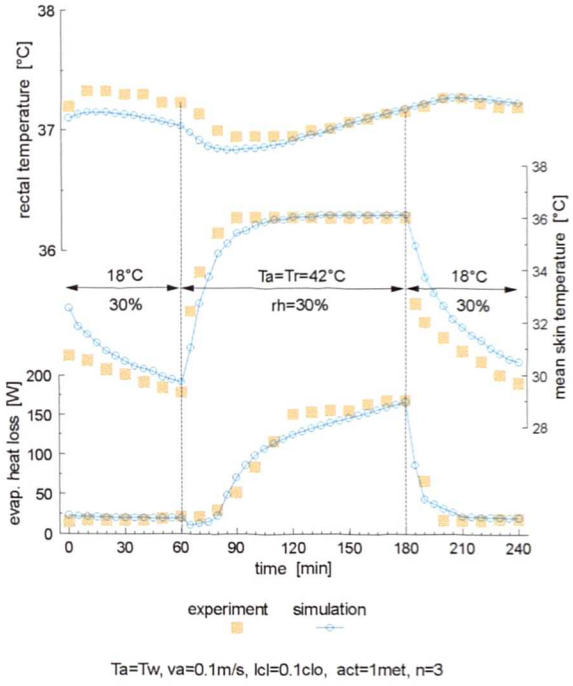

Fig.4.23

Sudden changes in ambient temperature from a cold- into a hot environment of T_a 42°C and back again investigated by Stolwijk et al. [175]. The experimental conditions and the number of subjects are noted in the legend.

There was a very good general agreement with the experimental data except for the hottest environment (***Fig.4.24***) where the predictions differed appreciably from the data measured by Stolwijk et al. The comparison with measured body core tem-

perature obtained from Gagge [57] for the same exposure (also plotted in ***Fig.4.24***), however, provided better agreement.

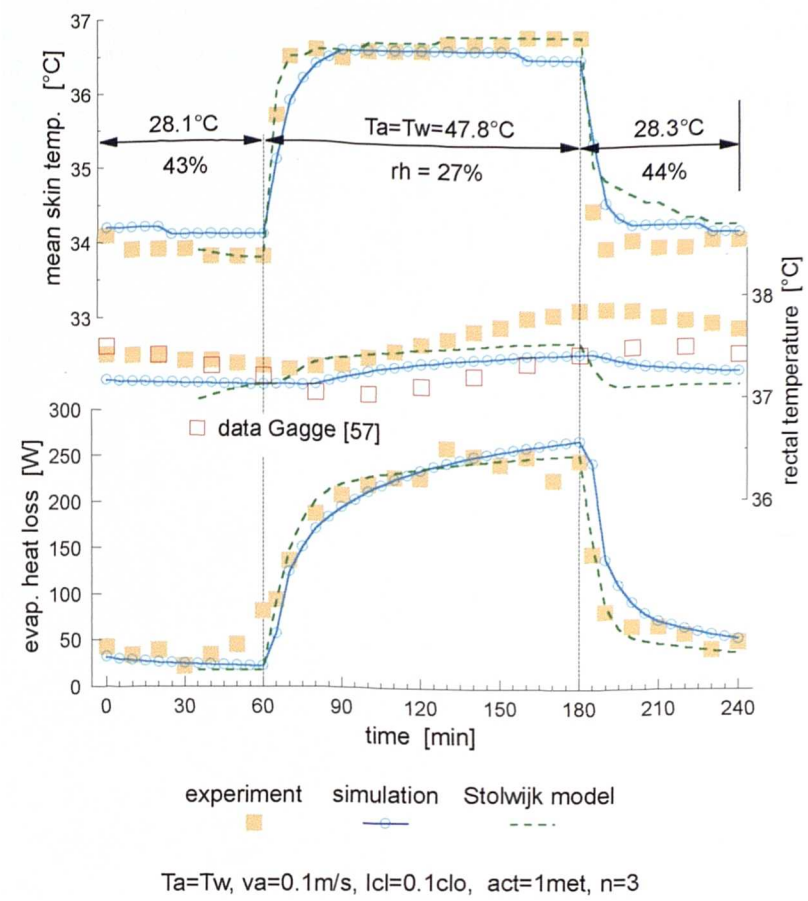

Fig.4.24

Exposure to sudden changes in ambient temperature of T_a=28-48-28°C investigated by Stolwijk et al. [175]. The experimental conditions and the number of subjects are noted in the legend.

As can be seen, the non-linear sweating model simulated the sudomotor regulatory behaviour quite well even for a wide range of warm and hot ambient conditions (see also ***Fig.B.54*** - ***Fig.B.58*** in appendix B.3). Both the transient behaviour, and the final levelling-off of skin evaporation, were predicted appropriately. The model was also able to reflect the delay of the onset in sweating (of about 20 minutes) after moving from a cold environment into a hot one (***Fig.4.23***).

In contrast to cold air exposures, where the thermal state of the body's periphery is mainly a result of environmental temperatures, skin temperature in hot conditions is substantially influenced by the rate of sweat evaporation from the skin. Thus, reliably

predicted sweat rates led to confident predictions of skin temperatures.

Systematic discrepancies between predicted and measured skin temperatures were observed for transient sweating induced by internal hot stress in the cold. Measurements typically showed an increase in skin temperature as subjects began to work and started to sweat. This behaviour is illustrated in ***Fig.4.25***. A subsequent cooling of the skin was observed after terminating the work when the production of sweat liquid declined. The model predicted the reverse pattern: decreasing skin temperatures during the initial phase of exercise with a small increase in the recovery-phase. This discrepancy seemed to be more crucial when sweating in the cold (***Fig.4.25***) than in moderate environments, as illustrated in ***Fig.4.26***. Wissler [201] also obtained similar predictions for the mean skin temperature in these two types of condition.

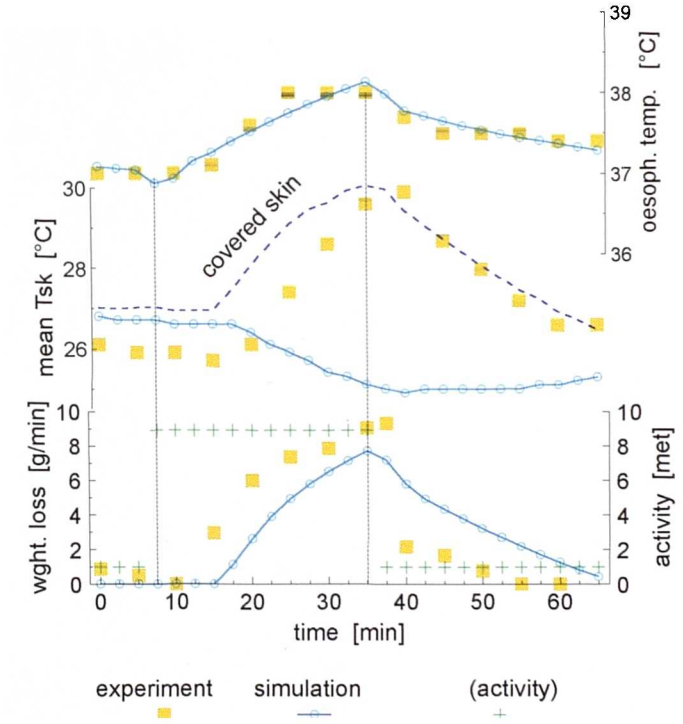

Ta=Tw=10°C, va=0.1m/s, rh=40%, Icl=0.1clo, act=8.9met, n=1

Fig.4.25

Discrepancies between predicted and measured skin temperature during working in a cold environment of T_a 10°C investigated by Saltin et al. [165]. Also shown is the predicted skin temperature which resulted from the simulation when evaporation was prevented, and this imitated a small area of sticking tape on the skin as used in the experiments.

The authors of the corresponding experiments [165] attributed increasing skin temperatures to the rise in the heat gain due to vasodilatation in the skin. To investigate this statement further, a special study was undertaken using the model. The aim was to see whether temporal increases in *SBF* could reverse the trend of the predicted mean skin temperature during working. For this purpose, the model was arranged to allow manual variations of the *DI*-variable for each time instance of an experiment. The thermal state of the body was then predicted for these artificial changes in *SBF*. It was found that increases in *SBF* during work-periods did not significantly affect the predicted skin temperatures. This conflicts with the explanation of Saltin et al. Moreover, artificially elevated vasodilatation during the exercise-phase caused an appreciable fall in the predicted body core temperatures; this would contradict measured data.

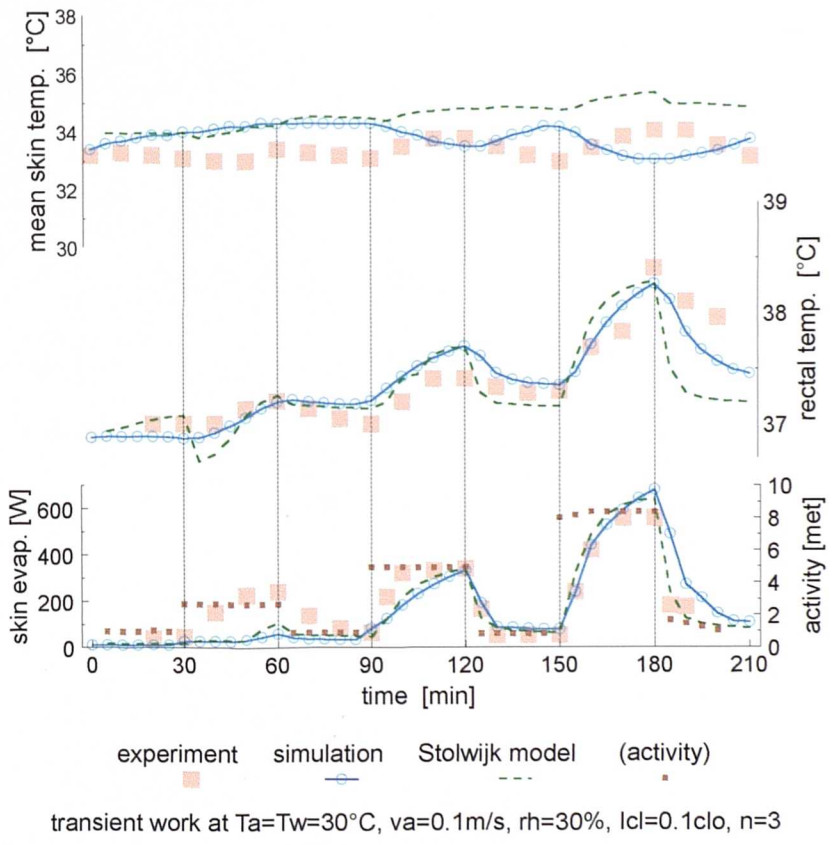

Fig.4.26

Exercise at three levels of activity at T_a 30°C [177]. The experimental conditions and the number of subjects are noted in the legend.

It appeared that other effects are probably responsible for the discrepancies between the measured and predicted skin temperatures for the conditions described above.

Skin temperatures were measured by Saltin et al. using thermocouples taped on the skin. In reality, however, the tape may prevent evaporation of sweat exactly at those locations on the skin where temperatures are measured. This will cause evaporation (and also perhaps convective cooling) to be suppressed, leading to higher skin temperatures. The extent to which suppressed evaporation may influence measurements of skin temperature was investigated further by a theoretical study, a literature review, and also by some preliminary experimentation (appendix B.4).

In the theoretical study the effect of preventing local sweat evaporation by a small impermeable sticker (a circle with a radius of 8mm) was investigated numerically using a specially developed, two-dimensional dynamic skin model (appendix ***B.4.1***). The resulting temperatures of the skin covered by the sticker are plotted as dashed lines in ***Fig.4.25***. As can be seen, the predicted values now fitted the measurements (surprisingly) well. The results indicated that spot-like suppression of skin evaporation by sticking tape can considerably affect the surface heat exchange. The measured skin temperature therefore differs from that of the uncovered skin. This effect could explain the discrepancies between the predicted and measured skin temperatures shown in ***Fig.4.25*** (see also appendix B.3, ***Fig.B.62***).

This conclusion, however, needed the support of experimental verification before casting serious doubts on a measurement method which has been employed in many experimental studies. Unfortunately, the available literature did not provide experiments which could directly verify the finding. Nevertheless, some insight was gained from experiments in which alternative methods of recording skin temperatures were used. Clark and co-workers [32] utilized infrared thermography to measure the skin temperature of unclothed subjects running on a treadmill in an climate chamber at 11°C. They found that skin temperatures were not rising but - in contrast - T_{sk} began to fall on starting running, and decreased by about 5K over-all during the experiment. This marked decrease in skin temperatures was observed even though there was no wind. When a fan was turned on there was a further decrease in T_{sk} of about 4°C. This result agrees with the predicted fall in $T_{sk,m}$ for the period of exercise in ***Fig.4.25***. Similarly, a rise in skin temperatures was observed in the case of an athlete who showed inhibition of sweating (due exhaustion at the end of exercise).

Unfortunately, in their paper, Clark et al. did not compare results of these non-contact temperature-measurements with measurements using thermocouples.

A simple experiment was, therefore, designed to compare directly the temperatures of covered and uncovered skin as measured by a thermocouple and by an optical, non-contact method, respectively (for a description see appendix B.4.2). The differences between the results were similar to the differences observed between the measured and predicted data using the whole-body model (see ***Fig.B.64*** and ***Fig.B.65*** in appx. B.4.2).

One may, therefore, conclude that skin temperature predicted by the present model for transient work when sweating in the cold corresponds to the temperature of the uncovered skin rather than skin temperature covered by a non-porous tape.

4.6 Validation

Some examples of validation work on the model are given here. The validation was performed using experiments which were not involved in the formulation procedure.

The model's predicted thermal behaviour due to a cold air exposure of 10°C is compared with measured data obtained by Budd et al. [22] in ***Fig.4.27***.

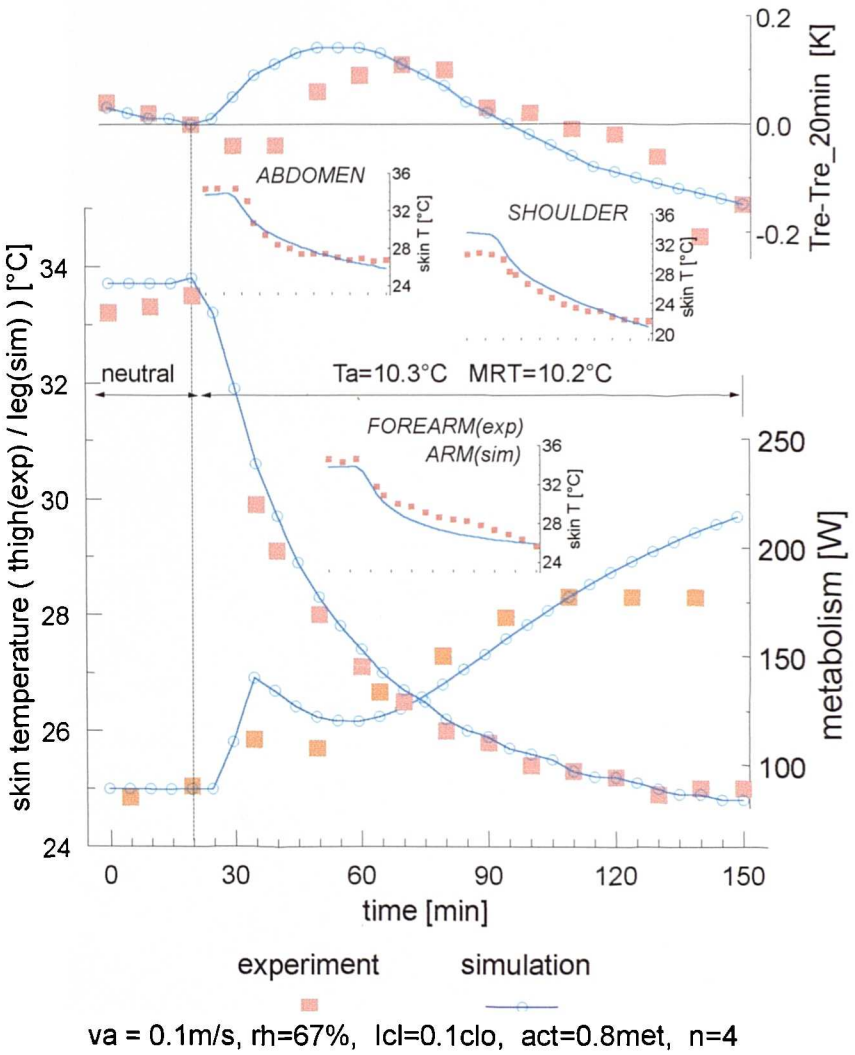

Fig.4.27

Exposure to an environment of T_a 10°C investigated by Budd et al. [22] (T_{re} rectal temperature). The experimental conditions and the number of subjects are noted in the legend.

The experimental report provided neither absolute values of the rectal temperature, T_{re}, nor information on the mean skin temperature, $T_{sk,m}$. So, the trend of T_{re} and the

local skin temperatures from four body sites were considered instead. Although there is some temporal discrepancy, the model reproduces the pattern of the body core temperature quite well: after 20 minutes there is an initial, transient rise of T_{re} of about 0.2K followed by a decrease reaching finally about -0.15K. The skin temperatures also showed a generally good agreement with measurements, although the forearm (experiment) and the arm (simulation) skin temperature deviated temporarily by about 2K. However, it should be noted that the forearm skin temperature in particular differed by 3K from one measurement site to the next. Also, the skin temperature of shoulders showed significant differences for t<20min which was, however, a result of different ways of simulating the subjects' thermal neutrality. The neutral environment for t<20min was simulated by 'exposing' the computer dummy to ambient temperatures of 28°C, whereas the reclining subjects were covered (not entirely) by a blanket which was then removed to start the cold stress exposure. The model overestimated somewhat the metabolic heat production at 30<t<50min, and for t >110min, whereas the predicted values rose due to a continuous fall in skin and body core temperature, the experimental measurement became steady.

A study by Olesen et al. [150], investigating the skin temperature distribution of subjects in a state of thermal comfort, was used to examine the model's performance in neutral ambient conditions. Thirty-two subjects participated in the experiment and spent, 2.5 hrs seated in neutral ambient temperatures of T_a=*MRT*=25.5°C. The participants were clad in the standard KSU-uniform comprising a cotton twill shirt and trousers, cotton undershorts and cotton socks (no shoes). The measured mean values of 32 subjects, averaged over the last two hours of the experiment are compared with predictions in ***Tab.4.6***. As can be seen, the body core temperature, the skin temperature distribution, as well as the evaporative weight loss (including evaporation by respiration and skin water vapour diffusion) agreed well with the corresponding measurements. Predicted values were always within the bounds of the intra-individual fluctuation.

Another comparison of the skin temperature distribution for clothed subjects in a moderate environment as measured by Nielsen et al. [143] and as predicted is provided in ***Tab.B.4*** (appendix B.5). Mean skin temperatures and rectal temperatures as

predicted for various combinations of environmental parameters and different garments are compared with measured values in ***Tab.B.2*** [149] and ***Tab.B.3*** [143].

skin temperature distribution for resting man in comfort (Olesen et. al 1973)

body temperatures			experiment *)	simulation
rectal		[°C]	36.9 ± 0.3	36.98
mean skin		[°C]	33.5 ± 0.5	33.76
forehead skin		[°C]	34.2 ± 1.0	34.65
neck skin	posterior	[°C]	34.7 ± 0.8	34.09
thorax skin	anterior	[°C]	34.4 ± 0.6	34.39
	posterior		34.5 ± 0.9	34.36
arm skin	upper	[°C]	*33.5 ± 0.9*	
	lower		*32.7 ± 0.8*	
	average		33.1 ± 0.9	33.25
hand skin	back	[°C]	33.5 ± 1.0	33.63
abomen skin	anterior	[°C]	34.9 ± 1.0	34.36
	posterior		33.5 ± 0.8	34.33
leg skin (anterior)	upper	[°C]	*33.7 ± 0.8*	
	lower		*32.6 ± 1.1*	
	average		33.2 ± 1.0	33.69
leg skin (posterior)	upper	[°C]	*32.9 ± 0.9*	
	lower		*32.2 ± 1.0*	
	average		32.6 ± 1.0	33.69
foot skin	instep	[°C]	32.2 ± 2.0	31.57
evaporative weight loss		[g/m²h]	20.1 ± 6.9	19.12

*) mean values ± SD of 32 subjects

Tab.4.6

Skin and body core temperatures during the exposure to thermoneutral conditions of T_a = 25.5°C investigated by Olesen et al. [150]. The mean radiant temperature was equal to T_a and there was still air (v_a<0.1 m s^{-1}). The subjects were seated and clad in the so called KSU-uniform (I_{cl}= 0.6clo).

The dynamic behaviour of the model, with respect to sudden changes in ambient temperatures from hot (T_a=43°C) to cold (T_a=17°C) and back again, is shown in ***Fig.4.28***, together with the experimental data of Hardy et al. [75], and simulation data from the Stolwijk model obtained from literature [13] [177]. This type of ex-

posure was not considered when formulating the active system. Another example, for step changes in ambient temperature can be seen in ***Fig.B.67*** (appendix B.5).

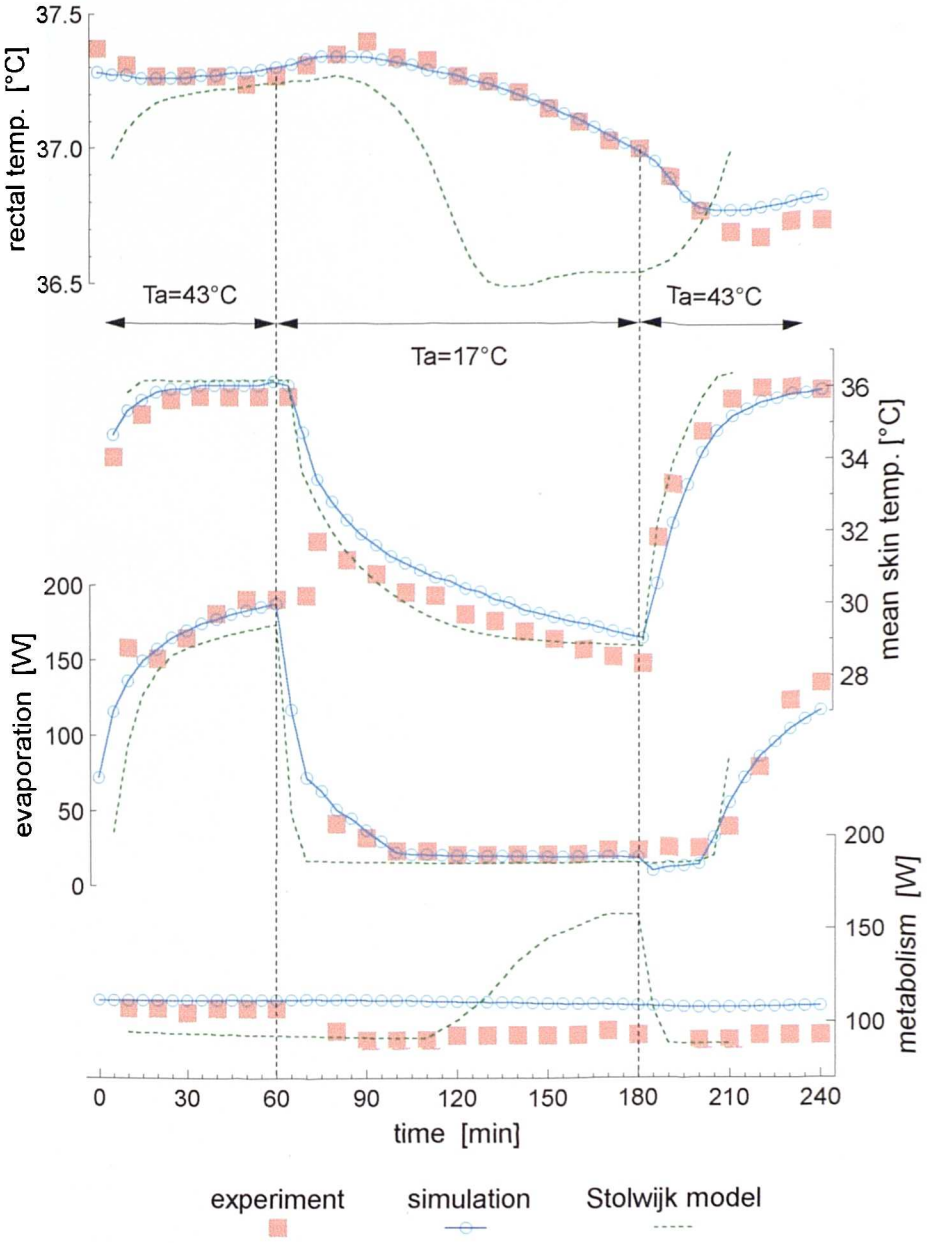

Fig.4.28

Exposure to sudden changes in ambient temperature, from a hot environment of 43°C to a cold environment of 17°C and back again, investigated by Hardy et al. [75]. The experimental conditions and the number of subjects are noted in the legend.

The first hour of the experiment was characterized by hot stress reactions in response to elevated skin- and body core temperature. After entering the cold room the

subjects experienced a rapid fall in the mean skin temperature which was reproduced, but less dramatically, by the model using time steps of Δt = 5 min. There might have been some differences between the experimental conditions and those assumed in the simulation during the 5-minute-period in which subjects moved from the hot space into the cold room.

During the initial (30min.) phase of cold exposure both the experimental and predicted rectal temperature behaved in the opposite way to the skin temperature. In the model, T_{re} rose as a result of peripheral vasoconstriction and the simultaneous inhibition of sweat production in response to the decreasing skin temperatures. The sweat production predicted for 70<t<100 minutes arose, therefore, exclusively from the elevated body core temperature. During the cold exposure, the mean skin temperature continued to fall and did not reach equilibrium even after 2 hours. The predicted mean skin temperature differed from the measurements by a constant 0.6-0.7K. After levelling off at t=90min, the rectal temperature began to fall due to the high convective and radiative heat losses to the environment. Nevertheless, the subjects did not shiver during the entire period of the cold exposure, which was in accordance with the model's predictions.

After returning to the hot room there was an immediate increase in the subjects' mean skin temperature which was also predicted by the model. However, due to the dynamic effect of heat storage in the body, the measured rectal temperature lagged in trend behind the measured skin temperatures and continued to fall for a further 20 minutes before warming began. The model predicted similar patterns. Despite the decreasing core temperatures, the model predicted the onset of sweating with a delay of about 20 minutes after entering the hot environment. This is consistent with experimental observation. Since, at this time the model's head core temperature was below the setpoint for sweating ($\Delta T_{hy} \approx$-0.1K) the onset of sweating was attributed exclusively to the influence of warm skin thermoreceptors.

The following example is concerned with the performance of the model during exercise (for another example see ***Tab.B.2*** appendix B.5). Givoni and Goldman [63] conducted a series of experiments (groups of n=4 subjects) in which (only) the rectal

temperature was measured for different combinations of work load, ambient temperature, relative humidity, and clothing insulation. Some of the results for these rest-work-recovery cycles are shown in ***Fig.4.29***. The model underestimated the rectal temperature of unclothed (I_{cl}=0.1clo) subjects especially for the high air speed of v_a= 5 m s^{-1}, where the predicted T_{re} was constantly about 0.3K below the measured values. Nevertheless, there was very good general agreement between predicted and measured rectal temperatures.

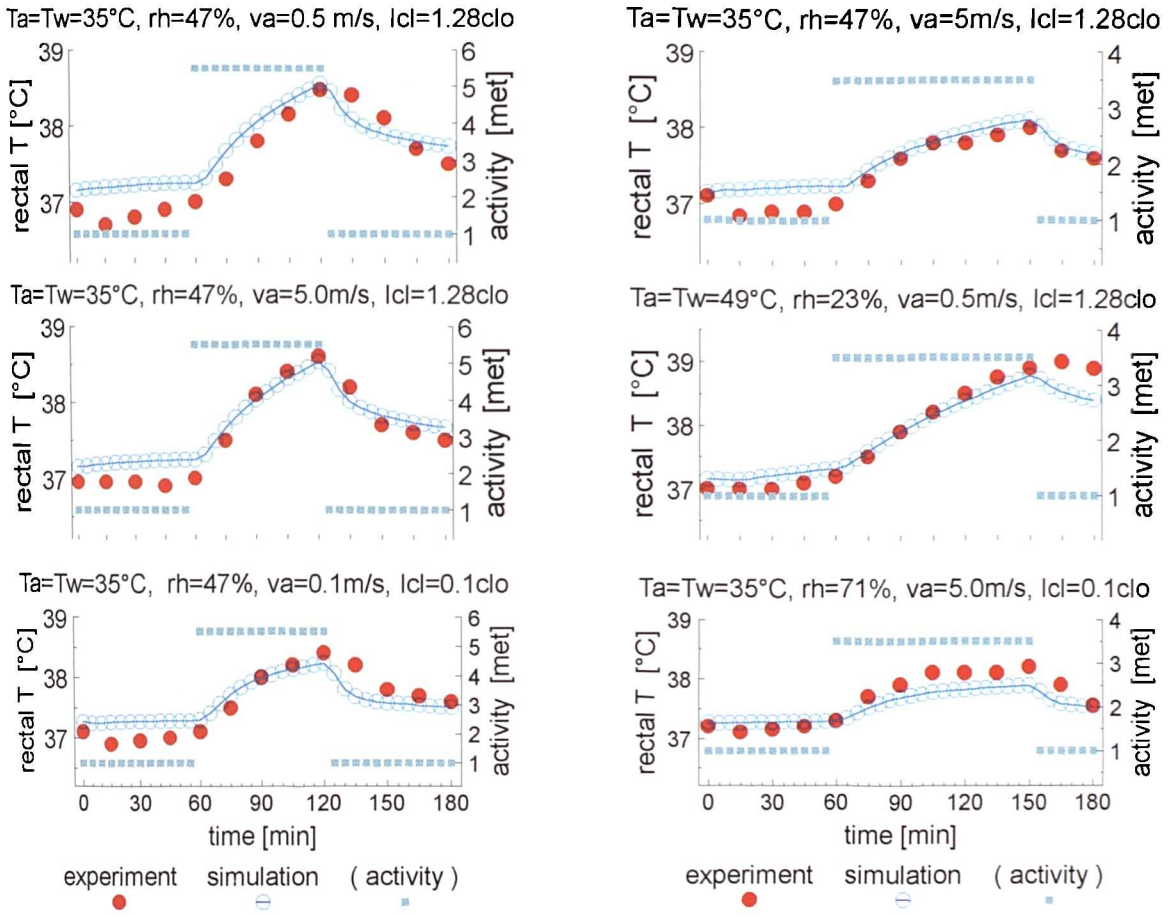

Fig.4.29

Rectal temperature during sequences of exercise and recovery with different clothing levels and for different environmental conditions [63].

Finally, the model's predictions are compared with the average physiological data (± standard deviation) of three or more seminude, seated subjects exposed to ambient temperatures of 12°C to 48°C [57] (***Fig.4.30***). The data points represent averages after approximately one hour's exposure to each particular temperature. This test was useful for examining the predictive behaviour of the model with respect to a wide

range of environmental conditions (see also appx. B.5, ***Fig.B.66*** [204]).

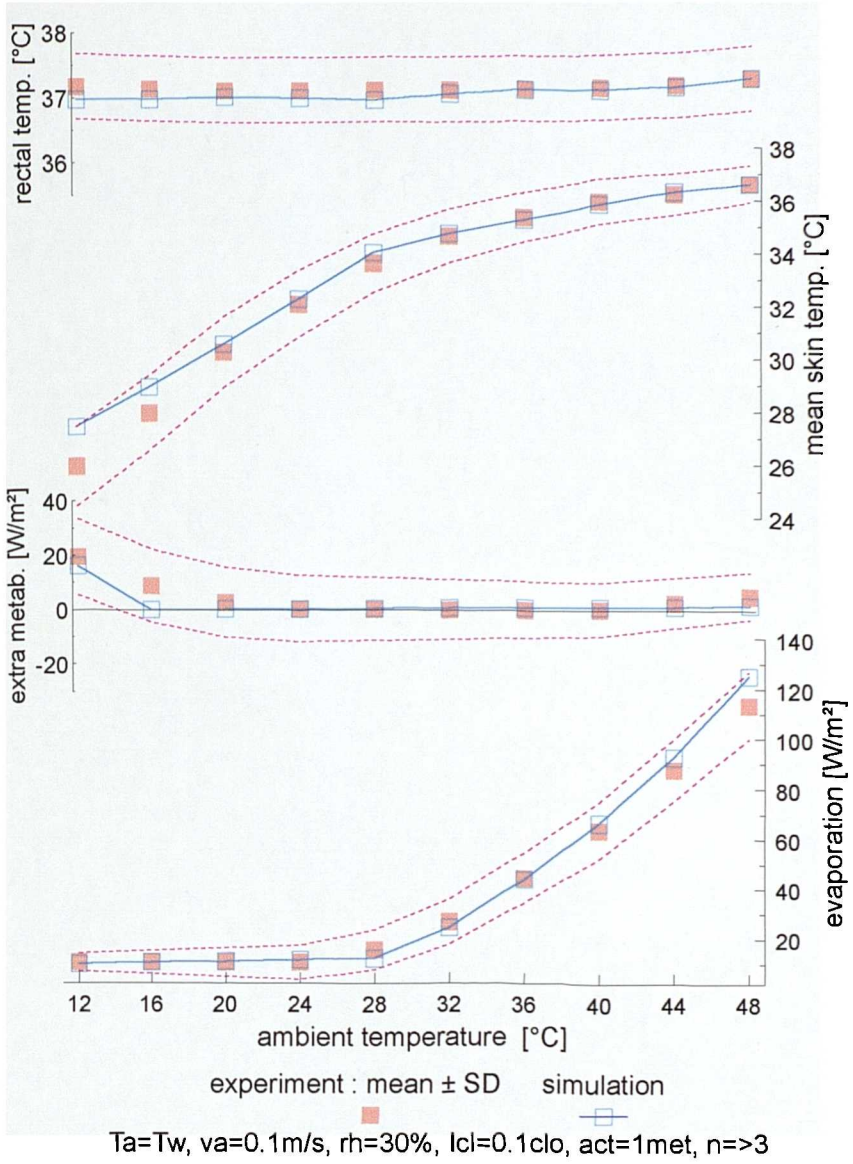

Fig.4.30

Skin temperature, body core temperature and regulatory responses as measured and as predicted by the model over a wide range of environmental conditions [57] [75]. Each data point represents a separate 1-hr exposure to the particular ambient temperature.

As can be seen, the mean skin temperature rises in a non-linear fashion. It is elevated from about 26°C at T_a=12°C to about 34°C at T_a=28°C. In warm and hot environments, the temperature rises less rapidly with increasing ambient temperature and reaches about 37°C at T_a=48°C. This trend, as well as the absolute values, were also predicted by the model although there were some discrepancies at the lowest ambient temperatures. In contrast to skin temperature, the rectal temperature remained

constant (to within 0.5K) over the range of 12°C<T_a< 48°C, the model predicted this behaviour. The metabolic heat production rate remained relatively constant over a wide range of ambient temperatures; it began to rise at about T_a=16°C (measurement) and T_a=12°C (predicted). There was also a very slight increase in metabolism in the hot (caused by the Q_{10}-effect). The evaporative heat loss, including respiration, skin diffusion and sweating in the warmth increased non-linearly with ambient temperature reaching ten times the basal value. The model also reproduced this regulatory behaviour (including the onset of sweating).

4.7 Discussion of the Active System Model

In sections 4.3 and 4.4 a statistically founded active system for a wide range of boundary conditions was developed. The analysis of already published thermal and thermoregulatory responses of about 140 test persons in 27 different experiments covering a range of environmental temperatures between T_a=5°C and T_a=50°C, and exercise intensities between *act*=0.8met and *act*=10met led to a non-linear, temperature-based, active system model. This is summarised schematically in ***Fig.4.31***.

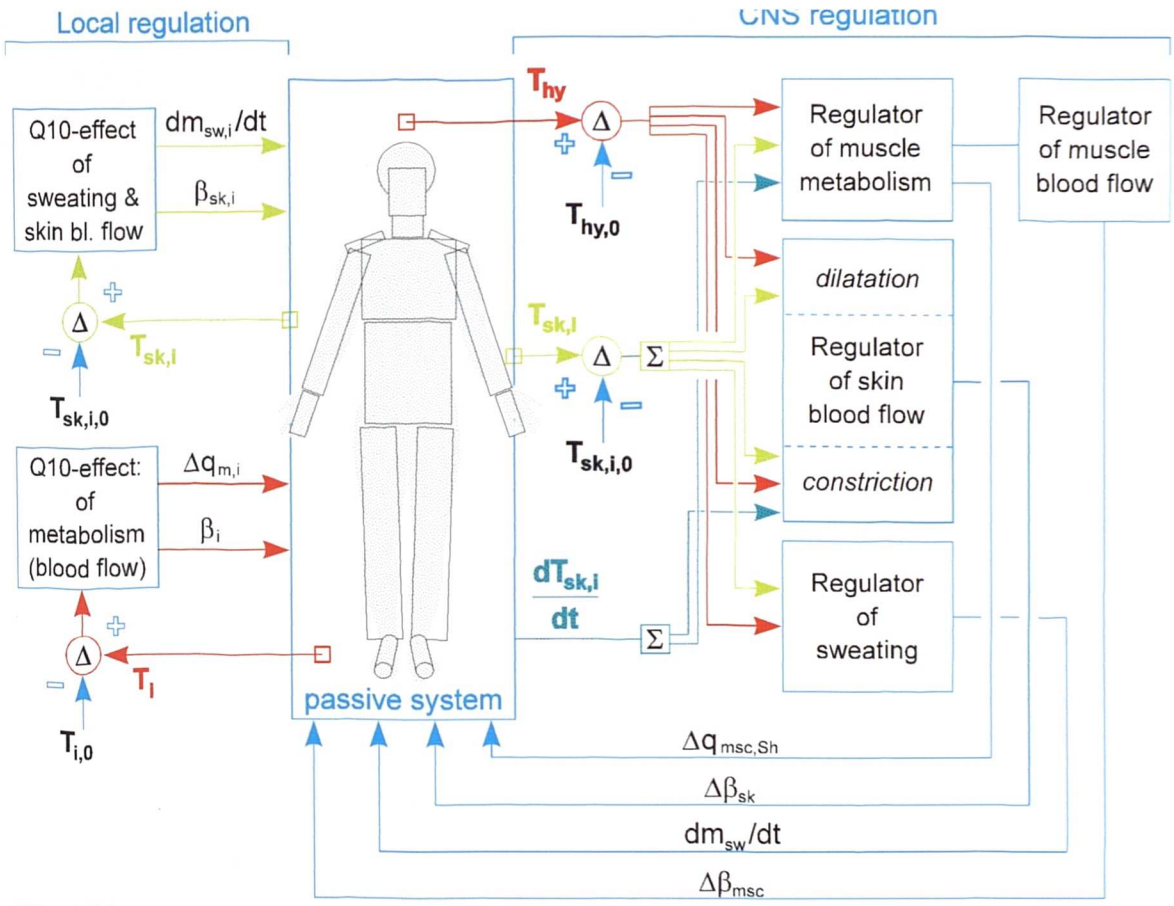

Fig.4.31

Block diagram of the active system. The central nervous system (CNS) thermoregulation accounts for overall changes in muscle metabolism $\Delta q_{msc,Sh}$ [W m^{-3}] via shivering (and the corresponding changes in muscle blood flow $\Delta\beta'_{msc}$), skin blood flow $\Delta\beta'_{sk}$ [W K^{-1}] via vasodilatation and vasoconstriction, and skin moisture extraction dm_{sw} dt [g min^{-1}] via sweating. The model uses temperatures of the skin (T_{sk} [°C]) and of the head core (hypothalamus, T_{hy} [°C]) as well as the rate of change of skin temperature (dT_{sk} dt [K h^{-1}]) as input signals into the regulatory centre. Local skin temperatures $T_{sk,i}$ are substracted (Δ) from the corresponding setpoint values $T_{sk,i,0}$ and form error signals $\Delta T_{sk,i}$ [K]. Positive error signals represent 'warm' cutaneous recepetors, negative differences represent 'cold' thermoreceptors. The local afferent signals $\Delta T_{sk,i}$ are summed (Σ) to the integral signal from the skin ($\Delta T_{sk,m}$) which governs - together with ΔT_{hy} [K] - the four responses of the CNS-regulation, eqs. (4.19) (4.24) (4.28) (4.32). The local autonomic regulation utilizes local skin and tissue temperatures, $T_{sk,i}$ and T_i, to modify nodal sweat rates, $dm_{sw,i}$ dt (eq.(4.29)), skin blood flows, $\beta'_{sk,i}$ (eq.(4.25)), tissue metabolic rates, $q_{m,i}$ (eq.(4.21)), and blood flows, β'_i (eq.(4.22)) by the Q_{10}-effect.

Skin temperature was found to play a major role in human thermoregulation for the entire spectrum of environmental conditions. Cold cutaneous receptors (simulated by error signals $\Delta T_{sk,m}$<0) were found to be the source of afferent signals which may elicit and govern regulatory responses against cold, ie. vasoconstriction, *Cs*, and shivering, *Sh*. This is in agreement with various experimental findings [11] [184]. An inhibiting effect of 'cold' cutaneous receptors (which also has experimental verification, eg. [11]) was assessed for the *Sw*-variable. In contrast to some literature sources [11], the present study indicated a substantial role for 'warm' skin thermoreceptors, ie. error signals $\Delta T_{sk,m}$>0. In the model, positive $\Delta T_{sk,m}$-signals are involved in the regulation of both sweating and vasodilatation. Experimental support of this exists, eg. in [120] [21].

Negative rates of change of the mean skin temperature, $dT_{sk,m}/dt$, were found to govern the dynamic behaviour of shivering and vasoconstriction. In the model, $dT_{sk,m}/dt$ appears as the product together with $\Delta T_{sk,m}$ in corresponding control equations. Such a multiplicative interaction between a static (temperature) and a dynamic (rate of change of temperature) component of a thermal stimulus characterizes also the discharge behaviour of cutaneous thermoreceptors [88]. The approach ensures that shivering (and *Cs*) is restricted to conditions where $\Delta T_{sk,m}$< 0 and is not started at any arbitrary occurrence of negative $dT_{sk,m}/dt$-signals under any environmental conditions.

The hypothalamus temperature signal, ΔT_{hy}, was found to be an important afferent signal for controlling regulatory responses against warmth, ie. vasodilatation, *Dl*, and sweating, *Sw*. This agrees with common physiological knowledge of the role of body core temperature in human thermoregulation (eg. [88] [11]). The *Sh*-response also showed a statistically provable dependence on ΔT_{hy} although the resultant sensitivities fluctuated erratically from one experiment to another. However, no clear influence of ΔT_{hy} was discovered for the *Cs*-response using methods of linear regression analysis.

The analysis of the *Sw*-response for sudden changes in internal temperature, eg. as experienced during sudden changes in periods of heavy work and recovery, indi-

cated that the rate of change of the hypothalamus temperature dT_{hy}/dt may represent a further afferent signal into the regulatory centre. Wissler [201] modelled rapid changes of sweating during transient exercise using this signal. Also, the addition of this signal into the present sweating model provided, in some cases, improved predictions of sweating - causing sweat rates to rise within shorter time-periods during the onset of exercise and causing massive suppression of Sw after terminating the exercise. Unfortunately, this behaviour was not always appropriate (see ***Fig.B.60***) so the dT_{hy}/dt signal was removed from the present active system. Nevertheless, this signal seems to be an afferent signal which affects transient thermoregulation in extraordinary conditions of such changes from heavy work to recovery and vice versa. The implementation of this signal in statistically founded models, however, will require more data from independent experiments.

In addition to the skin and the hypothalamus, reports of further thermosensitive sites are contained in the literature (see chap. 2). Afferent signals from receptors located in muscles, however, do not seem to play an important role in the overall regulatory behaviour of man either in the cold or under hot stress. Although the *mean* muscle temperature, $T_{msc,m}$, exceeded the head core temperature (on some occasions by about 1K) no regulatory effects were observed which would justify the implementation of a temperature error signal from muscles, $\Delta T_{msc,m}$, in addition to ΔT_{hy} (and $\Delta T_{sk,m}$). Similar conclusions were drawn by Nadel et al. [165].

In contrast to earlier models [177] [69] [132] [198], the present active system is essentially non-linear. Some evidence of non-linear shivering is found in [11], and non-linear sweating in eg. [68] [77] [78] (quoted in [80]). Non-linearities in vasomotor reactions have been noted in [208].

The non-linearity of the present active-system was derived by considering thermoregulatory behaviour over a wide range of environmental and internal conditions. It is a result of the temperature dependency of (linear-) regression coefficients as found in the supra-experimental analysis. Responses measured in individual experiments - each representing a limited range of boundary conditions - could often be fitted satisfactorily by linear regression relationships. These coefficients, however, showed a

temperature-dependency when they were considered over a wide range of bodily thermal states. The shapes of the coefficient-curves, which are common to all responses, also bear some likeness to curves of thermally stimulated electrical events within the 'operational range' of single afferent nerve fibres [88]. So, one can hypothesize that some characteristics of man's thermoregulatory behaviour are due to the thermosensitivity-properties of warm and cold-sensors.

The (steady) *Sh*-response is plotted over $\Delta T_{sk,m}$ and $\Delta T_{sk,m}$ in ***Fig.4.32*** and ***Fig.4.33***, respectively. The non-linear *Sh*-curves in ***Fig.4.32*** are similar to those observed experimentally by Benzinger [11]. The model's shivering action is not responsive to punitive signals from 'warm' cutaneous receptors [136], ie. for $\Delta T_{sk,m}>0$. The onset of shivering is predicted for a mean skin temperature $T_{sk,m}<29°C$ but depends on the actual level of body core temperature. Benzinger stated that neither of the two afferent signals, ie. $\Delta T_{sk,m}$ or ΔT_{hy}, can elicit shivering alone. This means, that punitive signals (ie. negative temperature error signals) from both the skin and the hypothalamus must be present simultaneously to initiate shivering. The results of the present study contradict Benzinger's finding. It can be seen from ***Fig.4.16*** and ***Fig.4.17*** (see also ***Fig.4.27***) that entry into a cold room always causes an increase in the internal temperature (ie. $\Delta T_{hy}>0$; both as measured and as predicted by the model) for a prolonged period of time. Nevertheless, appreciable shivering occurs.

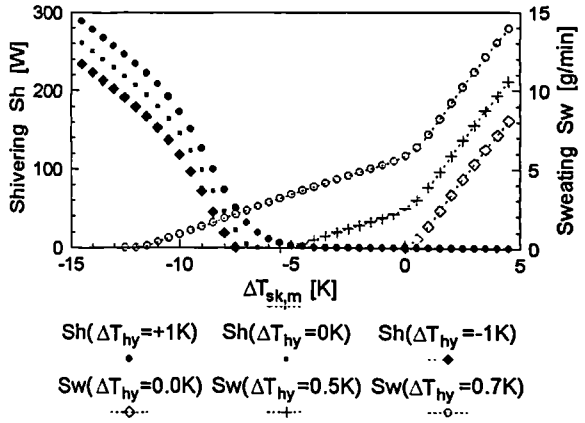

Fig.4.32

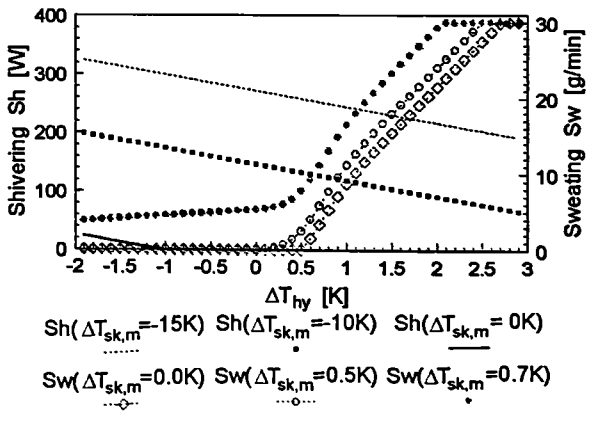

Fig.4.33

The responses of shivering (Sh) and sweating (Sw), predicted using eq. (4.19) and eq. (4.28), respectively, are plotted against the temperature error signal from the skin $\Delta T_{sk,m}$ (for three different body core temperatures), and against the temperature error signal from the head core ΔT_{hy} (for three different skin temperatures).

The *Sh*-response is proportional to ΔT_{hy} (***Fig.4.33***), and the sensitivity of *Sh* to ΔT_{hy} (ie. the $b_{sh,hy}$-coefficient) is of the same magnitude as that found by Timbal et al. [184] for subjects immersed to cold water. The proportional dependency of *Sh* on ΔT_{hy} suggests that positive ΔT_{hy}-signals have an inhibitory effect to shivering. When sweating is elicited due to $\Delta T_{hy}>0$ (eg. when working in a cold environment) *Sh* is set to zero.

In the literature [137] [178], sweating is usually described as a linear function of both the body core- and the mean skin temperature. Also the *Sw*-variable can be considered as linear over sections of the $\Delta T_{sk,m}$-scale (see ***Fig.4.32***). In the present model, the non-linearity of sweating with respect to the mean skin temperature is primarily a result of appreciable differences between the intensity with which 'cold' and 'warm' skin temperatures affect sweating, whereas - in physiological terms - the sensitivity of *Sw* to cold skin receptors is lower than to warm skin receptors. Thus, in cold environments the *Sw*-regulator is increasingly oriented toward elevating body core temperatures while afferent signals from the periphery are discriminated. Similarly, a minor influence of internal temperature on *Sw* results for negative ΔT_{hy}-signals while there is a steep rise of sweating for $\Delta T_{hy}>0.5$K (***Fig.4.33***) until a maximum sweat rate of 30 g min^{-1} is reached.

The role of warm skin thermoreceptors in elevating sweat excretion in the model contradicts some literature reports. According to Benzinger [11], who's hypothesis has found widespread acceptance, elicitation and elevation of sweating is solely governed by the central, but not by the peripheral, 'warm'-sensitive organ. Thus, skin temperatures would exert an influence upon the rate of sweating only by depression, namely, when the mean skin temperature falls below 33°C. However, during sudden changes in environmental temperatures towards hot conditions, sweating was evidently increased by rising skin temperature. This phenomenon occurred even though body core temperatures were falling as a result of (evaporative) cooling of the vasodilated skin bood flow. This somewhat paradoxical behaviour was repeatedly observed experimentally (eg. ***Fig.4.23***, ***Fig.B.56***) and is reproduced also by the model.

The *Cs*-response is a primary function of ('cold') skin temperature (***Fig.4.34***) whereas the effect of central temperature on the model's vasoconstriction action appears to be negligible (***Fig.4.35***) [164]. As for the shivering-response, *Cs* is independent of the drive from 'warm' cutaneous receptors (the effects of positive $\Delta T_{sk,m}$-signals on skin blood flow are governed by the *Dl*-variable in the model). The model's vasoconstriction action increases proportionally with the mean skin temperature for $\Delta T_{sk,m}$< -10K. Effectively, however, the *Cs*-response reduces *SBF* to a minimum of about 10% of the basal value. This is, because the distribution coefficients a_{cs} (see ***Tab.B.1*** in appx. B.1) attribute the bulk of the overall *Cs*-variable to the extremities, whereas the skin blood flow of the trunk remains almost unchanged by the *CNS*-governed response. This *Cs*-distribution over the body surface can be interpreted from the thermophysical point of view. Namely, the trunk's insubstantially suppressed[1)] *SBF* can operate as a sort of *active insulation system* in the cold by which the skin surface is heated to minimize temperature gradients within the trunk core, thereby sustaining uniform temperatures over wide regions in the trunk. This in turn might be a condition for the optimal biological function of organs in the trunk.

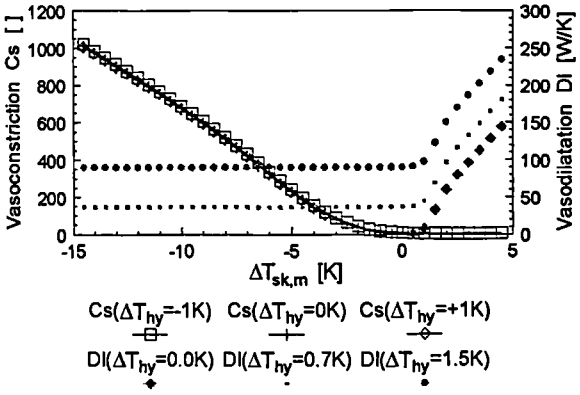

Fig.4.34

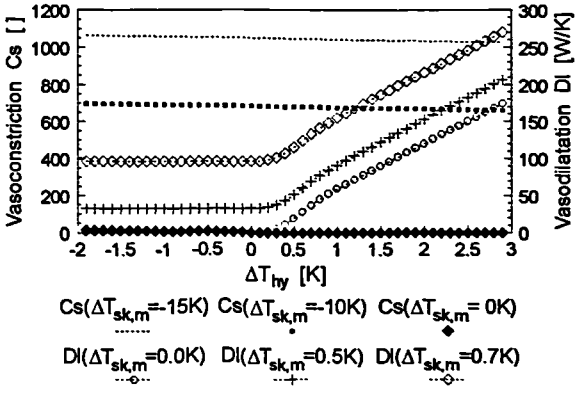

Fig.4.35

Cutaneous vasomotor responses Cs and Dl, calculated using eq. (4.24) and eq. (4.32), respectively, are plotted against the temperature error signal from the skin $\Delta T_{sk,m}$ (for three different body core temperatures), and against the temperature error signal from the head core ΔT_{hy} (for three different skin temperatures).

In contrast to *Cs*, the model's *Dl*-response depends on both positive $\Delta T_{sk,m}$- and positive ΔT_{hy}-signals and is independent of negative temperature error signals from the

1) local constriction via the Q_{10}-effect remains active

skin and from the body core (***Fig.4.34*** and ***Fig.4.35***). Negative $\Delta T_{sk,m}$-values ('cold' skin receptors) exert an influence upon *SBF* exclusively via vasoconstriction in the model [164]. The importance of core temperature in vasodilatation is well recognized (see eg. [88]). However, the control equation of *Dl* shows a stronger dependence on skin temperature than found experimentally (for overheated subjects with both high skin and high body core temperatures [208]). One reason for this might be the fact [164] that at high body core temperatures and high skin temperatures there is an inhibited (or zero) influence of skin temperature on *SBF*. The present model of the *Dl*-response as a function of skin temperature was developed using experiments where little or no elevation in body core temperature occurred. The analysis has shown that the maintenance of constant internal temperature after step changes into hot environments was due to vasodilatation associated with sweating.

Each vasomotor response showed similarities in its dependence on afferent signals with their associated response, ie. *Cs* with *Sh* and *Dl* with *Sw*. This can be interpreted as a sort of coupling between related responses. In fact, in the absence of dilatation, the cooling effect of sweating in hot conditions, cannot be as effective as when a simultaneous elevation of *SBF* is able to supply the skin with heat carried by blood from within the body core.

5 MODELLING THERMAL COMFORT

5.1 Introduction

The challenge of the work was to create a computer model of man's thermal and perceptual response to thermal influences within a wide range of boundary conditions and a variety of different thermal situations. One way of judging a given set of thermal influences is to examine their combined effect to the bodily thermal strain as indicated by body temperatures and the associated regulatory reactions. In addition, it is often necessary to have information on responses of the human warmth sense to quantify how a given set of thermal circumstances is perceived.

Body core temperatures, for instance, are useful indicators of thermal stress and can be compared with health and safety limits [199]. In thermally less stressful situations, however, indices of human thermal perception are more useful measures of thermal effects on man than temperatures inside the body. Therefore, in addition to models of the passive and the active system, a predictor which is an index of human thermal feelings is required.

In European countries and elsewhere, the Fanger model [46] represents the current standard in thermal comfort theory [94]. This steady state model is based on a *'physical'* consideration of comfort, whereas the thermal sensation is described in terms of 'calorimetric' variables, ie. a (hypothetical) heat load on the body. Fanger did not consider the role of thermoregulatory effects in the bodily thermal state and thus in the perception of thermal (dis)comfort. Physiological research seems to contradict the 'philosophy' of a *calorimetrically* oriented human thermal perception, indicating that man's thermoreception and thermoregulation are based on *temperature* as a physical quantity (see chaps. 2 and 4). For these reasons the model is restricted to steady state conditions near the zone of thermal neutrality [94]. The model is not valid for non-moderate (and asymmetric) climatic conditions, transients, and/or activity levels higher than 3 met.

A conceptually different method of predicting thermal (dis)comfort was developed by

Gagge [61]. Gagge used a simple two-node (core and shell) model of human thermoregulation to obtain the temperature of a standardized environment where subjects would perceive the same level of (dis)comfort as the actual climate. Thermal sensation (*TSENS*) was described as a function of *climatic* variables which was found experimentally for sedentary subjects [158]. Another comfort variable, ie. *DISC*, was used to predict discomfort in warm and hot environments as a function of the skin wettedness. Since the 'neutral' skin wettedness [46], as well as the *sensitivity* of thermal sensation and discomfort to environmental influences, varies with the activity level [127] [46], the Gagge comfort model is restricted to conditions of light (sedentary) work. Similarly, the model is not valid for environmental transients (where specific dynamic comfort effects occur, see section 5.4.3).

Azer et al. [7] also predicted thermal (dis)comfort by means of a two-node model of human thermoregulation. The thermal sensation was assumed to be a function of skin 'conductance' and skin wettedness for which 'neutral' values were defined - in contrast to the Gagge model depending on the amount of heat production, ie. activity level. Since skin conductance, skin wettedness, and activity level represent calorimetric variables, the Azer concept - like the Fanger model - has to be interpreted as being oriented toward a 'physical' consideration of thermal comfort rather than the real nature of comfort.

The following sections are concerned with the development, verification, and validation of a new comfort model which is based on physiological effects. The opportunity to consider the *dynamic* behaviour of the human thermal system was of special importance for modelling comfort within a wide range of climatic conditions, different types of transient circumstances, and for studying the nature of thermal comfort during exercise. Furthermore, the multi-segmental model of human thermoregulation described in chapters 3 and 4 opens doors for future studies of the perception of local thermal (dis)comfort by means of one, common, simulation model.

5.2 Methods of Model Development

Most applied work on thermal comfort has dealt directly with the relationship between sensory estimates and features of the thermal environment. The nature of human thermal comfort, however, is based on physiological principles. Man cannot sense ambient temperature directly. The sensation of temperature and comfort arises from the actual thermal state of the body as detected by thermoreceptors (see chap. 2).

The thermal state of the human body is a result of several thermophysical and regulatory processes occurring within the body and at its periphery. Any comfort model which produces predictions based only on parameters of the thermal environment will therefore be of limited validity. For instance, the effect of recent history on an individual's comfort perception cannot be assessed. An overheated individual (eg. due to recent exercise or prolonged heat exposure) will give different judgements about the thermal environment than an individual who had not previously undergone hot stress conditions. Thermophysiological parameters, ie. parameters of the actual thermal state of the human body, appear therefore to be of special relevance when extending comfort predictions to *transient conditions* and to a *wide range* of boundary conditions - including non-moderate situations where thermoregulatory adjustments and changes in the bodily heat content occur.

One challenge of theoretical work on thermal comfort is to *generalize* experimental results for arbitrary thermal situations. Fanger [46], for example, was able to generalize Nevins' experimental observations [141] from conditions of equal air and radiant temperatures to arbitrary combinations of environmental parameters by utilizing (hypothetical) heat loads on the human body. By extension of this generalization, the *first principles* method of considering the dynamic behaviour of the human thermal system, enables different transient situations to be treated in a common manner. Any temporal change, eg. in a boundary condition parameter, will elicit the same transient comfort sensation as any other boundary factor which causes the same dynamic change in the body's thermal state. Experimentally obtained knowledge about comfort during transient changes (eg. in air temperature) can so be extended to other transient changes (eg. in radiant temperature, air velocity, solar radiation, etc.)

or even arbitrary combinations of them.

The present model was used as an interface to comfort experiments to provide the necessary physiological data. The model is capable of simulating all parameters of bodily thermal state which might be of importance for modelling comfort within a wide range of boundary conditions and for a variety of different thermal situations. The model predicts dynamically skin-, muscle-, and body core-temperatures, rates of change of body temperatures, heat fluxes through the skin, parameters of sweating (sweat liquid production, wetted skin area, evaporative weight/heat loss) and other regulatory responses from phenomena of human heat transfer occurring within the body and at its periphery. All parameters are also predicted for conditions when the body is not in thermal balance with the environment, and when considering inhomogeneities occurring within the body and at its surface (see chapter 3 and 4).

Thus, the results of comfort experiments described in the literature were evaluated for *standardized* human thermal behaviour as predicted by the present model. In this procedure, each individual experiment was re-simulated for the specific boundary conditions and the duration of the experiment. Analysis of afferent signals was performed in order to investigate the nature of thermal (dis)comfort due to a variety of different boundary conditions. Methods of statistical correlation analysis were employed for this purpose and for the purpose of describing comfort perception in quantitative terms.

The *general* thermal comfort arising from the *overall* thermal state of the body was the subject of investigation in the present study. It should be noted that under asymmetric conditions *local* discomfort may be perceived as a further response - in addition to the general thermal (dis)comfort (see chap. 2). The modelling of this specific response, which does depend on the state of general comfort [88], should, however, be the subject of more ambitious future work.

In common with previous modelling work [7] [46], thermal comfort was dealt with in terms of the *Thermal Sensation (TS)* as defined by the so called *ASHRAE-scale* and modified by Fanger, ***Fig.5.1***. Most experimental work has been conducted to investi-

gate the perceived responses of occupants in terms of thermal (or temperature) sensation. As a result, currently, the largest experimental data base is available for this variable[1].

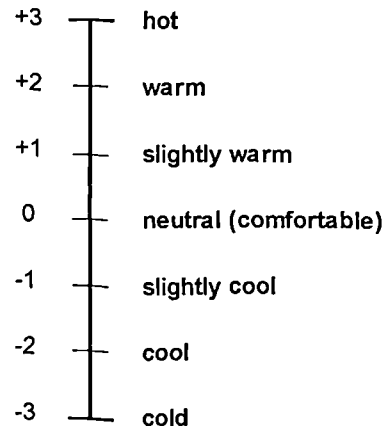

Fig.5.1
The 7-point ASHRAE-scale

According to Hensel [88] *"Temperature sensation is a rational experience that can be described as being directed toward an objective world"*. On the other hand *"thermal comfort is an emotional ... experience referring to the subjective state of the observer"*. Thus, thermal sensation, as a more objective measure of the impact of thermal influences on man, appears to be the preferred quantity for thermal modelling rather than (dis)comfort itself which is affected more strongly by subjective and perhaps non-thermal factors.

For these reasons, the only experiments used to develop the present comfort model were those in which subjects judged according to the 7-point ASHRAE-scale. It should be noted that in the literature, an enhanced, 9-point scale, was also sometimes used. However, the results of these experiments, eg. Rohles et al. [161], and Jones et al. [100], showed incompatibilities with sensation votings made using the 7-point scale, so they were excluded from this study. As noted by McIntyre [126], Miller [131] found *"that in general people cannot deal with more than about seven levels of*

---

[1] In the Fanger model the original seven-point ASHRAE-scale running from +1 to +7 was modified to indicate sensations of 'warm' and 'hot' by positive *TS*-values, 'cool' and 'cold' by negative *TS*-values, and the state of thermal neutrality by *TS=0*, see the left hand side of Fig.5.1. This modification was also used in the present model.

sensation without confusion".

There were further criteria for selecting the appropriate comfort experiments from literature. Only *air exposure*, which is the primary area of the model's intended application, was analysed. Results from climate chamber experiments were used because, in contrast to field studies, boundary conditions, ie. climatic variables, levels of activity and clothing insulation, were carefully controlled and so numerous sources of uncertainty were eliminated.

An aim of the study was to develop a statistically well founded thermal comfort model. Therefore, extensive experimental series (Nevins et al. [141] Rohles et al. [158] and McNall et al. [127]) involving a large number of (unacclimatized) test-persons were used to formulate the model.

In these experiments, sensation votings of sedentary and working subjects were reported for a wide range of environmental conditions. To extend the available range of boundary conditions for thermally stressful situations and heavy work, experiments conducted by Gagge et al. for sedentary [57] and exercising subjects [58] were added to the analysis.

During transient changes in boundary conditions dynamic comfort effects occur which do not appear under (quasi-) steady-state conditions. Thus, the experiments of Gagge et al. [57] were analysed for dynamic comfort behaviour during sudden changes in ambient temperature both in a direction away from neutral conditions (toward both cold and warm conditions), and in a direction from cold and hot environments toward thermal neutrality.

In section 5.3 each individual experiment is re-simulated, and the simulation results are discussed. The development of model is described subsequently for a wide range of steady state environmental conditions and sedentary activity, conditions of exercise, and for transient conditions in section 5.4. In section 5.5, the complete comfort model is tested using experiments described in section 5.3, validated using independent experiments in section 5.7, and discussed in section 5.8.

5.3 Simulating Thermal Comfort Experiments

5.3.1 Sedentary Subjects in Steady Environments

The experimental series of Nevins et al. [141] and Rohles et al. [158] provided the major data source for the present comfort model. In these extensive climate chamber tests, 1600 (800 male, 800 female) college students were involved. The subject of investigation was the effect of steady ambient temperatures on the thermal sensation of *sedentary* subjects. Ambient temperatures and relative humidity ranged between $15.6°C \leq T_a \leq 36.7°C$, and $15\% \leq rh \leq 85\%$, respectively. The subjects were clad in standardized clothing, the so called KSU-uniform.

Nevins [141] investigated the responses of 720 sedentary subjects in the narrow range of temperatures from 18.9°C to 27.8°C. The results of these mild exposures were generalized by Fanger [46] from conditions of equal air and radiant temperatures to arbitrary combinations of environmental parameters. Rohles et al. [158] extended the range of Nevins' moderate environments downward to 15.6°C and upward to 36.7°C. With this extension, nearly the whole range of the ASHRAE seven point scale was covered.

5.3.1.1 Experiments

In the experiments groups of ten subjects (5 males, 5 females) were exposed to 20 different ambient temperatures, T_a:

15.6 16.7 17.8 18.9 20.0 21.1 22.2 23.4 24.4 25.6
26.7 27.7 28.9 30.0 31.1 32.2 33.3 34.4 35.6 and 36.7 °C.

At each temperature, eight different relative humidities were examined:

15 25 35 45 55 65 75 and 85%.

Thus, all combinations of ambient temperature and relative humidity constituted 160 different 3-hr experiments.

Before each exposure, the subjects put on the prescribed clothing and spent about 30 minutes in a conditioned pretest room. After entering the test chamber the subjects sat at tables and were allowed to read, talk quietly or play cards. One hour later they gave their first votings on thermal sensation and they repeated this reporting on each subsequent half hour.

Rohles et al. presented their observations in tabular form. Here, the results are shown graphically to illustrate the existence of some non-linear effects which occur at the ends of the investigated temperature spectrum which were not noted by the authors.

Observed mean thermal sensation votings of a group[1)] of 10 subjects are plotted against ambient temperature in ***Fig.5.2***. Sensation votings given after the first, second and third hour of exposure are plotted for each ambient temperature and relative humidity.

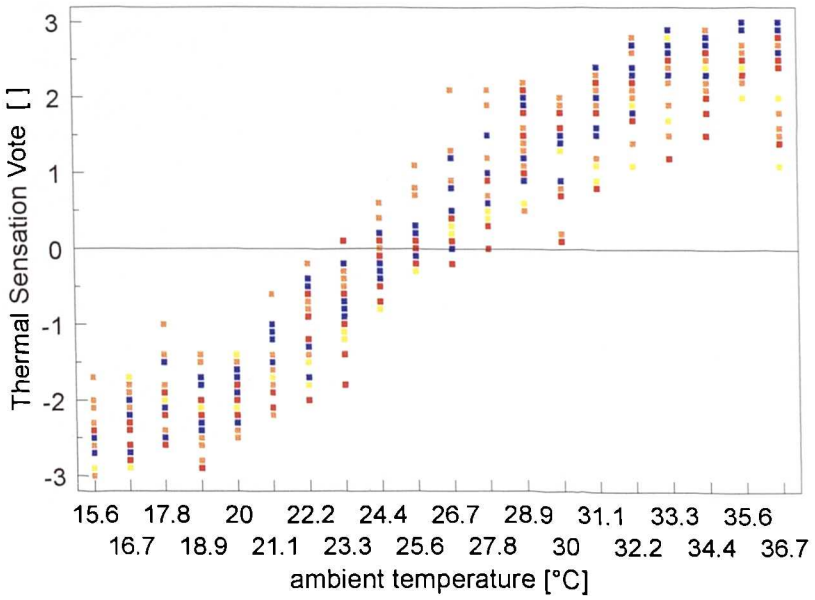

Fig.5.2

Mean thermal sensation of groups of ten subjects (5 males, 5 females) voted after 1, 2, and 3 hours of exposure for relative humidities ranging between 15% rh 85% [141][158].

1) There were no statistically significant differences (except for the first hour of exposure) between votings of male and female subjects.

Within the range of moderate environmental temperatures investigated by Nevins et al., subjects' thermal sensations can be considered to be proportional to ambient temperature. However, outside the mild zone the votings showed deviations from the linear trend by approaching asymptotically the lower and the upper limit of the thermal sensation scale.

The impact of relative humidity on thermal sensation (TS) is shown in ***Fig.5.3***. The data represents time-averaged values of the votings given after t=1.0, 1.5, 2.0, 2.5, and 3.0 hours of exposure. For simplicity, only values for rh=15, 35, 55, and 75% are drawn in ***Fig.5.3***. Since even these four trends of *TS* appears to be quite erratic, two integral curves as averaged for *rh*<50% and *rh*>50%, are plotted to demonstrate more clearly the partial effect of relative humidity on *TS*. The curves indicate that relative humidity had little influence on the temperature feelings of the subjects. However, the role of relative humidity was more pronounced at the warm end (T_a>25.6°C) than on the cold end of the temperature spectrum.

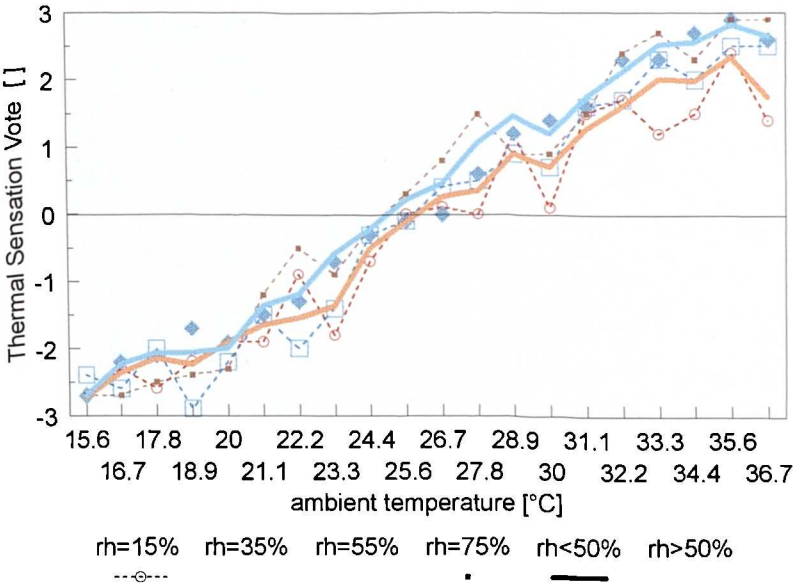

Fig.5.3

The effect of relative humidity on thermal sensation. The plotted TS-values are averaged over exposure time.

The time-dependency of subjects' sensation votings as averaged over the eight different relative humidities is shown in ***Fig.5.4***. In general, there was a slight decrease

in TS with time even for 'warm' temperatures.

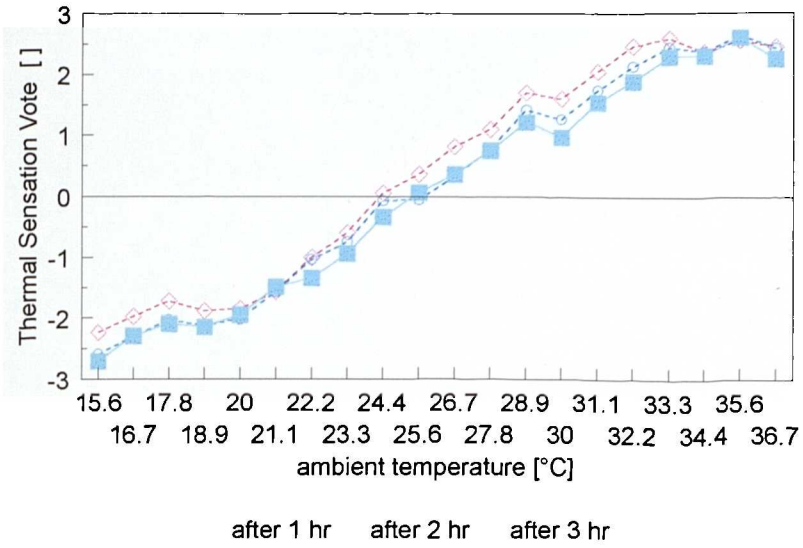

Fig.5.4

The impact of exposure time on thermal sensation. The plotted TS-values are averaged over different relative humidities.

5.3.1.2 Simulation

The aim of the simulations was to achieve proper characterisation of subjects' thermophysiological behaviour in the experimental tests. Thus, each experiment was simulated by detailed modelling of the particular boundary conditions. These consisted of ambient temperatures (air temperature, and the mean temperature of the surrounding surfaces), air velocity, relative humidity, the activity level actually performed, and local characteristics of clothing ensembles. These parameters (except clothing) represented time-dependent input variables to the model.

Each of the 160 different exposures was simulated separately using a thirty-minute pretest period followed by a 180-minutes steady state exposure to the particular combinations of ambient temperature and relative humidity. Simulations were performed for time steps of Δt=5min.

The pretest room conditions were assumed to be common for all exposures and consisted of room temperatures of T_a=T_W=24.5°C, v_a=0.17 m s^{-1}, and rh=50%. The activity level of the subjects was taken to be act=1.2 met: a value slightly higher than that for quietly seated subjects.

Immediately before entering the test room, ie. for simulation time -5<t<0 min., the activity level was increased to act=2.0 met to account for the phase of walking from the pretest room into the test chamber. In the experiment, the persons were seated and had an activity level between 1.0 and 1.1 met. In an attempt to simulate the impact of ambient temperature on subjects' activity, an activity level of 1.1 met was used for exposures to T_a<22°C. For exposures of T_a>22°C, an activity level of act=1.0 met was assumed. The mean wall temperature was set equal to the air temperature. An emissivity coefficient of 0.93 was used for the envelope to simulate the heat exchange of the body with the environment by long wave radiation. Relative humidities were chosen according to the experimental plan. The experimental report provided only rough information on air velocity, ie. v_a≤0.15 m s^{-1}. In the simulations a mean air speed of v_a= 0.12 m s^{-1} was used.

The so called KSU uniform worn by the subjects in the experiments consisted of cotton twill shirts and trousers, cotton undershorts, and woollen sweat socks without shoes. The overall clo-value, as measured using a thermal copper manikin, was 0.6 clo [159]. The overall moisture permeability was estimated to be i_{cl} = 0.34 [122].

The individual garments of the uniform were modelled taking into account their local, ie. garment-oriented characteristics, as calculated from measurements by McCullough et al. [122] [121] and as described in chap. 3. The data on the intrinsic clothing insulation, I_{cl}^*, local clothing area factor, f_{cl}^*, and the local moisture permeability index, i_{cl}^* of the individual items of clothing are summarised in ***Tab.5.1***. A long wave emissivity of ε=0.95 was used for all garments - a commonly used value in literature. The *overall* resistances of the KSU-uniform, I_{cl} and i_{cl}, were calculated by the model from the individual values for each clothing item, and the dry and sensible heat losses to the environment from each body part (as described in chap.3). These

resulted in a value for I_{cl} of 0.59 clo, and for i_{cl} of 0.34[1)].

Garment	I_{cl}^* [clo]	f_{cl}^* [ ]	i_{cl}^* [ ]	body elements covered
twill shirt (cotton) long sleeved	0.570	1.23	0.478	shoulders, thorax, abdomen, arms
undershorts (cotton) knit	0.211	1.04	0.413	abdomen
trousers, loose denim	0.596	1.18	0.485	abdomen, legs
socks (wool) knit	0.686	1.18	0.445	feet
chair	0.600	1.27	0.300	(posterior) legs

Tab.5.1

Local, ie. garment-oriented, insulation characteristics of clothing item s for the KSU-uniform. I_{cl}^*: local intrinsic clothing insulation, f_{cl}^*: local clothing area factor, i_{cl}^*: local moisture permeability index.

In the experiments the subjects sat on chairs. The impact of a chair on the heat loss of the subjects was considered in the simulations. The chair was modelled as 7 mm of wood (λ= 0.15 $W m^{-1}K^{-1}$ [39]) and 5mm of foam (λ= 0.04 $W m^{-1}K^{-1}$ [39]) and this was applied to the posterior sectors of the leg body elements, see ***Tab.5.1***. The overall characteristics as calculated by the model for the KSU-uniform with the chair resulted in I_{cl}= 0.68 clo, and i_{cl}=0.28.

Simulated parameters of the bodily thermal state after 3 hours of exposure are shown against ambient temperature in ***Fig.5.5*** for three different relative humidities. As can be seen, the internal (hypothalamus) temperature predicted by the model varied only moderately with ambient temperature, and was maintained within 0.5K over a range of about $\Delta T_a \approx$20K. This constancy was achieved by thermoregulatory adjustments of skin blood flow, *SBF*, and skin evaporation in the warm. Increases in metabolic heat generation (shivering) were not predicted even for the coldest conditions of T_a=15.6°C.

---

1) determined for T_a=22.2°C and *rh*=50% [121]. The *overall* values may vary slightly with ambient temperature due to adjustments of the human thermoregulatory system.

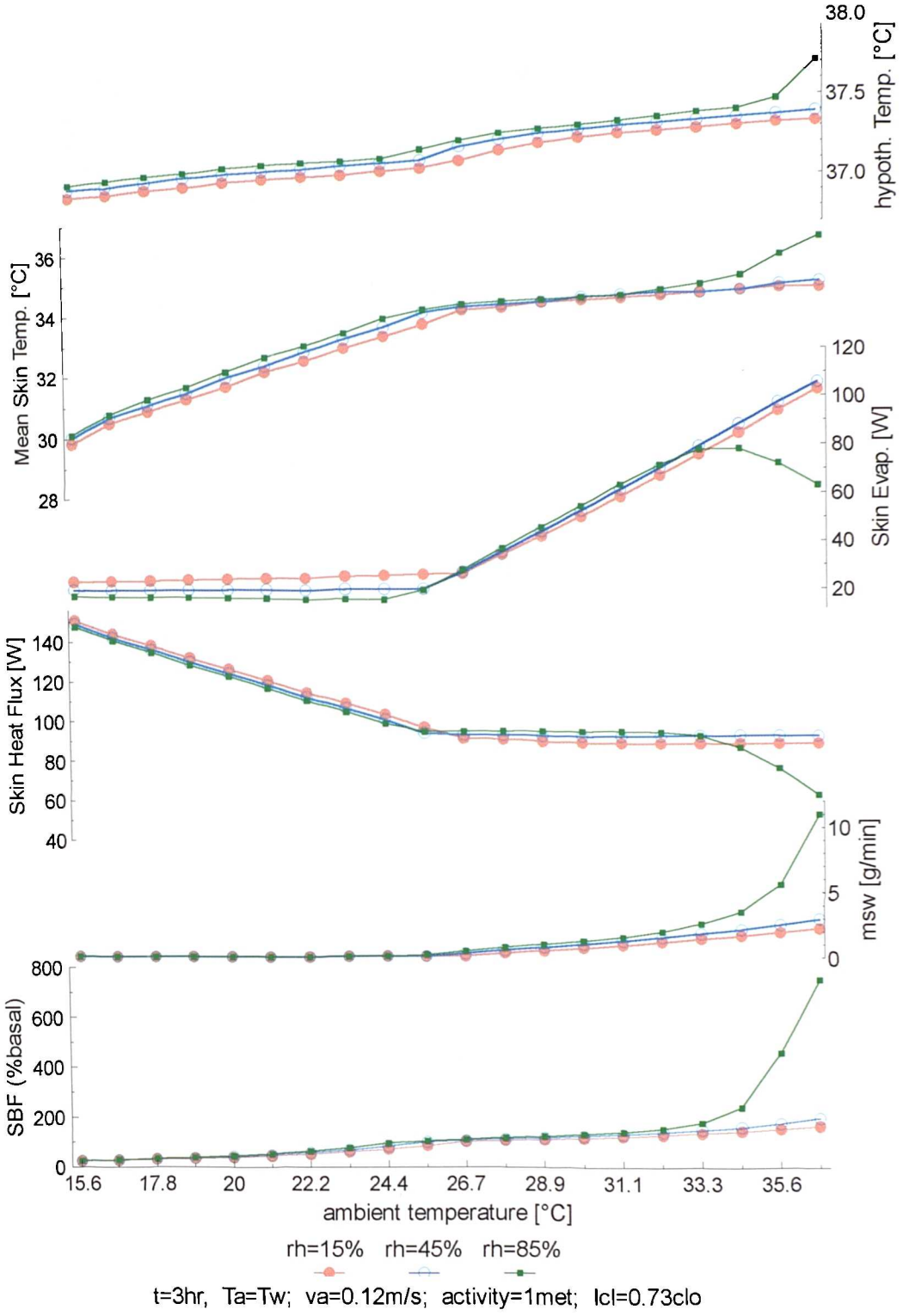

Fig.5.5

Parameters of bodily thermal state as predicted for the experimental series of Nevins et al. [141] and Rohles et al. [158]. The subjects were sedentary, and clad the KSU-uniform. The plotted parameters - from top to bottom - are: hypothalamus temperature T_{hy} [°C], mean skin temperature $T_{sk,m}$ [°C], evaporative heat loss from the skin E_{sk} [W], skin heat flux Q_{sk} [W], sweat liquid production m_{sw} [g min^{-1}], and overall skin blood flow SBF [°obasal]. For more information see text.

Changes in *SBF* occurred due either to vasoconstriction, ie. in ambients of about T_a< 26°C, or to vasodilatation in warm conditions, ie. about T_a>26°C. Cutaneous blood was constricted to a minimum of about *SBF*≈20% of its basal value at T_a=15.6°C. In contrast *SBF* was - averaged over relative humidities - elevated above the base to three or four fold due to dilatation in warm conditions.

Additional cooling of the body due to evaporation of moisture from the skin occurred for about T_a>27°C and reached an average maximum of about E_{sk}≈90W at ambients of T_a= 36.7°C. Skin evaporation of about 19W for T_a<27°C (***Fig.5.5***) was not due to regulatory sweating but arose from diffusion of water vapour through the skin. It should be noted that some evaporative heat loss also occurred by respiration. This component (not shown in ***Fig.5.5***) was predicted to be about 14W under cold, dry conditions but decreased with hot, humid exposures reaching a minimum of only about 1W.

In contrast to core temperature, skin temperature was significantly affected by ambient temperature. The mean skin temperature varied on average by about 6K from $T_{sk,m}$≈ 30°C at T_a=15.6°C to $T_{sk,m}$≈35.8°C at T_a=36.7°C. The most pronounced effect of ambient temperature on the skin was found in cool and cold environments (T_a<25.6°C). In these conditions, the elevated amount of convective and radiative heat loss to the environment was the main reason for the fall in skin temperature. In addition, there was a reduced supply of warm blood to the skin due to increasing vasoconstriction. In warm conditions, skin temperature rose only moderately being restrained by the evaporation of sweat moisture.

Heat flow through the skin (Q_{sk}) increased steeply with falling ambient temperature reaching a maximum of nearly 150W at T_a=15.6°C compared to about 90W in warm and hot conditions.

Generally, relative humidity had little effect on the thermal state of the body. An increase in *rh* from 15% to 85% affected the central temperature by about 0.1K over a wide range of environmental conditions. Similarly, no appreciable impact of *rh* was

observed on $T_{sk,m}$, E_{sk}, *SBF*, and Q_{sk}.

However, high relative humidities became important for T_a>34°C. This was because, in these conditions, it was not possible for all the sweat to evaporate which would be necessary to counteract the reduction in environmental heat loss due to convection and radiation. The barrier of the clothing ensemble and the increase in partial water vapour pressure of the ambient air hindered moisture evaporation.

As a result of reduced evaporation, heat was stored in the body and the central and peripheral temperatures increased, indicating conditions of hot stress in which subjects were unable to maintain their thermal state by thermoregulatory adjustments. A marked increase in *SBF*, and an overshoot of regulatory sweat production m_{sw} were the effects associated with overheating of the body, whereas skin evaporation declined with rising ambient temperature in the most humid climatic conditions.

The impact of time on the bodily thermal state in the experiments of Rohles et al. is shown in ***Fig.5.6***. Individual parameter values are averaged over relative humidities from 15% to 85%, and are plotted against T_a for 1, 2 and 3 hours of exposure.

The results of the dynamic simulations indicated that transient conditions do occur in the thermal state of the body although *static* environmental and personal (activity, clothing) conditions were applied. These transient occurrences became more pronounced at temperatures away from the point of thermal neutrality. When the ambient temperature was between 20°C<T_a<27°C there was no significant change in body temperature or the regulatory actions, so the body was in quasi-equilibrium with the thermal environment.

However, exposures to ambient temperatures of T_a<18°C induced a continuous cooling of the body and hence a fall in the internal temperature. As a result of the decreasing body core temperature (and thus blood temperature) and the inhibition of *SBF* the skin temperature declined with time.

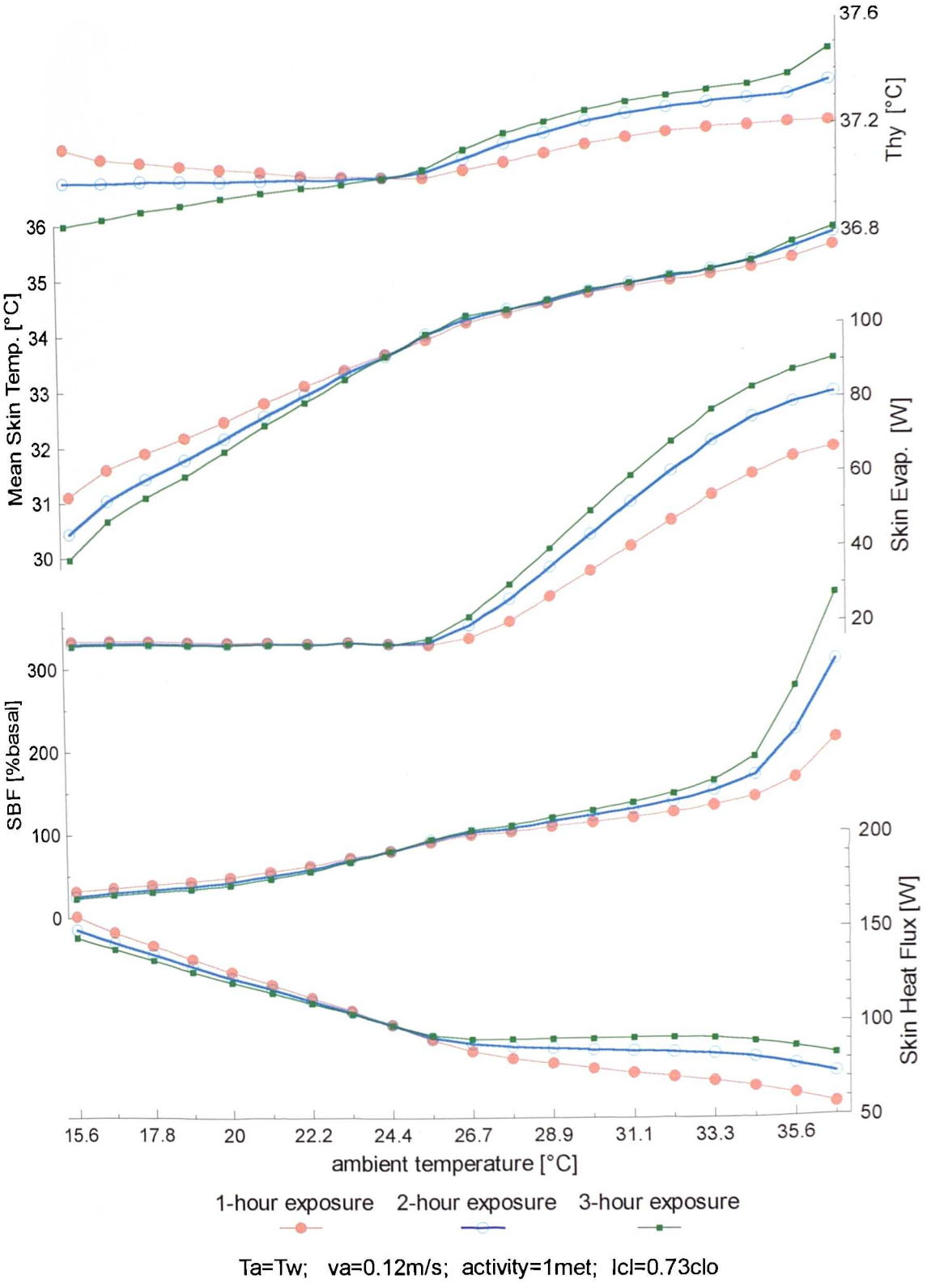

Fig.5.6

Parameters of bodily thermal state as predicted for the experimental series of Nevins et al. [141] and Rohles et al. [158]. The subjects were sedentary, and clad in the KSU-uniform. The plotted parameters - from top to bottom - are: hypothalamus temperature T_{hy} [°C], mean skin temperature $T_{sk,m}$ [°C], evaporative heat loss from the skin E_{sk} [W], overall skin blood flow SBF [% basal], and skin heat flux Q_{sk} [W]. For more information see text.

In warm ambient conditions the skin temperature remained fairly constant over a relatively wide range of temperatures; there was slight warming of the body core. This maintenance of skin temperature arose from temporal changes in the regulatory adjustments, ie. increases in E_{sw} and *SBF*.

5.3.2 Thermally Stressful Environments

In order to extend the environmental conditions investigated by Nevins et al. and Rohles et al., experiments reported by Gagge et al. [57] were also included in the development of the present comfort model. In these experiments three seminude subjects were exposed for two hours to steady ambient temperatures of 13°C, 18°C, and 48°C.

The two-hour exposures to 18°C and to 48°C were part of two separate four-hour experiments in which the subjects underwent sudden changes in ambient temperature from neutral to the particular climate and back to neutral. Therefore, these experiments were also used to investigate the dynamics of the human thermal sensation (see chap. 5.4.3).

5.3.2.1 Experiment

In the experiments with transient exposures, quietly seated male subjects spent 1 hour in a thermally neutral environment of T_a=28°C. They were quickly transferred at t=60 min. into another room at either 18°C or 48°C. After 180 minutes the subjects (clad only in shorts) moved back into the neutral environment for one hour. The wall temperature was equal to the temperature of the still air. The observed thermal sensation is shown for both the cold and warm exposure in ***Fig.5.7***.

The cold-stress experiment with an ambient temperature of 13°C (T_a=T_W=13°C) represented a two-hour exposure of sedentary subjects wearing shorts to constant ambient conditions. In contrast to the other two experiments, the subjects' sensation of

temperature was not continuously recorded over time, so only the final sensation vote of *TS*=**-2.98**, taken after two hours, was used to develop the comfort model.

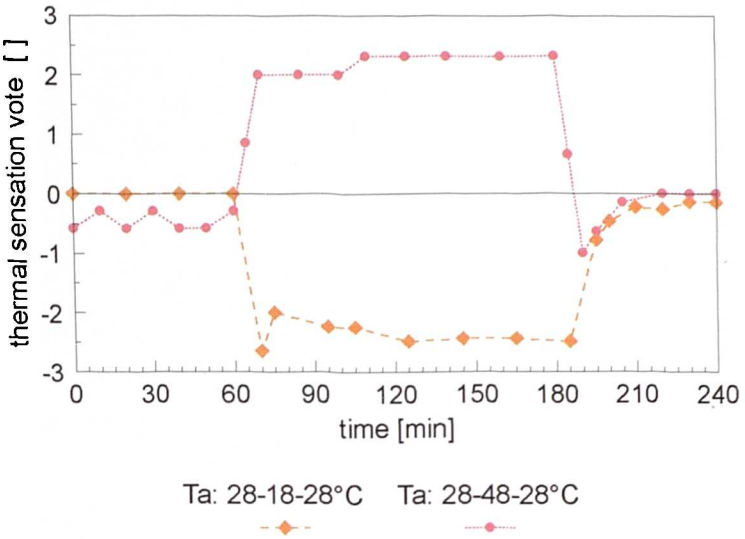

Fig.5.7

Average dynamic thermal sensation of 3 subjects undergoing sudden changes in ambient temperature from neutral (t 60min) toward hot and cold, respectively. The two-hour exposures to thermal stress conditions were followed at t 180 min. by a return to the initial, thermally neutral environment [57].

5.3.2.2 Simulation

The simulated transient environmental conditions were chosen to match the experimental design. In the transient simulations the wall temperature was set equal to the ambient air temperature (13°C, 28°C, 18°C or 48°C) and a typical emissivity for indoor walls of ε_W=0.93 was chosen. An air velocity of v_a= 0.1 m s^{-1}, a relative humidity of *rh*=30%, and time steps of Δt=5 min were used to simulate the three exposures. The local insulating characteristics of the shorts was as applied to the abdomen element (***Tab.5.1***).

Rectal temperature, mean skin temperature and the metabolic heat production predicted by the model for the transient exposure to T_a=18°C are plotted over time in ***Fig.5.8***.

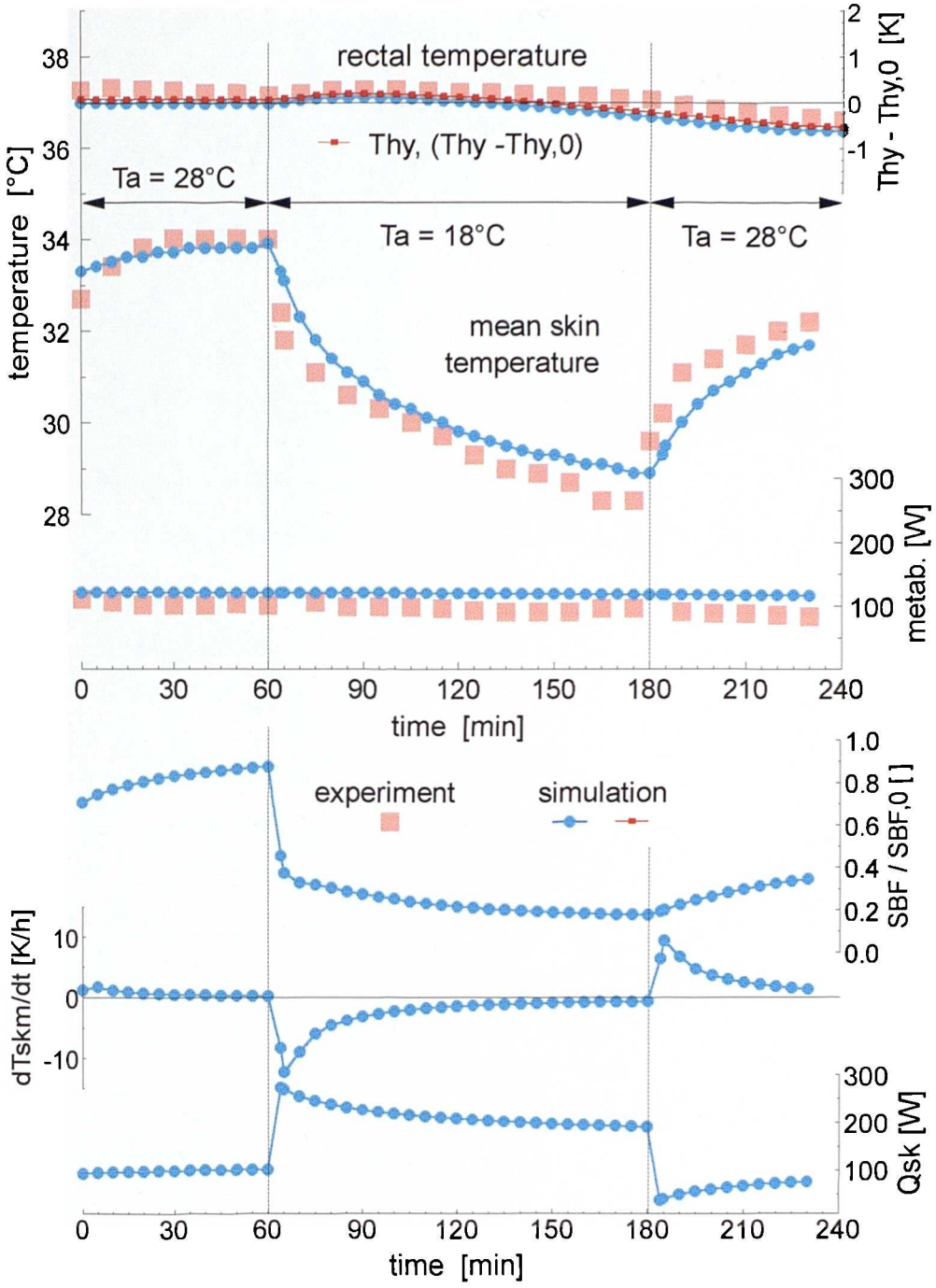

Fig.5.8

Parameters of the bodily thermal state as predicted by the model for sudden changes from a thermally neutral environment to a cold climate of T_a 18°C and back to neutral. Predicted rectal temperature, mean skin temperature and the metabolic heat production - from top to bottom - are compared with the corresponding measured values. Further simulated variables (not measured in the experiment) are plotted: the hypothalamus temperature (and the corresponding error signal T_{hy}-$T_{hy,0}$, see the upper right-hand scale), relative skin blood flow SBF SBF_0, rate of change of the mean skin temperature $dT_{sk,m}$ dt, and skin heat flux Q_{sk}

Further important variables (not measured in the experiments) are also included in ***Fig.5.8***, ie. the hypothalamus temperature T_{hy}, (or the corresponding temperature error signal T_{hy}-$T_{hy,0}$ indicated by the upper, right-hand scale), skin blood flow *SBF*, rate of change of the mean skin temperature $dT_{sk,m}/dt$, and skin heat flux Q_{sk}.

As can be seen, the cold exposure was accompanied by a continuous fall in the mean skin temperature whereas there was an initial rise in the body core temperature (both as measured and as predicted) before both T_{re} and T_{hy} began to fall at about t=105 min. During the whole cold exposure no increase in metabolic heat production occurred. After a rapid reduction in the predicted skin blood flow, the value decreased further only slightly. The minimum *SBF* was about 20% of its basal value at the end of the cold exposure. Sharp changes in $dT_{sk,m}/dt$ and Q_{sk} occurred upon entry into the cold climate followed by a relaxation period for both variables.

After re-entering the neutral environment the skin temperature immediately began to rise. However, the response to warming occurred more slowly than the cooling due to entering the cold room. The trend of internal temperature, and metabolic rate remained unaffected by the change in ambient temperature whilst the *SBF* showed a moderate increase for t>180 min. The transient behaviour of $dT_{sk,m}/dt$ and Q_{sk} after the positive step-change in T_a was the reverse of the behaviour observed after the negative step-change on entering the cold room.

A comparison of the predicted and observed values for a transient exposure to T_a=48 °C is shown in ***Fig.5.9***. Subjects' initial sensation of thermal neutrality (see ***Fig.5.7***) was accompanied by measured (and predicted) mean skin temperatures ranging between 33-34°C. However, there was a discrepancy between the *'thermally neutral'* measured and predicted body core temperatures for the first hour of the experiment. In the experiment, the subjects felt 'thermally neutral' despite an internal (rectal) temperature of about 37.5°C at the beginning of the experiment. In contrast, the model predicted body core temperatures nearer to 37°C (ie. $\Delta T_{hy} \rightarrow 0$K, see the corresponding right-hand scale).

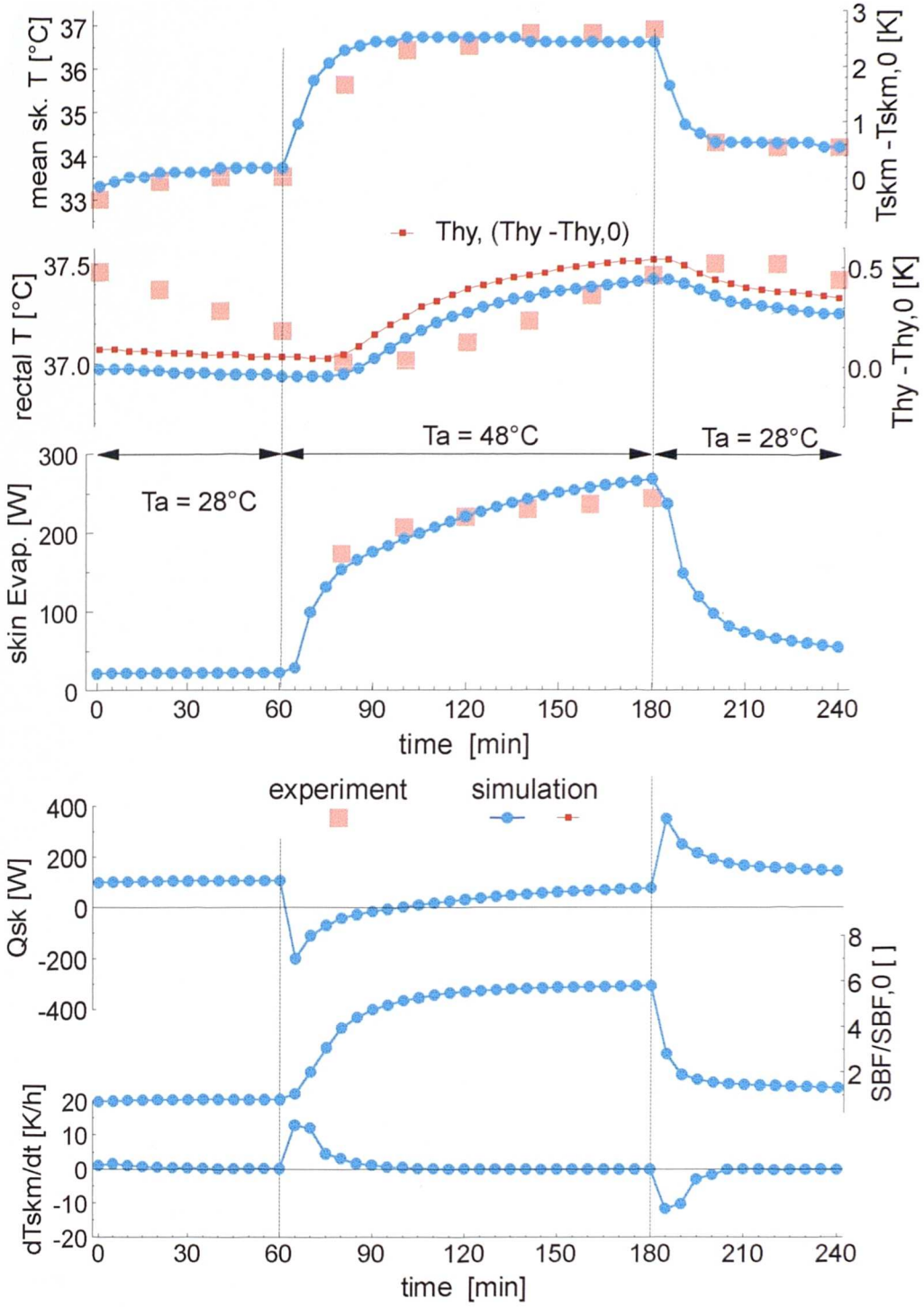

Fig.5.9

Parameters of the bodily thermal state as predicted by the model for sudden changes from a thermally neutral environment to a hot climate of T_a=48°C and back to neutral. Predicted mean skin temperature, rectal temperature, and the evaporative skin heat loss - from top to bottom - are compared with the corresponding measured values. Further simulated variables (not measured in the experiment) are plotted: the hypothalamus temperature (and the corresponding error signal T_{hy}-$T_{hy,0}$, see the upper right-hand scale), skin heat flux Q_{sk}, relative skin blood flow SBF/SBF_0, and rate of change of the mean skin temperature $dT_{sk,m}/dt$.

After entering the hot environment the subjects started to sweat appreciably. The corresponding evaporative heat loss from the skin continued to rise up to about 270W at t=180 minutes. The mean skin temperature increased rapidly in the hot climate and had reached its maximum of about $T_{sk,m}$=36.7°C (ie. about $\Delta T_{sk,m}$=+2.3K, see the upper right-hand scale) already after only about 30 minutes of the exposure to 48°C. As a result of this hot stress exposure the body core (both rectal and hypothalamic) temperature rose continuously. However, the onset of body core warming occurred later in the experiment than in the simulation. At t=65 min a minimum value of Q_{sk} and a maximum value of $dT_{sk,m}/dt$ occurred. Both signals were then very small for the rest of the hot exposure.

On re-entering the neutral environment, skin temperature, sweating, and *SBF* responded immediately to the fall in ambient temperature. Predicted and measured changes in core temperatures were delayed by about 5 min and 30 min, respectively, and they did not decline to the initial level before the end of the experiment.

5.3.3 Intermediate Work

The effect of work intensity on thermal sensation was investigated extensively by McNall et al. [127]. These climate chamber experiments involved 210 male and 210 female college-age subjects. The experimental design consisted of exposing subjects in groups of ten (5 male, 5 female) to different combinations of globe temperature, relative humidity, and levels of activity. The three different metabolic rates investigated resulted from *intermittent* exercise cycles involving standing and walking.

5.3.3.1 Experiments

The subjects spent 30 minutes in a pretest room before entering the climate chamber where they were exposed for 3 hours to steady ambient conditions whilst performing intermittent work. The pretest conditions were not explicitly specified in [127]. The three different activity levels resulted from varying the standing period and using 5 minutes of walking over two steps. Each test began with the stand period. The 'low activity level' arose from a sequence of 25 minutes standing and 5 minutes walking. The other cycles were: stand 10 min - walk 5 min ('medium activity level'), and stand 5 min - walk 5 min. ('high activity level'). A detailed study of the corresponding (time) average metabolic rates [128] provided values which differed between the sexes being 182W (females: 144W), 242 (191)W, and 310 (242)W, respectively, for low, medium, and high activity level.

The subjects - wearing the standard KSU-uniform (see ***Tab.5.1***) - were exposed to the following steady dry bulb temperatures, each combined with a relative humidity of 25, 45, and 65%:

"low" activity	-	18.9°C	22.2°C	25.6°C
"medium" activity	15.6°C	18.9°C	22.2°C	25.6°C
"high" activity	12.2°C	15.6°C	18.9°C	-

Throughout the tests the mean radiant temperature was maintained equal to the air

temperature. The recorded air velocity ranged between 0.10 and 0.15 m s^{-1}.

The results of subjects' mean thermal sensation after three hours of exposure are summarised in ***Fig.5.10*** (all votes were taken during the standing period).

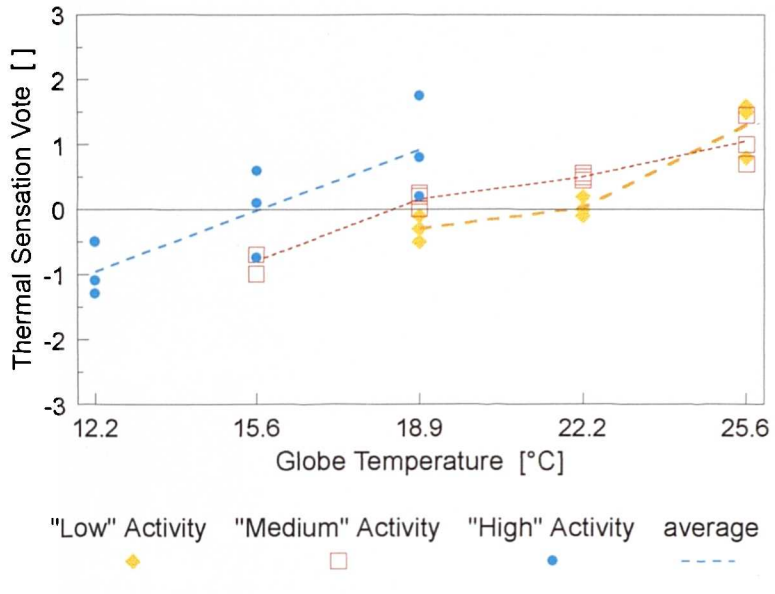

Fig.5.10

Observed [127] mean thermal sensation of groups of ten subjects after three hours of exposure to different ambient temperatures and for three levels of intermittent work, ie. low activity (1.6met), medium activity (2.1met) and high activity (2.7met).

5.3.3.2 Simulation

Each of the 30 different experiments was simulated using time-steps of Δt=5 min and included a thirty-minutes pretest-simulation followed by a 180-minutes exposure to the particular combination of globe temperature (T_a=T_W), relative humidity, and activity level. The pretest room period was simulated assuming an ambient temperature of T_a= T_W=25°C, v_a= 0.1m s^{-1}, rh=50%, and an activity level of 1.2 met. The KSU-uniform worn by the participants was simulated by the clothing ensemble described in chap. 5.3.1.2 but excluding the chair.

The step into the climate chamber was simulated by a temporarily increased activity level to act=2 met for the last 5 minutes of the pretest phase. According to the expe-

rimental design, each exposure began with the stand-period. Experimental investigations [128] indicated that subjects exercised on average at a level of *act*=1.2 met when standing, and *act*=4.2 when walking. These values were obtained from measured metabolic rates of male and female subjects normalized for unit clothed body *weight* to obtain sex-independent values [128] and were used in the simulations for the respective activities.

Each activity was associated with a specific relative air velocity. When moving, the measured mean relative air speed was about v_a=0.5 m s^{-1} [128]. This value was used to simulate walk-periods, whereas the mean chamber air speed of v_a=0.13 m s^{-1} was taken for periods of standing activity.

In ***Fig.5.11***, the principal trends of the predicted physiological parameters are indicated for the intermittent work experiments. This simulation reproduces an exposure to T_a= 18.9°C and *rh*=45% which was perceived to be thermally neutral by subjects exercising at the 'medium' activity level. For comparison, parameters resulting from continuous exercise which would yield the same time-averaged metabolic rate are also given.

It can be seen that intermittent exercise, where metabolic rates fluctuated between about 130W (standing) and 400W (walking), caused both long term and short term changes in the physiological parameters. The 'long-term' transient behaviour indicated that quasi-equilibrium of the bodily thermal state was approached after about *t*> 60 min. Within the first hour, the body core temperature rose by about 0.3K to a level of more than 37.4°C, and the mean skin temperature declined from about 34°C to about 32°C due to an overall increase in the evaporative heat loss of about 30W.

This transient trend was overlaid with fluctuations due to each change in activity level. While this 'short-term' transient effect had a negligible influence on skin temperature, it influenced significantly the evaporative heat losses, which fluctuated by about 50W between periods of standing and walking.

It is interesting to note that the use of a constant bodily heat production of about 220

W (obtained by time-averaging the partial metabolic rates of the stand-walk cycles) produced simulated data which corresponded to the average thermal behaviour predicted for intermittent work. The strategy of time-weighting metabolic rates to depict the mean activity level of periodically repeated changes in exercise intensity, which is frequently adopted in literature (eg. [127] [128] [46]) seems, therefore, to be adequate from the thermophysiological point of view.

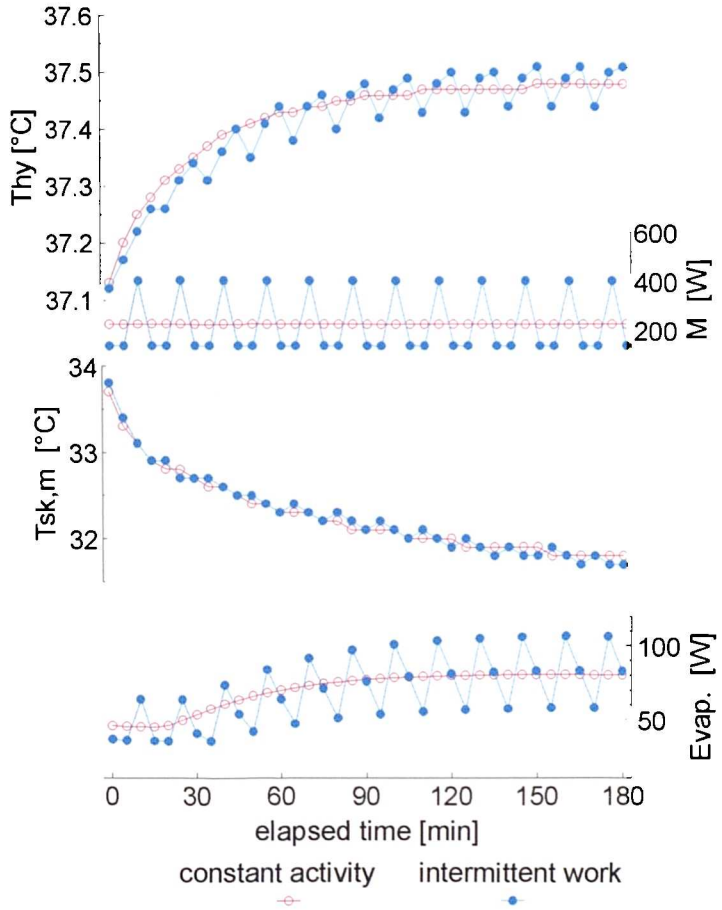

Fig.5.11

Temporal trends of the hypothalmus temperature, metabolic rate, mean skin temperature, and evaporative heat loss as simulated for intermittent and continuous work and exposure to T_a 18.9°C and rh 45%.

In ***Fig.5.12***, physiological data predicted after three hours of exposure (the time at which the test-subjects voted on their thermal sensation) are drawn against ambient temperature for the three levels of intermittent work. Relative humidity was found to be insignificant in affecting both the sensory estimates of the subjects [127] and the physiological parameters predicted by the model.

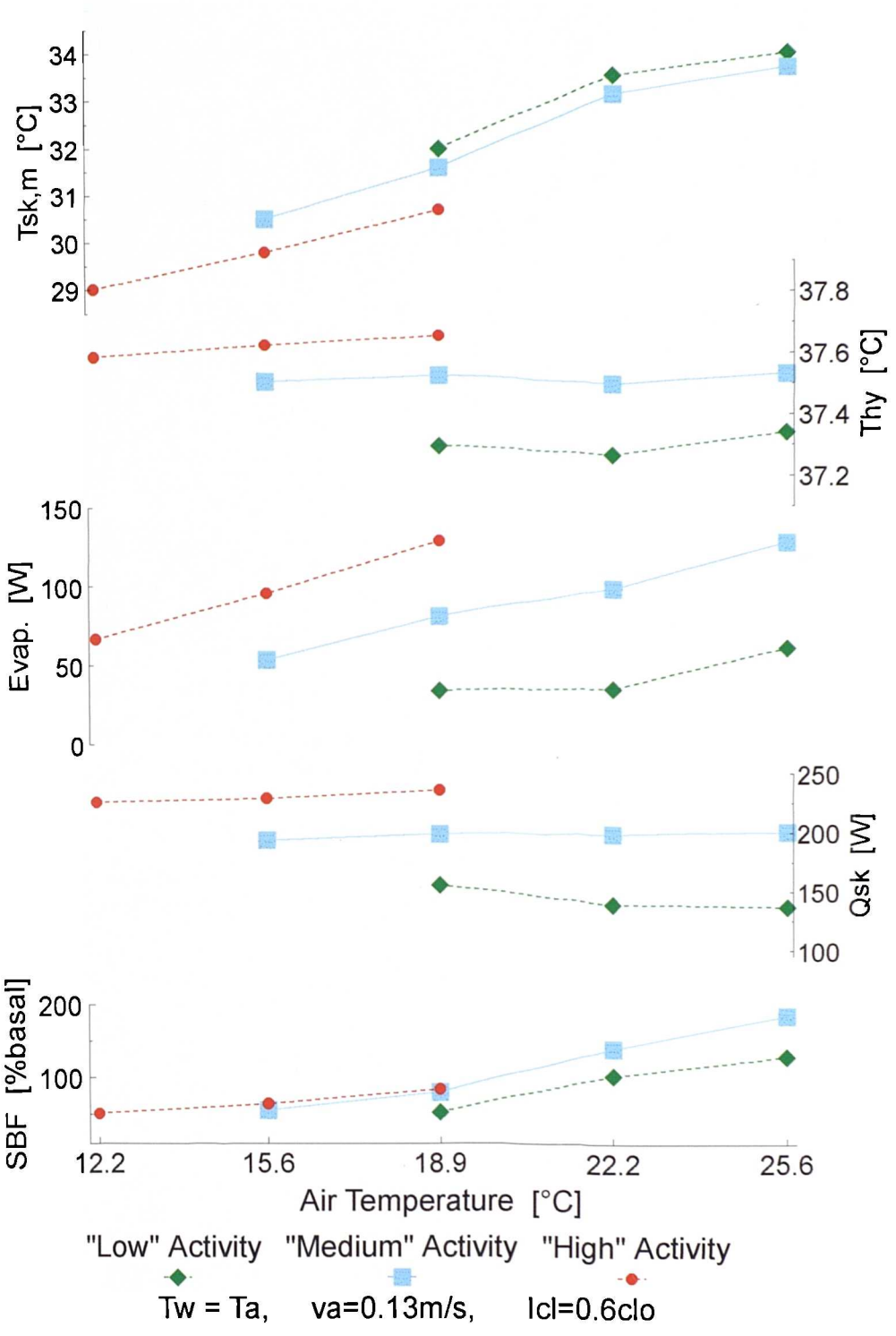

Fig.5.12

Predicted thermophysiological responses after three hours of exposure to the respective ambient temperatures and averaged over relative humidity. The values were simulated for three levels of intermittent work as investigated by McNall et al. [127] resulting in average activity levels of 1.6 (low), 2.1 (medium), and 2.7 met (high).

Therefore, in ***Fig.5.12*** plotted values of the mean skin temperature, hypothalamus temperature, total evaporative heat loss, and skin blood flow were averaged over the three relative humidities, ie. 25, 45, and 65%.

The simulations revealed skin temperature to be influenced primarily by the thermal environment, with activity level having a minor effect. In contrast, predicted internal temperatures were found to be strongly affected by exercise intensity, whereas the ambient temperature played a negligible role. This thermal behaviour has been repeatedly observed in different experimental studies, eg. [111] [165].

The skin heat flux was largely independent of ambient temperature. This was predominantly because there was adequate heat loss by evaporation which varied due to both internal and external influences.

5.3.4 Heavy Exercise

McNall et al. [127] studied subjects' responses for lower levels of activity (act<3 met) resulting from *intermittent* work. In contrast, *continuous* work (pedalling a bicycle ergometer) was used by Gagge et al. [58] in 72 experimental runs to study the sensory estimates of four seminude male participants for activity levels between 3<act<10 met and ambient temperatures ranging from 10°C to 30°C.

5.3.4.1 Experiment

The subjects spent about 30 min. reclining in a thermally neutral room (26°C<T_a<28 °C) before entering the test chamber where they sat on the bicycle and performed constant exercise at three different levels of their maximum oxygen uptake, ie. 25%, 50%, and 75%. The corresponding average metabolic rates were:

M:	410W	700W	1080W.

These three exercise intensities were combined with each of the following levels of ambient air temperature:

T_a : 10°C 20°C 30°C.

In all the tests, the relative humidity was maintained between 30-40%. The air movement in the chamber was constant at around 0.20-0.25 m s^{-1}.

The subjects were dressed in shorts, socks, and shoes. The two lowest work loads were performed in sequence during the same experimental period. The heaviest work loads were carried out in separate sessions. Each period of constant work rate lasted about 40 minutes.

Thermal sensation votes for each ambient temperature, after 30-40 minutes of exercise, for the three different activity levels, are shown in ***Fig.5.13***.

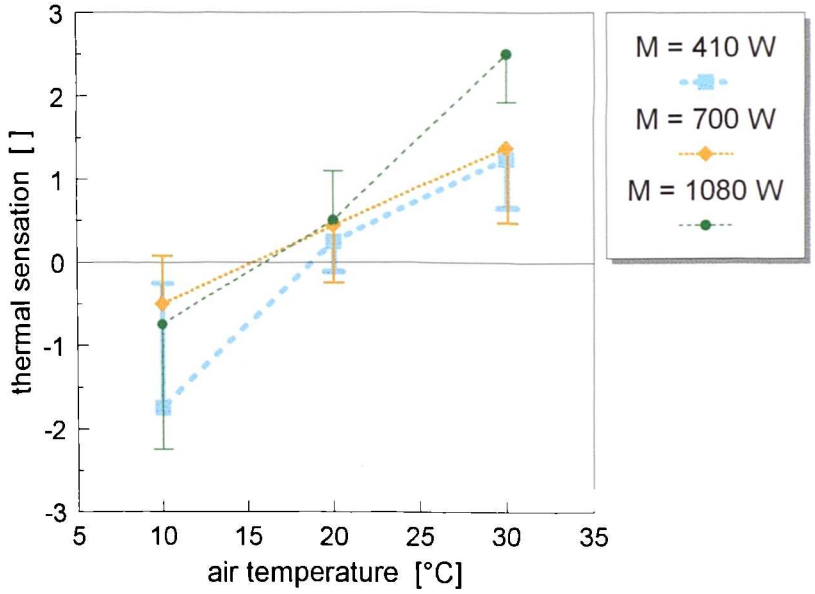

Fig.5.13

Mean thermal sensation votes (±sd) of four seminude male subjects pedalling at 25%, 50%, and 75% maximal oxygen uptake and 10°, 20°, and 30°C ambient temperature [58].

5.3.4.2 Simulation

Gagge's experiments were simulated using a 30-minutes pretest exposure to T_a= 27°C (v_a= 0.1m s^{-1}, *rh*=40%, *act*=0.9met) and a forty minute exposure to the relevant ambient air temperature. According to the experimental design, the two lower work loads were simulated in one sequence resulting in 80 minutes total duration. The highest work loads were studied in separate simulation runs. The surrounding wall temperature was assumed to be equal to the air temperature. The measured metabolic rates corresponded to activity levels of *act*=3.6met, 6.4met, and 9.9met. The corresponding relative air velocities used were 0.3, 0.4, and 0.5 m s^{-1}, for low, medium and high activity, respectively. A constant relative humidity of 35% was assumed for all the exposures, and the clothing items listed in ***Tab.5.2*** were adopted.

Garment	I_{cl}^* [clo]	f_{cl}^* [ ]	i_{cl}^* [ ]	body elements covered
short shorts (cotton) knit	0.363	1.21	0.354	abdomen
socks (cotton) knit	0.510	1.18	0.407	feet
athletic shoes soft soled	0.585	1.53	0.130	feet

Tab.5.2

Local, ie. garment-oriented insulation characteristics of clothing items. I_{cl}^*: local intrinsic clothing insulation, f_{cl}^*: local clothing area factor, i_{cl}^*: local moisture permeability index.

In ***Fig.5.14***, predicted mean skin temperature, rectal temperature, and the total weight loss are compared with measured data for the three levels of activity. Also, included are thermophysiological data for sedentary activity both as measured and as predicted. All predicted parameters were averaged over exposure times of 30 to 40 minutes to reproduce the time of observation in the experiments.

In general, there was a good agreement between predicted and measured values. This was the case even for the highest level of activity - representing exhausting work - where the body core temperature was appreciably elevated reaching a value

of about 38.6°C (independently of the prevailing climatic conditions, compare section 5.3.3.2).

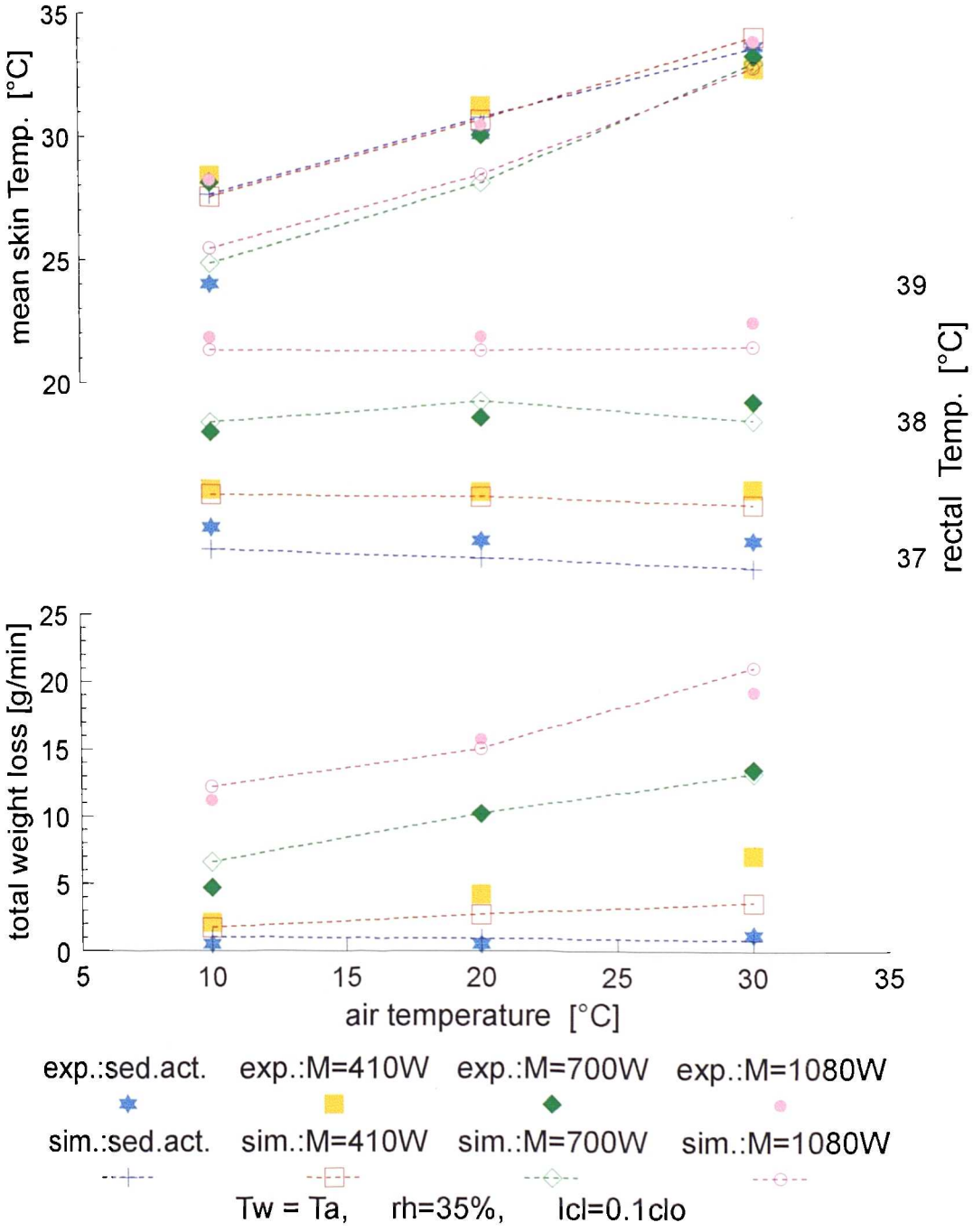

Fig.5.14

Comparison between measured [58] and simulated physiological data for three levels of activity at 25, 50, and 75% maximal oxygen uptake and 10, 20, and 30°C ambient temperature.

5.4 Derivation of the Comfort Model

The dynamic comfort model was developed by correlating the thermal sensation votes of subjects observed for a variety of different experimental conditions, with parameters describing the bodily thermal state as predicted by the model. At first, simple and multiple linear regression analysis was employed to examine the possibility of describing thermal sensation in terms of body temperatures, overall skin heat flux, individual regulatory responses and associated parameters (eg. skin wettedr and/or sets of them [147].

The studies indicated that linear regression was unable to reproduce the non-linear behaviour of thermal sensation at the boundaries of the 7-point ASHRAE scale (noted in section 5.3.1.1). Instead of approaching asymptotically the limits of |TS|=3, the regression lines continued into the undefined regions outside the ASHRAE scale. Furthermore, there were systematic errors in predicting thermal sensation in the zone of thermal neutrality due to inappropriate representation of non-linear trends by means of linear regression. Also, the multiple linear regressions produced implausible thermal sensation trends. In particular, the regression coefficients for individual physiological variables often had the opposite sign from that which one would expect, eg. a negative coefficient for the ΔT_{hy}-variable indicating an inhibited sensation of 'warm' or 'hot' when body core temperature is rising.

The non-linarity of the problem can also be seen in ***Fig.5.15*** where the mean sensation votes of 1600 subjects (5 men + 5 women for each of 160 exposures) are shown for five different variables of the predicted bodily thermal state. These variables are (from top to bottom) the integral temperature error signal from the skin $\Delta T_{sk,m}=T_{sk,m}-T_{sk,m,0}$, the hypothalamus temperature error signal $\Delta T_{hy}= T_{hy}- T_{hy,0}$, overall skin heat flux error signal ΔQ_{sk}, the regulatory response of sweating Sw, and of the overall skin blood flow *SBF*.

To achieve an adequate, and physiologically sensible, relationship between the thermal state of the body and the thermal sensation vote for a wide range of environmental conditions complex, rather than linear, regression was adopted.

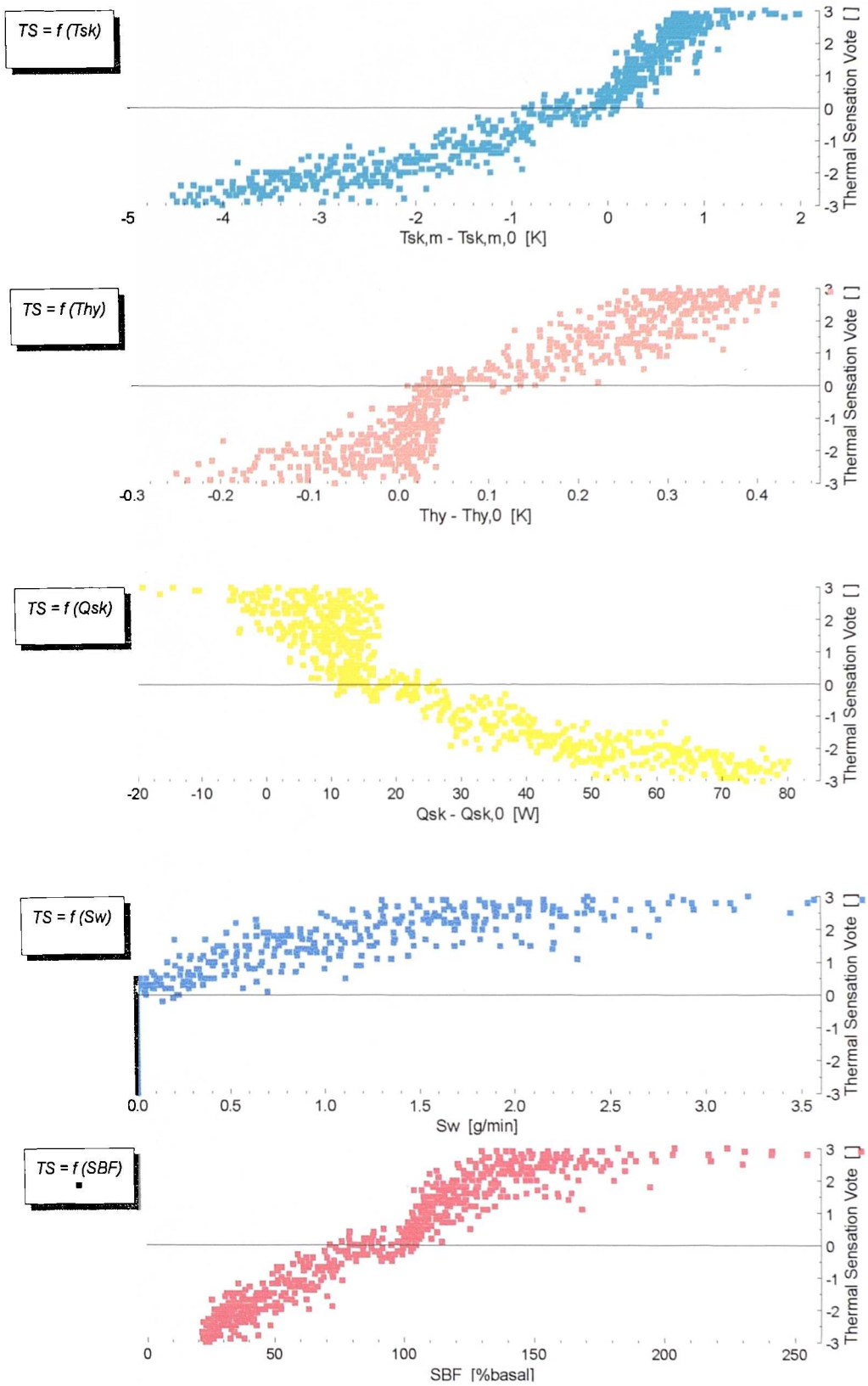

Fig.5.15

Thermal sensation votes observed by Nevins et al. [141] and Rohles et al. [158] for ambient temperatures and relative humidities between 15.6°C T_a 36.7°C and 15% rh 85%, are drawn (from top to bottom) against predicted values of the integral temperature error signal from the skin $T_{sk,m}$-$T_{sk,m,0}$, hypothalamus temperature error signal T_{hy}-$T_{hy,0}$, overall skin heat flux error signal Q_{sk}-$Q_{sk,0}$, sweat rate Sw, and overall skin blood flow SBF.

The mean skin temperature (ie. $\Delta T_{sk,m}$) was found to be the best predictor of thermal sensation for sedentary subjects for the whole spectrum of steady ambient temperatures investigated by Nevins et al. and Rohles et al. Even in warm environments, *TS* correlated better with skin temperature than, for example, with internal temperature which (as the second best predictor) produced a wide scatter in the data points. The analyses have shown that in air exposures, the *TS* is independent of cold signals from the brain (as can be seen for ΔT_{hy}<0K in ***Fig.5.15***). This is consistent with experimental findings [11].

Analysis of afferent signals indicated that skin heat flux Q_{sk} as a physical variable was a less successful indicators of human thermal sensation. In exposures to cool and cold air there is a good correlation between ΔQ_{sk} and *TS*; however, under these conditions Q_{sk} and $T_{sk,m}$ are themselves correlated. However, as can be seen from ***Fig.5.15***, there is no clear relationship between *TS* and ΔQ_{sk} in warm environments, ie. for *TS*>0.

In ***Fig.5.15***, *TS* is also plotted against sweating and skin blood flow across the whole bandwidth of ambient temperatures. This examines the question of whether thermal sensation represents a response which is associated with thermoregulatory effects, ie. whether regulatory adjustments are felt to be uncomfortable in themselves, or whether thermal sensation has to be described as an additional, autonomic response. In steady state exposures, as illustrated in ***Fig.5.15***, sweating and *SBF*, however, did not correlate better with experimentally observed sensation votes than with the single variable of skin temperature although they represent multiple functions which involve effects of both internal and skin temperature. Moreover, the concept of utilizing regulatory variables for modelling *TS* is neither applicable to transient conditions (see section 5.4.3) nor it can be used successfully for non-sedentary activities (section 5.4.2).

So, thermal sensation had to be treated as a further, separate (perceptual) response in addition to the four responses of the human thermoregulatory system. In the following sections, the integral temperature error signal from the skin, $\Delta T_{sk,m}$, and the

temperature error signal from the head core, ΔT_{hy}, will be used to develop the *static comfort model*. The active-system concept of utilizing *relative* temperatures, ie. $\Delta T_{sk,m}$ and ΔT_{hy} instead of *absolute* values $T_{sk,m}$ and T_{hy}, will be helpful when determining the type of thermal strain on the body and so the type of discomfort. Negative error signals from the skin, ie. $\Delta T_{sk,m}<0$, representing 'cold' cutaneous receptors, are usually coincident with the perception of cold discomfort. Positive error signals from the hypothalamus, and/or from the skin, indicate warm discomfort, whereas thermal neutrality is accompanied by an absence of driving thermal impulses; ie. $\Delta T_{sk,m}=\Delta T_{hy}=0$.

In addition to $\Delta T_{sk,m}$ and ΔT_{hy}, the rate of change of the mean skin temperature $dT_{sk,m}/dt$ will have to be employed as an further signal in order to describe the *dynamic* components of human thermal sensation (sec. 5.4.3).

5.4.1 The Static Effect of Cutaneous Thermoreceptors

Comfort experiments investigating the impact of *steady state* ambient conditions on *sedentary* subjects were used to explore the *static* influence of 'cold' and 'warm' cutaneous thermoreceptors on *TS*.

The foregoing analysis revealed the skin temperature to be the best predictor of thermal sensation for sedentary subjects within a wide range of steady ambient conditions. In ***Fig.5.16*** the *TS* votes observed by Nevins et al. [141] and Rohles et al. [158] for 15.6°C≤T_a≤36.7°C and 15%≤*rh*≤85%, and by Gagge et al. [57] for thermally stressful situations of T_a=13°C, 18°C, and 48°C are plotted against $\Delta T_{sk\,m}$.

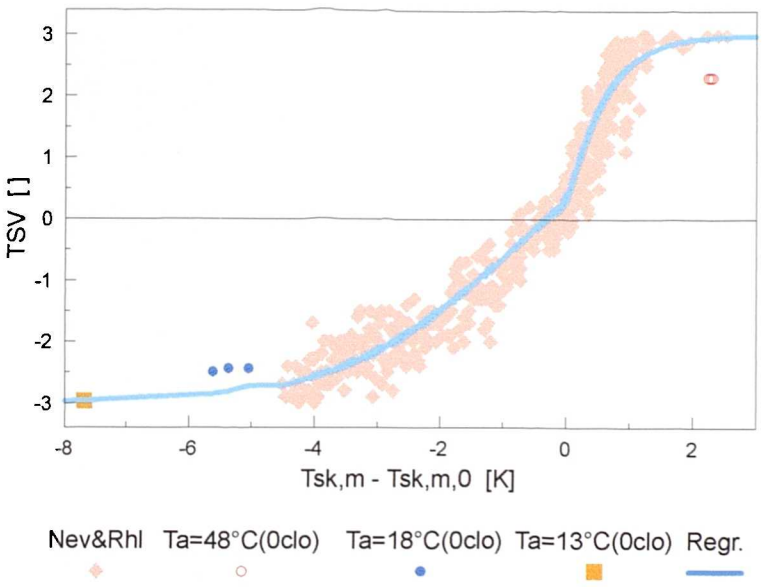

Fig.5.16

Thermal sensation votes of sedentary subjects exposed to a wide range of steady state ambient conditions as investigated by Nevins et al. [141] and Rohles et al. [158] and Gagge et al. [57] plotted against the predicted integral skin temperature error signal $\Delta T_{sk\,m}$. For more information see text.

The data of Nevins et al. and Rohles et al. reflect the mean group votes obtained from 160 experiments after *t*=120, 150, and 180 minutes of exposure. Observations made for t≤1.5h were excluded from the analysis because of inconsistencies in the votings of groups of different sex and (dynamically induced) deviations from subsequent votings in warm conditions (see chap. 5.3.1.2). Gagge's data represent the

mean votes of three subjects taken for t>90min of exposure. The initial votes taken after stepping from neutral conditions into ambient temperatures of T_a=13, 18, and 48 °C were discarded to exclude any dynamic component in the *TS*-response.

Thermal sensation appears to be a non-linear function of $\Delta T_{sk,m}$ (***Fig.5.16***). *TS* votings rise steeply due to positive skin error signals, they fall less rapidly in response to cold signals, and approach both limits of the sensation scale asymptotically. The data points do not pass exactly through the origin of the sensation scale but range between 0<*TS*<0.5 for $\Delta T_{sk,m}$=0. This indicates a secondary effect on *TS* due to body core temperature.

The relationship between *TS* and $\Delta T_{sk,m}$ can be described using a modified *tanh*-function (this type of function was adopted for modelling the regulatory actions of the active system). Modifications to the standard *tanh* function were concerned with extending the functions limits from -1, and +1 to -3, and +3, respectively, and fitting the trend using a linear function f_{sk} of the integral skin temperature error signal:

$$TS = 3 \times tanh\,(f_{sk}) \tag{5.1}$$

where

$$f_{sk} = b_1 \Delta T_{sk,m} + b_0 \tag{5.2}$$

The coefficients b_0 and b_1 of the linear function, f_{sk}, had to be determined by means of regression analysis of the linearized eq. (5.1).

It should be noted that for exposures to ambient temperatures of T_a>26°C, as investigated by Nevins and Rohles, the head core temperature rose above its setpoint and also influenced *TS*. However, experiments investigating the impact of *steady state* ambient conditions on *sedentary* subjects were not used to study the impact of internal temperature on *TS*. In steady state exposures where the exercise intensity is kept at a constant, low level the thermal state of the body core is not independent of the thermal state of the bodies periphery. Thus, multiple regression analyses employing both signals, $\Delta T_{sk,m}$ and ΔT_{hy} would not provide correct information on the

two partial effects. In the present work, the influence of core temperature on *TS* was derived using experiments where the body core temperature varied independently of skin temperature by changes in exercise intensity (see chap. 5.4.2).

The regression to establish the impact of skin temperature on *TS* was performed by recognizing the role of the head core temperature as described by a function ϕ. This function represents an additive term in the argument of the *tanh*-function and is developed further in section 5.4.3. Considering ϕ and linearizing eq. (5.1) the following expression was then subjected to regression analysis:

$$Y = \left\{ artanh\left(\frac{TS}{3}\right) - \phi \right\} = b_1 \Delta T_{sk,m} + b_0 \qquad (5.3)$$

In the regression procedure, ϕ and f_{sk} influenced each other. Since ϕ is neither linear, nor linearizeable for purposes of regression analysis, iterations had to be undertaken to evaluate the regression coefficients of f_{sk}. In this procedure, for any change in ϕ the regression for determining the coefficients b in eq. (5.3) had to be repeated (and vice versa) until the results became stable and accurate.

The regression procedure was performed separately for negative and positive error signals $\Delta T_{sk,m}$ to account for the difference in sensitivity of the human temperature sense to cold and to warm stimuli at the skin. To ensure that the new, skin-temperature-dependent *TS*-function vanished for $\Delta T_{sk\,m} \rightarrow 0$ (where there are no driving impulses) the regressions were performed by setting b_0=0 in eq. (5.3). As a result a slope of b_1= **1.026**±0.031 was obtained for positive $\Delta T_{sk,m}$ values (ie. 'warm' cutaneous receptors) with a correlation coefficient of r=0.76. A coefficient of b_1= **0.298**±0.005 with r=0.88 was obtained for $\Delta T_{sk,m}$<0 K ('cold' receptors).

The following expression summarizes the results for both 'warm' and 'cold' skin temperature:

$$f_{sk} = \left(\begin{matrix}1.026\\0.298\end{matrix}\right) \cdot \Delta T_{sk,m} \Big|_{-}^{+} \qquad (5.4)$$

5.4.2 The Effect of Core Temperature

The model of *TS* based on only the skin temperature, ie. $TS(f_{sk})$, accounts for external (ie. environmental) influences on (dis)comfort. This approach, however, is not applicable for conditions in which subjects perform exercise. As can be seen from ***Fig.5.17*** (which reproduces the average sensation votes observed by McNall et al. [127] for three different activity levels), the higher the intensity of work the greater the discrepancy between experimental observations and predictions using the *TS* (f_{sk}) model.

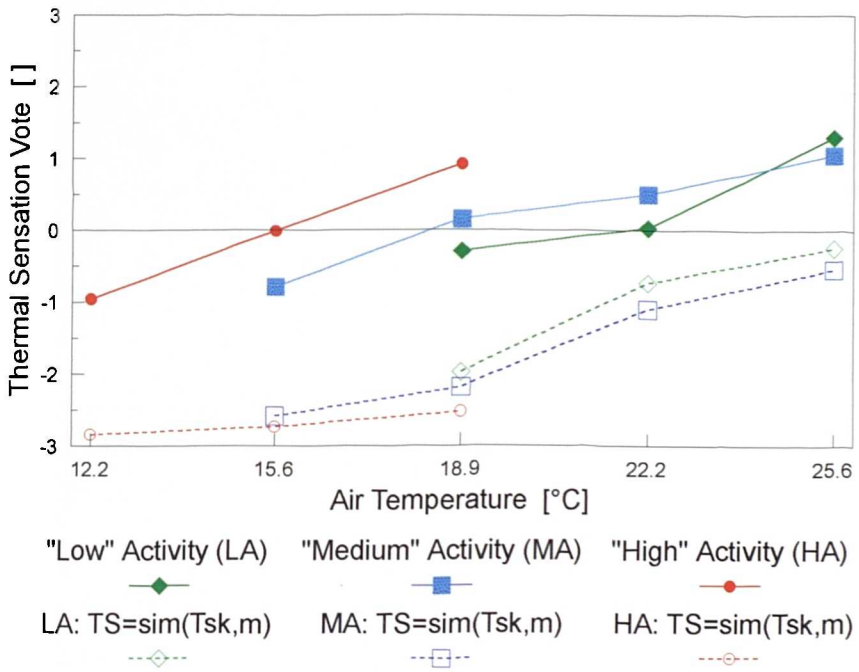

Fig.5.17

Subjects' judgements of TS (filled symbols) at different ambient temperatures and three levels of activity (1.6, 2.1, and 2.7 met), and the TS-index as predicted by the f_{sk}-model.

The impact of exercise on (dis)comfort has usually been modelled by taking into account the metabolic heat generated at a given level of activity. In these models, eg. [7] [46], thermal sensation appears to be a function of internal heat production with decreasing sensitivity to ambient influences as the activity level increases. This physical approach, however, does not reflect the physiological origin of (dis)comfort because the humans do not possess thermosensors which would detect the rate of heat production in the body.

An alternative, physiological concept was postulated by Benzinger [11] to explain the specifics of comfort perception during exercise using the terms *ideal* and *relative* (*mixed*) comfort. According to Benzinger, *ideal* comfort can only be assured for resting individuals in the absence of punitive signals from both peripheral and central thermoreceptors. When working, internal temperature is elevated above the threshold for central warmth-reception, ie. $\Delta T_{hy}>0$. An adequate decrease in skin temperature is then required to balance the internally generated sensation of warmth, and thereby to ensure the condition of *mixed* comfort. A person is at comfort even though he/she receives two conflicting warnings of warm and cold from the core and the periphery, respectively. According to Benzinger, this 'physiological' concept of *relative* comfort is not limited to working individuals. The balancing mechanism is also the basis of many transient observations, eg. when an overheated subject enters an air-conditioned shopping centre, etc.

Unfortunately, literature does not provide any quantitative description of the mixed comfort concept. Moreover, Benzinger's idea needs to be extended to arbitrary (ie. also uncomfortable) combinations of skin and core temperature to quantify the thermal feelings of exercising subjects according to the ASHRAE-scale.

In the present model, the effect of the temperature error signal from the head core ΔT_{hy} was investigated using the extensive experimental series undertaken by McNall et al. [127] (see also chap. 5.3.3). In addition, the results obtained by Gagge et al. [58] (see chap. 5.3.4) were included to extend the predictability of (dis)comfort to high levels of activity (up to 10 met) and to a wide range of ambient temperatures from 10°C to 30°C.

A preliminary analysis of experimental and simulated data indicated that central temperature affects *TS* in a complex way. Firstly, the contribution of the internal temperature milieu seemed to be non-linear. Secondly, the partial contribution of core temperature did not seem to be simply additive because of some interaction between internal and skin temperature signals. Because of this complication, the appropriate functions were not directly apparent from experimental data, as eg. for the effect of $\Delta T_{sk,m}$ on *TS* in chap. 5.4.1.

The first step in modelling this multiple, non-linear problem (for which the mathematical functions to be linearized are unknown) consisted, therefore, of applying polynomial regression analysis. The strategy of using polynomial approximation opened doors for studying several multiple approaches. However, only the following model provided an useful solution[1]:

$$TS = 3\,tanh\left(f_{sk} + \phi\right) \tag{5.5}$$

where

$$\phi = g_{hy} \cdot g_{sk}$$

and where f_{sk} is a function of $\Delta T_{sk,m}$ as prescribed by eq. (5.4) in chap. 5.4.1, and g_{hy} and g_{sk} are a function of ΔT_{hy} and $\Delta T_{sk,m}$, respectively. These are approximated by power-series polynomials:

$$g_{hy} = a_0 + a_1 \Delta T_{hy} + a_2 \Delta T_{hy}^2 + \ldots \tag{5.7}$$

and

$$g_{sk} = b_0 + b_1 \Delta T_{sk,m} + b_2 \Delta T_{sk,m}^2 + \ldots \tag{5.8}$$

The multiplication of eqs. (5.7) and (5.8), and the linearization of eq. (5.5) gives:

$$Y = \left\{ artanh\left(\frac{TS}{3}\right) - f_{sk} \right\} = \sum_{i=0}^{m} \sum_{j=0}^{n} a_i b_j \Delta T_{hy}^{\,i} \Delta T_{sk,m}^{\,j} \tag{5.9}$$

The application of this equation to data sets of experimentally obtained sensation votes and predicted error signals $\Delta T_{sk,m}$ and ΔT_{hy} led to a system of linear equations

---

[1] The function of ΔT_{hy} was handled as a term of the argument of the *tanh*-function in eq. (5.1) to avoid predicted values penetrating into the undefined zones outside the 7-point ASHRAE scale, ie. $|TS|>3$.

which had to be solved by multiple regression analysis for the combined coefficients $a_0 b_0$, $a_0 b_1$... Truncated polynomials appeared to be most appropriate and were able to describe the principal trends of g_{hy} and g_{sk} reasonably well. In contrast, polynomials of higher degree produced implausible and erratic matchings to the individual dispersed data points. Thus, the shape of the required g_{hy}-function was approximated using a polynomial of the second degree (m=2 in eq. (5.9)). The absolute coefficient a_0 was set to zero for the regression analysis to ensure that g_{hy} vanished as $\Delta T_{hy} \rightarrow 0$. The role of skin temperature in the interacting mechanism, was, in this phase, considered as a polynomial of the first (n=1) degree. This was sufficient to obtain a very good correlation of R=0.97 between sensory estimates and pairs of skin and body core temperatures.

The resultant polynomial of the g_{hy}-function (with a_1=0.98±0.16, a_2=-0.09±0.14) is shown in ***Fig.5.18***. This curve rises almost linearly with positive ΔT_{hy}, passes through

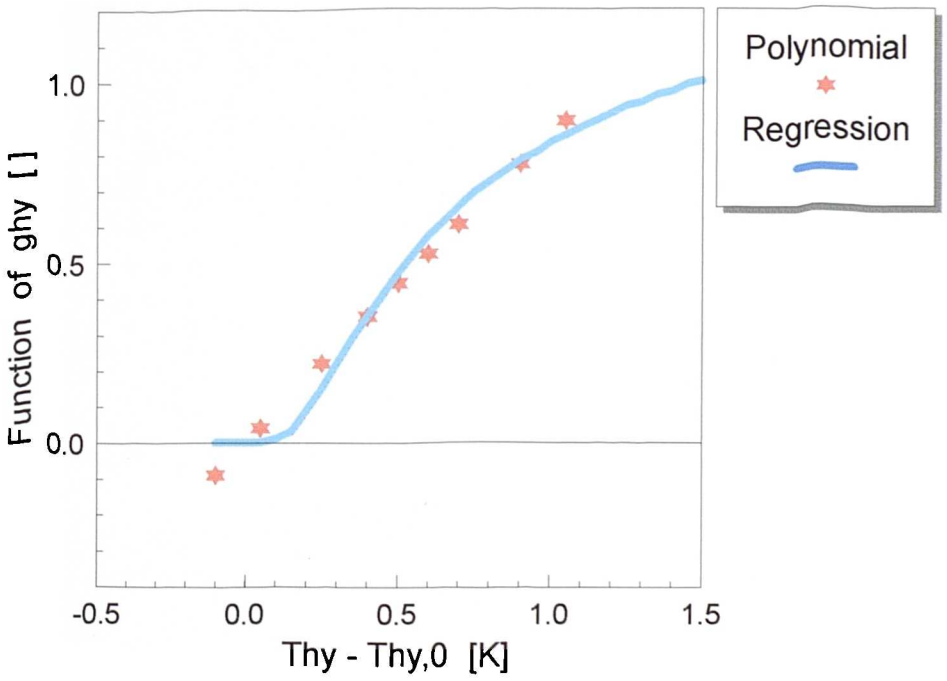

Fig.5.18

The impact of elevated body core temperature due to exercise on thermal sensation, the 2nd-degree polynomial of the g_{hy} -function, and the corresponding exponential regression fit.

the origin and becomes negative for $\Delta T_{hy} < 0$. For modelling the final g_{hy}-function, how-

ever, one had to consider that core temperature does not affect *TS* for $\Delta T_{hy} < 0$ (see ***Fig.5.15*** and the corresponding text) and that g_{hy} will likely not continue to rise for any ΔT_{hy}. The g_{hy}-polynomial was therefore matched (for the domain of central temperature $0<\Delta T_{hy}<1.5$) by the following exponential function:

$$g_{hy} = \exp\left\{\frac{b_1}{\Delta T_{hy}} + b_0\right\} \tag{5.10}$$

The regression coefficients were b_1= **-0.565**±0.122 and b_0= **0.376**±0.027 with r=0.96. The resulting function is drawn ***Fig.5.18***.

Once the partial effect of internal temperature on *TS* was defined, the interacting influence of skin temperature, described by the g_{sk}-function, could now be obtained directly from the experimental data. For this purpose g_{sk} was separated from eq. (5.5) and calculated for each measured *TS*-vote:

$$Y = \left\{\frac{artanh\left(\frac{TS}{3}\right) - f_{sk}}{g_{hy}}\right\} = g_{sk} \tag{5.11}$$

where *TS* represent reported sensation votes, and f_{sk} and g_{hy} result from the corresponding predicted values of $\Delta T_{sk,m}$ and ΔT_{hy} according to eqs. (5.4) and (5.10), respectively. The data-points of g_{sk} are plotted against $\Delta T_{sk,m}$ in ***Fig.5.19***. A similar mathematical function to eq. (5.10) was used to match the data-points in ***Fig.5.19***:

$$g_{sk} = \exp\left\{\frac{b_1}{5 - \Delta T_{sk,m}} + b_0\right\} \tag{5.12}$$

The regression coefficients were b_1=**-7.634**±1.243 and b_0=**1.521**±0.177 with r=0.71.

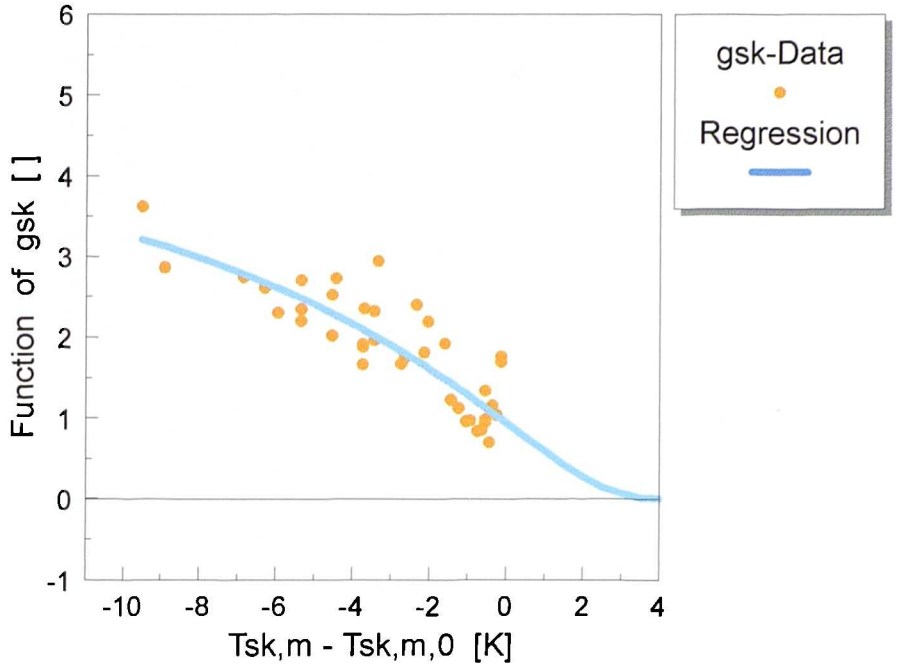

Fig.5.19

The function of skin temperature g_{sk} weighting the effect of body core temperature to thermal sensation. The trend of the data-points resulting from eq. (5.11) was fitted by exponential regression, eq. (5.12).

Summarising, the above analysis revealed the body core (hypothalamus) temperature to affect the thermal sensation in a complex, non-linear manner whereas the contribution of ΔT_{hy} was found to be weighted by the level of thermal strain detected at the skin, $\Delta T_{sk,m}$. The function ϕ, obtained by multiplying eqs. (5.10) and (5.12) reflects these multiple influences:

$$\phi = 6.662 \exp\left\{\frac{-0.565}{\Delta T_{hy}}\right\} \exp\left\{\frac{-7.634}{5-\Delta T_{sk,m}}\right\} \qquad (5.13)$$

with ϕ=0 for $\Delta T_{hy} \leq 0$ or $\Delta T_{sk,m} \geq 5$K.

5.4.3 Dynamic Components of the Human Thermal Sensation

In the foregoing two sections a static, ie. temperature-based, comfort model was developed. The time dependency of body temperatures accounts for some of the effects of time in thermal sensation. For instance, the impact on *TS* of the duration of a cold exposure (causing a fall in skin temperature with time) becomes recognized by the static comfort model. Furthermore, the consideration of the central temperature in addition to skin temperature gives rise to transients due to discrepancies between the thermal states of the body core and the body's periphery. Herein, the internal temperature accounts for the effect of heat storage in the body on the subject's perception of the thermal environment.

Nevertheless, additional, specifically transient phenomena - the subject of investigation in this section - dominate the sensation of temperature in rapid environmental transients. To illustrate this, a comparison between the instantaneous thermal sensation as observed by Gagge et al. [57] as a result of a step change from a neutral to a cold climate (T_a=18°C) and the predicted 'static' TS-index as calculated using eq. (5.5) is shown in ***Fig.5.20***.

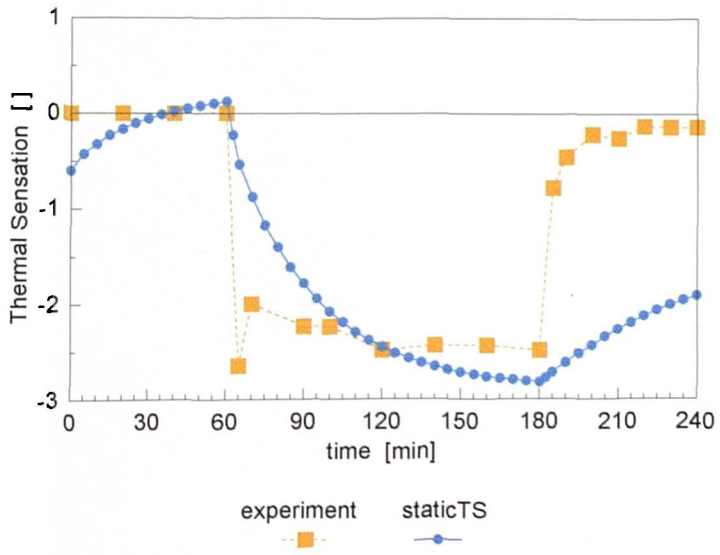

Fig.5.20

Discrepancy between the static comfort model and the dynamic response of subjects exposed to sudden changes in ambient temperature of T_a 28 - 18 - 28°C.

The entry into the cold room, t=60~70 min. in ***Fig.5.20***, was accompanied by an immediate cold-sensation-'overshoot'. In contrast, the static model predicted a gradual fall in *TS* as the mean skin temperature decreased with time. After the initial 'cold-peak' the subjects felt 'cool' with a drift toward 'cold' as the exposure to T_a=18°C persisted [1].

Another appreciable discrepancy between the statically predicted *TS*-index and the actual dynamic response appears for the period after re-entering the thermally neutral room, ie. for t>180min in ***Fig.5.20***. In the experiment, occupants' thermal feelings were close to 'neutral' after just 15min, in contrast, the model predicted continued cold discomfort.

In contrast to step changes downward, the sudden increase in ambient temperature from 28°C to 48°C, ***Fig.5.21***, did not show any 'overshoot' effect in thermal sensation. Thus, *TS* correlated best with skin temperature for 60<t<180 min. It is interesting to note that during this period *TS* did not correlate with the ΔT_{hy}-signal as can be seen from ***Fig.5.9*** in section 5.3.2.2. This observation demonstrates clearly that skin temperature, not core temperature, governs the sensation of temperature in these hot conditions[2].

In the experiment the subjects voted 'warm' but the static model predicted 'hot' when T_a=48°C. This discrepancy, however, was attributed to inter-individual differences in the thermal sensation of the subjects studied in [57] and the *'average'* thermal sensation as predicted by the model (compare also ***Fig.5.16*** in section 5.4.1).

On return to the neutral environment at t=180 min. in ***Fig.5.21***, the subjects voted 'neutral' within 20 min. In contrast, the static model predicted a gradual fall in *TS* re-

---

[1] This indicates the correlation of *TS* with the skin temperature after the initial phase. In contrast, the continuously decreasing trend in skin heat loss $Q_{sk\,m}$, (see for example *Fig.5.8* in section 5.3.2.2), contradicts the thermal sensation votes of the subjects during prolonged cold exposures. Hence, this transient observation provides an argument for rejecting the hypothesis of a calorimetrically oriented human thermal sensation.

[2] A similar conclusion can also be drawn for the impact of skin heat flux in the hot, ie. for 60<t<180 min. in *Fig.5.21*.

aching $TS \approx +1$ at t=240 min. Since the temperature error signal from the skin had approached zero ($\Delta T_{sk,m} \rightarrow 0$) the predicted plateau of 'slightly warm' was exclusively due to core temperature which ranged between $0.35K < \Delta T_{hy} < 0.55K$ above its setpoint at that period of time. The analysis showed that the discrepancy between the predicted, static *TS*-index and the experimentally observed value for $t > 180$ min. did not indicate any special dynamic effect. The participants in the experiment showed a similar, atypical behaviour even at the beginning of the experiment, ie. for $0 < t < 60$ min., where they voted to be thermally neutral despite body core temperatures ranging between $37.2°C < T_{re} < 37.5°C$ (see ***Fig.5.9*** in section 5.3.2.2). The static model, however, predicted $TS \approx 0$ (see ***Fig.5.21***) for this initial exposure because both the mean skin temperature and the hypothalamus temperature as predicted by the model did not deviate noticeably from their reference values of 34.4°C and 37.0°C, respectively.

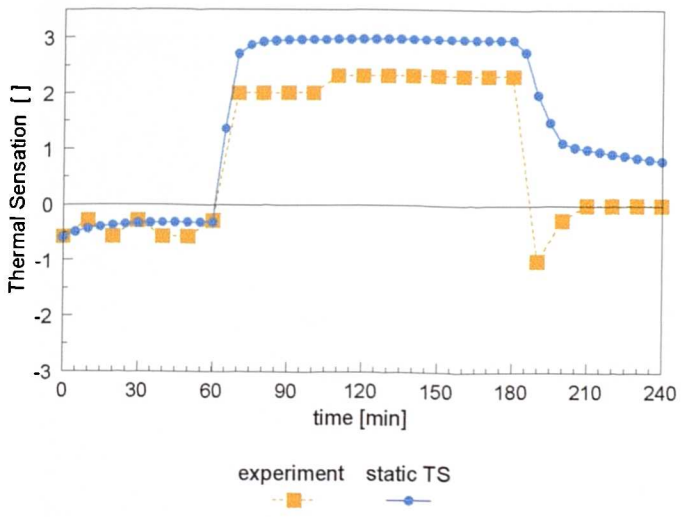

Fig.5.21

Discrepancy between the static comfort model and the dynamic response of subjects exposed to sudden changes in ambient temperature of T_a 28 - 48 - 28°C.

Based on observations made in [57], Gagge was able to demonstrate that the correlation between thermal sensation and skin temperature or regulatory sweating does not apply to transient conditions. This conclusion (to be extended also to *SBF*) is drawn by comparing temporal trends in *TS* (ie. 60<t<90 min. in ***Fig.5.20***, and 180 t<210 min. ***Fig.5.21***) after sudden downward changes in T_a with the corresponding trends for $T_{sk,m}$ and for skin evaporation in ***Fig.5.8*** and ***Fig.5.9***, respectively.

An important result arises from the discrepancy between temporal trends of *TS* and regulatory responses. Namely, that the human thermal sensation does not appear to be directly associated with effector mechanisms of the human themoregulatory system but appears to be an autonomic response.

5.4.3.1 Negative Rates of Change in $T_{sk,m}$

Any transient change in ambient conditions which cause sudden cooling the skin is characterized by an abrupt decrease in thermal sensation. This 'overshoot'-response can occur because of a fall in ambient temperature or any other environmental parameter including relative humidity (see chap. 5.7.1).

Analysis of the rate of change of the *TS*-votes and the predicted rate of change of skin temperature (ie. 60<t<90 min. in ***Fig.5.20*** and ***Fig.5.8*** in chap. 5.3.2.2; and 180<t<210 min. in ***Fig.5.21*** and ***Fig.5.9*** in chap. 5.3.2.2) reveals that the $dT_{sk\,m}/dt$ - signal is the physiological origin of *dynamic* effects on thermal sensation which occur when changes in environmental parameters cause transient cooling of the skin. The appearance of this 'overshoot'-response is not restricted to conditions where cutaneous thermoreceptors send warnings of 'cold' skin temperature. The sensation of 'warm' and 'hot' might also be subject to this transient effect as demonstrated for t> 180 min. in ***Fig.5.21***.

Concluding from this observation and expressed in terms of mathematics, the negative rate of change of the mean skin temperature represents a further, additive signal in the function of *TS*. Its influence was therefore modelled using an *additive* term ψ which was attached to the static terms of *TS*, ie. f_{sk} and ϕ, in the argument of the *tanh*-function in eq. (5.5):

$$TS = 3\,tanh\left(f_{sk} + \phi + \psi\right) \tag{5.14}$$

The rate of change of skin temperature did not seem to be the only determinant

when modelling ψ. Although there is a lack of adequate experimental proof, people seem to be less sensitive to temporal changes in ambient temperatures when working [123]. The authors own simulation results, however, have shown that the impact of temporal changes in ambient temperature on *TS* is more pronounced during periods of exercise than when resting. This is because exercise is associated with additional thermal loads such as increased surface convection due to body motion and/or the evaporation of sweat even in cold climates. In effect, the predicted dynamic thermal sensation would, therefore, respond by increased sensitivity to transient changes in climatic parameters when the level of activity increases and when ψ would be a function only of $dT_{sk\,m}/dt$. Hence, the term of negative $dT_{sk\,m}/dt$-rates, τ_-, was hypothetically weighted by ϕ - the term which is responsible for changes in *TS* due to exercise in the model :

$$\psi = \frac{\tau_-}{1 + \phi} \qquad \tau_- = b \frac{dT_{sk,m}}{dt} . \tag{5.15}$$

The coefficient b was determined by linear regression using a rearranged equation (5.14):

$$Y = \left\{ \left[artanh\left(\frac{TS}{3}\right) - \left(f_{sk} + \phi\right) \right] \times \left(1 + \phi\right) \right\} = b \frac{dT_{sk,m}}{dt}$$

where *TS* is the thermal sensation as reported in experiments; f_{sk} and ϕ are a function of predicted $\Delta T_{sk,m}$- and ΔT_{hy}-values according to eqs. (5.4) and (5.13); and $dT_{sk,m}/dt$ is the predicted rate of change of the mean skin temperature.

The regression coefficient b was determined separately for the step change in ambient temperature from neutral to cold, ie. for 60<t<90min in ***Fig.5.20***, and for the sudden change from hot to neutral, ie. for 180<t<210min in ***Fig.5.21***. In the latter case there was a continuous discrepancy between the predicted static *TS* and the reported thermal sensation which resulted from elevated body core temperature (which were about 0.5K above the setpoint and yet perceived to be neutral by the test-persons, see text above). In order to eliminate this systematic error from the

regression analysis only the relative effect of ψ was evaluated :

$$Y = \left\{ artanh\left(\frac{TS}{3}\right) \times (1 + \phi) \right\} = b \frac{dT_{sk,m}}{dt}$$

The linear approach of eq. (5.15) provided very good fits to the dynamic behaviour of *TS* for b = 0.112 ± 0.006 with r=0.96 (see ***Fig.5.22***), and b = 0.115 ± 0.006 with r=0.98 (see ***Fig.5.23***), respectively.

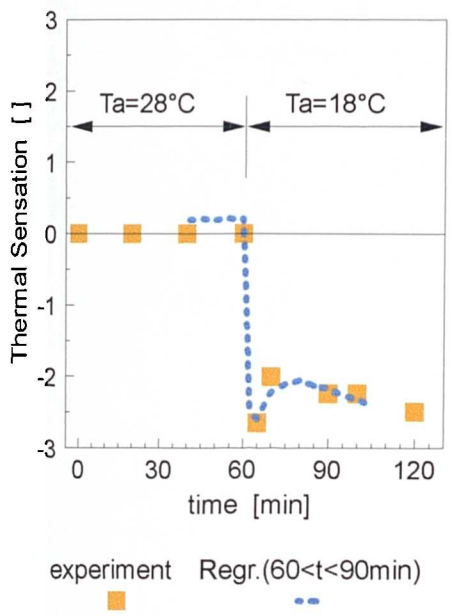

Fig.5.22

Regression fitting the 'overshoot' of cold sensation as experienced after entering a cold room by addition of the $dT_{sk,m}$ dt -signal to the static model.

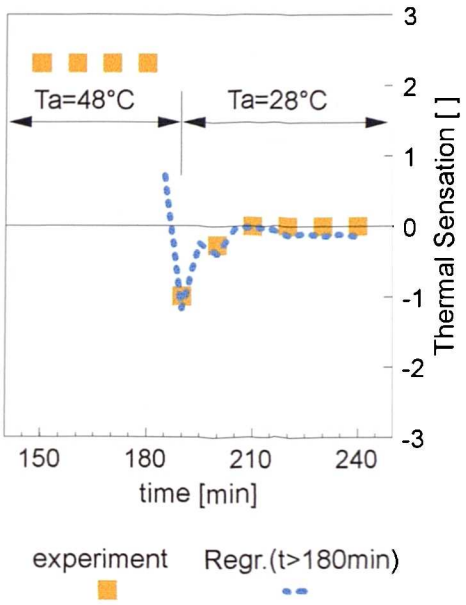

Fig.5.23

Regression fitting the relative effect of the $dT_{sk,m}$ dt-signal to thermal sensation as experienced after a sudden change in ambient temperature from hot to neutral.

The apparent similarity of b=0.112 and b=0.115 was obtained for the two disparate cases of sudden changes in T_a. This indicates that the b-coefficient which stands for the sensitivity of *TS* to $dT_{sk,m}$ dt is fairly independent of the level of skin temperature. Hence, a common value of ***b*=0.114** was used in the final model.

5.4.3.2 Positive Rates of Change in $T_{sk,m}$

A different approach from that developed in section 5.4.3.1 was required to model the dynamic component of thermal sensation when positive rates of change of the mean skin temperature occur. Neither the step change in ambient temperature from cold to neutral (t>180min in ***Fig.5.20***) nor from neutral to hot (t>60min in ***Fig.5.21***) was accompanied by any transient peak in sensation despite such predicted trends in the $dT_{sk,m}/dt$-variable in ***Fig.5.8*** and ***Fig.5.9*** (both section 5.3.2.2).

The lack of any 'peak'-shaped response gave reason to suppose that the signal-processing mechanism of the dynamic thermal sensation does not utilize sequences of $dT_{sk,m}/dt$ -rates while skin is warming. Instead, the 'shock'-experience and its strength appeared to dominate the sensation of temperature after the sudden increase in ambient temperature. Thus, the application of a 'memory'-function concept was employed to model the quick adaptation of *TS* to the new environmental situation after *t*>180 min. in ***Fig.5.20***. In this process of recent thermal history evaluation, the most 'dangerous' warning of skin heating (ie. the maximum positive rate $(dT_{sk,m}\ dt)_{max}$) is 'stored' to be weighted afterwards by a function of the time which has elapsed since the occurrence of this event:

$$\tau_{+} = \left(\frac{dT_{sk,m}}{dt}\right)_{max} \cdot \exp\left\{ b_1 \Delta t + b_0 \right\} \qquad (5.18)$$

where $\Delta t = t - t_0$, and t_0 is the time of occurrence of the highest rate $dT_{sk,m}\ dt$. The regression for obtaining the coefficients b_1 and b_0 was performed by recognizing the moderating role of the ϕ-term as described for negative rates of change of $T_{sk,m}$ in the foregoing section. Thus, the following expression was subjected to statistical analysis:

$$Y = \ln\left\{ \frac{artanh\left(\frac{TS}{3}\right) - (f_{sk} + \phi)}{\left(\frac{dT_{sk,m}}{dt}\right)_{max}} \times (1 + \phi) \right\} = b_1 \Delta t + b_0$$

As a result, regression coefficients of b_1=**-0.681** ± 0.029 [h^{-1}] and b_0=**-1.985** ± 0.029 [] (r=-0.99, ***Fig.5.24***) were obtained for the step change in ambient temperature from cold to neutral (180<t<240 min. in ***Fig.5.20***).

In contrast to the sudden change in ambient temperature from cold to neutral, no special dynamic thermal sensation effect was observed for the sudden increase in T_a from neutral to hot (t>60 min. in ***Fig.5.21***). This behaviour, ie. a vanishing influence of positive $dT_{sk,m}/dt$ -signals on *TS* when the basic, ie. 'static' thermal sensation indicates 'warm' or 'hot' (*TS*>2), is reproduced to a certain extent by the model. The reason for this arises from the non-linear behaviour of the *TS*-(*tanh*)-equation (5.14) near the upper limit of the sensation scale where additional positive signals do not elevate noticeably the *TS* -function any more.

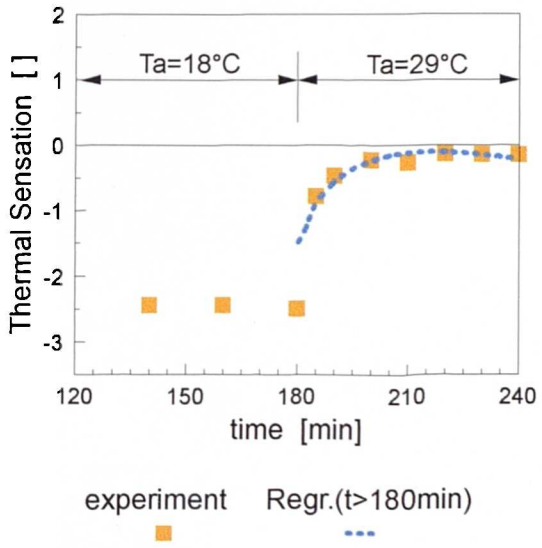

Fig.5.24

Regression to the transient effect of skin warming to thermal sensation as experienced after a sudden change in ambient temperature from cold to neutral (see text).

The model 'remembers' the impulse until it vanishes in time or until the next, more unfavourable, event occurs, ie. when:

$$\frac{dT_{sk,m}}{dt} > \frac{\tau_+}{0.137} .$$

Then, the $(dT_{sk,m}/dt)_{max}$ -signal is reset to the actual value of $dT_{sk,m}\ dt$.

5.4.4 Summary

In sections 5.4.1 to 5.4.3 a new, dynamic comfort model based on physiological principles was developed. The individual components of the human temperature sensation leads to the following equation for the *Dynamic Thermal Sensation*-index, ***DTS*** :

$$DTS = 3\,tanh\left(f_{sk} + \phi + \psi\right) \tag{5.21}$$

where

$$f_{sk} = 1.026 \cdot \Delta T_{sk,m} \qquad for \qquad \Delta T_{sk,m} > 0$$

and

$$f_{sk} = 0.298 \cdot \Delta T_{sk,m} \qquad for \qquad \Delta T_{sk,m} < 0$$

The term ϕ in eq. (5.21) stands for the effect of core temperature on thermal sensation as a multiple function of the temperature error signals from the hypothalamus, ΔT_{hy}, and from the skin, $\Delta T_{sk,m}$:

$$\phi = 6.662 \exp\left\{\frac{-0.565}{\Delta T_{hy}}\right\} \exp\left\{\frac{-7.634}{5 - \Delta T_{sk,m}}\right\}$$

and ϕ=0 when $\Delta T_{hy} \leq 0$K or $\Delta T_{sk,m} \geq 5$K. The last term of eq. (5.21), ψ, collects the dynamic components of *DTS* :

$$\psi = \frac{\tau_- + \tau_+}{1 + \phi} \tag{5.25}$$

where

$$\tau_- = 0.114 \frac{dT_{sk,m}}{dt} \qquad for \qquad \frac{dT_{sk,m}}{dt} < 0$$

and

$$\tau_+ = 0.137 \left(\frac{dT_{sk,m}}{dt}\right)_{max} \cdot e^{-0.681\Delta t} \qquad for \qquad \frac{dT_{sk,m}}{dt} > 0$$

In the model, the simultaneous appearance of both τ_- and τ_+ was permitted to avoid inconsistencies in predicting *DTS* which could result from the application the 'either-or' concept in eq. (5.25). In situations where τ_+ is active, eg. after moving from a cooler to a warmer space, any negligible temporal inversion of the $dT_{sk,m}/dt$ -rate (caused eg. by fluctuating air motion and sweating) would immediately cancel the process of adapting the thermal sensation to new thermal conditions. For such, rather unique situations, the governing $(dT_{sk,m}/dt)_{max}$-impulse was not dropped, instead it was reduced in a balanced way depending on the magnitude of the actual negative $dT_{sk,m}/dt$ -rate:

$$\tau_+ = 0.137 \frac{\left(\frac{dT_{sk,m}}{dt}\right)_{max}}{1 + z} e^{-0.681\Delta t}$$

where

$$z = \frac{-dT_{sk,m}/dt}{\left(\frac{dT_{sk,m}}{dt}\right)_{max}}$$

and z=0 for $dT_{sk,m}/dt$ >0.

5.5 Testing the Comfort Model

All the experiments described in section 5.3 were re-simulated using the complete comfort model. The results are presented in this section. The validation of the new model using additional experiments is discussed in section 5.7.

Comparisons of predicted *DTS*-values and the Thermal Sensation Votes (*TSV*) reported by Nevins et al. [141] and Rohles et al. [158] for ambient temperatures ranging from 15 to 37°C are shown in ***Fig.5.25*** and ***Fig.5.26***. Thermal sensation votes after 3 hours of exposure as predicted and as reported for relative humidities of 15% and 85% are drawn in ***Fig.5.25***. Also plotted are values of the *PMV*-index. There was a good agreement between *TSV*, *DTS* and Fanger's *PMV* within the zone of mild ambient temperatures, ie. from of about 20 to 30°C which approximately covers the range of validity of the Fanger model as recommended by ISO 7730 [94]. However, discrepancies in *PMV* resulted for exposures outside this zone where increasing bodily cold or warm stress occurred and where the linear *PMV*-model did not reproduce the non-linear trends of *TSV*.

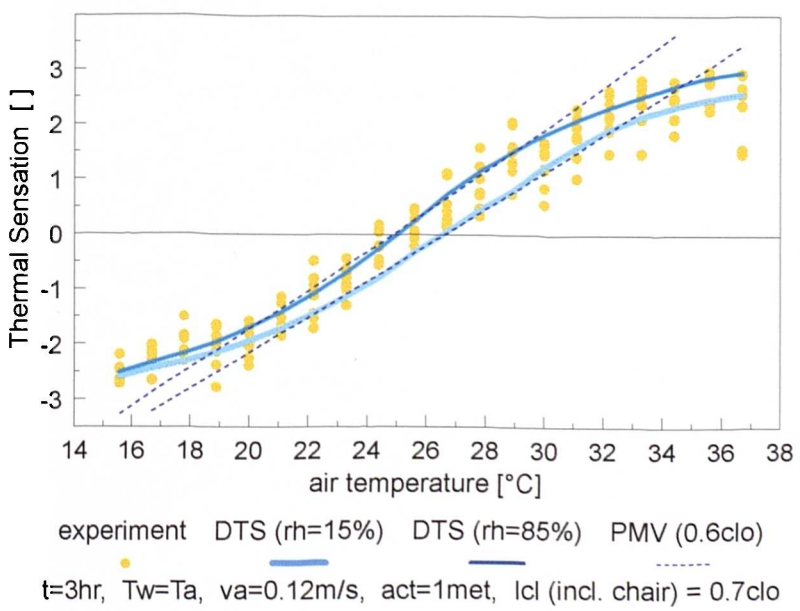

Fig.5.25

Thermal sensation values after 3 hours of exposure as reported by Nevins et al. [141] and Rohles et al. [158] for ambient temperature ranging from 15 to 37°C, and as predicted by the present DTS-model and Fanger's PMV-model for relative humidities of 15% and 85%.

In ***Fig.5.26***, *DTS*-values are shown for two different times, ie. 1hr and 3hr after exposure to constant climatic conditions. All thermal sensations were averaged over all relative humidities. As in the experimental observations made by Nevins et al. and Rohles et al. (see also ***Fig.5.4***), there was an effect of time on the *DTS*-response both in cold- and warm conditions. In environments where T_a<24°C *DTS* fell with time due to passive system cooling as the exposure continued. The model also predicted a fall in thermal sensation with time for warm conditions. The seemingly paradoxical behaviour of the model (also observed experimentally) arose from the effect of the positive $dT_{sk,m}/dt$-values (see section ***5.4.3.2***) predicted after the step change from the neutral pretest conditions into the warm climates.

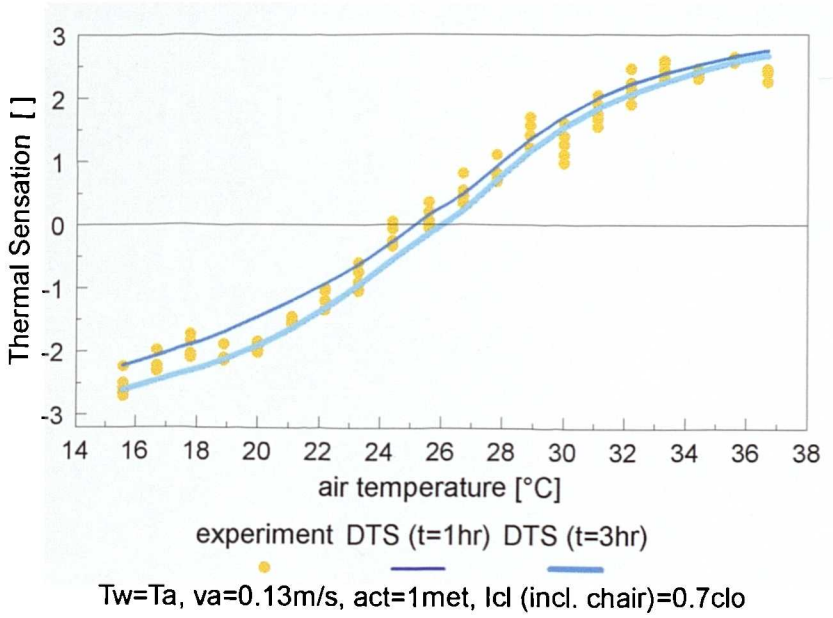

Fig.5.26

The time dependency of reported [158] and predicted thermal sensation as averaged over relative humidity.

It seems to be a common experience that test-subjects also perceive neutral conditions to be warmer at the beginning than at the end of the exposure. This effect is well known as the so called '*short-term adaptation*' and is sometimes ascribed to an increased metabolic rate at the beginning of experiments [158]. Unfortunately, the experimental data of Nevins et al. and Rohles et al. did not provide any quantitative information on metabolic rates and their variation over time. However, simulation results from the present model seem to support the hypothesis of gradually decrea-

sing metabolism as the origin for short-term adaptation in neutral conditions. In ***Fig.5.27***, the initial activity level was assumed to be higher, ie. 1.6 met for the first 10 minutes, than for the rest of the 3-hour exposure (1.0 met) to T_a=25.6°C.

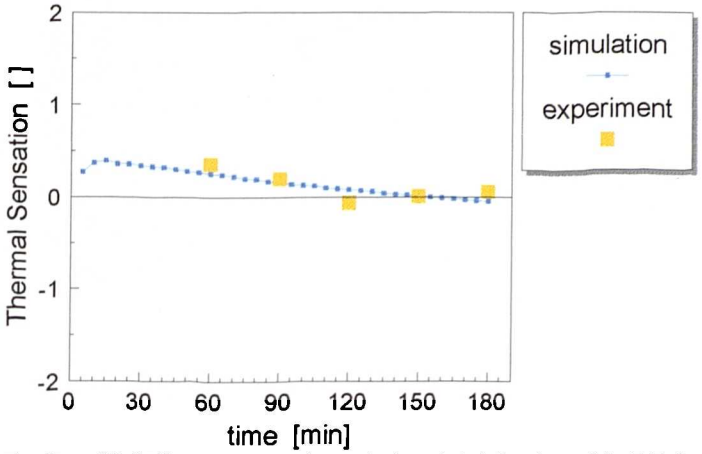

Fig.5.27

The course of DTS as predicted for slightly increased activity (1.6met) at the beginning (0<t<10min) of the exposure in a thermally neutral environment as an attempt to explain the "short-term adaptation" effect.

The predicted dynamic thermal sensation was compared with the experimental data for sudden changes in ambient temperature in ***Fig.5.28*** and ***Fig.5.29***. The model reproduced well both the dynamics and the statics of thermal sensation for changes in ambient temperature from neutral toward cold and back, and for the 2-hour exposure to 18°C, ***Fig.5.28***. In contrast, the application of the stationary *PMV*-model to the non-moderate ambient temperature of 18°C, with minimum clothing, did not provide reliable results (*PMV*<<-3).

Poorer agreement between *DTS* and *TSV* was obtained for the exposure to ambient temperatures of 28-48-28°C. The model predicted a sensation of 'hot' whilst T_a=48°C, instead of 'warm' as voted. Similarly, the model predicted a higher *DTS* than measured *TSV* for the overheated human body in the subsequent exposure to 28°C. These discrepancies, however, were found to arise from the rather atypical perceptions by the subjects studied in [57] (see also ***Fig.5.16*** in section 5.4.1, and section 5.4.3).

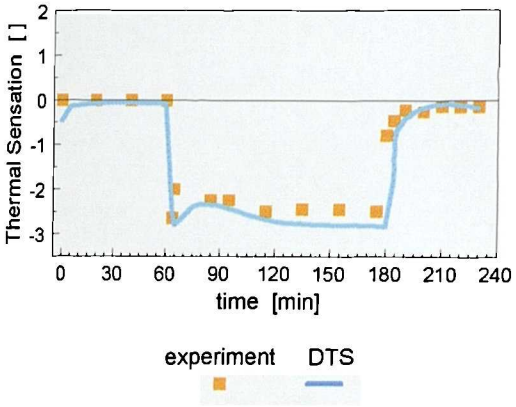

Fig.5.28

Thermal sensation during step-change exposures in ambient temperature of 28-18-28°C [57].

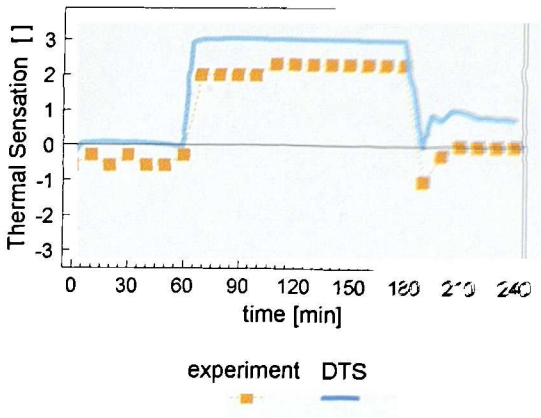

Fig.5.29

Thermal sensation during step-change exposures in ambient temperature of 28-18-28°C [57].

The performance of the comfort model when predicting thermal sensation during exercise is demonstrated in ***Fig.5.30*** and ***Fig.5.31***. *DTS* is compared with sensation votes reported by McNall et al. [127] and *PMV* for combinations of steady ambient temperatures and intermediate exercise in ***Fig.5.30***.

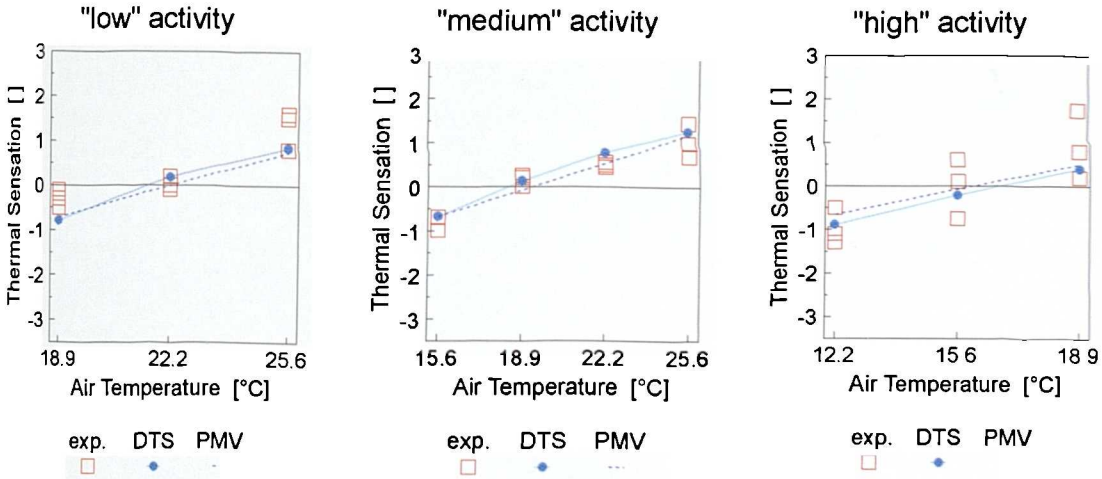

Fig.5.30

DTS, PMV and observed [127] mean thermal sensation votes after three hours of exposure to different ambient temperatures and for three moderate levels of intermittent work, ie. "low" activity (1.6met), "medium" activity (2.1met) and "high" activity (2.7met).

The three different metabolic rates of average 1.6 ('low' activity), 2.1met ('medium'

activity), and 2.7 met ('high' activity) resulted from intermittent exercise of various stand-walk cycles (see section 5.3.3). The *DTS* and experimental data correspond to thermal sensations after three hours of exposure. The experimental and simulated clothing ensemble correspond to the *KSU*-uniform (I_{cl}= 0.6). In general, there is good agreement between *DTS*, *TSV* and *PMV* for intermediate work and ambient temperatures in the narrow range of relative thermal comfort.

Finally, *DTS* predicted during high levels of continuous work (4, 6, and 10met) and a wide range of ambient temperatures are plotted together with the corresponding measured values in ***Fig.5.31***. The data corresponded to seminude subjects and exposure times of 35 minutes. The Fanger-model predicted *PMV*-values within the range of the ASHRAE-scale *only for the lowest level of activity (4met)*, otherwise *PMV*>>+3.

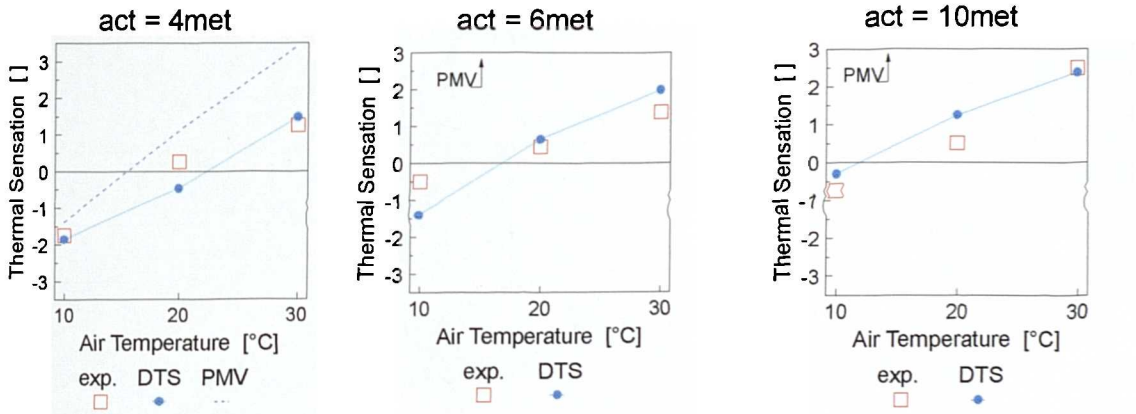

Fig.5.31

Thermal sensation as predicted by the present model and as observed by Gagge et al. [58] for three high levels of activity, minimum clothing, and ambient temperatures of 10°, 20°, and 30°C.

5.6 Further Indices

The dynamic thermal sensation (*DTS*) as predicted by the model for an average person can be used as an index for judging thermal situations. However, it is often useful to have a measure of the probability that environmental conditions will be acceptable, or expressed in the opposite way, the percentage of occupants likely to be dissatisfied with the actual climate.

Fanger [46] developed the index of Predicted Percentage of Dissatisfied (*PPD*) in order to estimate the number of persons *"who in practice will be inclined to complain about the environment"*. The *PPD*-formula was also employed in the present model, by substituting Fanger's original *PMV*-index with the *DTS*-variable. The predicted percentage dissatisfied is calculated following the Fanger formulation [94] by:

$$PPD = 100 - 95 \exp\left\{-0.03353 \cdot DTS^4 - 0.2179 \cdot DTS^2\right\}$$

This approach recognizes that even in thermally neutral conditions (ie. *DTS*=0) there are still about 5% of occupants who are dissatisfied with the "optimum" thermal environment.

In hot environments where there is the danger of heat disorder, the thermal sensation index no longer appears to be an adequate guide to physiological strain.

In the zone of environmental conditions where sweating is able to keep the core temperature fairly constant, indices based on sweat rate, eg. Predicted 4-hour Sweat Rate, *P4SR* [119], Heat Stress Index, *HSI* [10], and Index of Thermal Stress, *ITS* [64], are a sensitive measure of physiological strain. Heat stress indices such as *HSI* and *ITS* are defined as the ratio between the required rate of sweat evaporation and the maximum evaporative heat loss from the skin. The difference between internal heat production and the heat loss by radiation and convection is the required rate of sweat evaporation.

The skin wettedness w_{sk} as predicted by the present model represents, conceptually, the same measure of physiological strain as *HSI* and *ITS*. Therefore, although various simplifying assumptions were made in the models of *HSI* and *ITS*, the individual heat stress categories as listed in *appx.* C, ***Tab.C.1***, are directly applicable to predicted w_{sk}-values.

In severe hot (humid) conditions the thermoregulatory mechanisms of vasomotion and sweating fail. There is not enough evaporative cooling power to maintain equilibrium between bodily heat generation and environmental heat loss. In effect, heat is accumulated and body temperatures rise with time. In these conditions, internal temperature rather than w_{sk} appears to be the suitable measure of physiological strain, tolerance and safety limits, and permissible exposure times. Exposures must be terminated before the deep body temperature is elevated to dangerous level. Many industrial working situations come into this category.

The requirements for an exposure standard were considered by the National Institute for Occupational Safety and Health [145] (quoted by McIntyre [126]). They adopted the WHO [199] criterion that the body core temperature should not be allowed to rise above 38°C for industrial workers.

A rise in body core temperature of about 1.4K (corresponding to a predicted internal temperature of 38.4°C) is considered to be the average voluntary tolerance limit [6]. Heat stroke may occur when the rectal temperature reaches the danger level of about 40.5°C [169] and collaps can then occur very suddenly (a rise in core temperature of about 3.8°C [6]).

On the other hand, a fall in body core temperature below 35°C threatens a loss of body thermoregulation, while 28°C is considered critical for survival [6].

The critical tolerance limit for the mean skin temperature of *resting* subjects is about 25 °C. However, exercising subjects may tolerate even lower skin temperatures. Pain is elicited by local hot and cold stimuli when skin temperatures reach 46°C and 5-7°C (hands and feet), respectively [6].

5.7 Validation of the Comfort Model

The performance of the comfort model can probably be best tested using experiments of comfort under transient conditions. Instationary conditions are associated with transient thermophysical effects in the body and provoke dynamic reactions in thermoregulation and comfort perception.

In general three types of non-steady-state climatic conditions can be identified. Discrete conditions are experienced daily when moving from one space to another which has different ambient conditions or when passing from indoors to outdoors or vice versa. Abrupt changes, for example, in clothing (eg. taking off the jacket), or solar irradiation (eg. partly-cloudy sky), frequently appear and also belong to this category.

Monotonic temporal changes in indoor temperature occur both in free-running buildings and actively controlled buildings. These effects are due to interaction between the climate and the building, the impact of occupants and the interia and capacity of the control-system. Cyclical temperature fluctuations in indoor spaces are attributed to room thermostat adjustments, and the deadband of HVAC-systems.

In addition to environmental transients, time-varying activity levels frequently occur. These affect the dynamic perception of comfort and temperature. In the following sections, the performance of the present comfort model will be validated for this effect as well as for the building and climatically induced transients noted above.

5.7.1 Sudden Changes in Ambient Temperature and Relative Humidity

An appropriate test of the model's behaviour due to positive and negative rates of $dT_{sk,m}/dt$ is a comparison with the sensation votes observed in experiments during *sudden* changes in environmental parameters.

Step changes in ambient temperature were investigated by de Dear et al. [38]. The subjects were exposed to four types of sudden change - slightly warm to neutral (sW/N), neutral to sl. warm (N/sW), sl. cool to neutral (sC/N), and neutral to sl. cool (N/sC). In the experiments, the operative temperature[1)] was adjusted to achieve the desired level of comfort according to the *PMV*-model for three different levels of clothing insulation - naked, 0.6 clo and 1.0 clo. However, as can be seen eg. from ***Fig.5.33*** and ***Fig.5.36*** the subjects' sensation votes in the experiments were not always coincident with the expected (dis)comfort level. Air velocities of v_a<0.1m s^{-1} and relative humidity of rh= 50% were common to all exposures. The seated subjects (n=12, act=1.0-1.1met) first spent 90 min in a climate chamber in steady environmental conditions, and they were moved for a further 90 min into an adjacent room with different ambient conditions.

Predicted *DTS*s are compared with the reported sensation votes in ***Fig.5.32*** to ***Fig.5.37***. Although the test-persons' sensation votes differed from the expected levels of (dis)comfort on some occasions, there was generally good agreement between observation and simulation. The model predicted constantly lower sensations by about 1 scale unit for the step change from slightly cool to neutral (sC/N in ***Fig.5.35***, I_{cl}=0.6clo) where the average vote of 6 subjects was near "neutral" throughout the whole 3-hr experiment. Discrepancies of a similar size between *DTS* and reported sensations arise also from ***Fig.5.37***.

The biggest difference, of more than one scale unit, resulted for the initial "neutral" exposure to 18°C (I_{cl}=1clo) in ***Fig.5.36*** (N/sC), whereas the test persons felt slightly warm, the model predicted a *DTS* close to the experimental expectation (N/sC). The deviations between prediction and observation lie within the expected standard error due to interindividual differences (the thermal sensation predicted by the model is for an average person). Statistical analyses of experiments involving a large number of test-subjects revealed that the standard deviation of the sensation vote ranged between 0.8 and 1.0 category of warmth [124] (noted in [126]).

---

1) Operative temperature T_o integrates the effects of air and radiant temperatures. T_o was simulated by setting T_a=T_w.

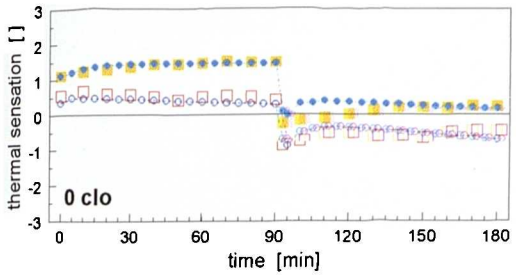

Fig.5.32

Responses of sedentary subjects, I_{cl} 0clo, to downward step-changes in T_o.

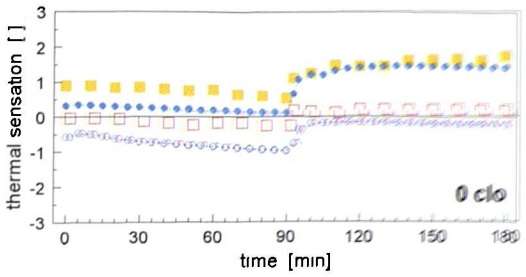

Fig.5.33

Responses of sedentary subjects, I_{cl} 0clo, to upward step-changes in T_o.

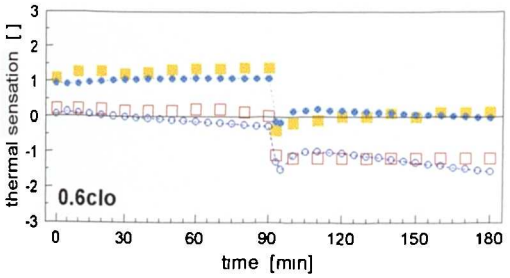

Fig.5.34

Responses of sedentary subjects, I_{cl} 0.6 clo, to downward step-changes in T_o.

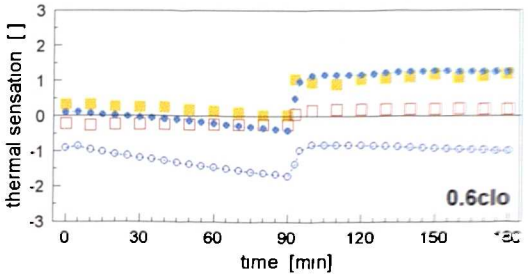

Fig.5.35

Responses of sedentary subjects, I_{cl} 0.6 clo, to upward step-changes in T_o.

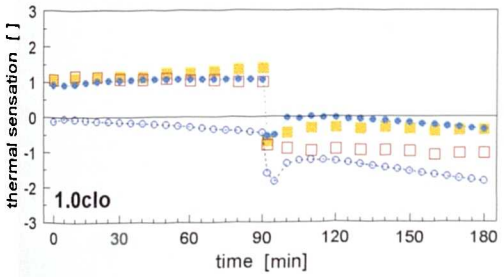

Fig.5.36

Responses of sedentary subjects, I_{cl} 1clo, to downward step-changes in T_o.

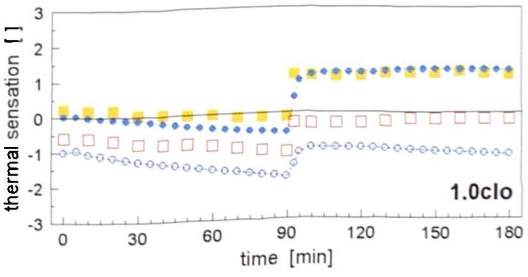

Fig.5.37

Responses of sedentary subjects, I_{cl} 1clo, to upward step-changes in T_o.

The model reproduced correctly the typical sudden decrease in sensation observed after downward-changes in ambient temperature (left-hand-side figures) by using the negative rate of change in $T_{sk,m}$ as a simple-additive afferent signal. Both the magnitude and the time of occurrence of the transient fall in *DTS* were coincident with experiment.

Upward-changes in T_a (right-hand-side figures) were also associated with strong dynamic responses in thermal sensation. The model reproduced well this instantaneous effect by using the "memory"-function of positive $dT_{sk,m}/dt$-signals: *DTS* adapted within 10 min to the final "steady-state" thermal sensation irrespective the preceding level of discomfort, either neutral or cold.

Sensation responses during step changes in relative humidity as occurring, for instance, when people walk from a humid outdoor environment into a dry indoor environment were studied in [37]. The experimental design consisted of exposing sedentary subjects (n=12) to two different relative humidities in quick succession. The experiments took place in twin climate chambers with the same ambient temperatures. Two directions of humidity-change were investigated, ie. downward steps from 80% to 20%, and upward steps from 20% to 85% for two levels of clothing insulation, ie. 0clo and 1clo. The results of the experiment and simulation are shown in ***Fig.5.38*** and ***Fig.5.39***.

It should be noted that reported feelings of warmth for I_{cl}=1clo corresponded to subjects dressed in non-hygroscopic materials (polyester). In hygroscopic textile materials special transient processes such as absorption and description of moisture can occur which may influence the perception of comfort [37]. These phenomena, however, are not considered in the model. At present, a steady-state clothing model is used which does not allow for thermodynamic responses of garments.

The figures demonstrate that dynamic thermal sensation responses can also be elicited by step-changes in relative humidity. Sudden changes in rh induce abrupt changes in the evaporation of sweat and/or the diffusion of moisture through the skin. This is accompanied by corresponding $dT_{sk,m}/dt$-signals which are considered as the

physiological reason for the dynamic response in thermal sensation in these conditions.

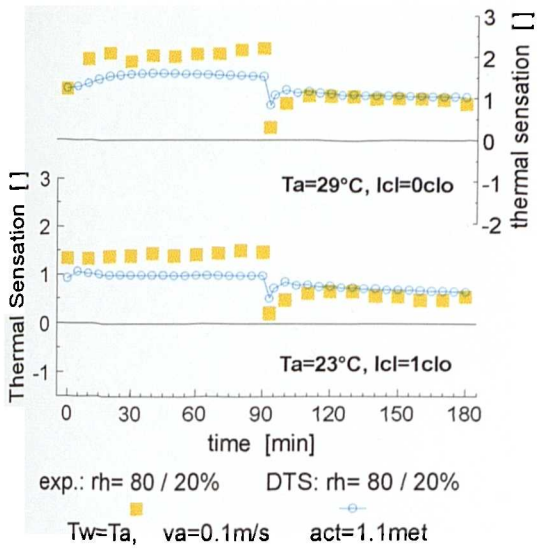

Fig.5.38

Thermal sensation during downward step changes in relative humidity.

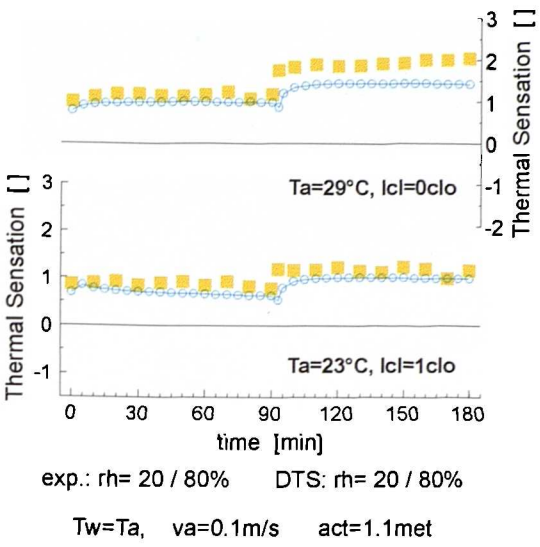

Fig.5.39

Thermal sensation during upward step changes in relative humidity.

5.7.2 Monotonic Changes in Ambient Temperature

Experiments on thermal comfort during monotonic, gradual changes in ambient temperature are appropriate to validate the comfort model for temporal changes in the heat content of the body. In this case rates of change in $T_{sk,m}$ are small, and so the effect of the $dT_{sk,m}/dt$-signal on *DTS* is minimal.

In an effort to provide a basis for new energy conservation strategies for the built environment, Berglund et al. [14] studied the thermal acceptability of occupants to slow, one-directional temperature changes. The test-persons (n=12) spent 30 minutes in an environment of 25°C before being exposed to each of the following ramps in ambient temperature starting at T_a=25°C: ±0.5 K h^{-1}, ±1.0 K h^{-1}, and ±1.5 K h^{-1}. Throughout the testing, the chamber's air and wall temperatures were equal, and the air velocity and the dew point were constant at 0.1 m s^{-1} and 12°C, respectively. During the experiment the subjects were allowed to converse, and played games, etc. - an

activity level near 1.1 met. Every thirty minutes the subjects walked slowly about the test chamber for 5 minutes (*act*≈2met).

The comparison between thermal sensation as predicted dynamically by the present model and the observed experimental data are shown in ***Fig.5.40*** to ***Fig.5.45***. There was good agreement between *DTS* and the voted thermal sensations for all changes in ambient temperature. The deviations between experiment and simulation were always lower than the expected standard error of the sensation vote (0.8 to 1.0 scale units noted above).

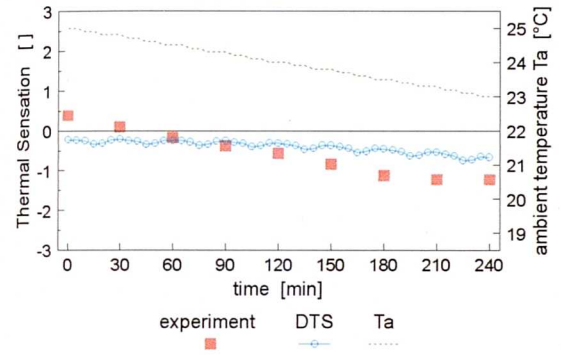

Fig.5.40

Temporal trends of thermal sensation as reported [14] and as predicted during a ramp of ***-0.5 K h^{-1}*** *and* I_{cl}*=0.5clo.*

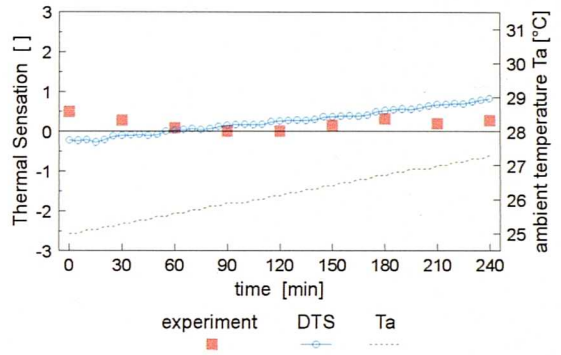

Fig.5.41

Temporal trends of thermal sensation as reported [14] and as predicted during a ramp of ***+0.5 K h^{-1}*** *and* I_{cl}*=0.5clo.*

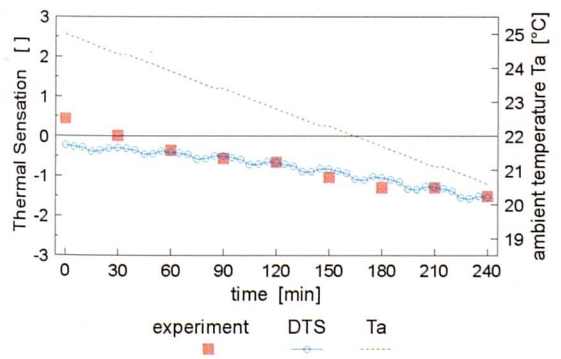

Fig.5.42

Temporal trends of thermal sensation as reported [14] and as predicted during a ramp of ***-1.0 K h^{-1}*** *and* I_{cl}*=0.5clo.*

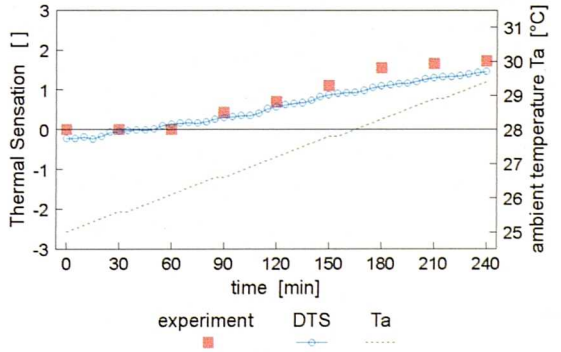

Fig.5.43

Temporal trends of thermal sensation as reported [14] and as predicted during a ramp of ***+1.0 K h^{-1}*** *and* I_{cl}*=0.5clo.*

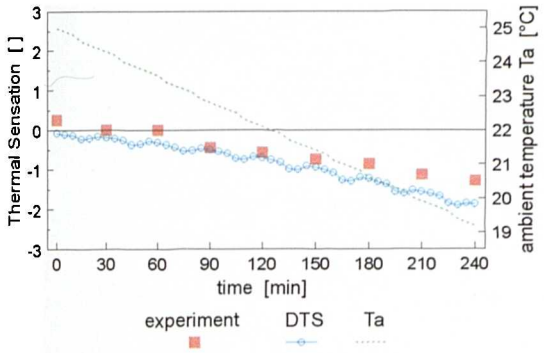

Fig.5.44

Temporal trends of thermal sensation as reported [14] and as predicted during a ramp of $-1.5\ K\ h^{-1}$ *and* I_{cl} *0.5clo.*

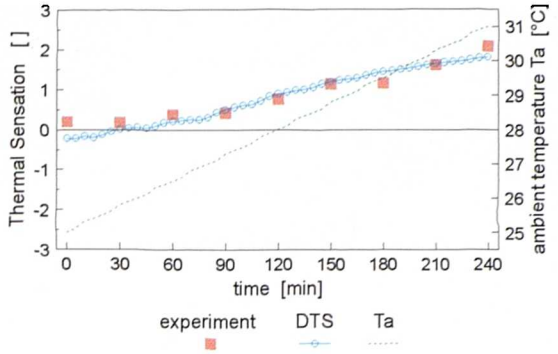

Fig.5.45

Temporal trends of thermal sensation as reported [14] and as predicted during a ramp of $+1.5\ K\ h^{-1}$ *and* I_{cl} *0.5clo.*

5.7.3 Periodic Changes in Ambient Temperature

From a thermophysiological point of view periodic changes in environmental temperature represent complex conditions where several dynamic effects overlap. Under these conditions *DTS* is a composite of temporal changes in skin temperature, changes in the rate of change in $T_{sk,m}$, and time-varying body core temperatures.

Nevins [142] studied the effect of cyclic variations in ambient temperature on subjects (n=11) performing light office-type activity. The ambient temperature altered by ±5K from a starting temperature of 25°C at rates of ±0.3 K min^{-1} over a period of 2 hours. Relative humidity was kept constant at 50%. The subjects rested on (office) chairs for 15 minutes (*act*=1.0met) and walked slowly about the chamber. The resultant activity level during the walk-period was determined to be *act*=1.5met. The mean air velocity for both resting and walking was 0.25 m s^{-1}. Thermal sensation as voted by males and females, and as predicted by the model, are plotted in ***Fig.5.46***.

The model predicted correctly both the trend and the level of the thermal sensation. For the last 15 minutes of the experiment the prediction was closer to the sensation votes of females rather than of males who were at comfort for this period of time.

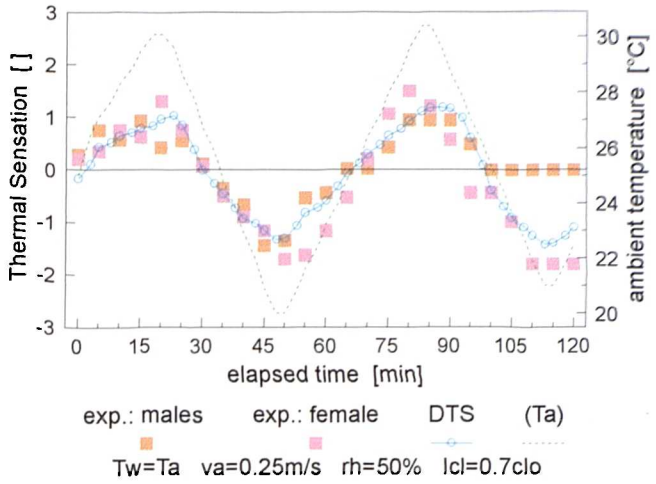

Fig.5.46

Temporal trends of thermal sensation as reported [142] and as predicted for cyclic changes in air temperature of ±5K about the initial temperature of T_a 25.6°C.

In ***Fig.5.47*** and ***Fig.5.48*** the *DTS* is compared with reported sensation votes for two different sinusoidal swings in air temperature [173]. In the experiments, subjects (n= 12) were exposed to various amplitudes and rates of change above the base air temperature of 25.6°C. In all the tests, the mean radiant temperature, relative humidity, and air velocity were kept constant at 25.6°C, 45%, and 0.14 m s^{-1}, respectively. The sedentary subjects were clad in the standard KSU-uniforn and were allowed to study, read, or engage in conversation (*act*≈1.0met). The experimental results were presented in the form of regression equations where the thermal sensation was described using ambient temperature and the rate of change in ambient temperature. The two best correlations obtained in the experiments were selected for validation.

The predicted *DTS*-values agreed reasonably well with the observed sensation votes that followed closely the changes in ambient temperature. For the slower sinusoidal changes of dT_a/dt=5 K h^{-1} (***Fig.5.48***) *DTS* was almost identical to the subjects' sensation votes. However, the model appeared to be less sensitive to the faster fluctuations in ambient temperature (10.9 K h^{-1}, ***Fig.5.47***) by up to 0.5 scale units. The question arises as to whether the model systematically underpredicts the level of discomfort for higher rates of change in ambient temperature. The previous example, ***Fig.5.46***, where rates of dT_a dt=18 K h^{-1} were applied, however, contradicts this generalization. Thus, the differences between experiment and prediction in ***Fig.5.47***,

which fall within the bounds of the expected standard deviation of the sensation vote (0.8-1 scale units) will most probably be due to random error.

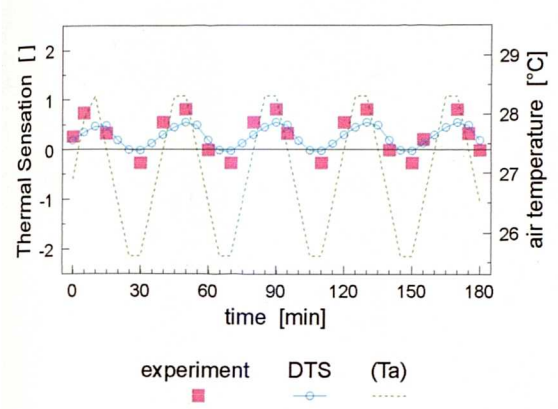

Tw=25.6°C va=0.14m/s rh=45% act=1.0met Icl=0.7clo

Fig.5.47

Thermal sensation during sinusiodal changes in air temperature. The peak-to-peak amplitude was 2.8K, and the frequency was 10.9 K h^{-1}.

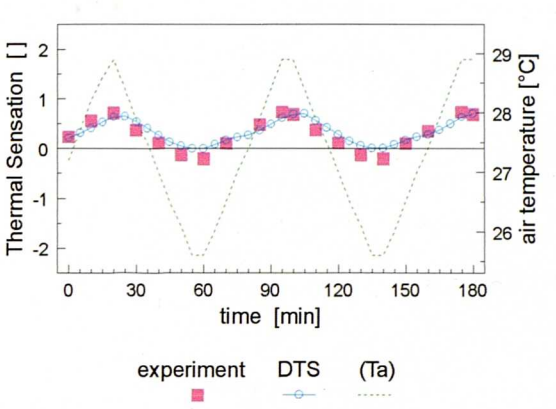

Tw=25.6°C va=0.14m/s rh=45% act=1.0met Icl=0.7clo

Fig.5.48

Thermal sensation during sinusiodal changes in air temperature. The peak-to-peak amplitude was 1.4K, and the frequency was 5 K h^{-1}.

5.7.4 Transients Due to Exercise

The model's algorithms for predicting temporal variations in *DTS* due to changes in internal temperature can best be tested using experiments in which subjects performed transient work. After beginning the work, there is increased heat input to the body which causes a transient rise in internal temperature and is associated with an increase in thermal sensation. After terminating the work there is usually a phase of body cooling accompanied by falling core temperature and a decreasing thermal sensation.

Thermal sensation during a work/rest sequence in ambient temperatures of T_a=10°C was observed by Nielsen [144]. The subjects (n=10) were dressed in clothing of I_{cl} = 1.2 clo, and exercised for 60 min on an ergometer at about *act* = 2.6 met. After the work period they sat quietly on the bicycle. Time-dependent sensation votes and the predicted *DTS* are plotted in ***Fig.5.49***.

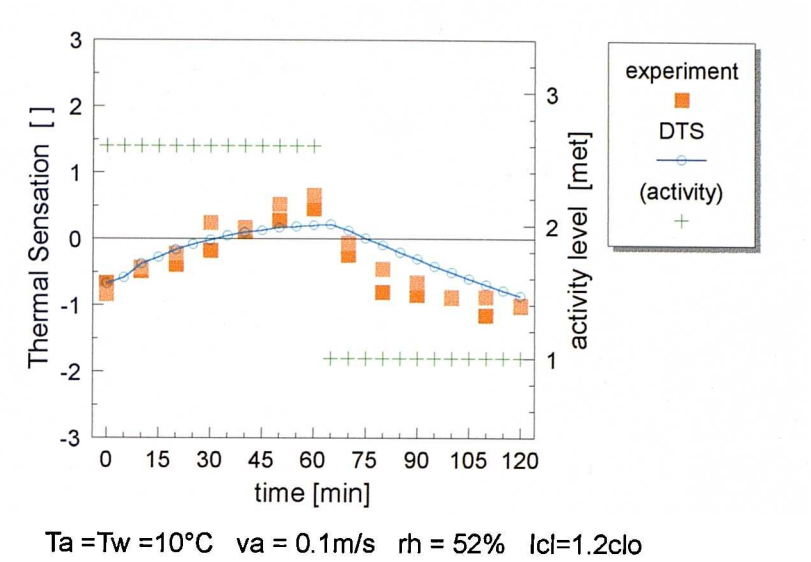

Fig.5.49

Thermal sensation in an environment of T_a=10°C as observed [144] and as predicted for a period of 60 min exercise at act=2.6 met followed by 60 min recovery.

The model reproduced reasonably well both the temporal rise and fall in thermal sensation during the work- and recovery phase. The mean deviation between DTS and sensation votes was lower than 0.3 scale units; the maximum deviation was 0.7 scale units.

Fahnestock et al. [44] studied the responses of exercising subjects (n=6) in two different environmental conditions: ambient temperature of T_a=24°C and relative humidity of 45%; and ambient temperature of T_a=35°C and relative humidity of 50%. In each environment the participants were pedalling on a bicycle ergometer for 90 min at four different activity levels: 1.9 met, 2.2 met, 3.1 met, and 3.6 met. The work period of the 120-minute-exposures was preceded by a 30 minute rest. The subjects' sensation votes and the corresponding *DTS*-values are plotted in ***Fig.5.50*** to ***Fig.5.57***. The two environmental conditions showed markedly different comfort responses. In the climate of T_a=35°C - a test of the model performance whilst working in a non-moderate environment - the general level of discomfort was 'warm'. There were no significant changes in thermal sensation between different exercise intensities including the rest period. The model reproduced this behaviour showing general validity of the $\Delta T_{sk,m}$-ΔT_{hy}-concept even for conditions far away from conditi-

ons of the body's thermal balance with the environment.

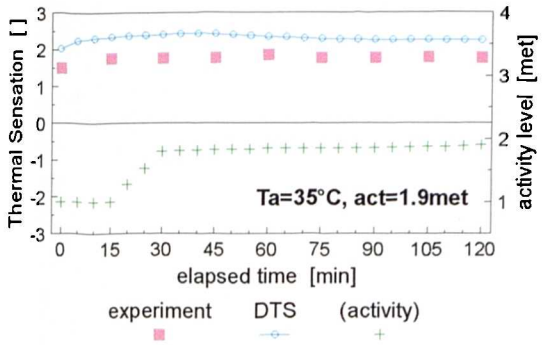

Fig.5.50

Work at act 1.9met in an environment of T_a 35°C, I_{cl} 0.6 clo, [44].

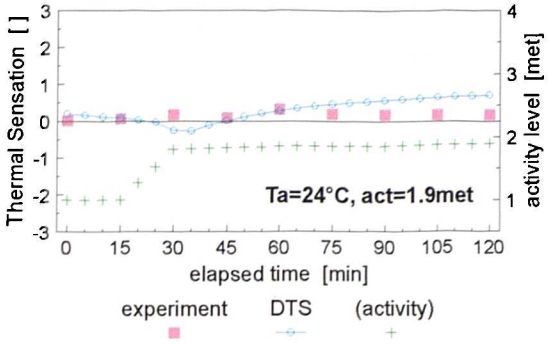

Fig.5.51

Work at act 1.9met in an environment of T_a 24°C, I_{cl} 0.6 clo, [44].

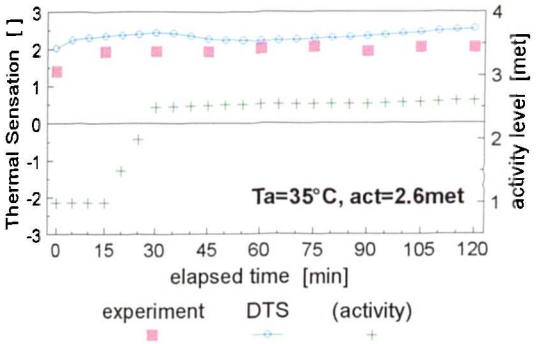

Fig.5.52

Work at act 2.6met in an environment of T_a 35°C, I_{cl} 0.6 clo, [44].

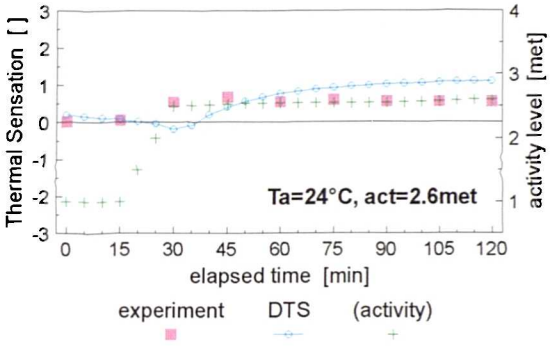

Fig.5.53

Work at act 2.6met in an environments of T_a 24°C, I_{cl} 0.6 clo, [44].

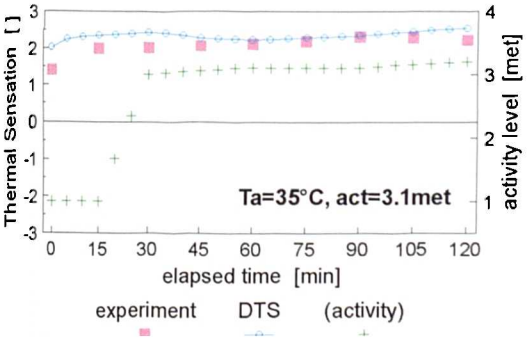

Fig.5.54

Work at act 3.1met in an environment of T_a 35°C, I_{cl} 0.6 clo, [44].

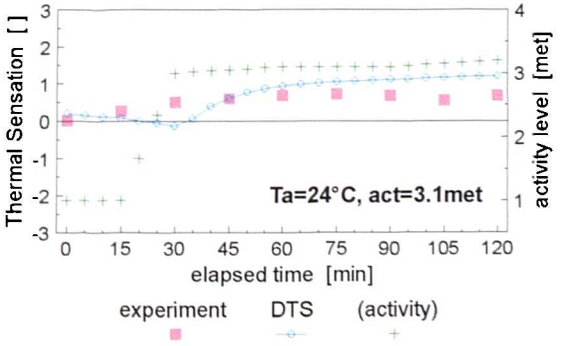

Fig.5.55

Work at act 3.1met in an environment of T_a 24°C, I_{cl} 0.6 clo, [44].

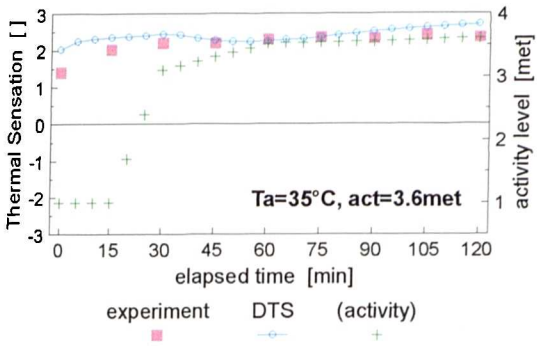

Fig.5.56

Work at act 3.6met in an environment of T_a 35°C, I_{cl} 0.6 clo, [44].

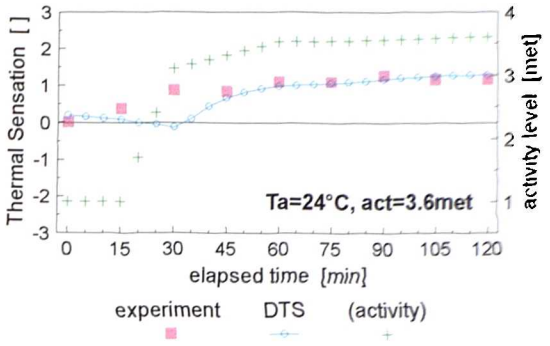

Fig.5.57

Work at act 3.6met in an environment of T_a 24°C, I_{cl} 0.6 clo, [44].

In the mild climate of T_a=24°C, the participants felt thermally neutral while they were seated. The sensation of temperature began to rise as the subjects started to work. This transient phase lasted on average about 30 minutes. Except for the lowest activity where there was no noticeable change in thermal sensation due to exercise, thermal sensation levelled off at values which exceeded the initial sensation by up to 1 warmth category. The model simulated both the general levels of discomfort and the transient changes in sensation quite well. The typical deviation between expe-riment and simulation did not exceed 0.5 scale units.

5.8 Discussion of the Comfort Model

In sections 5.4.1-5.4.3 a statistically founded thermal comfort model for a wide range of boundary conditions was developed. About seven thousand sensation responses from more then two thousand male and female subjects observed in different experiments were involved. This is much more data than was used in the development of earlier models (eg. [46]). The enlarged experimental base was achieved, on the one hand, by including results of additional comfort experiments, ie. [158] [57] [58], and on the other hand by evaluating - when appropriate - sequences of reported sensation votes [141] [158] [57] instead of only the final votes taken at the end of each exposure.

In the model, thermal sensation was related to parameters of the body's thermal state as predicted by a dynamic model of the human thermoregulatory system. Human body properties (anatomical, physical, physiological) and human thermoregulatory behaviour were introduced to enable investigation of the nature of comfort, and to achieve a higher universality of comfort prediction. Thereby, the extensions concerned the range of evaluable environmental conditions, high levels of activity, and transient conditions.

Regression analyses revealed the temperature error signals from the skin, $\Delta T_{sk\,m}$, and from the head core, ΔT_{hy}, and the rate of the change of the mean skin temperature, $dT_{sk,m}\ dt$, to be the responsible thermophysiological variables which govern the overall human thermal sensation. This temperature-orientation of the *DTS*-model contradicts the 'philosophy' of comfort models presuming a calorimetrically operating system [46] [7]. Skin heat flux, as a calorimetric variable, was discovered to be an inadequate signal in warm and hot environments, as well as in transient conditions.

Both negative and positive temperature error signals from the skin, ie. punitive signals from cutaneous 'cold' and 'warm' receptors, were found to affect the sensation of temperature. The importance of skin temperature throughout the whole range of climatic conditions, as found in this study, coincides with the nature of thermal sensation as a *"rational experience that can be described as being directed toward*

an objective world" [88], however, the finding that punitive signals from 'warm' cutaneous receptors also influence man's overall thermal perception, contradicts a widely held belief that internal temperature is the only origin of 'warm' discomfort [11] [118]. A partial explanation to this discrepancy might arise from differences in definitions of thermal sensation and thermal comfort.

The analysis of hot transient environmental conditions [57] clearly indicated that subjects' sensory estimates correlate best with positive skin temperature error signals. As a result, subjects perceived warm temperatures and warm discomfort much earlier than any increase of internal temperature could account for. Therefore, from the cybernetic point of view, positive $\Delta T_{sk,m}$-signals represent 'feed forward' signals which enable the human organism to respond quickly to environmental disturbances by conscious action before the body is penetrated by environmental heat.

The influence of core temperature on thermal sensation was found to be a complex, multiple process in which any elevation of central temperature is weighted by the level of thermal strain found at the body's periphery, ie. integral skin temperature error signal. This mechanism emphasizes the partial contribution of central temperature with rising cold stress at the skin. It operates in a balancing way against massive warnings of cold which can be detected on the skin (ie. the function of f_{sk}) when working in the cold and sweating. This approach, therefore, underlines the primary role of the human thermoregulatory system: the regulation of *internal* temperature that occurs by autonomic (*SBF*, *Sw*, *Sh*) and conscious (ie. behavioural) action.

The model predicts a vanishing effect of internal temperature on thermal sensation when the head core temperature approaches, or falls below, its setpoint (37.0°C). This result agrees with Benzinger [11] who stated that "*... the origin of cold-discomfort is the skin with its cold-receptors*" and that "*... central thermoreception*" makes "*... no appreciable contribution to the sensation of cold* ".

Under transient conditions there are several factors which affect the human perception of warmth. The dynamic thermal sensation is a composite of overlapping effects arising from *static*, ie temperature based, cutaneous and central thermoreception, as

well as from specifically *transient* phenomena due to temporal changes in skin temperature. The static components (ie. the temperature error signals $\Delta T_{sk,m}$ and ΔT_{hy}) themselves account for some of the temporal effects in prediction of *DTS*. For instance, the impact of the duration of exposures which cause falling skin temperatures with time becomes recognized. Furthermore, the consideration of the central temperature in addition to skin temperature gives rise to the physical impact of heat storage in the body. In these dynamic processes human thermoregulatory behaviour is involved.

The complex nature of the dynamics of thermal sensation might easily be overlooked when designing comfort experiments for transient exposures. This might be a reason for the inconsistencies found in experiments on transient thermal comfort (for a review see eg. [89]).

The study revealed both positive and negative rates of change of the mean skin temperature to be additional, dynamic components in human thermal sensation. These signals were considered as the common basis for every transient comfort effect which occurred in response to temporal changes in climatic parameters (or clothing).

A sudden decrease in ambient temperature elicited an immediate drop in the sensation of temperature. This phenomenon is not restricted to cold environments but can appear at any level of the actually prevailing climatic conditions. Negative rates of change of the mean skin temperature were found to be the physiological origin of these specifically dynamic sensation events.

The initial impulse of the maximum positive rate of change of the mean skin temperature arising from a sudden increase in ambient temperature was found to be the governing thermophysiological principle which dominates the dynamics of subsequent perceptive responses. This process of recent thermal history evaluation, where the maximum skin heating rate $(dT_{sk,m}/dt)_{max}$ is weighted by time, enables an agile and quite precise adaptation of thermal sensation to the new, warmer environmental situations.

Stolwijk [179] stated that "*Optimal thermal comfort appears to be coincident with minimum thermoregulatory response: almost any level of involuntary autonomic physiological response leads to reports of discomfort and to a drive for behavioural adjustments in the thermal environment*". Concluding from this statement, thermal perceptual responses appear to be associated with reactions of the human thermoregulatory system, ie. regulatory effectors themselves might be perceived as being uncomfortable.

The experimental results of Gagge et al. [57], and the results of the present study indicate, however, that the sensations of comfort and temperature represent independent, additional responses. They do not correlate with reactions of the human thermoregulatory system in transient conditions but respond to temporal variations in ambient conditions much earlier by appropriate changes. Thus, due to the strong dynamic component in the human response, the sensation of temperature and comfort gives man both an anticipatory, and early motivating drive for conscious action to effect a necessary change in the body's microclimate. In addition to the autonomic adjustments man also possesses the ability to correct for disturbances of the bodily thermal state by *behavioural thermoregulation*, such as changes in clothing insulation, active movement, body posture, seeking shade, etc. This seems to be the origin of the human ability of perceiving thermal comfort.

The sensitivity of the comfort model was analysed for different parameters of steady boundary conditions, ***Fig.5.58*** to ***Fig.5.61***. Where possible, the results were compared with predictions of the *PMV*-model representing the current standard [94]. The *DTS*-values refer to two-hour-exposures to the respective steady conditions following the state of thermal neutrality. Except for ***Fig.5.60***, the following parameters were common to the simulations: relative humidity of 50%, sedentary activity of 1.0met, clothing insulation of 0.7clo (KSU-uniform plus chair, see ***Tab.5.1***, chap. 5.3.1.2). Since the Fanger model was developed by neglecting the chair for sedentary activities in the experiments of Nevins et al. [141], the *PMV*-calculations were performed for Icl= 0.6 clo.

The behaviour of the model with respect to a wide range of ambient air temperatures

and different relative humidities has already been presented together with *PMV* in ***Fig.5.25***, section 5.5. In ***Fig.5.58***, a similar graph is shown for three different temperatures of surrounding surfaces, T_W, ie. mean wall temperatures equal to air temperature, and mean wall temperatures 10K higher and lower than the actual air temperature. In general, *DTS* agreed well with *PMV* within the range of -2<*PMV*<+2 including the prediction of the point of thermal neutrality for sedentary subjects. Outside the domain of mild ambient temperatures, however, *DTS* approached asymptotically the limits of the 7-point ASHRAE-scale, whereas the linear trends of the *PMV*-lines produced values outside the ASHRAE-scale.

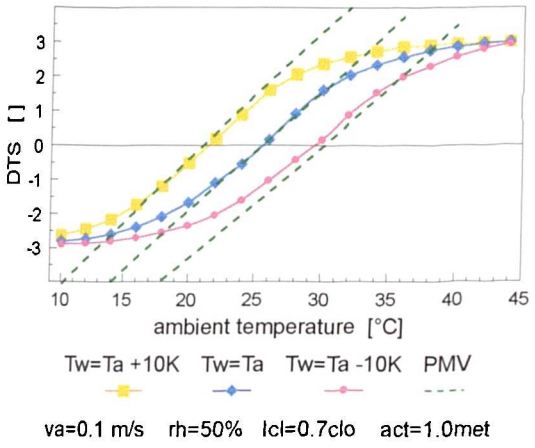

Fig.5.58

DTS as function of steady air temperatur e drawn for 3 different wall temperatures

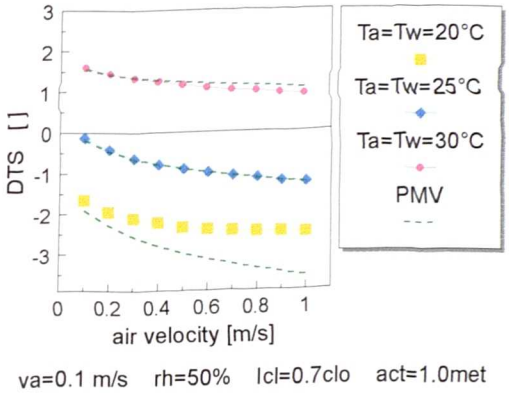

Fig.5.59

DTS as function of steady air velocity drawn for 3 different ambient temperatures.

The relative air velocity had a moderate impact on comfort (***Fig.5.59***). The *DTS* and *PMV* corresponded reasonably well with each other except for -2<*DTS*<-3. This difference is due to the non-linear behaviour of the present comfort model in the cold.

The effect of exercise intensity on thermal sensation is shown in ***Fig.5.60***. The subject of the analysis was continuous exercise performed by man clad in the KSU-uniform in standing position (ie. without a chair, I_{cl}=0.6clo). In the study, the relative air velocity was assumed to be a function of the activity level (to account for body motion during exercise [6] [103]). Appreciable discrepancies between *DTS* and *PMV* resulted for activity levels of *act*>3met. The Fanger model, which was calibrated for lower levels of activity (*act*<3 met), predicted an steep rise in thermal sensation for

high intensities of exercise. However, man seems to be able to maintain a thermal balance (ie. thermal comfort) within a much wider range of activity levels due to thermoregulatory adjustments, ie. peripheral vasomotion and sweating. There was also an initial steep elevation of *DTS* (for *act*<3 met) which concurs with the experimental results of McNall et al. [127]. However, according to comfort experiments for heavy exercise and a wide range of ambient temperatures [58], only a moderate rise in *DTS* occurs for *act*>4 met. This allows man to tolerate heavy work, up to 10 met, in a wide range of climatic conditions.

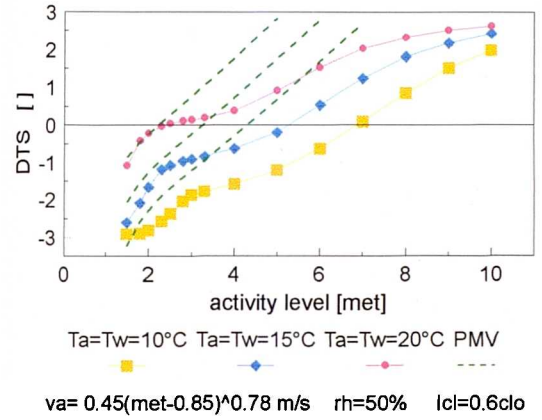

Fig.5.60

DTS as function of continuous work drawn for 3 different ambient temperatures.

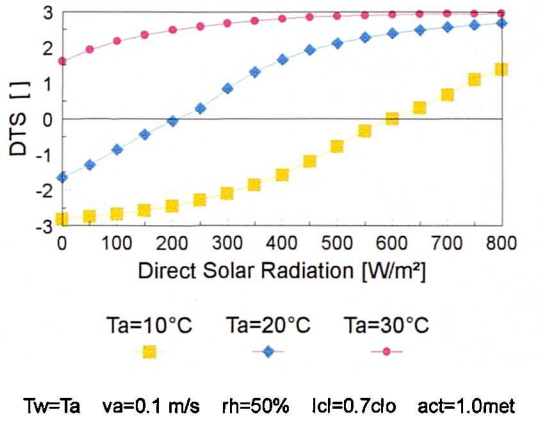

Fig.5.61

DTS as function of direct solar radiation drawn for 3 different ambient temperatures.

The sensitivity of the present comfort model to direct solar radiation (on the anterior site of the body) is presented in ***Fig.5.61***. The simulations were performed assuming an average short wave absorptivity for clothing of 0.7 (uncovered skin segments: 0.6). The Fanger model does not account for the effect of solar gain on comfort; so no comparison with *PMV*-index was possible. According to ***Fig.5.61***, lightly clad man can be in comfort or even feel warm discomfort in environments of T_a=10°C due to solar radiation.

The dynamic behaviour of the new comfort model is shown for both sudden changes and monotonic changes (drifts) in ambient temperature in ***Fig.5.62*** to ***Fig.5.64***. These two types of climatic transients frequently occur in practice. In the case of time-

varying conditions a comparison with the steady-state *PMV*-model appeared to be inappropriate.

The variation of dynamic thermal sensation with changes in ambient temperature from T_a=26°C to T_a=10, 20, 30 and 40°C, and back are shown in ***Fig.5.62***. The model typically predicted a transient peak in *DTS* for sudden downward changes in T_a. As can be seen, this dynamic response (elicited by negative $dT_{sk\,m}/dt$-signals) provided anticipatory warnings of cold ambient temperature allowing early adaptation. This transient mechanism enabled adjustment of the thermal sensation up to 1 hour before any body temperature could effect a change. For downward steps in ambient temperature from warm or hot to neutral, an additional 'transient' effect, ie. heat accumulation within the body, influenced the sensation of temperature (***Fig.5.62***).

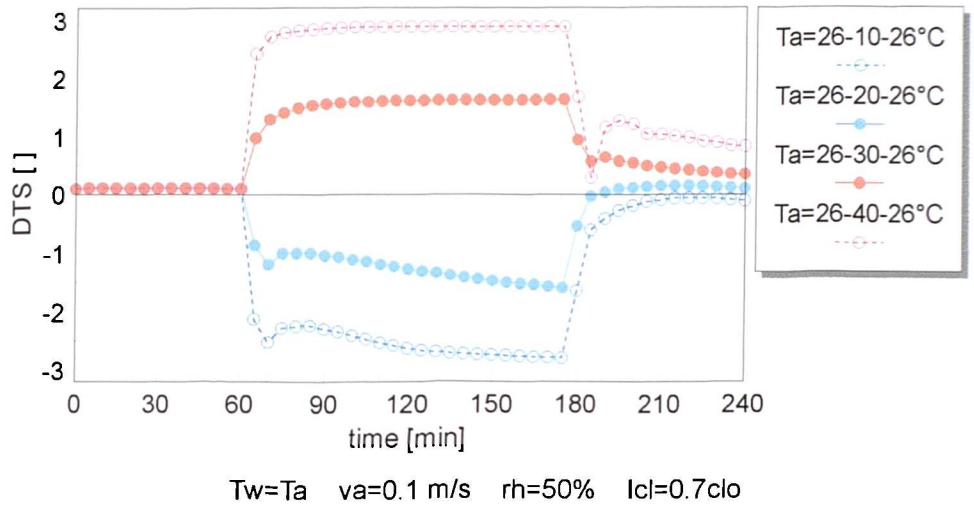

Fig.5.62

The dynamic behaviour of DTS when applying downward and upward steps in ambient temperature.

The 'anticipatory' nature of the *DTS*-index arose also for positive step-changes in ambient temperature thereby providing proper estimates on the level of the future thermal sensation in the new steady climatic conditions. The involvement of positive $dT_{sk,m}/dt$-signals in warmth perception was found to affect *DTS* most effectively in cool and cold environments. This principle, however, appeared to be less pronounced for upward-steps into warm and hot conditions (see ***Fig.5.62***). This was because rates of change in $T_{sk,m}$ due a rise in T_a are generally higher in the cold than in the

warmth where *DTS* followed changes in skin temperature more closely.

The behaviour of the comfort model with respect to monotonic, steady changes in ambient temperature (beginning at T_a=26°C) is shown in ***Fig.5.63*** and ***Fig.5.64*** in which *DTS* is plotted for a linear decrease in T_a of -2, -4, and -8 K h^{-1}, and a near rise in T_a of +2, +4, and +8 K h^{-1}. The effect of these drifts on thermal sensation can be directly considered when plotted against T_a instead of time.

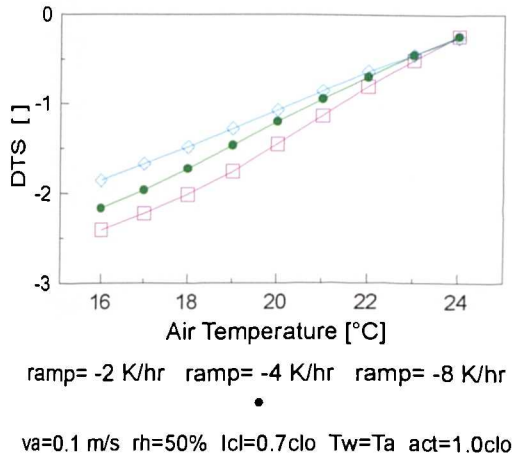

Fig.5.63

DTS as function of ambient temperature drawn for 3 different negative rates of change in ambient temperature.

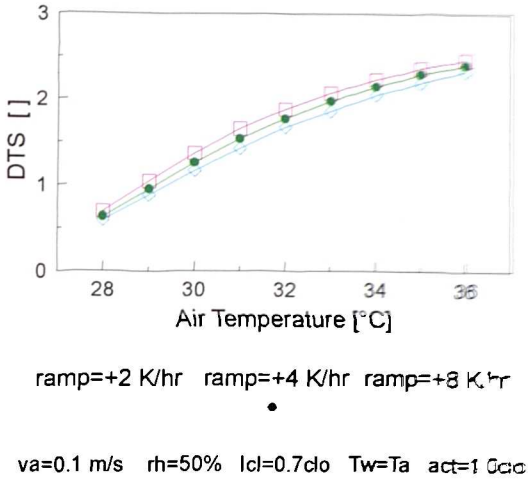

Fig.5.64

DTS as function of ambient temperature drawn for 3 different positive rates of change in mabient temperature.

In warm environments there were no significant changes in *DTS* with varying rates of change in ambient temperature. However, during cooling equal ambient temperatures are not perceived equally because of dynamic effects in thermal sensation. Lower rates of change in ambient temperature provoke a higher degree of discomfort than do higher rates of change. This result, which is coincident with experimental findings [14], seems to be in conflict with the results for the previous transient exposures, ***Fig.5.62***. However, another thermal effect dominated the dynamics of thermal sensation under these slow transient circumstances. Changes in body's heat content caused the time varying response to gradual changes in T_a, rather than $dT_{sk,m}/dt$-signals - these were vanishingly small.

6 CONCLUSIONS

A mathematical model predicting human thermal responses and the associated thermal feelings in steady state and in transient conditions has been developed. The dynamic model predicts body temperatures, thermoregulatory responses, components of the environmental heat exchange and the overall, dynamic thermal sensation DTS in cold stress, cool, neutral, warm and hot stress conditions. Thermal influences on human beings can be analysed for a range of activity of up to 10 met, as well as for various asymmetric environmental conditions and non-uniform clothing ensembles.

6.1 Passive System Model

A multi-segmental model of the human body incorporating thermally important body elements has been developed. Each element was made up of different body tissue materials by utilizing anatomical, thermophysical and geometrical data of the human body obtained from literature. The humanoid represents an average (adult, white) person with respect to body weight, body fat content, body surface-area, basal values of body metabolism, skin evaporation, and cardiac output. Body compartments were subdivided further into spatial sectors to permit direction-dependent simulation of environmental heat exchange in asymmetric conditions. Heat dissipation within the body was modelled by accounting for the combined effect of metabolic heat generation, blood circulation, and conductive heat transport. The calculation of body metabolism includes the impact of the human work efficiency as a function of the activity level.

Efforts were made to model the environmental heat exchange in some detail to reflect the importance and complexity of these phenomena in practice. Convective heat losses were simulated by accounting for free and forced convection and their variation over the human body using local convection coefficients obtained from measurements reported in the literature. The simulation of the radiant heat exchange is body posture dependent and considers spatial asymmetric radiant fields, and the effect of solar direct and diffuse irradiation. The skin evaporation model is based on

local mass and heat balances incorporating the effect of moisture diffusion through the skin, evaporation of regulatory sweat, accumulation of the sweat liquid on the skin, and the evaporative resistance of garments. A clothing model was developed which provides non-uniform thermal and evaporative insulation properties for use with the multi-segmental model. Respiration was modelled by considering both the convective and latent heat losses.

For solving the complex mathematical problem of heat transfer in the human body advanced hybrid techniques were applied which provide fast and accurate numerical solutions associated with stable numerical behaviour. A finite-difference formulation of the bioheat equation has been developed which applies - with slight modifications - to a steady state and to transient heat transport in body tissue cylinders or spheres. The formulation of the boundary conditions at tissue interfaces and on the skin surface considers the effect of geometry on the dissipation of heat.

The numerical formulation of the passive system was tested using different analytical solutions for heat dissipation in cylinders and spheres. The validation was performed for diverse steady-state and transient analytical solutions and showed both good agreement with the analytical solutions and a numerically stable behaviour. Even for large time-steps of one hour, the model provided reasonable results. In the case of (disproportionally) large time-steps and sudden changes of boundary conditions the model was stable and rapidly converged on the final temperature values.

6.2 Active System Model

The active system model of human thermoregulation was developed by means of statistical regression methods. The analysis of thermal and thermoregulatory responses obtained from different experimental studies covering a range of environmental temperatures between 5 and 50°C, and exercise intensities between 0.8 and 10 met, led to a *temperature-based*, *non-linear* active system model. Skin temperature was found to play a major role in human thermoregulation for the entire spectrum of environmental conditions, whereas elevated internal temperature was an important affe-

rent signal for regulatory reactions against warmth and during exercise. Negative rates of change of the mean skin temperature were found to govern the *dynamics* of regulatory responses in the cold. The afferent signal analysis indicated that calorimetric variables, such as the skin heat flux, were inappropriate input signals into the regulatory centre. The non-linearity of the active system model was a result of considering the human thermoregulatory behaviour over a wide range of environmental and internal conditions.

The sweating response, Sw, was found to be a function of both positive and negative skin temperature error signals, $\Delta T_{sk,m}$, and positive and negative error signals from the head core, ΔT_{hy}. There were appreciable differences between the intensity with which 'cold' and 'warm' cutaneous receptors affect sweating. In cold environments the Sw-regulator seemed to be increasingly oriented toward maintaining body core temperature (during exercise) while warnings of 'cold' from the periphery were discriminated. Little effect resulted for negative error signals from the hypothalamus, whereas a pronounced effect on Sw resulted for ΔT_{hy}>0.5K.

The shivering action, Sh, was revealed to be responsive to punitive signals from 'cold' cutaneous receptors, ie. $\Delta T_{sk,m} < 0$. Negative rates of change in the mean skin temperature, $dT_{sk,m}/dt$ appeared to govern the dynamic behaviour of Sh after a sudden fall in ambient temperature. The effect of ΔT_{hy}-signals on Sh was weak. The model's shivering response was unaffected by positive $\Delta T_{sk,m}$-signals as well as positive $dT_{sk,m}/dt$-signals.

The vasoconstriction response, Cs, was found to be a primary function of 'cold' cutaneous receptors, ie. negative signals $\Delta T_{sk,m}$ and $dT_{sk,m}/dt$. The effect of core temperature on the model's vasoconstriction appeared to be practically negligible. Cs was independent of the drive from 'warm' cutaneous receptors. The involvement of 'warm' cutaneous receptors (positive $\Delta T_{sk,m}$-signals) in the regulation of skin blood flow was found to be associated exclusively with the vasodilatation response, Dl, which depended also on positive ΔT_{hy} -signals. However, Dl appeared to be independent of negative temperature error signals from either body site. It can be

seen, therefore, that the functional relationships between *Cs* and afferent signals was similar to the relationship between *Sh* and these signals. Likewise, *Dl* responded to afferent signals similar to *Sw*. These results were interpreted as a sort of coupling principle between related responses that provide increased efficiency of regulatory defense mechanisms against thermal disturbances of the body.

6.3 Verification and Validation of the Thermoregulatory Model

The complete model was tested for a spectrum of ambient temperatures between 5 and about 50°C in chapters 4.5 and 4.6. The transient behaviour of the model was tested using transient changes in activity and in climatic conditions, eg. step changes from neutral to cool, cold, warm and hot and vice versa, and from cold to hot and vice versa. Good general agreement with measured data was obtained for the predicted thermoregulatory responses and the resultant body temperatures for the whole range of climatic conditions and types of exposure[1]. The mean and local skin temperatures were reproduced to within the bounds of the measurement error observed in different experiments, typically ±1K. Larger differences, however, resulted for skin temperature when sweating in the cold (see below). The predicted body core temperature(s) deviated from corresponding measurements by less than ±0.5K as the typical uncertainty of experimental data. This elevated accuracy in the prediction of body core temperature arose from appropriate modelling of vasomotor responses.

The predicted increase in metabolism due to shivering in cold and severe cold environments differed from experimental observations generally by less then the assumed error band of the experimental data, ie. about 50W. Greater discrepancies between measurement and prediction might, however, be expected for atypically lean or obese subjects especially for the shivering response [104]. The passive system reflects an average person in terms of body size and fat content. The model also reproduced the dynamic thermal behaviour of subjects exposed to sudden

[1] Reliable simulation results were obtained also for conditions outside the range of ambient temperature of 5-50°C, eg. for finish-sauna conditions (not presented in the thesis).

downward changes in ambient temperatures, ie. a transient peak of the metabolic activity (due to a rapid cooling of the skin), and an increase with time of the body core temperature (due to cutaneous vasomotor adjustments).

In moderate and thermally neutral environments, where body temperatures were regulated by vasomotor responses and where neither shivering nor sweating occurred, the predicted body core temperatures and skin temperatures deviated from measured data typically by less than 0.2K and 1K, respectively. Similar accuracies were also obtained for moderately exercising subjects, as well as for diverse combinations of environmental parameters, and for different clothing ensembles.

The sweating model reproduced the sudomotor regulatory behaviour of non-exercising subjects for the whole range of warm and hot ambient conditions. Differences between prediction and experimental observation were less than 50W. Both the transient behaviour, and the stationary plateau of skin evaporation, were predicted appropriately. The reliability of the sweating model led to confident predictions of skin and core temperature in warm and hot conditions. Seemingly paradoxical dynamic effects such as the fall in core temperature observed in experiments after moving from a cold to a hot climate were predicted.

The predictions of sweat rates during alternating periods of heavy work and recovery were in poorer agreement with experimental results than predictions for environmentally induced sweating. More independent experimental investigations seem to be required before more reliable algorithms for sweating during abrupt, large changes in exercise can be included in an active system model.

Systematic discrepancies (in some instance up to 5K) were observed between predicted and measured skin temperatures during sharp transient changes in exercise intensity in the cold where subjects were sweating. Based on an pilot experimental and a numerical study it was concluded that this was due to the manner in which experimentalists had attached thermocouples to the skin of subjects (ie. sticky tape). Care over the attachment of temperature sensors, which might prevent skin evaporation, needs to be exercised when undertaking physiological studies.

The model showed good agreement with measured body core temperatures for steady as well as instantaneous exercise activity, and for different combinations of work load, ambient temperature, relative humidity, and clothing insulation.

6.4 Comfort Model

A statistically founded thermal comfort model has been developed which predicts the *dynamic thermal sensation, DTS*, for a wide range of environmental conditions and activity levels. Regression analyses revealed the temperature error signals from the skin, $\Delta T_{sk\,m}$, from the head core, ΔT_{hy}, and the rate of the change in the mean skin temperature, $dT_{sk,m}/dt$, to be the responsible thermophysiological variables which govern the overall human warmth sense.

Both *negative* and *positive* signals from the skin, ie. punitive signals from cutaneous 'cold' and 'warm' receptors, were involved in the sensation of temperature. Analysis of sensation votes during environmental transients and in warm and hot environments revealed, on the other hand, that the skin heat flux, as a calorimetric quantity was inadequate for modelling thermal sensation.

The influence of core temperature, that affects the comfort perception eg. during exercise, was found to be a multiple process in which any elevation in core temperature appeared to be weighted by the level of thermal strain at the body's periphery, ie. $\Delta T_{sk,m}$. This mechanism emphasizes the partial contribution of core temperature with rising cold stress at the skin. However, the model predicts a vanishing effect of negative ΔT_{hy}-signals to *DTS*.

A strong dynamic component in thermal sensation was discovered which gives man anticipatory drive toward conscious behavioural action. Rates of change in the mean skin temperature were found to be the physiological origin of dynamic sensation events during skin cooling. However, the initial impulse of the maximum rate of change in the mean skin temperature was found to be the governing drive which dominates the dynamic thermal sensation during skin warming.

The transient comfort model was validated for gradual-, sinusoidal-, and sudden-changes in environmental conditions, for transient exercise, and for steady climatic conditions. The predicted levels of (dis)comfort agreed well with experimental observations. The deviations were typically less than the expected standard error of inter-individual differences which is about 0.8 - 1.0 categories of warmth on the ASHRAE scale.

7 OUTLOOK AND SUGGESTIONS FOR FUTURE WORK

7.1 Intended Model's Applications

The new model should enable thermal influences on human beings to be studied for complex conditions met in reality: steady states; transients; thermal inhomogeneities; moderate and thermally stressful conditions. It can therefore find application in various fields of human endeavour:

- When designing new buildings, the model will enable architects to gain information on the effect of the building's design or its individual built-constructions on human beings at the design stage. In particular the method of direction-dependent partitional calorimetry can be utilized for selective judgements of indoor climate conditions. Transient comfort, eg. in passively ventilated buildings, can be analysed.

- As an application tool in the hands of HVAC engineers the model can aid the dimensioning and optimization of heating and air conditioning systems. Critical aspects of the HVAC-design such as the impact of the air flow pattern and temperature stratification in spaces as induced by different HVAC-systems on the (three dimensional) human body and its effect to thermal comfort can systematically be investigated.

- In the automobile, textile and aerospace industries, in meteorology, in the military, and in medicine, where thermal interactions between man and his environment are important.

- In future research into human thermal comfort (see also further below):
  - modelling the perception of local thermal (dis)comfort;
  - modelling conscious behavioural reactions in response to thermal discomfort;
  - modelling long term adaptation in thermal comfort.

One mode of the model's intended future application is as a *stand-alone module* for studies on human thermal responses in various air exposures, analysis of critical

thermal conditions for heath and safety margins, etc. The predictive abilities of the model can thereby be used in connection with simulation programs predicting parameters of the thermal environment, eg. building simulation programs (BSP) [3] [33], and computational fluid dynamics codes (CFD) [2]. Examples for application of the present model together with these programs are eg. studies on thermal conditions in the Australia Stadium, Year 2000 Olympics [113], and the European project on Passive Downdraft Evaporative Cooling (PDEC) in southern European countries [115].

Future work might focus on the *integration of the model* into CFD and BSP to allow integrative computer analyses of thermal environments, human heat transfer and thermal comfort. A link with a sophisticated CFD would lead to an advanced design and research tool for detailed analyses in complex environments. The inclusion of the model into BSP would help to meet efforts in achieving more realistic simulations of energy consumption in buildings by adjusting indoor climate conditions (via HVAC-regulation) according to the occupants' expected wishes (ie. according to the DTS-index at a given activity level and clothing insulation) instead of presuming fixed target indoor temperatures.

7.2 Perception of Local (Dis)comfort in Asymmetric Conditions

The dynamic thermal sensation index, DTS, represents an overall response which reflects an integration of thermal afferents from various sites of the human body. Under asymmetric conditions, however, *local discomfort* may be perceived as a further response in addition to the overall sensation response.

In various comfort experiments local (dis)comfort has been investigated for environmental asymmetries, such as: asymmetric radiant fields [130] [4] [49] [65]; draughts [50] [48] [117]; and vertical air temperature gradients [152] [206]. As a result, limits on the allowable asymmetry of environmental parameters have been set. Unfortunately, environmental limits cannot be used when combinations of different inhomogeneities occur. A universal model predicting the perception of local thermal

(dis)comfort under arbitrary asymmetric conditions, and combinations, of them is required.

The present multi-segmental model of human thermoregulation with spatial subdivisions can be used as a research tool into this area. In addition to arbitrary climatic asymmetries, the model also treats inhomogeneities due to non-uniforn clothing and uneven distribution of skin evaporation over the body. In contrast to current strategies of evaluating (dis)comfort under asymmetric conditions, simulation on the basis of thermophysiological effects is proposed in order to obtain a model for local comfort perception of enhanced validity.

The physiological mechanisms governing the local sensation of comfort are associated with local cutaneous thermoreception [87], whereas the skin temperature appears to be the indicator for local perception [16] [95] [90]. If the temperature of a skin area deviates too much from the mean skin temperature, local comfort or discomfort can be experienced in this area [87]. In order to obtain a universal model the impact of the actual state of general comfort on the local perception, known as the *alliesthesia*-effect [24] [135], which usually has been neglected in comfort research, should also be considered. Seemingly paradoxical, but in practice often experienced events might then be clarified, for example, the improved comfort that is experienced by local cooling (eg. from a fan) in hot conditions, or the pleasantness of warm feet in a cool space (produced eg. by underfloor heating). Both cases are perceived as comfortable despite the existence of an appreciable asymmetry in the environmental heat exchange.

7.3 Behavioural Thermoregulation

The model can form the basis for future research work into *behavioural* aspects of human thermoregulation. The drive for behaviour thermoregulation is the perception of thermal (dis)comfort [57] which gives man both an anticipatory, and early motivating drive for conscious action to effect a change in the body's microclimate. In addition to the autonomic thermoregulatory adjustments man also possesses the

ability to correct for disturbances of the bodily thermal state by *behavioural thermoregulation*, such as changes in clothing insulation, active movement, body posture, and seeking shade.

A self-regulatory model, perhaps based on the fuzzy-logic method, could be developed in which conscious responses are initiated by the DTS-index as an indicator of (dis)comfort.

7.4 Long Term Adaptation

Fanger [46] has shown time and time again that the thermally neutral ambient temperature of a group of people does not vary and is not affected by seasonal experience, country of domicile, or other factors. Humphreys, on the other hand, has demonstrated [93] that the *preferred* ambient temperature can vary depending on the thermal experience of the people even if the effect of varying clothing insulation and (perhaps) changing metabolism with the climate is taken into account. This suggests that some form of acclimatization to the climate (and/or activity) might take place.

There is clear experimental evidence of acclimatory changes in thermoregulatory responses and body temperatures in hot climatic conditions (eg. [68] [157])[1)]. It has been repeatedly observed (for a review see eg. [80]) that over a 8 to 12 days period thermal adaptation can occur. There is an increase in the rate of sweating whilst the body core temperature (and skin temperature) falls. This might be the physiological origin of adaptation in thermal comfort. A study could be undertaken to support or to disapprove this hypothesis. The acclimatory shift of sweating could be modelled by permitting a decline in the set-point temperatures for sweating and perhaps vasodilatation during the acclimatization period[2)].

---

1) no clear effect seems to arise for seasonal changes in metabolic heat generation in human subjects [125].

2) Note: in the present work, themal comfort, ie. DTS, was revealed to be a function of body temperatures, not of sweating (skin wettedness), and seems to be coincident with acclimatory processes: a decrease in warm discomfort despite an increase in sweating.

7.5 Suggestions For Experimental Investigation

The present work also leads to suggestions for experimental investigations.

- There is some indication that the rate of change of the hypothalamus temperature dT_{hy}/dt may affect the dynamic behaviour of sweating during sudden changes in exercise intensity. To implement this variable as an further afferent signal more independent experimental data is required.

- The appropriateness of measuring skin temperatures using thermocouples taped on the skin during sweating in the cold has been questioned. The tapes were found to suppress evaporation of sweat skin just at the location of temperature measurement. Alternative methods of recording skin temperature, eg. by non-contact (optical) measurements, could be *investigated.*

- Future experiments on thermal comfort might include more extensive experimentation in the area of transient comfort during sudden changes in ambient temperature at *arbitrary* levels of discomfort, as well as studies of comfort at high levels of activity. Furthermore, appropriate experiments can be designed which enable an investigation of the effect of acclimatization on the perception of (dis)comfort.

REFERENCES

[1] Adair E.R. Hypothalamic control of thermoregulatory behaviour. In *"Recent Studies of Hypothalamic Function"*, Karger, Basel, pp. 341-358. 1974.

[2] AEA Harwell. Computational Fluid Dynamics Services CFX 4.1. Flow Solver User Guide. 1995.

[3] Alexander D.K. HTB2 version 1.1, User manual. Welsh school of Architecture, UWIST, Cardiff (UK), 1993.

[4] Anguez J., and M. Croiset. Thermal comfort requirements adjacent to cold walls - application to glazed openings. *CSTB No.96*, Jan/Feb. English translation: NBS-TN-710-4, may 1972, US Dept. of Commerce, Washington D.C., 1969.

[5] ANSI/ASHRAE 55-1992. Thermal Environmental Conditions for Human Occupants. *American Society of Heating, Refrigerating and Air-Conditioning Engineers*, Inc., 1791 Tullie Circle, NE Atlanta, GA 30329, 1992.

[6] ASHRAE Handbook. 1985 Fundamentals. *American Society of Heating, Refrigerating and Air-Conditioning Engineers,* chap. 8: Physiological Principles for Comfort and Health, Atlanta, 1985.

[7] Azer N.Z., and S. Hsu. The prediction of thermal sensation from a simple model of human physiological regulatory response. *ASHRAE Trans.* 83 (1), pp. 88-102, 1977.

[8] Bach, H. Behaglichkeit in Räumen. *Heizung-Lüftung-Haustechnik (HLH)*, vol. 42, no. 7, July 1991.

[9] Bedford T. The warmth factor in comfort at work: a physiological study of heating and ventilating. *Industrial Health Research Board Report No. 76*, HMSO London, 1936.

[10] Belding H.S., and Hatch T.F. Index for evaluating heat stress in terms of resulting physiological strain. *Heating, Piping and Air Conditioning*, vol. 27, pp. 129-136.

[11] Benzinger T.H. The physiological basis for thermal comfort. In *"Indoor Climate"*, ed. P.O. Fanger & O. Valbjorn, Danish Building Research Institute, Copenhagen, pp. 441-476, 1979.

[12] Berglund, L.G. A Theoretical and Experimental Study of the Thermoregulatory Effect of Salt Accumulating on Human Skin During Sweating. PhD dissertation, Kansas State University, 1971.

[13] Berglund L.G., and J.A.J. Stolwijk. The use of simulation models of human thermoregulation in assessing acceptability of complex dynamic thermal environments. In *'Energy Conservation Strategies in Buildings'*, chap. 10, pp. 157-191, J. B. Pierce Foundation of Connecticut, Inc., ed. J.A.J. Stolwijk, 1978.

[14] Berglund L.G., and R.R. Gonzalez. Application of acceptable temperature drifts to build environments as a mode of energy conservation. *ASHRAE Trans.* 84(1), pp. 110-121, 1978.

[15] Berglund L.G., and Cunningham D.J. Parameters of human discomfort in warm environments. *ASHRAE Trans.*, vol. 92, 1986.

[16] Beste R. Perzeption statischer thermischer Reize beim Menschen. *Inaugural-Dissertation zur Erlangung des Doktorgrades der Humanbiologie des FB Humanmedizin*, Phillips-Universität Marburg, 1977.

[17] Birkebak, R.C. Heat transfer in biological systems. *Iner. Rev. Gen. and Exp. Zoology*, Vol. 2: 269-344, 1966.

[18] Blight J. Temperature regulation in mammals and other vertebrates. *North-Holland Publ. Comp.*, Amsterdam, London, NY. 1973.

[19] Blight J. Regulation of body temperature in man and other mammals. In: Shitzer A., and R.C. Eberhardt. *Heat Transfer in Medicine and Biology - Analysis and Applications*, vol. 1, chap. 2. Plenum Press, New York and London, 1985.

[20] Brager G.S., A.E. Fountain, Ch.C. Benton, E.A. Arens, and F.S. Bauman. A comparison of methods for assessing thermal sensation and acceptability in the field. Proceedings of the BRE-Conference held 9-10 June 1993: *Thermal Comfort: Past, Present and Future*. Editors N.A. Oseland and M.A. Humphreys, Building Research Establishment Report, Garston, pp. 17-39, 1994.

[21] Brengelmann G.L. Control of sweating rate and skin blood flow during exercise. In *'Problems with temperature regulation during exercise'*, ed. E.R. Nadel, *Academic Press Inc.*, New York - San Francisco - London, 1977.

[22] Budd, G. M., and N. Warhaft. Body temperature, shivering, blood pressure and heart rate during a standard cold stress in Australia and Antarctica. *J. Physiol.* (London), vol. 186, pp. 216-232, 1966.

[23] Bullard R.W., M.R. Banerjee, F. Chen, R. Elizondo, and B.A. McIntyre. Skin temperature and thermoregulatory sweating: A control systems approach. In *"Physiological and Behavioral Temperature Regulation."* ed. Hardy & Gagge & Stolwijk, Springfield, pp. 597-610, 1970.

[24] Cabanac M., and J.D. Hardy J.D. Réponses unitaires et thermorégulatrices lors de réchauffements et réfroidissements localisés de al région préoptigue et du mésencéphale chez le lapin. *J. Physiol. (Paris)*, vol. 61, pp. 331-347, 1969.

[25] Cannistraro, G., G. Franzitta, and C. Giaconia. Algorithm for the calculation of the view factors between human body and rectangular surfaces in parallelepiped environments. *Energy and Buildings* 19: 51-60, 1992.

[26] Consolazio, C.F., L.R. Matoush, R.A. Nelson, J.B. Torres, and G.J. Isaac. Environmental temperature and energy expenditures. *J. Appl. Physiol.* 18, pp. 65-68, 1963.

[27] Chang, S. K., E. Arens, and R. R. Gonzalez. Determination of the effect of walking on the forced convective heat transfer coefficient using an articulated manikin. *ASHRAE Trans.* 94 (1): 71-81, 1988.

[28] Charny, C. K., S. Weinbaum, and R. L. Levin. An evaluation of the Weinbaum-Jiji bioheat equation for normal and hyperthermic conditions. *ASME J. Biomech. Eng.* 112: 80-87, 1990.

[29] Chato, J. C. Selected thermophysical properties of biological materials. In: Shitzer A., and R.C. Eberhart. *Heat Transfer in Medicine and Biology - Analysis and Applications*, vol. 2, appx. 2, Plenum Press, New York and London, 1985.

[30] Chen, M. M., and K. R. Holmes. Microvascular contributions in tissue heat transfer. *Annals of New York Academy of Science*, vol. 355, pp. 137-150, 1980.

[31] Chen, M. M. The tissue energy balance equation. In: Shitzer A., and R.C. Eberhart. *Heat Transfer in Medicine and Biology - Analysis and Applications*, vol. 1, chap. 7. Plenum Press, New York and London, 1985.

[32] Clark, R.P., B.J. Mullan, and L.G.C.E. Pugh. Skin temperature during running - a study using infra-red colour thermography. *J. Physiol. (London)*, 26: 53-62, 1977.

[33] Clark J.P., and D. McLean. ESP - A building and plant energy simulation system. Version 6, release 8, Energy Simulation Research Unit, University of Strathclyde and ABACUS Simulations Ltd., Glasgow (UK), 1988.

[34] Colin, J., and Y. Houdas. Experimental determination of coefficients of heat exchange by convection of the human body. *J. Appl. Physiol.* 22, p.31, 1952.

[35] Crawshaw L.I., E.R. Nadel, J.A.J. Stolwijk, and B.A. Stamford. Effect of local cooling on sweating rate and cold sensation. *Pflügers Arch.*, vol. 354, pp. 19-27, 1975.

[36] Davson H. A textbook of general physiology. *J. and A. Churchill Ltd*, London, 1964.

[37] de Dear R.J., H.N. Knudsen, and P.O. Fanger. Impact of air humidity on thermal comfort during step-changes. *ASHRAE Trans.* 95 (2), pp. 336-350, 1989.

[38] de Dear R.J., J.W. Ring, P.O. Fanger. Thermal sensation resulting from sudden ambient temperature changes. *Indoor Air*, vol. 3, pp. 181-192, 1993.

[39] DIN 4108 Wärmeschutz im Hochbau, Teil 4: Wärme- und Feuchteschutztechnische Kennwerte, 1981.

[40] Doherty T.J., and E. Arens: Evaluation of the physiological bases of thermal comfort models. *ASHRAE Trans.*, vol. 94, p. 1371-1385, 1988.

[41] Downey J.A., C.E. Huckaba, P.S. Kelley, H.S. Tam, R.C. Darling, and H.Y. Chen. Sweating responses to central and peripheral heating in spinal man. *J. Appl. Physiol.*, vol. 40, pp. 701-706, 1976.

[42] Ducharme M.B., and P. Tikuisis. In vivo thermal conductivity of the human forearm tissues. *J. App. Physiol.*, vol. 70, pp.2682-2690. 1991.

[43] Eberhart, E. C. Thermal models of single organs. In: Shitzer A., and R.C. Eberhart. *Heat Transfer in Medicine and Biology - Analysis and Applications*, vol. 1, chap. 12. Plenum Press, New York and London, 1985.

[44] Fahnestock M.K., F.E. Boys, F. Sargent II, L.D. Siler. Energy Cost, Comfort, and Physiological Responses to Physical Work in 95F-50% rh and 75%-45% rh Environments. ASHRAE Trans. 73, pp. I.1.1 - I.1.20, 1967.

[45] Fanger, P.O. Thermal Comfort - Analysis and Applications in Environmental Engineering. *McGraw-Hill*, New York - London - Sidney - Toronto, pp. 28-30, 1973.

[46] Fanger P.O.: Thermal comfort - Analysis and applications in environmental engineering. *McGraw-Hill*, New York - London - Sidney - Toronto, 1973.

[47] Fanger P.O. Thermal discomfort caused by radiant asymmetry, local air velocities, warm and cold floors, and vertical air temperature gradients. In "*Thermal Comfort*" J.Durrand and J.Rayuand, Eds., vol. 75, Editions INSERM, Paris, pp.145-152, 1977.

[48] Fanger P.O., and C.J.K. Pedersen. Discomfort due to air velocities in spaces. Proceedings of the meeting of Commission El (Air Conditioning) of the International Institute of Refrigeration, Belgrade, 1977.

[49] Fanger P.O., B.N. Ipsen, G. Langkilde, B.W. Olesen, N.K. Christensen, and S. Tanabe. Comfort limits for asymmetric thermal radiation. *Energy and Buildings* 8, pp. 225-236, 1985.

[50] Fanger P.O., A.K. Melikov, H. Hanzawa, and J. Ring. Air turbulence and sensation of draught. *Energy and Buildings*, vol. 12, pp. 21-39, 1988.

[51] Fanger P.O. How to apply models predicting thermal sensation and discomfort in practice. Proceedings of the BRE-Conference held 9-10 June 1993: *Thermal Comfort: Past, Present and Future*. Editors N.A. Oseland and M.A. Humphreys, Building Research Establishment Report, Garston, pp. 11-14, 1994.

[52] Fiala, D. Bestimmung von Einstrahlzahlen zwischen rotationssymmetrischen Körpern und Rechteckflächen mit Analyse eines Halbraum-Strahlungssensors. Diplomarbeit im FB Bauphysik, FHT Stuttgart, Germany, January 1991.

[53] Fiala D. Literature survey on thermal comfort. *Interim Report #1*, De Montfort University Leicester, ECADAP-Centre, 1992.

[54] Fiala D. Computer simulation of the human thermoregulatory system. Mathematical formulation. *Interim Report #2*, 123 pages, DMU-Leicester, ECADAP-Centre, 1993.

[55] Fiala D. Application of the Fanger comfort theory to draught. *Interim Report #3*, De Montfort University Leicester, ECADAP-Centre, 1993.

[56] Fiala D. Mathematical models of the human thermoregulatory system. A literature review. *Interim Report #4*, De Montfort University Leicester, ECADAP-Centre, 1993.

[57] Gagge A.P., J.A.J. Stolwijk, and J.D. Hardy. Comfort and thermal sensation and associated physiological responses at various ambient temperatures. *Environmental Research* 1, pp. 1-20, 1967.

[58] Gagge A.P., J.A.J. Stolwijk, and B. Hardy. Comfort and thermal sensations and associated responses during exercise at various ambient temperatures. *Environmental Research* 2, pp. 209-229, 1969.

[59] Gagge A.P., and R.R. Gonzalez. Physiological bases of warm discomfort for sedentary man. *Arch. Sci. Physiol.*, vol. 27, pp. A409-A424, 1973.

[60] Gagge A.P. Rational temperature indices of man's thermal environment and their use with a 2-node model of his temperature regulation. *Fed. Proc.*, vol. 32, pp. 1572-1582, 1973.

[61] Gagge A.P.: Rational temperature indices of man's thermal environment and their use with a two node model of his temperature regulation. Federation Proceedings, vol. 32, no.5, Federation of American Societies for Experimental Biology, pp.1572-1582, 1973.

[62] Gagge A.P. The role of humidity during warm discomfort. In *"Indoor Climate"*, ed. P.O. Fanger & O. Valbjorn, Danish Building Research Institute, Copenhagen, pp. 527-538, 1979.

[63] Givoni B., and R.F. Goldman. Predicting rectal temperature response to work, environment, and clothing. *J. Appl. Physiol.,* vol. 32, pp.812-822, 1972.

[64] Givoni B. Man, climate and architecture. 2nd edition *Applied Sciences*, London, 1976.

[65] Glück B. Zulässige Strahlungstemperatur-Asymmetrie. *Gesundheits Ingenieur (gi), Haustechnik - Bauphysik - Umwelttechnik* 115 (6), pp. 285-344, 1994.

[66] Gonzalez R.R., and A.P. Gagge. Magnitude estimates of thermal discomfort during transients of humidity and operative temperature and their relation to the new ASHRAE effective temperature (ET^*). *ASHRAE Trans.*, vol. 79, pp. 88-96, 1973.

[67] Gonzalez R.R., Pandolf K.B., and A.P. Gagge. Physiological responses and warm discomfort during heat strain. *Arch. Sci. Physiol.*, vol. 27, pp. A563-A571, 1973.

[68] Gonzalez R.R., Pandolf K.B., and A.P. Gagge. Heat acclimation and decline in sweating during humidity transients. *J. Appl. Physiol.*, vol. 36, pp. 419-425, 1974.

[69] Gordon, R. G. The Response of Human Thermoregulatory System in the Cold. PhD-Thesis in Mechanical Engineering, University of California, Santa Barbara CA, 1974.

[70] Gordon R. G., and R. B. Roemer. The effect of radial nodal spacing on the performance of a mathematical model of the human temperature regulatory system. *IEEE Trans. on Biomech. Eng.*, vol. BME-22, pp. 80-83, January 1975.

[71] Gordon R. G., and R. B. Roemer. The effect of radial nodal spacing on finite difference calculations of temperatures in living tissue. *IEEE Trans. on Biomech. Eng.*, vol. BME-22, pp. 77-80, January 1975.

[72] Gordon R.G., R.B. Roemer, and S.M. Horvath. A mathematical model of the human temperature regulatory system - transient cold exposure response. *IEEE Trans. Biomed. Eng.*, vol. 23, pp. 434-444. 1976.

[73] Gröber, H., S. Erk, and U. Grigull. Die Grundgesetze der Wärmeübertragung. *Springer-Verlag*. Berlin- Heidelberg, pp. 53-60, 1988.

[74] Hald A. Statistical Theory with Engineering Application. John Wiley & sons, Inc. New York-London-Sydney, 1989.

[75] Hardy J.D., and J.A.J. Stolwijk. Partitional calorimetric studies of man during exposures to thermal transients. *J. Appl. Physiol.*, vol. 21, pp. 1799-1806, 1966.

[76] Hardy J.D. Thermal comfort: skin temperature and physiological thermoregulation. In *"Physiological and Behavioural Temperature Regulation"*, Hardy, Gagge & Stolwijk, Springfield, pp. 856-873, 1970.

[77] Hardy J.D. Regulation of body temperature in man - an overview. In *'Energy Conservation Strategies in Buildings'*, chap. 2, pp. 14-37, J. B. Pierce Foundation of Connecticut, Inc., ed. J.A.J. Stolwijk, 1978.

[78] Haslag W.M., and A.B. Hertzman. Temperautre regulation of young woman. *J. Appl. Physiol.*, vol. 20, pp. 1283-1288, 1965.

[79] Haslam R.A., and K.C. Parsons: An evaluation of computer-based models that predict human responses to the thermal environment. ASHRAE Trans., vol. 94, pp. 1342-1360, 1988.

[80] Havenith D.G. Individual parameters in thermoregulatory control; a review. Report No. IZF 1985-26, Inst. Perc. TNO, Nat. Def. Res. Org., the Netherlands, 1985.

[81] Hayward J.S., J.D. Eckerson, and M.L. Collis. Thermoregulatory heat production in man: prediction equation based on skin and core temperatures. *J. Appl. Physiol.*, vol. 42, pp. 377-384, 1977.

[82] Heising M., Werner J. Control of sweating in man after work-induced thermal load and symmetrically applied cooling. *Eur. J. Appl. Physiol.*, vol. 56, pp. 608-614, 1987.

[83] Hemmingsen A. M. Energy metabolism as related to body size and respiratory surfaces, and its evolution. *Rep. Steno. Mem. Hosp. Nord. Insulin Lab.* 9, pp.1–110, 1960.

[84] Hensel H. Physologie der Thermoreception. *Ergebnisse der Physiologie*, vol. 47, pp. 166-368, 1952.

[85] Hensel H., and I. Witt. Spatial temperature gradient and thermoreceptor stimulation. *J. Physiol. (London)*, vol. 148, pp. 180-189, 1959.

[86] Hensel H., and K.K.A Boman. Afferent impulses in cutaneous sensory nerves in human subjects. *J. Neurophysiol.*, vol. 23, pp. 564-578, 1960.

[87] Hensel H. Thermoreception and human comfort.. In *"Indoor Climate"*, ed. P.O. Fanger & O. Valbjorn, Danish Building Research Institute, Copenhagen, pp. 426-440, 1979.

[88] Hensel H. Thermoreception and temperature regulation. (Monographs of the physiological society; no.38), *Academic Press*, London, 1981.

[89] Hensen J.L.M. Literature review on thermal comfort in transient conditions. *Building and Environment*, vol. 25, pp.309-316, 1990.

[90] Hildebrandt G., P. Engel, and M. Attia. Temperaturregulation und thermischer Komfort. *Zeitschrift für Physikalische Medizin* 10, pp. 49-61, 1981.

[91] Höppe P.R. Heat balance modelling. *Experientia*, vol. 49, Birkhäuser Verlag, CH-Basel, pp. 741-746, 1993.

[92] Horikoshi, T., T. Tsuchikawa, Y. Kobayashi, E. Miwa, Y. Durazumi, and K. Hirayama. The effective radiation area and angle factor between man and a rectangular plane near him. *ASHRAE Trans. 96(I)*, pp. 60-66, 1990.

[93] Humphreys M.A. Outdoor temperatures and comfort indoors. *Building Research and Practice*, vol. 6, pp. 92-105, 1978.

[94] ISO 7730: Moderate Thermal Environments - Determination of the PMV and PPD Indices and Specification of the Conditions for Thermal Comfort. *International Organisation for Standardization*, Geneva, 1984.

[95] Issing K., and H. Hensel. Temperaturempfindung und thermischer Komfort bei statischen Temperaturreizen. *Z. Phys. Med. Baln. Med. Klim.*, vol. 11, pp. 354-365, 1982.

[96] Jiji, L. M., S. Weinbaum, and D.E. Lemons. Theory and experiment for the effect of vascular microstructure on surface tissue heat transfer - part II model formulation and solution. *ASME J. Biomech. Eng.* vol. 106, pp. 331-341, 1984.

[97] Johnson K.O., I. Darian-Smith, and C. LaMotte. Peripheral neutral determinants of temperature discrimination in man: A correlative study of response to cooling skin. *J. Neurophysiol.*, vol. 36, pp. 347-370, 1973.

[98] Johnson J.L., L.B. Rowell, and G.L. Brengelmann. Modification of the skin blood flow - body temperature relationship by upright exercise. *J. Appl. Physiol.* vol. 37, pp. 880-886, 1974.

[99] Johnson J.M., G.L. Brengelman, and L.B. Rowell. Interaction between local and reflex influences on human forearm skin blood flow. *J. Appl. Physiol.*, vol. 41, pp. 826-831, 1976.

[100] Jones B.W., K. Hsieh, and M. Hashinaga. The effect of air velocity on thermal

comfort at moderate activity levels. *ASHRAE Trans.* 95, pp. 761-768 1989

[101] Jones, B. W., and Y. Ogawa. Transient interaction between the human and the thermal environment. *ASHRAE Trans.* 98, pp. 189-196, 1992.

[102] Keller, K. H., and L. Seiler jun. An analysis of peripheral heat transfer in man *J Appl. Physiol.* 30(5): 779-786, 1971.

[103] Kerslake D. McK. The stress of hot environments *Cambridge University Press* Cambridge, 1972.

[104] Kollias J., L. Barlett, V. Bergsteinova, J.S. Skinner, E.R. Buskirk, and W.C. Nicholas. Metabolic and thermal responses of women during cooling in water. *J. Appl. Phyisol.*, vol. 36, pp. 577-580, 1974.

[105] Konietzny F., and H. Hensel. The neutral basis of the sensory quality of warmth. In *"Sensory Functions of the Skin of Humans"* (D.R. Kenshalo, Ed.) Plenum Press NY-London, pp. 241-259, 1979.

[106] Konz S., C. Hwang, B. Dhiman, J. Duncan, and A. Masud. An experimental validation of mathematical simulation of human thermoregulation. *Comput. Biol. Med.*, vol. 7, pp. 71-82, 1977.

[107] Kundt H.W., K. Brück, and H. Hensel. Hypothalamustemperatur und Hautdurchblutung der nichtnarkotisierten Katze. *Pflügers Arch. ges. Physiol.*, vol. 264, pp. 275-285, 1957.

[108] Kuznetz, L. H. A two-dimensional transient mathematical model of human thermoregulation. *Am. J. Physiol.* 6(3), pp. R266-R277, 1979.

[109] Libert J.P., V. Candas, and J.J. Vogt. Effect of rate change in skin temperature on local sweating rate. *J. Appl. Physiol.*, vol. 47, pp. 306-311, 1979.

[110] Libert J.P., V. Candas, J.J. Vogt. Sweating response in man during transient rises of air temperature. *J. Appl. Phyisol.*, vol. 44, pp. 284-290, 1978.

[111] Lind A.R. A physiological criterion for setting thermal environmental limits for everyday work. *J. Appl. Physiol.* 18(1), pp. 51-56, 1963.

[112] Livingstone S.D., J. Grayson, J. Frim, C.L. Allen, and R.E. Limmer. Effect of cold exposure on various sites of core temperature measurements. *J. Appl. Physiol.*, vol. 54, pp. 1025-1031. 1983.

[113] Lomas, K.J., H. Eppel, M.J. Cook, and J. Mardaljevic. Ventilation and Thermal

Performance of Design Options for Stadium Australia. PRoc. 5th IBPSA Conf. BS'97, Prague, vol. 1, pp. 135-142, 1997.

[114] Lotens W.A.: Comparison of thermal predictive models for clothed humans. *ASHRAE Trans.*, vol. 94, pp. 1321-1340, 1988.

[115] Mansour M.A., M.J. Cook, A.H. Taki, and K.J. Lomas. Use of Computational Fluid Dynamics of Modelling Passive Downdraught Evaporative Cooling. Proc. 18th Ann. AIVC Conf., Vol. 2, pp. 603-611, ISBN 0-946075-96-4, 1997.

[116] Maruhashi I., K. Mizuguchi, and I. Tasaki. Action current in single afferent nerve fibres elicited by stimulation of the skin of the toad and the cat. *J. Physiol. (London)*, vol. 117, pp. 129-151, 1952.

[117] Mayer, E., and R. Schwab. Untersuchungen der physikalischen Ursachen von Zugluft. *Gesundheitsingenieur 111*, Heft 1, pp.17-30, 1990.

[118] Mayer E. Wie behaglich ist Quellüftung. *Bauphysik (Wärme Energie Schall Brand Feuchte Licht Mikroklima)*, Sonderdruck aus: 15 (1993), Heft 2, pp. 68-71, 1993.

[119] McArdle B., Dunham W., Holling H.E., Ladell W.S.S., Scott J.W., Thomson M.L., and Weiner J.S. The prediction of the physiological effect of warm and hot environments. *Med. Res. Council*, London, RNP Rep. 47/391, 1947.

[120] McCaffrey T.V., R.D. Wurster, H.K. Jacobs, D.E. Euler, and G.S. Geis. Role of skin temperature in the control of sweating. *J. Appl. Physiol.*, vol. 47, pp. 591-597, 1979.

[121] McCullough, E. A., B. W. Jones, and J. Huck. A comprehensive data base for estimating clothing insulation. *ASHRAE Trans.,* vol. 91, pp. 29-47, 1985.

[122] McCullough, E. A., B. W. Jones, and T. Tamura. A data base for determining the evaporative resistance of clothing. *ASHRAE Trans.*, vol. 95, pp. 316-328, 1989.

[123] McIntyre D.A., R.R. Gonzalez. Man's thermal sensitivity during temperature changes at two levels of clothing insulation and activity. *ASHRAE Trans.* 82(2), pp. 219-233, 1976.

[124] McIntyre D.A. Seven point scales of warmth. *Building Services Engineer* 45, pp. 215-226, 1978.

[125] McIntyre, D. A. Indoor Climate. *Applied Science Publishers Ltd.*, London, 1980.

[126] McIntyre D.A. Indoor Climate. *Applied Science Publishers*, London, Chap. 5.7: Scales of Warmth Sensation, p. 134, 1980.

[127] McNall, P.E., J. Jaax, F.H. Rohles, R.G. Nevins, and W. Springer. Thermal comfort (thermally neutral) conditions for three levels of activity. *ASHRAE Trans.* vol. 73(1), pp. I.3.1-I.3.14, 1967.

[128] McNall P.E., P.W. Ryan, F.H. Rohles, R.G. Nevins, and W.E. Springer. Metabolic rates at four activity levels and their relationship to thermal comfort. *ASHRAE Trans.* vol. 74(1), pp. IV.3.1-IV.3.14, 1968.

[129] McNall P.E., and J.C. Schlegel. The relative effect of convective and radiation heat transfer on thermal comfort (thermal neutrality) for sedentary and active human subjects. *ASHRAE Trans.*, vol. 74, pp. 131-143, 1968.

[130] McNall Jr. P.E., and R.E. Biddison. Thermal and comfort sensation of sedentary persons exposed to asymmetric radiant fields. *ASHRAE Trans.*, vol. 76, pp. 123-176, 1970.

[131] Miller G.A. The magical seven, plus or minus two. *Physiol. Review*, vol. 63, pp. 81-97, 1956.

[132] Miller, N. C., and R. C. Seagrave. A model of human thermoregulation during water immersion. *Comput. Biol. Med.*, vol. 4, pp. 165-182, Pergamon Press 1974.

[133] Mitchell D., and C.H. Wyndham. Comparison of weighting formulas for calculating mean skin temperature. *J. Appl. Physiol.*, vol. 26, pp. 616-622, 1969.

[134] Mitchell, J. W., T. L. Galvez, J. Hengle, G. L. Meyers, and K. L. Siebacker. Thermal response of human legs during cooling. *J. Appl. Physiol. 29*, pp. 859-865, 1970.

[135] Mower G.D. Perceived intensity of peripheral thermal stimuli is independent of internal body temperature. *J. Comp. Physiol. Psychol.*, vol. 90, pp. 1152-1155, 1976.

[136] Nadel E.R., S.M. Horvath, C.A. Dawson, and A. Tucker. Sensitivity to central and peripheral thermal stimulation in man. *J. Appl. Physiol.*, vol. 29, pp. 603-609, 1970.

[137] Nadel E.R., R.W. Bullard, and J.A.J. Stolwijk. Importance of skin temperature in the regulation of sweating. *J. Appl. Physiol.*, vol. 31, pp. 80-87, 1971.

[138] Nadel E.R., J.W. Mitchell, and J.A.J. Stolwijk. Differential thermal sensitivity in the human skin. *Pflügers Arch.*, vol. 340, pp.71-76. 1973

[139] Nakayama T., H.T. Hammel, J.D. Hardy, and J.S. Eisenmann. Thermal stimulation of electrical activity of single units in the preoptic region. *Am. J. Physiol.*, vol. 204, pp. 112-1126, 1963.

[140] Nakayama T., and J.D. Hardy. Unit responses in the rabbit's brain stem to changes in brain and cutaneous temperature. *J. Appl. Physiol.*, vol. 27, pp. 848-857. 1969.

[141] Nevins R.G., F.H. Rohles, W. Springer, and A.M. Feyerherm. Temperature-humidity chart for thermal comfort of seated persons. *ASHRAE Trans.* 72, pp. 283-291, 1966.

[142] Nevins R.G., R.R. Gonzalez, Y. Nishi, and A.P. Gagge. Effect of changes in ambient temperature and level of humidity on comfort and thermal sensation. *ASHRAE Trans.* 81(2), pp. 169-182, 1975.

[143] Nielsen M., and L. Pedersen. Studies on the heat loss by radiation and convection from the clothed human body. *Acta Physiol. Scand.*, vol. 27, pp. 272-294, 1952.

[144] Nielsen R., and B. Nielsen. Influence of skin temperature distribution on thermal sensation in a cool environment. *Eur. J. Appl. Physiol.*, vol 53, pp. 225-230, 1984.

[145] NIOSH. Occupational Exposure to Hot Environments. *National Institute for Occupational Safety and Health*, HSM 72-10269. Department of Health Education and Welfare, USA, 1972.

[146] Nishi, Y. Direct evaluation of the convective heat transfer coefficient for various activities and environment. *Arch. Sci. Physiol. 27*, pp. A59-A66, 1973.

[147] Oeffinger M., M. Stohrer, G. Claus., and D. Fiala. Entwicklung eines physiologischen Behaglichkeitsmodells zur Beurteilung der thermischen Behaglichkeit. Diplomarbeit im Fachbereich Bauphysik, FH Stuttgart - Hochschule für Technik, Stuttgart, Januar 1995.

[148] Ohno H., S. Kuno, M. Kida, and N. Nakahara. Physiological and psychological responses in thermal transients with ramp change. *ASHRAE Trans.*, vol. 93, 1987.

[149] Olesen S., J.J. Bassing, and P.O. Fanger. Physiological comfort conditions at sixteen combinations of activity, clothing, air velocity and ambient temperature. *ASHRAE Trans.*, vol. 78, pp. 199-206, 1972.

[150] Olesen, B. W., and P. O. Fanger. The skin temperature distribution for resting man in comfort. *Arch. Sci. Physiol. 27*, pp. A385-A393, 1973.

[151] Olesen S., P.O. Fanger, P.B. Jensen, and O.J. Nielsen. Comfort limits for man exposed to asymmetric thermal radiation. Proceedings of the CIB Commission W45 Human Requirements Symposium: Thermal Comfort and Moderate Heat Stress. Building Research Station, London, Spt.1972, HMSO, pp.133-150, 1973.

[152] Olesen B.W., M. Schöler, and P.O. Fanger. Discomfort Caused by Vertical Air Temperature. Indoor climate, ed. P.O. Fanger and O.Valbjorn, Danish Building Research Institute, Copenhagen, pp.561-579, 1979.

[153] Pennes, H. H. Analysis of tissue and arterial blood temperatures in the resting human forearm. *J. Appl. Physiol.*, Vol. 1, pp. 93-121, August 1948.

[154] Press, W.H., B.P. Flannery, S.A. Teukolsky, and W.T. Vetterling. Numerical recipes in C - The art of scientific computing. Chap. 9, *Cambridge University Press*, Cambridge - New York - Port Chester - Melbourne - Sydney, 1988.

[155] Rapp, G. M. Convective heat transfer and convective coefficients of nude man, cylinder and spheres at low air velocities. *ASHRAE Trans. 79 (1)*, pp. 75-87, 1973.

[156] Raven, P. R., and S. M. Horvath. Variability of physiological parameters of unacclimatized males during a two-hour cold stress of 5°C. *Int. J. Biometeor.*, vol. 14, number 3, pp. 309-320, 1970.

[157] Roberts M.F., C.B. Wenger, J.A.J Stolwijk, and E.R. Nadel. Skin blood flow and sweating changes following exercise and heat acclimation. *J. Appl. Physiol.*, vol. 43, pp. 133-137, 1977.

[158] Rohles F.H. Thermal Sensation of Sedentary Man in Moderate Temperatures. Special report of *Institute for Environmental Research, Kansas State University*, June 1970.

[159] Rohles F.H., and R.G. Nevins. The nature of thermal comfort for sedentary man. *ASHRAE Trans.* 77 (1), pp. 239-246. 1971.

[160] Rohles F.H., J.E. Woods, and R.G. Nevins. The effect of air movement and temperature on the thermal sensation of sedentary man. *ASHRAE Trans.*, vol. 80, pp. 101-118. 1974.

[161] Rohles F.H., G.A. Milliken, D.E. Skipton, and I. Krstic. Thermal comfort during cyclical temperature fluctuations. *ASHRAE Trans.*, vol. 86, pp. 125-140, 1980.

[162] Rowell L.B., J.A. Murray, G.L. Brengelmann, and K.K. Kraning. Human cardiovascular adjustments to rapid changes in skin temperature. *Circulation Res.*, vol. 24, pp. 711-724, 1969.

[163] Rowell L.B. Human cardiovascular adjustments to exercise and thermal stress. *Physiol. Rev.*, vol. 54, pp. 75-159, 1974.

[164] Rowell, L.B., and C.R. Wyss. Temperature regulation in exercising and heat-stres-

sed man. In: Shitzer A., and R.C. Eberhart: *Heat Transfer in Medicine and Biology - Analysis and Applications*, vol. 1, chap. 3, pp. 53-78, Plenum Press, New York and London, 1985.

[165] Saltin B.A., Gagge A.P., and Stolwijk J.A.J. Body temperatures and sweating during thermal transients caused by exercise. *J. Appl. Physiol.* 28(3), pp. 318-327, 1970.

[166] Scherer, P. W., and L. M. Hanna. Heat and water transport in the human respiratory system. In: Shitzer A., and R.C. Eberhart. *Heat Transfer in Medicine and Biology - Analysis and Applications*, vol. 2, chap. 23. Plenum Press, New York and London, 1985.

[167] Schuh, H. Differenzenverfahren zum Berechnen von Temperatur-Ausgleichsvorgängen bei eindimensionaler Wärmeströmung in einfachen und zusammengesetzten Körpern. *VDI-Forschungsheft 459*, Beilage zu "Forschung auf dem Gebiete des Ingenieurwesens", Ausgabe B, Band 23, VDI-Verlag GmbH Düsseldorf, 1957.

[168] Schweinberger, M., Fiala, D. Simulationsmodell zur Berechnung der mittleren Strahlungstemperatur und Strahlungsasymmetrien für den stehenden und sitzenden Menschen. *Diplomarbeit im FB Bauphysik, HfT-Stuttgart,* Sommersemester, 1997.

[169] Shibolet S., Lancaster M.C., and Danon Y. Heat Stroke: A review. *Aviation Space and Environmental Medicine*, vol. 47, pp. 280-301, 1976

[170] Shih, T.-M. Numerical Heat Transfer. *Hemisphere Publishing Corporation*. Washington, New York, London, 1984.

[171] Shitzer, A. General analysis of the bioheat equation. In: Shitzer A., and R.C. Eberhart. *Heat Transfer in Medicine and Biology - Analysis and Applications*, vol. 1, chap. 10. Plenum Press, New York and London, 1985.

[172] Song, W. J., S. Weinbaum, and L. M. Jiji. A theoretical model for peripheral tissue heat transfer using the bioheat equation of Weinbaum and Jiji. ASME - *J. Biomech. Eng.*, vol 109, pp. 72-78, February 1987.

[173] Sprague C.H., and P.E. McNall jr. The effect of fluctuating temperature and relative humidity on the thermal sensation (thermal comfort) of sedentary subjects. *ASHRAE Trans.* 76, pp. 146-156, 1970.

[174] Stevens J.C., L.E. Marks, and D.E. Simonson D.E. Regional and spatial summation in the warmth sense. *Physiology and Behaviour*, vol. 13, pp.825-836. 1974.

[175] Stolwijk J.A.J., and J.D. Hardy. Partitional calorimetric studies of responses of man to thermal transients. *J. Appl. Physiol.*, vol. 21, pp. 967-977, 1966.

[176] Stolwijk J.A.J., and J.D. Hardy. Temperature regulation in man - a theoretical study. *Pflügers Archiv 291*, pp. 129-162, 1966.

[177] Stolwijk, J.A.J. A mathematical model of physiological temperature regulation in man. *NASA contractor report, NASA CR-1855*, Washington DC, August 1971.

[178] Stolwijk J.A.J., E.R. Nadel, J.W. Mitchell, and B.Saltin. Modification of central sweating drive at the periphery. *Int. J. Biometeor.*, vol. 15, pp.268-272, 1971.

[179] Stolwijk J.A.J. Physiological responses and thermal comfort in changing environmental temperature and humidity. In *"Indoor Climate"*, ed. P.O. Fanger & O. Valbjorn, Danish Building Research Institute, Copenhagen, pp. 491-505, 1979.

[180] Strong L.H., G.K. Gee, and R.F. Goldman. Metabolic and vasomotor insulative responses occurring on immersion in cold water. *J. Appl. Physiol.*, vol. 58, pp. 964-977, 1985.

[181] Tick-Waider A. M. Signalverarbeitung in einem Sinneskanal: menschliche Sinnesempfindung als Aussage im Vergleich zur Rezeptorantwort als Eingangssignal bei dynamisch-thermischen Reizen. *Dissertation zur Erlangung eines Doktors der Naturwissenschaften.* Institut für Zoophysiologie der Universität Hohenheim, Germany, 1991.

[182] Tikuisis, P., and M. B. Ducharme. Finite-element solution of thermal conductivity of muscle during cold water immersion. *J. Appl. Physiol. 70*, pp. 2673-2681, 1991.

[183] Tikuisis P., D.G. Bell, and I. Jacobs. Shivering onset, metabolic response, and convective heat transfer during cold air exposure. *J. Appl. Physiol.*, vol. 70, pp. 1996-2002, 1991.

[184] Timbal J., Ch. Boutelier, M. Loncle, and L. Bougues. Comparison of shivering in man exposed to cold water and air. *Pflügers Arch.*, vol. 365, pp. 243-248, 1976.

[185] Veicsteinas A., G. Ferretti, and D.W. Rennie. Superficial shell insulation in resting and exercising men in cold water. *J. Appl. Physiol.*, vol. 52, pp. 1557-1564.

[186] Vendrik A.J.H., and J.J. Vos. Comparison of the stimulation of the warmth sense organ by microwave and infrared. *J. Appl. Physiol.*, vol. 13, pp. 435-444. 1958.

[187] Vogelaere P., and F. De Meyer. Rheological modelling of physiological variables during temperature variations at rest. *Int. J. Biometeorology*, vol. 34, pp. 76-86, 1990.

[188] Wagner J.A., and S.M. Horvath. Influences of age and gender on human thermore-

gulatory responses to cold exposures. *J. Appl. Physiol.*, vol. 58, pp. 180-186, 1985.

[189] Wang, X.-L. Convective heat losses from segments of the human body. *Climate and Buildings*, no. 3, pp. 8-14, Stockholm, 1990.

[190] Wang, X.-L. Convective heat transfer coefficients from head and arms. *Climate and Buildings*, no. 2, pp. 3-7, Stockholm, 1990.

[191] Wang, X.-L. Free convective heat transfer coefficients of a heated full-scale manikin. *Climate and Buildings,* no. 1, pp.17-31, Stockholm, 1990.

[192] Webb-Peploe M.M., and J.T. Shepherd. Response of dogs' cutaneous vein to local and central temperature changes. *Circulat. Res.*, vol 23, pp. 693-699, 1968.

[193] Weinbaum, S., L. M. Jiji, and D.E. Lemons. Theory and experiment for the effect of vascular microstructure on surface tissue heat transfer - part I: anatomical foundation and model conceptualization. ASME *J. Biomech. Eng.*, vol. 106, pp. 321-330, 1984.

[194] Weinbaum, S., and L. M. Jiji. A new simplified bioheat equation for the effect of blood flow on local average tissue temperature. ASME *J. Biomech. Eng.*, vol. 107, pp. 131-139, 1985.

[195] Wenger C.B., M.F. Roberts, E.R. Nadel, and J.A.J. Stolwijk. Thermoregulatory control of finger blood flow. *J. Appl. Physiol.*, vol. 38, pp. 1078-1082, 1975.

[196] Werner J., M. Heising, W. Rautenberg, and K. Leimann. Dynamic and topography of human temperature regulation in response to thermal and work load. *Eur. J. Appl. Physiol.*, vol. 53, pp. 353-358, 1985.

[197] Werner, J., and M. Buse. Temperature profiles with respect to inhomogeneity and geometry of the human body. *J. Appl. Physiol. 65(3)*: 1110-1118, 1988.

[198] Werner J., M. Buse, and A. Foegen. Lumped versus distributed thermoregulatory control: results from a three-dimensional dynamic model. Biol. Cybern., vol. 62, pp. 63-73, 1989.

[199] WHO. Health factors involved in working under conditions of heat stress. *World Health Organisation Technical Report* 412, Geneva, 1969.

[200] Wissler, E. H. A mathematical model of the human thermal system. *Buletin of mathematical biophysics*, vol. 26, pp.147-166, 1964.

[201] Wissler E.H. Mathematical simulation of human thermal behaviour using whole body

models. In: Shitzer A., and R.C. Eberhart: *Heat Transfer in Medicine and Biology - Analysis and Applications*, vol. 1, chap. 13, pp. 325-373, Plenum Press, New York and London, 1985.

[202] Wulff, W. The energy conservation equation for living tissue. *ISEE Trans.*, BME-21, no. 6, pp. 494-495, 1974.

[203] Wurster R.D., and R.D. McCook. Influence of rate of change in skin temperature on sweating. *J. Appl. Physiol.*, vol. 27, pp. 237-240. 1969.

[204] Wyndham C.H., J.S. Ward, N.B. Strydom, J.F. Morrison, C.G. Williams, G.A.G. Bredell, J. Peter, M.J.E. Von Rahden, L.D. Holdsworth, C.H. Van Graan, A.J. Van Rensburg, and A. Munro. Physiological reactions of caucasian and bantu males in acute exposure to cold. *J. Appl. Physiol.*, vol. 19, pp. 538-592, 1964.

[205] Wyndham, C. H., J. F. Morrison, C. G. Williams, N. B. Stryndom, M. J. E.von Rahden, L. D. Holdsworth, A. J. Van Rensburg, A. Joffe, and A. Heyns. Inter- and intra-individual differences in energy expenditure and mechanical efficiency. *Ergonomics*, vol. 9, pp. 17-29, 1966.

[206] Wyon D.P., and M. Sandberg. Thermal manikin prediction of discomfort due to displacement ventilation. *ASHRAE Trans.* 96, pp. 67-75, 1990.

[207] Wyss C.R., G.L. Brengelmann, J.M. Johnson, L.B. Rowell, and M. Niederberger. Control of skin blood flow, sweating, and heart rate: role of skin vs. core temperature. *J. Appl. Physiol.*, vol. 36, pp. 726-733, 1974.

[208] Wyss C.R., G.L. Brengelmann, J.M. Johnson, L.B. Rowell, and D. Silverstein. Altered control of skin blood flow at high skin and core temperatures. *J. Appl. Physiol.*, vol. 38, pp. 839-845, 1975.

[209] Young, A.J., S.R. Muza, M.N. Sawka, R.R. Gonzalez, and K.B. Pandolf. Human thermoregulatory responses to cold air are altered by repeated cold water immersion. *J. Appl. Physiol.* 60(5): 1542-1548, 1986.

Bibliography

During the course of this research several comprehensive interim reports were produced. These are listed in following.

IR1: Literature survey on thermal comfort. 152 pages, DMU-Leicester, ECADAP-Centre, 1992.

IR2: Reasons and proposal for estimating thermal comfort in highly glazed spaces. 27 pages, DMU-Leicester, ECADAP-Centre, 1992.

IR3: Application of the Fanger comfort theory to draught. 26 pages, DMU-Leicester, ECADAP-Centre, 1993.

IR4: Mathematical models of the human thermoregulatory system: A literature review. 69 pages, DMU-Leicester, ECADAP-Centre, 1993.

IR5: Computer simulation of the human thermoregulatory system. Mathematical formulation. 123 pages, DMU-Leicester, ECADAP-Centre, 1993.

IR6: Computer simulation of the human thermoregulatory system. Calibration & Validation. Part I-III. 254 pages, DMU-Leicester, ECADAP-Centre, 1994.

IR7: Modelling Thermal Comfort. 112 pages, DMU-Leicester, IESD, 1997.

A paper has also been accepted for publication in the *Journal of Applied Physiology* (a journal of the American Physiological Society):

Fiala D., K.J. Lomas, and M. Stohrer. A Computer Model of Human Thermoregulation for a Wide Range of Environmental Conditions: The Passive System.

Acknowledgements

This research was carried out at De Montfort University Leicester (UK), Institute of Energy and Sustainable Development (IESD), working in collaboration with Fachhochschule Stuttgart - Hochschule für Technik (Germany), Joseph-von-Egle Institut, and Department of Building-Physics. This work could not have been completed without the support and help of many people in both institutions and elsewhere.

I am especially grateful to Prof. Dr. Kevin J. Lomas for his encouragement and enthusiastic support throughout the whole project and for his careful and critical review of this thesis. In the early stages of the project, Prof. Lomas contributed decisively to my motivation to enter new pathways in the comfort research. I am also deeply indebted to Prof. Dr. Martin Stohrer who encouraged me to extend work in the area of thermal comfort established years ago at the Hochschule für Technik, and thereby, gave me support in many ways.

I would like to thank Prof. Neil Bowman who - as the leader of IESD - took care that the collaboration with the German institution was possible and successful. I am grateful to Prof. Christian Kupke for his instructive cooperation and support in the thermophysical aspects of the research project, Prof. Dr.-Ing. H. Winter for fruitful advices to numerical methods and matrix processing, and Prof. Dr. H.H. Heizmann for advice on methods of statistical data analysis.

I wish to express my particular thanks to Prof. Miloslav V. Jokl, DrSc, Technical University of Prague, for his devoted interest in the present work and his help on aspects of thermal comfort modelling.

This work could not have succeeded without the funding of different institutions, to which I would like to express my gratitude:

- the Deutsche Akademische Austauschdienst (DAAD) for British-German Academic Research Collaboration (ARC) - project funding;

- the Joseph-von-Egle Institut of Hochschule für Technik, Stuttgart;

- the Knödler Stiftung (Club of the Friends of the Fachhochschule für Technik Stuttgart).

While realizing that a complete listing of all people which supported this work is impossible I would gratefully acknowledge the following.

- Herbert Eppel for assistance and supervision on the use of the software and hardware at the IESD, and his organisation talent; and other members of the IESD research group for creating an atmosphere in which it was a pleasure to work.

- The students Micheal Oeffinger and Michael Schweinberger who contributed to this research during their diploma works, mainly by participating in the development of the thermal comfort model (preliminary linear regression analyses), and the application of the model to environments with inhomogeneous radiant fields.

Finally, I would like to thank my wife, my children and my parents who always stand by my side. I am deeply grateful to the Lord Jesus who provided for me and my family faithfully throughout the work and gave me peace, strength and confidence.

APPENDICES

A. Passive System

A.1 Tables

BODY ELEMENTS	L	h_x	$h_{c,mix}$			a_{sk}	$a_{m,w}$		sector	φ^i	$\Psi_{sf\text{-}sr}$		ε_{sf}	material	n	r	k	ρ	c	$w_{bl,0}$	$q_{m,0}$
	[cm]	[W/K]	a_{nat}	a_{frc}	a_{mix}	[-]	sed	stnd		[Deg]	sed	stnd	[]			[cm]	[W/m/K]	[kg/m³]	[J/kg/K]	[ltr/s/m³]	[W/m³]
HEAD (sphere)	•	0.00	3.0	113.0	-5.7	0.0835	0.00	0.00	forehead	10	1.00	1.00	0.99	brain	5	8.60	0.49	1080	3850	10.1320	13400
									head	170	0.90	0.90	0.80	bone	2	10.05	1.16	1500	1591	0.0000	0
														fat	2	10.20	0.16	850	2300	0.0036	58
														skin	4	10.40	0.47	1085	3680	5.4800	368
FACE (cylinder)	9.84	0.00	3.0	113.0	-5.7	0.0418	0.00	0.00		210	0.90	0.90	0.99	muscle	1	2.68	0.42	1085	3768	0.5380	684
														bone	1	5.42	1.16	1500	1591	0.0000	0
														muscle	1	6.80	0.42	1085	3768	0.5380	684
														fat	2	7.60	0.16	850	2300	0.0036	58
														skin	2	7.80	0.47	1085	3680	11.1700	368
NECK (cylinder)	8.42	0.00	1.6	130.0	-6.5	0.0417	0.03	0.01	anterior	180	0.70	0.70	0.99	bone	1	1.90	0.75	1357	1700	0.0000	0
									posterior	180	0.75	0.75	0.99	muscle	4	5.46	0.42	1085	3768	0.5380	684
														fat	2	5.56	0.16	850	2300	0.0036	58
														skin	4	5.67	0.47	1085	3680	6.8000	368
SHOULDERS (cylinder)	32.00	0.80	5.9	216.0	-10.8	0.0300	0.05	0.02		130	0.90	0.90	0.99	bone	1	3.70	0.75	1357	1700	0.0000	0
														muscle	2	3.90	0.42	1085	3768	0.5380	684
														fat	2	4.40	0.16	850	2300	0.0036	58
														skin	2	4.60	0.47	1085	3680	1.0100	368
THORAX (cylinder)	30.60	0.00	0.5	180.0	-7.4	0.3060	0.12	0.07						lung	1	7.73	0.28	550	3718	~ card.out	600
									anterior	150	0.80	0.90	0.99	bone	3	8.91	0.75	1357	1700	0.0000	0
									posterior	150	0.95	0.95	0.99	muscle	3	12.34	0.42	1085	3768	0.5380	684
									inferior	60	0.05	0.10	0.99	fat	6	12.68	0.16	850	2300	0.0036	58
														skin	6	12.90	0.47	1085	3680	1.5800	368
ABDOMEN (cylinder)	55.20	0.00	1.2	180.0	-9.0	0.1210	0.46	0.20						core	1	7.85	0.53	1000	3697	4.3100	4100
									anterior	150	0.80	0.90	0.99	bone	3	8.34	0.75	1357	1700	0.0000	0
									posterior	150	0.95	0.95	0.99	muscle	3	10.90	0.42	1085	3768	0.5380	684
									inferior	60	0.20	0.30	0.99	fat	6	12.44	0.16	850	2300	0.0036	58
														skin	6	12.60	0.47	1085	3680	1.4400	368
ARMS (cylinder)	127.40	4.13	8.3	216.0	-10.8	0.1800	0.19	0.08						bone	1	1.53	0.75	1357	1700	0.0000	0
									anterior	135	0.75	0.85	0.99	muscle	3	3.43	0.42	1085	3768	0.5380	684
									posterior	135	0.80	0.90	0.99	fat	6	4.01	0.16	850	2300	0.0036	58
									inferior	90	0.10	0.20	0.99	skin	6	4.18	0.47	1085	3680	1.1000	368
HANDS (cylinder)	62.00	0.57	8.3	216.0	-10.8	0.0900	0.02	0.01						bone	1	0.70	0.75	1357	1700	0.0000	0
									handback	180	0.80	0.80	0.99	muscle	2	1.74	0.42	1085	3768	0.5380	684
									palm	180	0.10	0.20	0.99	fat	2	2.04	0.16	850	2300	0.0036	58
														skin	4	2.26	0.47	1085	3680	4.5400	368
LEGS (cylinder)	139.00	6.90	5.3	220.0	-11.0	0.2080	0.11	0.60						bone	1	2.20	0.75	1357	1700	0.0000	0
									anterior	150	0.85	0.90	0.99	muscle	6	4.80	0.42	1085	3768	0.5380	684
									posterior	150	0.95	0.90	0.99	fat	6	5.33	0.16	850	2300	0.0036	58
									inferior	60	0.10	0.65	0.99	skin	6	5.53	0.47	1085	3680	1.0500	368
FEET (cylinder)	48.00	3.40	6.8	210.0	-10.5	0.0750	0.02	0.01						bone	1	2.00	0.75	1357	1700	0.0000	0
									instep	180	0.90	0.90	0.99	muscle	2	2.50	0.42	1085	3768	0.5380	684
									sole	180	1.00	1.00	0.99	fat	4	3.26	0.16	850	2300	0.0036	58
														skin	4	3.50	0.47	1085	3680	1.5000	368
BLOOD																		1069	3650		

Tab.A.1

*Passive system parameters: **L** length, h_x CCX coefficient, $h_{c,mix}$ heat exchange coefficient for mixed convection, a_{nat}, a_{frc}, a_{mix} corresponding regression coefficients (nat=natural, frc=forced, mix=absolute term), a_{sk} skin sensitivity coefficients used for calculating the mean skin temperature, $a_{m,w}$ workload distribution coefficient (sed=sedentary activity, stnd=standing activities), φ_i sector angle, $\psi_{sf\text{-}sr}$ view factor between a sector and the surrounding, ε_{sf} surface emission coefficient, **n** number of nodes, **r** outer radius, **k** heat conductivity, ρ material density, **c** heat capacitance, $w_{bl,0}$ and $q_{m,0}$ basal values for blood perfusion and metabolic rate in thermal neutrality, respectively.*

Wght	**Body Fat**	**A_{sk}**	**wt_{sk}**	**Cardiac Output**	**$M_{bas,o}$**
[kg]	[%]	[m^2]	[%]	[$l\,min^{-1}$]	[W]
73.5	14.0	1.9	6.0	4.9	87.1

Tab.A.2

Overall data of the passive system. ***Wght*** *body weight,* ***body fat*** *fat body-mass ratio,* wt_{sk} *wetted skin area ratio,* A_{sk} *skin surface area,* ***cardOut*** *cardiac output,* $M_{bas,o}$ *basal metabolism.*

T_a	**T_{sf}**	**v_a**	**rh**	**ε_w**	**act**
[°C]	[°C]	[$m\,s^{-1}$]	[%]	[ ]	[met]
30.0	30.0	0.05	40.0	0.93	0.8

Tab.A.3

Boundary conditions of the 'thermal neutrality'. T_a *ambient air temperature,* T_{sf} *temperature of the surrounding wall-surfaces,* v_a *air velocity,* ***rh*** *relative humidity,* ε_w *emissivity of the surrounding wall-surfaces,* act_{bas} *reclining activity.*

$T_{sk,m}$	**$T_{msc,m}$**	**T_{hy}**	**T_{re}**	**$h_{c,m}$**	**$h_{r,m}$**
[°C]	[°C]	[°C]	[°C]	[$W\,m^{-2}K^{-1}$]	[$W\,m^{-2}K^{-1}$]
34.40	36.20	37.00	36.88	2.7	5.0

Q_{sk}	**$Q_{sk,c}$**	**$Q_{sk,r}$**	**$Q_{sk,e}$**	**Q_{rsp}**
[W]	[W]	[W]	[W]	[W]
78.5	21.5	38.9	18.1	8.5

Tab.A.4

Simulated values resulting from a steady state exposure to thermoneutral conditions specified in Tab.A.3. $T_{sk,m}$ *mean skin temperature,* $T_{msc,m}$ *(volume weighted) mean muscle temperature,* T_{hy} *head core (hypothalamus) temperature,* T_{re} *abdomen core (rectal) temperature,* $h_{c,m}$ *calculated mean convective heat transfer coefficient,* $h_{r,m}$ *calculated mean radiative heat transfer coefficient,* Q_{sk} *skin heat loss,* $Q_{sk,c}$ *heat loss by convection,* $Q_{sk,r}$ *heat loss by (long wave) radiation,* $Q_{sk,e}$ *heat loss by skin evaporation,* Q_{rsp} *heat loss by respiration.*

A.2 Formulation of Boundary Conditions

A.2.1 Interfaces Between Tissue Layers

The boundary conditions at the interface between two nodes with different material properties or with different nodal distances, Δr, are given by satisfying the equality of heat fluxes passing the interface calculated for each tissue layer, and by defining a common interface temperature. To increase the accuracy of the calculations the heat flux passing the interface as well as the corresponding interface temperature were derived separately for cylindric and spherical body geometries.

A.2.1.1 Cylindric Coordinates

Consider the interface between the tissue layer *n* and *n+1*. The last node of the layer *n* possesses the following properties: r_n, Δr_n, k_n. The first node of the next different tissue layer *n+1* is characterized by r_{n+1}, Δr_{n+1}, k_{n+1}. The required equality of heat fluxes through the interface calculated for each layer of a cylinder sector (angle $\Delta\varphi$) per length unit *h* [m], and for steady state conditions yields:

$$\frac{\dot{Q}_{ifc}}{h} : \Delta\varphi \frac{k_n}{\ln\left(\frac{r_{(n+1)''}}{r_n}\right)} \left(T_{r_n} - T_{r_{(n+1)''}}\right) = \Delta\varphi \frac{k_{n+1}}{\ln\left(\frac{r_{n+1}}{r_{n''}}\right)} \left(T_{r_{n''}} - T_{r_{n+1}}\right) \qquad (A.1)$$

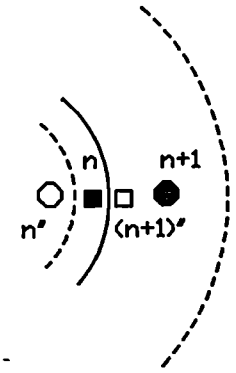

Fig.A.1

For further consideration $\Delta\varphi$ can be eliminated. The heat flux through the interface from the regular actual node *n* (*direction forward*) is calculated using an imaginary node *(n+1)"* [167]. The case of the so called *'forward direction'* occurs when the adjacent node is the next higher node number *n+1* with respect to the actual node *n*. The imaginary node *(n+1)"* is used in place of the node *n+1* to provide homogeneous node properties (Δr_n, k_n) which are the same as of the tissue layer

n. The corresponding radius is $r_{(n+1)''} = r_n + \Delta r_n$. The heat flux through the interface into the regular node *n+1* (next tissue layer) is calculated similarly, however, using an imaginary node *n''* which substitutes the node *n*. The spacing of the regular and the corresponding imaginary nodes is demonstrated in ***Fig.A.1*** (filled rectangle for node *n*, filled polygon for node *n+1*). To obtain the temperatures of the imaginary nodes one additional boundary condition must be satisfied, ie. the temperature of the interface. This temperature results from the steady heat flow within a cylinder, and is calculated for the *n*-th and the *n+1*-th tissue layer by following formulae:

$$\frac{T_{r_n} \cdot \ln\left(\frac{r_{ifc}}{r_{(n+1)''}}\right) - T_{r_{(n+1)''}} \cdot \ln\left(\frac{r_{ifc}}{r_n}\right)}{\ln\left(\frac{r_n}{r_{(n+1)''}}\right)} = T_{ifc} = \frac{T_{r_{n''}} \cdot \ln\left(\frac{r_{ifc}}{r_{n+1}}\right) - T_{r_{n+1}} \cdot \ln\left(\frac{r_{ifc}}{r_{n''}}\right)}{\ln\left(\frac{r_{n''}}{r_{n+1}}\right)} \qquad (A.2)$$

For the *backward direction*, ie. if the tissue layer *n+1* becomes the actual tissue layer *n*, and simultaneously the tissue layer *n* becomes *n-1*, the subscripts of eqs. (A.1) and (A.2) are then changed according to:

$$\frac{k_{n-1}}{\ln\left(\frac{r_{n''}}{r_{n-1}}\right)}\left(T_{r_{n-1}} - T_{r_{n''}}\right) = \frac{k_n}{\ln\left(\frac{r_n}{r_{(n-1)''}}\right)}\left(T_{r_{(n-1)''}} - T_{r_n}\right) \qquad (A.3)$$

$$\frac{T_{r_{n-1}} \cdot \ln\left(\frac{r_{ifc}}{r_{n''}}\right) - T_{r_{n''}} \cdot \ln\left(\frac{r_{ifc}}{r_{n-1}}\right)}{\ln\left(\frac{r_{n-1}}{r_{n''}}\right)} = T_{ifc} = \frac{T_{r_{(n-1)''}} \cdot \ln\left(\frac{r_{ifc}}{r_n}\right) - T_{r_n} \cdot \ln\left(\frac{r_{ifc}}{r_{(n-1)}}\right)}{\ln\left(\frac{r_{(n-1)''}}{r_n}\right)} \qquad (A.4)$$

This change of subscripts is noted to indicate that the final equations of boundary conditions at interfaces for the *forward* and the *backward* direction differ from each other.

From equation (A.2) the temperature of the imaginary node *n''* is separated and

introduced into equation (A.1). Furthermore, when equation (A.1) is modified adequately, the temperature of the imaginary node *(n+1)"* for the *forward direction* yields:

$$T_{(n+1)''} = T_{r_n} \cdot A_{F,n} + T_{r_{n+1}} \cdot A_{F,n+1} \qquad (A.5)$$

With equation (A.5) a formula is found which describes the temperature of the imaginary node *(n+1)"*, which arises from the boundary conditions at the interface between two regular adjacent nodes *n* and *n+1* with different properties for the *forward direction*. The coefficients $A_{F,n}$ and $A_{F,n+1}$ can be understood as a kind of weighting coefficients ($A_{F,n} + A_{F,n+1} = 1$) with respect to the temperatures of the adjacent nodes. The subscript $_F$ stands for the forward direction. They are calculated as follows:

$$A_{F,n} = \frac{Ds_n\ \Lambda_{n+1} - D_{n+1}\ \Lambda_n}{D_n\ \Lambda_{n+1} - D_{n+1}\ \Lambda_n} \qquad A_{F,n+1} = \frac{\Lambda_{n+1}}{D_n\ \Lambda_{n+1} - D_{n+1}\ \Lambda_n}$$

where

$$\Lambda_n = \frac{k_n}{\ln\left(\frac{r_n+\Delta r_n}{r_n}\right)} \qquad \Lambda_{n+1} = \frac{k_{n+1}}{\ln\left(\frac{r_{n+1}}{r_{n+1}-\Delta r_{n+1}}\right)}$$

and

$$D_n = \frac{\ln\left(\frac{r_{ifc}}{r_n}\right)}{\ln\left(\frac{r_n+\Delta r_n}{r_n}\right)} \qquad Ds_n = \frac{\ln\left(\frac{r_{ifc}}{r_n+\Delta r_n}\right)}{\ln\left(\frac{r_n+\Delta r_n}{r_n}\right)} \qquad D_{n+1} = \frac{\ln\left(\frac{r_{ifc}}{r_{n+1}}\right)}{\ln\left(\frac{r_{n+1}}{r_{n+1}-\Delta r_{n+1}}\right)}$$

The following formulae apply to boundary conditions at interfaces for the *backward direction* (subscript $_B$):

$$T_{(n-1)''} = T_{r_{n-1}} \cdot A_{B,n-1} + T_{r_n} \cdot A_{B,n} \qquad (A.9)$$

$$A_{B,n} = \frac{D_{n-1}\,\Lambda_n - Ds_n\,\Lambda_{n-1}}{D_{n-1}\,\Lambda_n - D_n\,\Lambda_{n-1}} \qquad A_{B,n-1} = \frac{\Lambda_{n-1}}{D_{n-1}\,\Lambda_n - D_n\,\Lambda_{n-1}}$$

$$D_n = \frac{\ln\left(\frac{r_{ifc}}{r_n}\right)}{\ln\left(\frac{r_n}{r_n-\Delta r_n}\right)} \qquad Ds_n = \frac{\ln\left(\frac{r_{ifc}}{r_n-\Delta r_n}\right)}{\ln\left(\frac{r_n}{r_n-\Delta r_n}\right)} \qquad D_{n-1} = \frac{\ln\left(\frac{r_{ifc}}{r_{n-1}}\right)}{\ln\left(\frac{r_{n-1}+\Delta r_{n-1}}{r_{n-1}}\right)}$$

$$\Lambda_n = \frac{k_n}{\ln\left(\frac{r_n}{r_n-\Delta r_n}\right)} \qquad \Lambda_{n-1} = \frac{k_{n-1}}{\ln\left(\frac{r_{n-1}+\Delta r_{n-1}}{r_{n-1}}\right)}$$

A.2.1.2 Spherical Coordinates

Boundary conditions at interfaces of the head body element were formulated for spherical coordinates. The conditions to be satisfied are the same as for cylindrical body segments: the equality of heat fluxes passing the interface and the interface temperature. Thereby, the steady heat flux from the last node r_n of the tissue layer n to an imaginary node $r_{(n+1)''}$ with the same material properties as n, is set equal to the steady heat flux calculated from an imaginary node n'' to the first regular node r_{n+1} of the next tissue layer $n+1$. Equating heat fluxes leads to the following expression for the *forward direction* and for a given solid angle, $\varphi \sin\phi$:

$$\dot{Q}_{sph}: \quad \frac{k_n}{\frac{1}{r_n} - \frac{1}{r_{(n+1)''}}}\ \varphi\ \sin\phi\ \left(T_{r_n} - T_{r_{(n+1)''}}\right) = \frac{k_{n+1}}{\frac{1}{r_{n''}} - \frac{1}{r_{n+1}}}\ \varphi\ \sin\phi\ \left(T_{r_{n''}} - T_{r_{n+1}}\right) \tag{A.13}$$

The angle $\varphi sin\phi$ is constant for both adjacent nodes and can be eliminated from equation (A.13). The interface temperature formulated for spherical coordinates and for the

forward direction results in:

$$\frac{r_{(n+1)''}T_{r_{(n+1)''}} - r_n T_{r_n}}{r_{(n+1)''} - r_n} + \frac{T_{r_n} - T_{r_{(n+1)''}}}{\frac{r_{ifc}}{r_n} - \frac{r_{ifc}}{r_{(n+1)''}}} = T_{ifc} = \frac{r_{n+1}T_{r_{n+1}} - r_{n''}T_{r_{n''}}}{r_{n+1} - r_{n''}} + \frac{T_{r_{n''}} - T_{r_{n+1}}}{\frac{r_{ifc}}{r_{n''}} - \frac{r_{ifc}}{r_{n+1}}} \tag{A.14}$$

For the *backward direction*, ie. when the tissue node *n+1* becomes the actual tissue node *n*, and simultaneously, the tissue layer *n* becomes *n-1* the subscripts of the equations (A.13) and (A.14) are changed accordingly:

$$\dot{Q}_{sph}: \quad \frac{k_{n-1}}{\frac{1}{r_{n-1}} - \frac{1}{r_{n''}}} \left(T_{n-1} - T_{n''}\right) = \frac{k_n}{\frac{1}{r_{(n-1)''}} - \frac{1}{r_n}} \left(T_{(n-1)''} - T_n\right)$$

$$\frac{r_{n''}T_{r_{n''}} - r_{n\,1}T_{r_{n-1}}}{r_{n''} - r_{n\,1}} + \frac{T_{r_{n-1}} - T_{r_{n''}}}{\frac{r_{ifc}}{r_{n-1}} - \frac{r_{ifc}}{r_{n''}}} = T_{ifc} = \frac{r_n T_{r_n} - r_{(n-1)''}T_{r_{(n-1)''}}}{r_n - r_{(n-1)''}} + \frac{T_{r_{(n-1)''}} - T_{r_n}}{\frac{r_{ifc}}{r_{(n-1)''}} - \frac{r_{ifc}}{r_n}}$$

From equation (A.14) the temperature of the imaginary node *n"* is separated and is introduced into equation (A.13). When equation (A.13) is adequately modified the appropriate temperature of the imaginary node $r_{(n+1)''}$ of a sphere for the *forward direction* is:

$$T_{(n+1)''} = T_{r_n} \cdot A_{F,n} + T_{r_{n+1}} \cdot A_{F,n+1} \tag{A.17}$$

where

$$A_{F,n} = \frac{\Lambda_n - \Lambda_{n+1}\frac{r_n}{r_{n+1} - \Delta r_{n+1}}}{\Lambda_n + \Lambda_{n+1}\frac{r_n + \Delta r_n}{r_{n+1} - \Delta r_{n+1}}} \qquad A_{F,n+1} = \frac{\Lambda_{n+1}\left(1 + \frac{r_{n+1}}{r_{n+1} - \Delta r_{n+1}}\right)}{\Lambda_n + \Lambda_{n+1}\frac{r_n + \Delta r_n}{r_{n+1} - \Delta r_{n+1}}}$$

and

$$\Lambda_n = \frac{k_n}{\frac{1}{r_n} - \frac{1}{r_n+\Delta r_n}} \qquad \Lambda_{n+1} = \frac{k_{n+1}}{\frac{1}{r_{n+1}-\Delta r_{n+1}} - \frac{1}{r_{n+1}}}$$

As noted above the sum of the (weighting) coefficients equals to unity: $A_{F,n+1} + A_{F,n} = 1$. This property of the *'interface'* coefficients applies of course also for the *backward direction*, $A_{B,n-1}$, $A_{B,n}$. Using these interface coefficients the temperature of the imaginary node $r_{(n-1)''}$ is calculated by the following equations:

$$T_{(n-1)''} = T_{r_n} \cdot A_{B,n} + T_{r_{n-1}} \cdot A_{B,n-1} \qquad \text{(A.20)}$$

where

$$A_{B,n} = \frac{\Lambda_n - \Lambda_{n-1}\frac{r_n}{r_{n-1}+\Delta r_{n-1}}}{\Lambda_n + \Lambda_{n-1}\frac{r_n-\Delta r_n}{r_{n-1}+\Delta r_{n-1}}} \qquad A_{B,n-1} = \frac{\Lambda_{n-1}\left(1 + \frac{r_{n-1}}{r_{n-1}+\Delta r_{n-1}}\right)}{\Lambda_n + \Lambda_{n-1}\frac{r_n-\Delta r_n}{r_{n-1}+\Delta r_{n-1}}}$$

and

$$\Lambda_n = \frac{k_n}{\frac{1}{r_n-\Delta r_n} - \frac{1}{r_n}} \qquad \Lambda_{n-1} = \frac{k_{n-1}}{\frac{1}{r_{n-1}} - \frac{1}{r_{n-1}+\Delta r_{n-1}}}$$

The above formulae do not apply only to nodes adjacent to tissue interfaces but they can be used universally for any node of a body element simulated in the program. For two adjacent nodes with $k_r=k_{r+1}$ and $\Delta r_r=\Delta r_{r+1}$ (direction forward), and nodes with $k_r=k_{r-1}$ and $\Delta r_r= \Delta r_{r-1}$ (direction backward), respectively, the calculation of the *interface coefficients* yields:

$$A_{F,r} = 0 \qquad A_{F,r+1} = 1$$
$$A_{B,r} = 0 \qquad A_{B,r-1} = 1$$

A.2.2 The Isothermal Core

The boundary conditions near a cylinder axis or the midpoint of the sphere were formulated to allow for asymmetric conditions. The boundary condition at the cylinder axis, where no spatially asymmetric heat flux occurs, is given by setting the temperature gradient at the axis to zero:

$$\frac{\partial T}{\partial r} = 0 \qquad \text{for} \qquad r = 0$$

This condition, however, can not be used, when heat is transferred asymmetrically from the cylinder centre to its boundary. The temperature gradient at the axis does not equal zero. Therefore, another formulation of the boundary conditions at the cylinder axis or the midpoint of a sphere is required.

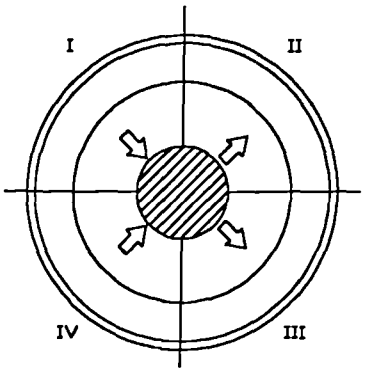

Fig.A.2

In the present model, the problem of asymmetric heat flow within a cylinder is solved by establishing an isothermal core around its axis and subdividing the cylinder into several spatial sectors (see ***Fig.A.2***) which may have different angles $\Delta\varphi_s$. Similar partitions are defined for a sphere (***Fig.A.3***). The boundary condition for the cylinder centre is then assessed by applying the following heat balance to the isothermal core: *heat which is stored within the core region is equal to the heat produced by metabolism and the heat gained by blood perfusion in the core node minus the sum of the conductive heat fluxes passing the core node surface to the individual cylinder sectors*:

$$V_1 \rho_1 c_1 \frac{dT_1}{dt} = \dot{Q}_{m_1} + \rho_{bl} c_{bl} w_{bl_1} \left(T_{bla} - T_1\right) - \sum_{s=1}^{n} \dot{Q}_{cond,1_s} \qquad \text{(A.25)}$$

The heat flux from the isothermal core into the *s*-th cylinder sector is described by:

$$\frac{\dot{Q}_{1_s}}{h} = \Delta\varphi_s \frac{k_1}{\ln\left(\frac{r_{2''}}{r_1}\right)} \left(T_{r_1} - T_{r_{2''}}\right) \qquad \text{(A.26)}$$

One obtains for the heat flux from the isothermal core into the *s*-th sector of a sphere (see ***Fig.A.3***):

$$\dot{Q}_{1_s} = \Delta\varphi_s \cdot 2 \frac{k_1}{\frac{1}{r_1} - \frac{1}{r_{2''}}} \left(T_{r_1} - T_{r_{2''}}\right) \quad \text{(A.27)}$$

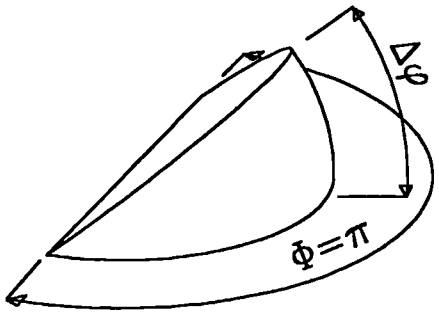

Fig.A.3

The introduction of the above boundary conditions into the numerical form of the *bioheat equation* for the isothermal core region of a cylinder results in:

$$T_1^{t+1}\left\{\frac{\zeta_1}{\Delta t} + \frac{2}{r_{ifc,1}^2} + \delta_1 \frac{\beta_1^{(t+1)}}{V_1}\right\} + \sum_{s=1}^{sides} T_{2,s}^{t+1} \cdot \left\{-\Delta\varphi_s \cdot \frac{2}{r_{ifc,1}^2 \sum_s \Delta\varphi_s}\right\} - \delta_1 \frac{\beta_1^{t+1}}{V_1} T_{bla}^{t+1}$$

and the right-hand side of the *bioheat equation*:

$$T_1^{t}\left\{\frac{\zeta_1}{\Delta t} - \frac{2}{r_{ifc,1}^2} - \delta_1 \frac{\beta_1^{(t+1)}}{V_1}\right\} + \sum_{s=1}^{sides} T_{2,s}^{t} \cdot \left\{\Delta\varphi_s \cdot \frac{2}{r_{ifc,1}^2 \sum_s \Delta\varphi_s}\right\} + \delta_1 \frac{\beta_1^{t}}{V_1} T_{bla}^{t} + q_{m_1}^{t} + q_{m_1}^{t+1}$$

The numerical formulation of the *bioheat equation* for the isothermal core in spherical coordinates is obtained by the following expression for the left hand side:

$$T_1^{t+1}\left\{\frac{\zeta_1}{\Delta t} + \frac{3}{r_{ifc,1}^3} + \delta_1 \frac{\beta_1^{(t+1)}}{V_1}\right\} + \sum_{s=1}^{sides} T_{2,s}^{t+1} \cdot \left\{-\Delta\varphi_s \cdot \frac{3}{r_{ifc,1}^3 \sum_s \Delta\varphi_s}\right\} - \delta_1 \frac{\beta_1^{t+1}}{V_1} T_{bla}^{t+1}$$

and for the right hand side:

$$T_1^{t}\left\{\frac{\zeta_1}{\Delta t} - \frac{3}{r_{ifc,1}^3} - \delta_1 \frac{\beta_1^{(t+1)}}{V_1}\right\} + \sum_{s=1}^{sides} T_{2,s}^{t} \cdot \left\{\Delta\varphi_s \cdot \frac{3}{r_{ifc,1}^3 \sum_s \Delta\varphi_s}\right\} + \delta_1 \frac{\beta_1^{t}}{V_1} T_{bla}^{t} + q_{m_1}^{t} + q_{m_1}^{t+1}$$

A.2.3 Skin Surface

The heat exchange between a body element sector and the environment is involved in the formulation of boundary conditions at the body's periphery. The heat exchange between the skin surface and the surroundings occurs by convection (*subscript* $_C$), radiation (subscript $_R$), and evaporation (subscript $_E$). The radiative heat exchange can further be subdivided into long-wave radiation (subscript $_R$) occurring between the skin and the surrounding *warm or cold wall surfaces*, and short-wave radiation (subscript $_{sR}$) occurring by diffuse and direct solar irradiation. The evaporative heat loss includes the heat loss by evaporation of sweat moisture and/or the vaporisation of water passing the skin by diffusion.

The first boundary condition at the skin surface is given by equating the heat flux by conduction passing the outer cutaneous layer and the sum of heat *fluxes from the skin* surface to the environment. The heat flux [W] per length unit *h* [m] in a cylinder sector with an angle $\Delta\varphi$ is then calculated as:

$$\frac{\dot{Q}}{h} : \Delta\varphi \frac{k_n}{\ln\left(\frac{r_{sk}}{r_n}\right)} \left(T_{r_n} - T_{sk} \right) = \Delta\varphi \, r_{sk} \left(q_C + q_R - q_{sR} + q_E \right) \tag{A.32}$$

where the subscript $_n$ denotes the last node of the cylinder, the subscript $_{sk}$ denotes the skin surface, whereas $r_{sk} = r_n + \Delta r_n/2$, and the *q*-terms denote the individual heat flux densities in [W m^{-2}]. The angle $\Delta\varphi$ can be eliminated from eq. (A.32).

The second boundary condition arises from the necessity of establishing an additional, imaginary node placed outside the skin surface symmetrically to the last cylinder node. The temperature of this imaginary node satisfies the second boundary condition, ie. the surface temperature of the skin. For cylindrical elements the skin temperature yields:

$$T_{sk} = \frac{T_{r_n} \ln\left(\frac{r_{sk}}{r_{(n+1)''}}\right) - T_{r_{(n+1)''}} \ln\left(\frac{r_{sk}}{r_n}\right)}{\ln\left(\frac{r_n}{r_{(n+1)''}}\right)} \qquad \text{(A.33)}$$

The two boundary conditions at the surface of a spherical element are:

$$\dot{Q}_{sk} = \frac{k_n}{\frac{1}{r_n} - \frac{1}{r_{sk}}} \varphi \sin\phi \left(T_{r_n} - T_{sk}\right) = r_{sk}^2 \varphi \sin\phi \left(q_C + q_R - q_{sR} + q_E \right)$$

and

$$T_{sk} = \frac{r_{(n+1)''} T_{r_{(n+1)''}} - r_n T_{r_n}}{r_{(n+1)''} - r_n} + \frac{T_{r_n} - T_{r_{(n+1)''}}}{\frac{r_{sk}}{r_n} - \frac{r_{sk}}{r_{(n+1)''}}} \qquad \text{(A.35)}$$

The temperature of the imaginary node is obtained by introducing eq. (A.33) into eq. (A.32) and rearranging:

$$T_{r_{(n+1)''}} = A_{F,n} T_{r_n} + Env \qquad \text{(A.36)}$$

where $r_{(n+1)''}$ in eq. (A.32) is substituted by $r_n + \Delta r_n$ to yield

$$A_{F,n} = \frac{\ln\left(\frac{r_n + \Delta r_n}{r_n}\right)}{\ln\left(\frac{r_{sk}}{r_n}\right)} \cdot \frac{\Lambda_{sk}/r_{sk}}{\Lambda_{sk}/r_{sk} + h_C + h_R} + \frac{\ln\left(\frac{r_{sk}}{r_n + \Delta r_n}\right)}{\ln\left(\frac{r_{sk}}{r_n}\right)} \quad \text{with} \quad \Lambda_{sk} = \frac{k_n}{\ln\left(\frac{r_{sk}}{r_n}\right)}$$

(A.37)

and

$$Env = \frac{\ln\left(\frac{r_n+\Delta r_n}{r_n}\right)}{\ln\left(\frac{r_{sk}}{r_n}\right)} \cdot \frac{h_C T_a + h_R T_R + q_E - q_{sR}}{\Lambda_{sk}/r_{sk} + h_C + h_R} \qquad (A.38)$$

For spherical coordinates coefficients $A_{F,n}$ and *Env* are calculated by:

$$A_{F,n} = \frac{2\, r_{sk}}{r_n+\Delta r_n} \cdot \frac{\Lambda_{sk}/r_{sk}^2}{\Lambda_{sk}/r_{sk}^2 + h_C + h_R} - \frac{r_n}{r_n+\Delta r_n} \qquad \text{where} \quad \Lambda_{sk} = \frac{k_n}{\frac{1}{r_n} - \frac{1}{r_{sk}}}$$

and

$$Env = \frac{2\, r_{sk}}{r_n+\Delta r_n} \cdot \frac{h_C T_a + h_R T_R + q_E - q_{sR}}{\Lambda_{sk}/r_{sk}^2 + h_C + h_R}$$

For use in the program further modifications were performed: the surface coefficient $A_{F,n}$ was separated into a time-dependent term and a time-*in*dependend term according to:

$$A_{F,n} = HTC(t) + A_n$$

where *HTC* represents a kind of combined heat transfer coefficient which depends on time as h_C and h_R vary temporarily with surrounding and body surface temperatures. The coefficient A_n stands for the time independent part of $A_{F,n}$. For cylinders, these two coefficients turn out to be:

$$HTC = \frac{\ln\left(\frac{r_n+\Delta r_n}{r_n}\right)}{\ln\left(\frac{r_{sk}}{r_n}\right)} \cdot \frac{\Lambda_{sk}/r_{sk}}{\Lambda_{sk}/r_{sk} + h_C + h_R} \qquad A_n = \frac{\ln\left(\frac{r_{sk}}{r_n+\Delta r_n}\right)}{\ln\left(\frac{r_{sk}}{r_n}\right)}$$

and for a sphere:

$$HTC = \frac{2\,r_{sk}}{r_n+\Delta r_n} \cdot \frac{\Lambda_{sk}/r_{sk}^2}{\Lambda_{sk}/r_{sk}^2 + h_C + h_R} \qquad A_n = \frac{r_n}{r_n+\Delta r_n}$$

A.3 Procedure to Solve the Common Matrix

As apparent from ***Fig.3.5*** it is not necessary to store all the coefficients of the common matrix because most of them are equal to zero. The coefficients not equal to zero constitute only about 10% of the total number.

The individual sub-matrices of the common matrix, ***Fig.3.5***, can be solved almost independently from each other. Only the *coupling coefficient*, eq. (3.52), represents a mathematical (and physical) connection between the individual body elements and link these sub-matrices. The sub-matrices have to be rearranged to obtain a triangular form according to the *Gaussian scheme*. Starting with the top sub-matrix the coefficients for the corresponding parts of the *blood pool temperature line* and *blood pool temperature column* (first $j_{(i)}$ coefficients), as well as the coupling coefficient *CplC* (taken from the bottom of the common matrix) have to be 'attached' to the first sub-matrix (***Fig.A.4***).

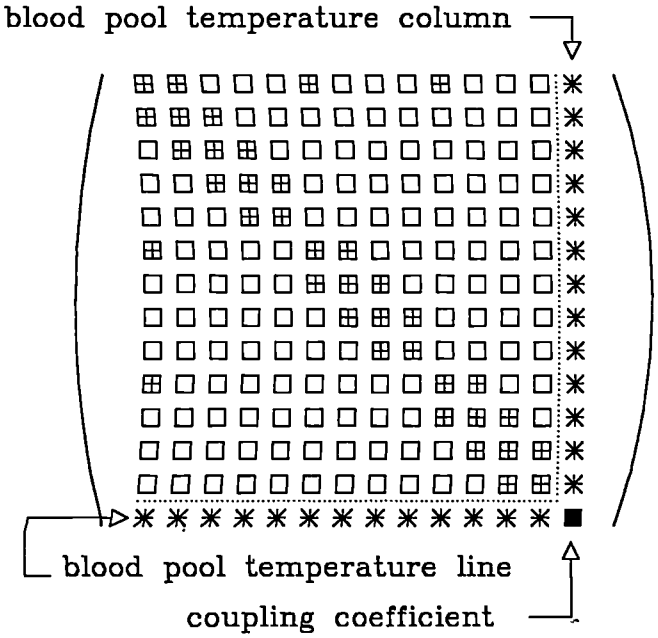

Fig.A.4

During the process of rearranging the first sub-matrix into a triangular form also the value of *CplC* will be changed. This coefficient has then to be transferred to the second sub-matrix to be rearranged, and so on. In ***Fig.A.5*** the situation is shown before transferring *CplC*:

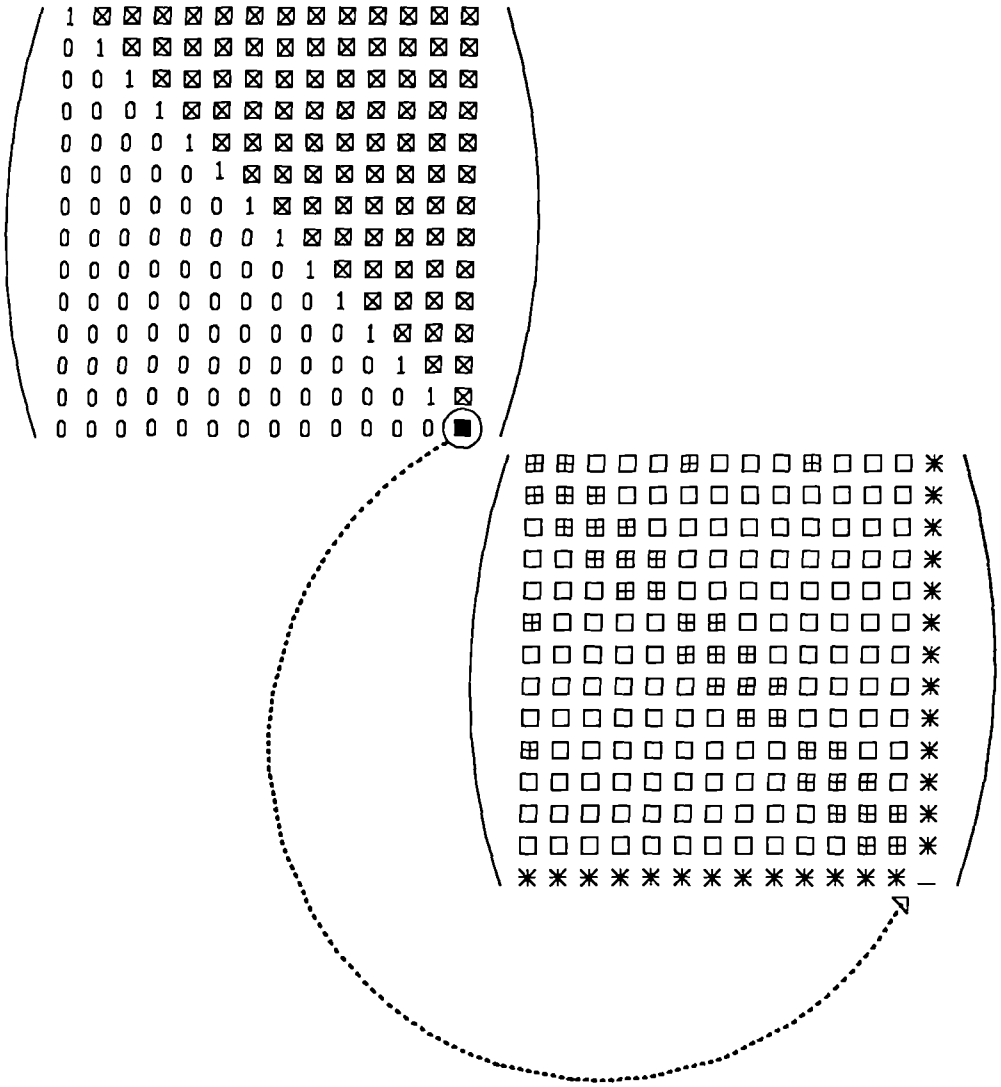

Fig.A.5

This solution procedure was found to be several times quicker than when the classical *Gaussian algorithm* was used to solve the common final matrix.

A.4 Analytical and Numerical Solutions of Heat Transfer in Cylinders and Spheres

A.4.1 Steady State Heat Conduction in Cylinders

In this test, the accuracy of temperature predicted for a thorax-cylinder of uniform material properties (k=0.3 $W K^{-1} m^{-1}$) and subject to steady conductive heat transfer was examined. The results were compared with temperatures calculated analytically [73] for various distances from the cylinder's centre. In order to simulate the pure heat conduction, the heat transfer by blood circulation and the heat generation by metabolism were switched off in the model. The temperature of the isothermal core was set to 40°C to induce a temperature gradient in the cylinder. The dry heat exchange (skin evaporation was switched off) with an environment of T_a=25°C represented the boundary condition at the cylinder surface. The results are compared in the following table:

r [m]	T_{exact} *[°C]*	$T_{num.}$ *[°C]*	*rel. error [%]*
0,06365	37,3130	37,3130	0,000
0,08320	36,0080	36,0087	0,002
0,09508	35,3580	35,3586	0,002
0,10703	34,7811	34,7816	0,001
0,11523	34,4211	34,4214	0,001
0,11970	34,2358	34,2360	0,001
0,12417	34,0573	34,0574	0,000
0,12705	33,9455	33,9455	0,000
0,12820	33,9016	33,9016	0,000

The numerical results agree with the analytical solution to within 0,0007°C. Whilst the numerical and analytical solutions for heat conduction in rectangular and spherical

coordinates are identical - in cylindrical coordinates the formulae are not identical. One obatains for the numerical solution:

$$T_r = T_2\left(\frac{r+r_2}{4\,r}\right) + T_1\left(\frac{r+r_1}{4\,r}\right)$$

whereas the analytical solution yields:

$$T_r = T_2\left(\frac{\ln\frac{r}{r_1}}{\ln\frac{r_2}{r_1}}\right) + T_1\left(\frac{\ln\frac{r}{r_2}}{\ln\frac{r_2}{r_1}}\right)$$

Although the above equations become equal first for $r_2 - r_1 \rightarrow 0$ the predicted error in the temperature appears to be negligible for the nodal spacing used in the present model. Calculations of the heat fluxes through interfaces and the interface temperatures confirmed the validity of the formulation of boundary conditions at interfaces between tissue layers.

A.4.2 Steady Heat Conduction in Cylinders with Heat Generation

The differential equation for steady conduction when overlaid by uniform heat generation W (in [W m^{-3}]) within a cylinder is described by:

$$\frac{\partial^2 T}{\partial r^2} + \frac{1}{r}\frac{\partial T}{\partial r} + \frac{W}{k} = 0$$

According to [73] the analytical solution of this differential equation for the temperature profile in the cylinder provides:

$$T = T_a + \frac{W \cdot R^2}{4 \cdot k} \left(1 + \frac{2 \cdot k}{h_c \cdot R} - \left(\frac{r}{R} \right)^2 \right)$$

The test was performed for the thorax body element with k = 0.3 W m^{-1}K^{-1}; W = 190 W m^{-3}; h_c = 1.2793 W m^{-2}K^{-1}; and T_a=25°C.

A comparison of the calculated and predicted temperatures at various distances ***r*** from the centre are given in the following table:

r [m]	T_{exact} [°C]	$T_{num.}$ [°C]	*rel. error* [%]
0,06365	36,538	36,604	0,18
0,08320	36,084	36,097	0,04
0,09508	35,749	35,762	0,04
0,10703	35,366	35,379	0,04
0,11523	35,077	34,080	0,01
0,11970	34,911	34,914	0,01
0,12417	34,739	34,741	0,01
0,12705	34,624	34,625	0,00
0,12820	34,578	33,579	0,00

The error of the predictions is greater than in the case of conduction only. Nevertheless, there is good agreement with the exact results. The maximum absolute error for the nodal configuration of the thorax body element used in the passive system model was 0.07°C whereas the mean absolute error was 0.01°C.

A.4.3 Steady State Solution of the Bioheat Equation for a Sphere

An analytical ,steady state solution of the *bioheat equation* for spherical coordinates was found in the literature [69]. This solution was used to check the validity of the numerical formulation of the *bioheat equation* as applied to the head element in the model. The quoted solution is:

$$T = T_{bla} - \frac{\frac{h_c R^2}{k \cdot r} \times \left(\vartheta_a + \vartheta_{bl} + \frac{q_m}{\rho_{bl} c_{bl} w_{bl}} \right) \times \sinh\left(r \sqrt{\frac{\rho_{bl} c_{bl}}{k} w_{bl}} \right)}{R \sqrt{\frac{\rho_{bl} c_{bl}}{k} w_{bl}} \times \cosh\left(R \sqrt{\frac{\rho_{bl} c_{bl}}{k} w_{bl}} \right) + \left(\frac{h_c R}{k} - 1 \right) \times \sinh\left(R \sqrt{\frac{\rho_{bl} c_{bl}}{k} w_{bl}} \right)} + \frac{q_m}{\rho_{bl} c_{bl} w_{bl}}$$

where T [°C] is the tissue temperature at the radius r [m], T_{bla} [°C] is the arterial blood temperature, T_a [°C] is the temperature of ambient air, and R is the outer radius of 10.45cm. The surface convective heat transfer coefficient was set to be $h_c = 3.0 W m^{-2} K^{-1}$, the conductive heat transfer coefficient of the tissue was set at $k = 0.5\ W m^{-1} K^{-1}$ corresponds to that of the brain. The density and the heat capacitance of blood were set as: $\rho_{bl} = 1050\ kg m^{-3}$ and $c_{bl} = 3600\ J kg^{-1} K^{-1}$. The parameters q_m [W m^{-3}] and w_{bl} [m$^3_{bl}$ s^{-1}m^{-3}] stand for the metabolic- and blood perfusion rate, respectively. In ***Fig.A.6*** the temperature profile of the sphere is plotted for the following conditions: T_a = 10°C; T_{bla} = 37°C; q_m = 10000 W m^{-3}; and w_{bl} = 0.01 m^{3}s^{-1}m^{-3}.

From ***Fig.A.6*** it can be seen that the deviation between the numerical and the analytical solution vanishes for the head core and the maximum error occurs at the head surface. For the given values of q_m and w_{bl} the maximum error ΔT was, however, lower than 0.1K.

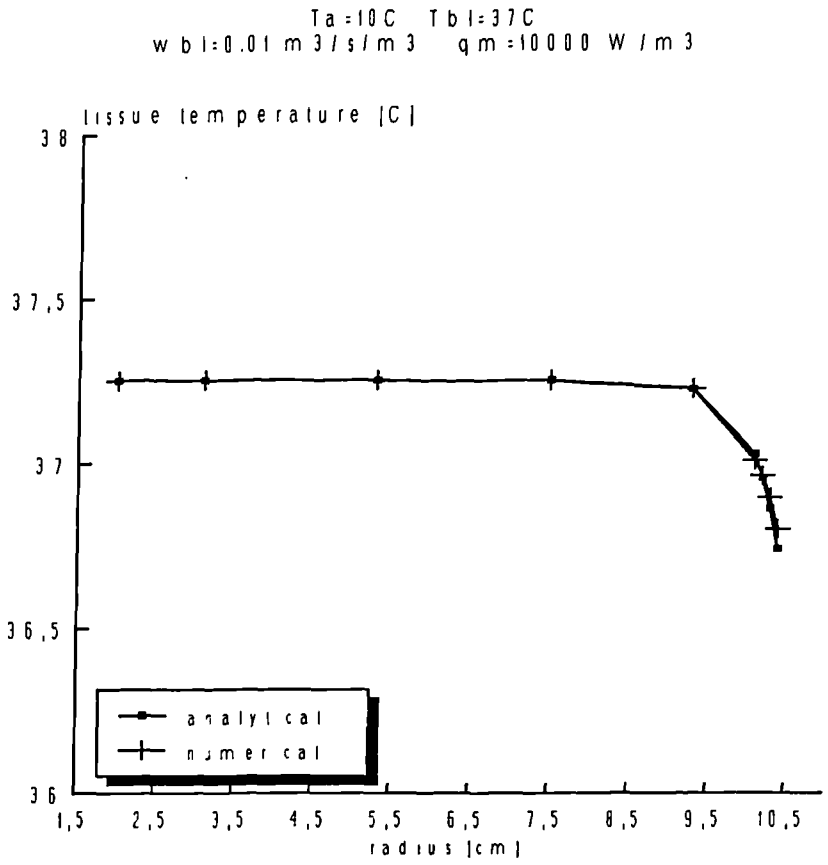

Fig.A.6

A.4.4 Transient Conduction in Cylinders

The analytical solution for transient conduction within a cylinder is provided by [73] as:

$$T = T_{t=0} \times \sum_{i=1}^{i=\infty} \frac{2}{\psi_i} \cdot \frac{J_1(\psi_i)}{J_0^2(\psi_i) + J_1^2(\psi_i)} e^{-\psi_i^2 \frac{a}{R^2} t} \times J_0\left(\psi_i \frac{r}{R}\right)$$

where $a = k/(\rho c)$ [m s^{-2}K^{-1}] is the thermal perfusivity, r [m] is the actual radius, and R [m] stands for the outer radius of the cylinder. J_0 and J_1 represent *Bessel functions* of the first kind for the zero order and the first order, respectively. The variable ψ is determined for each i and is calculated iteratively from the following transcendent relationship:

$$\psi \, J_1(\psi) \;=\; \frac{h_c}{k} \, R \, J_0(\psi)$$

In the test the initial temperature of the cylinder was assumed to be homogeneous and was set at $T_{t=0}$= 37°C. When an ambient temperature of T_a = 0°C is used the boundary condition at the cylinder surface results in:

$$- k \left. \frac{\partial \vartheta}{\partial r} \right|_{r=R} = h_c \, \vartheta_{r=R}$$

The thermophysical material properties of the cylinder were chosen to correspond roughly to the average values of the human body: $k=0.3\ W m^{-1}K^{-1}$, $\rho=1000\ kg\ m^{-3}$, $c=3000\ J kg^{-1}K^{-1}$. The convective heat transfer coefficient was set to be $h_c=4.0\ W m^{-2}K^{-1}$. The temporal variations of tissue temperature at three different locations are shown in *Fig.A.7*. The nodes were located as follows: one in the cylinder core, one in the middle between the isothermal core and the cylinder surface, and one at the surface. In the first example, temperatures were calculated for time steps of Δt=60s.

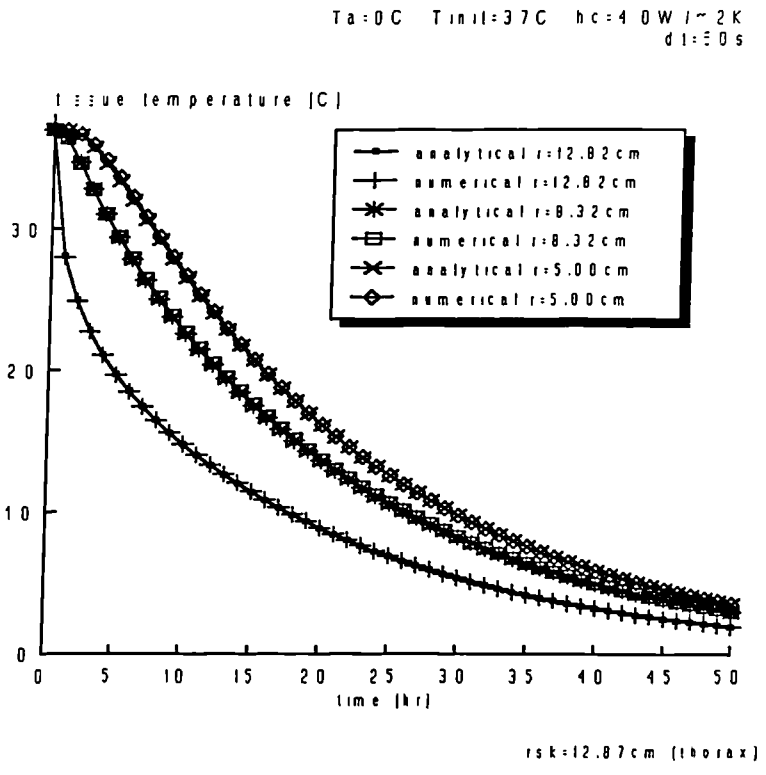

Fig.A.7

Good agreement with the analytical solution was achieved for this size of time step for each node. The maximum temperature error was found to be smaller than ΔT<0.3K. The mean error was in the range of about 0.05K. Predicted cylinder temperatures after 50 hours of exposure deviated from exact values by less than 0.01K. The impact of the time step size on the temperature predictions is demonstrated in ***Fig.A.8*** (Δt=20min) and ***Fig.A.9*** (Δt=60min).

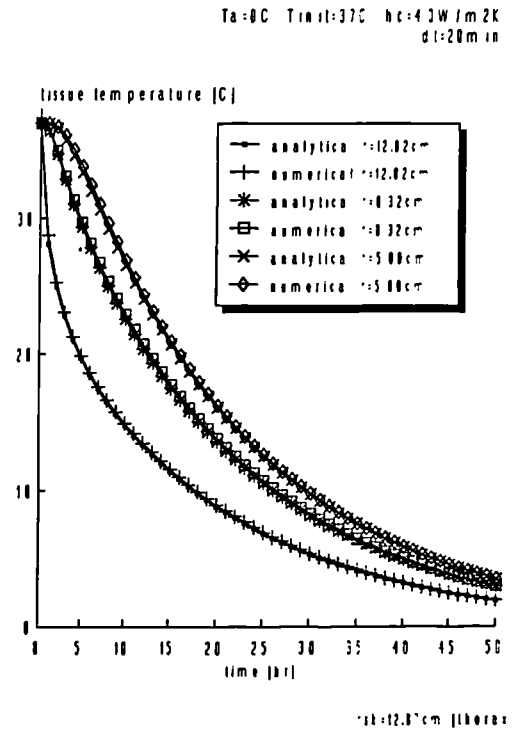

Fig.A.8

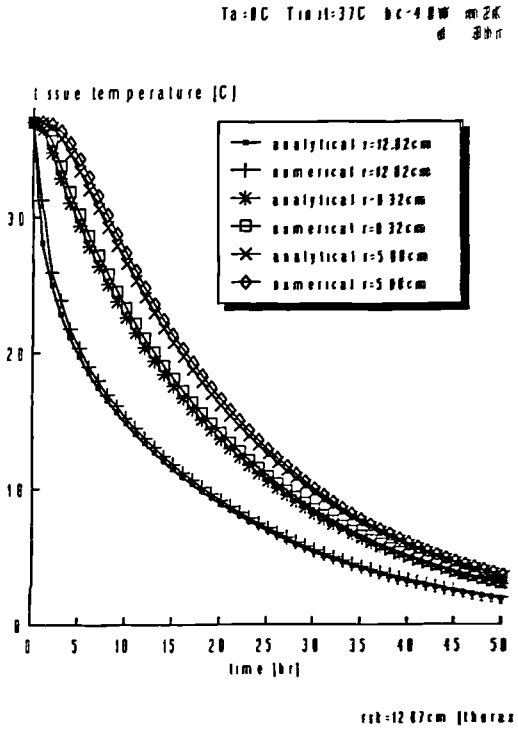

Fig.A.9

Fig.A.9 indicates that even time steps of the order of 1 hr provide reasonable results for this case of conditions. For both values of Δt the largest errors were found at the cylinder surface during the first time step. In the cylinder core, the largest errors occurred between 5h<t<7h. The maximum error was about 0.7K for Δt=20min and 3K for Δt=1hr. While for Δt=20min the mean error was about 0.2K, about 0.5K characterised the mean error of the Δt = 1hr simulation. After 50 hours exposure the errors were smaller than 0.05K and 0.1K for Δt=20min and Δt=1hr, respectively.

In ***Fig.A.10*** the simulation results are plotted as temperature profiles over the cylinder radius for both t=30min and t=1hr of exposure and a time step of Δt = 5min.

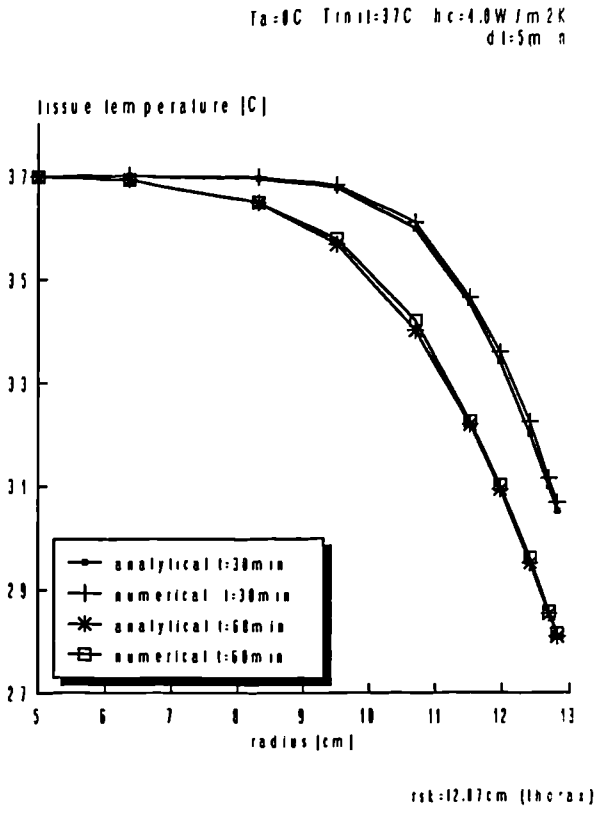

Fig.A.10

In order to investigate the transient behaviour of the model in the case of rapid cooling, the convective heat transfer coefficient was increased to a value of h_c=20 $W m^{-2}K^{-1}$. For this boundary condition the cylinder surface temperature dropped by more than 25K from its initial value within the first hour of exposure. A comparison between analytically calculated temperatures and temperatures predicted by the model, for a time step of Δt=60s, is shown in ***Fig.A.11***.

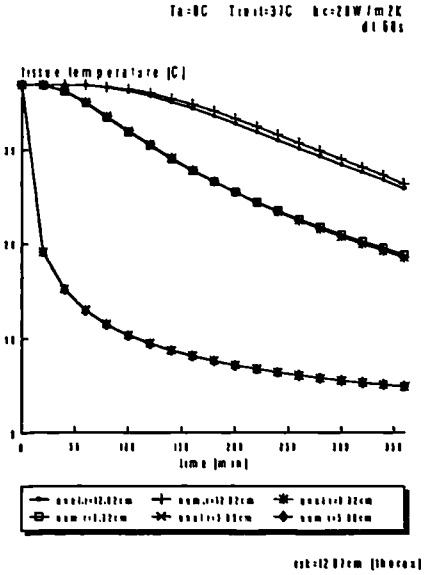

Fig.A.11

A.4.5 Analytical Solution for Transient Conduction In Spheres

The analytical solution for transient conduction within a sphere is provided by [73] as:

$$T = T_{t=0} \times \sum_{i=1}^{i=\infty} 2\frac{\sin\psi_i - \psi_i \cos\psi_i}{\psi_i - \sin\psi_i \cos\psi_i} e^{-\psi_i^2 \frac{a}{R^2} t} \times \frac{\sin\left(\psi_i \frac{r}{R}\right)}{\psi_i \frac{r}{R}}$$

where $a = k/(\rho c)$ [m s^{-2}K^{-1}] is the thermal perfusivity, r [m] is the actual radius, and R [m] stands for the outer radius of the sphere. The variable ψ has to be determined for each i and is calculated iteratively from the following transcendent relationship:

$$\psi \cos\psi = \left(1 - \frac{h_c}{k} R\right) \sin\psi$$

In the test, the initial temperature of the sphere was assumed to be homogeneous and was set to be $T_{t=0}$= 37°C. When an ambient temperature of T_a = 0°C is used the following expression for the boundary condition at the sphere surface is obtained:

$$-k \left.\frac{\partial \vartheta}{\partial r}\right|_{r=R} = h_c \vartheta_{r=R}$$

A.4.6 Transient Analytical Solution of the Bioheat Equation

An exact solution for transient heat transfer in cylinders according to the *bioheat equation* was found in [43]. The solution describes the tissue temperature at any location for sudden changes in q_m and w_{bl}:

$$\frac{V}{V_0} = 1 - \frac{Bi \cdot I_0(R\sqrt{\beta})}{\sqrt{\beta} \cdot I_1(R\sqrt{\beta}) + Bi \cdot I_0(\sqrt{\beta})} - 2\beta Bi \sum_{n=1}^{\infty} \frac{J_0(u_n R) \cdot e^{-\alpha r_0^{-2}(u_n^2+\beta)\cdot t}}{(u_n^2+\beta)\cdot(u_n^2+Bi^2)\cdot J_0(u_n)} \tag{A.59}$$

where V and V_0 arise from a dimensionless formulation of the *bioheat equation* repre-

senting differences between the actual temperature T at the location r and the corresponding initial value T_i, and the difference between the modified blood temperature T_0 and T_i:

$$V = T - T_i \qquad V_0 = T_0 - T_i$$

The modified blood temperature T_0 is prescribed by:

$$T_0 = T_{bl} + \frac{q_m}{\rho_{bl} c_{bl} w_{bl}}$$

J_1 and J_0 represent *Bessel functions* of the first kind for the zero-th and the first order, respectively. I_0 and I_1 are the *modified Bessel function* of the first kind for the zero-th and first order, respectively. A general relationship between the *modified n-th order Bessel function* I_n of the first kind and the corresponding *Bessel function* is given by:

$$I_n(x) = i^{-n} \cdot J_n(ix)$$

where $i^2 = -1$. The remaining parameters in equation (A.63) are obtained from the following relationships: $R = r/r_0$ whereby r_0 [m] is the outer radius of the cylinder, $Bi = h_c r_0 / k$ [ ], $\alpha = k/(\rho c)$ [$m^2 s^{-1}$], and $\beta = r_0^2 \rho_{bl} c_{bl} w_{bl} / k$ [ ]. Finally, the variable u_n is calculated for each n using the following transcendent relationship:

$$u_n \cdot J_1(u_n) - Bi \cdot J_0(u_n) = 0$$

B Active System

B.1 Distribution Coefficients for Regulatory Responses

Distribution Coefficients					
	a_{sk}	a_{sw}	a_{dl}	a_{cs}	a_{sh}
	[]	[]	[]	[]	[]
head	0.0835	0.0950	0.0550	0.0300	0.0000
face	0.0418	0.0540	0.0460	0.0330	0.0020
neck	0.0417	0.0420	0.0310	0.0250	0.0020
shoulders	0.0300	0.0370	0.0200	0.0100	0.0002
thorax	0.1290	0.1010	0.1410	0.0005	0.6305
abdomen	0.1210	0.1810	0.1610	0.0205	0.2400
arms	0.1800	0.1330	0.0950	0.1945	0.0400
hands	0.0900	0.0490	0.1210	0.1100	0.0020
legs	0.2080	0.2610	0.2300	0.2000	0.0813
feet	0.0750	0.0470	0.1000	0.3765	0.0020
sum	1.0000	1.0000	1.0000	1.0000	1.0000

Tab.B.1

Skin sensitivity coefficients a_{sk} [138] [35] and coefficients a_{sw} [177], a_{dl} [177], a_{cs}, and a_{sh} distributing the overall regulatory responses of sweating, cutaneous vasodilatation, cutaneous vasoconstriction, and shivering, respectively.

B.2 Curves of Simple and Multiple Regressions Using $\Delta T_{sk,m}$ and ΔT_{hy}

B.2.1 Shivering

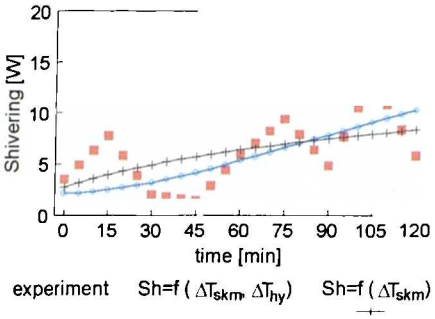

Fig.B.1 Steady T_a of 20°C [188]

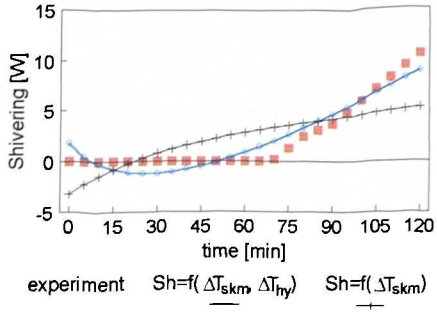

Fig.B.2 Steady T_a of 20°C [187]

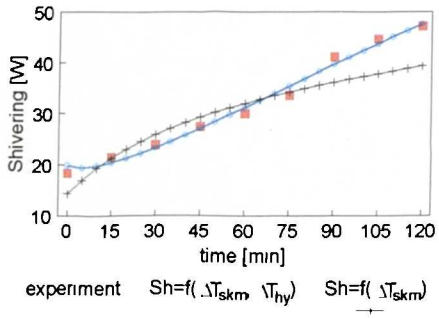

Fig.B.3 Steady T_a of 15°C [188]

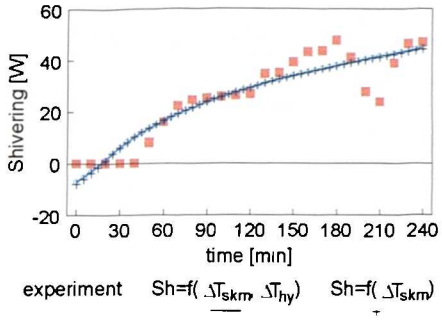

Fig.B.4 Steady T_a of 13°C [75]

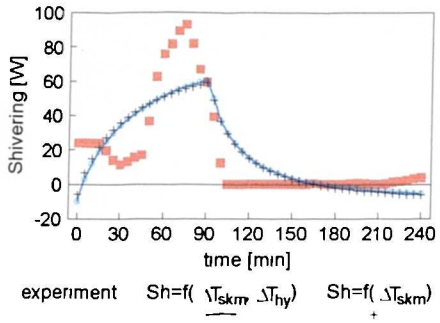

Fig.B.5 Step chng. in T_a=12-28°C [196]

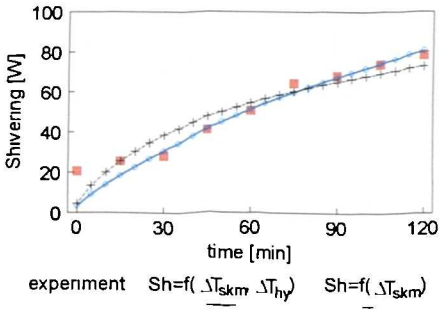

Fig.B.6 Steady T_a of 10°C [188]

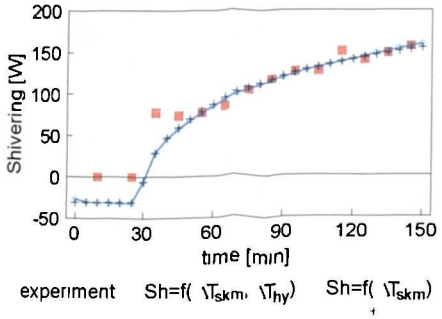

Fig.B.7 Step change into T_a=5°C [156]

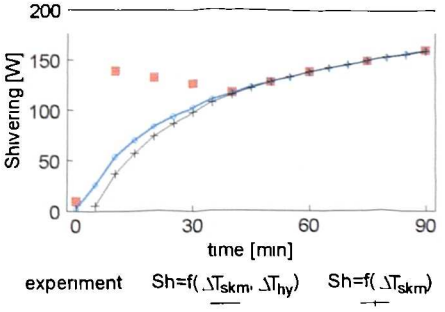

Fig.B.8 Step change into T_a=5°C [209]

B.2.2 Vasoconstriction

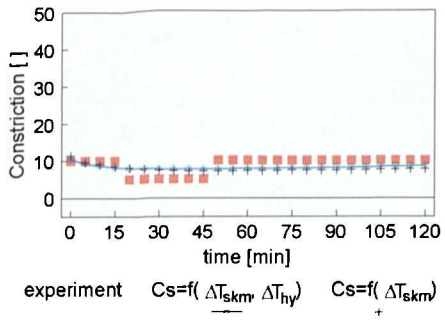

Fig.B.9 Steady T_a of 28°C [188]

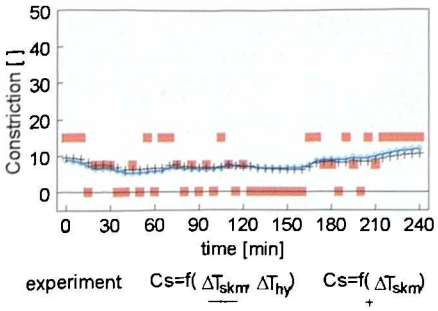

Fig.B.10 Steady T_a of 28°C [175]

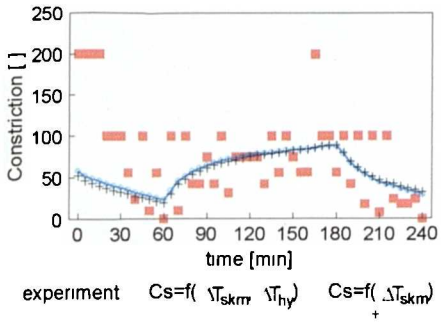

Fig.B.11 Step ch. in T_a: 29-22-29°C [75]

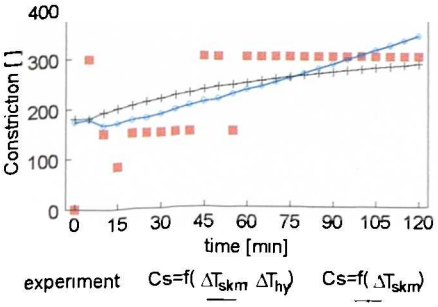

Fig.B.12 Steady T_a of 20°C [188]

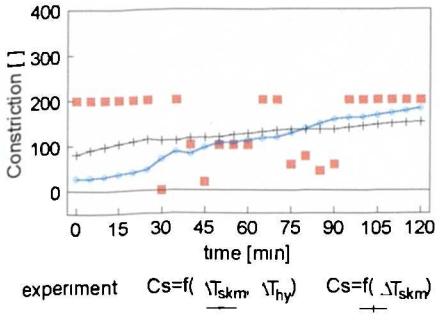

Fig.B.13 Steady T_a of 20°C [187]

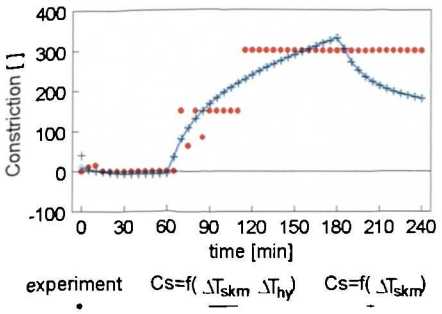

Fig.B.14 Step ch. in T_a: 28-18-28°C [75]

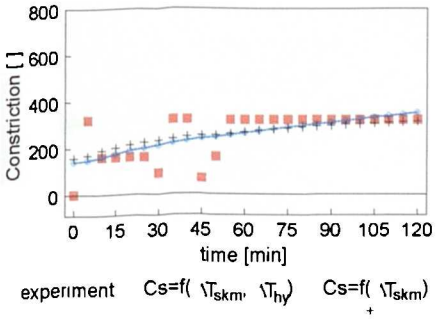

Fig.B.15 Steady T_a of 17.7°C [75]

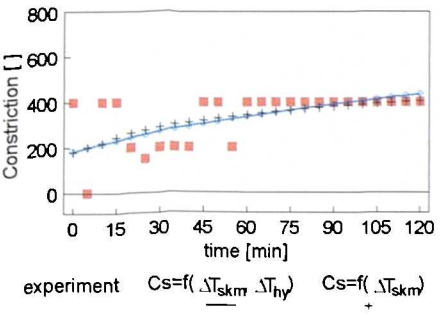

Fig.B.16 Steady T_a of 15°C [188]

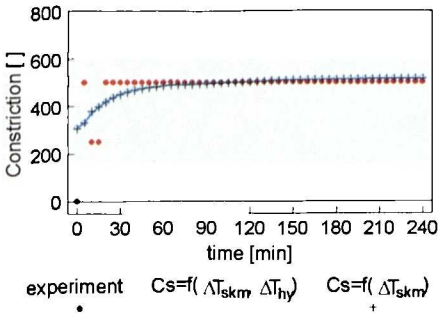

Fig.B.17 Steady T_a of 13°C [75]

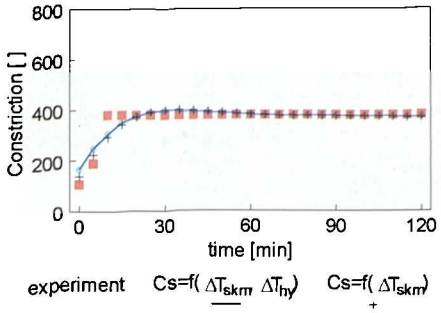

Fig.B.18 Steady T_a of 10°C [188]

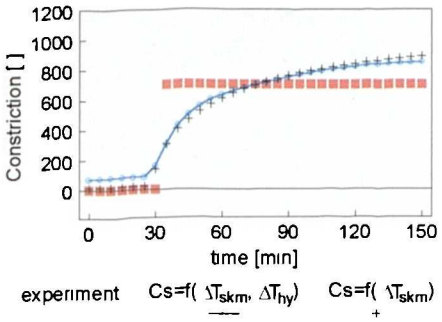

Fig.B.19 Step change into T_a=5°C [156]

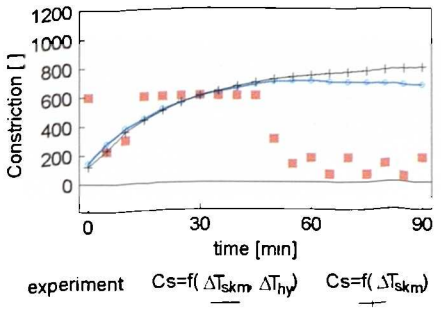

Fig.B.20 Step change into T_a=5°C [209]

B.2.3 Sweating

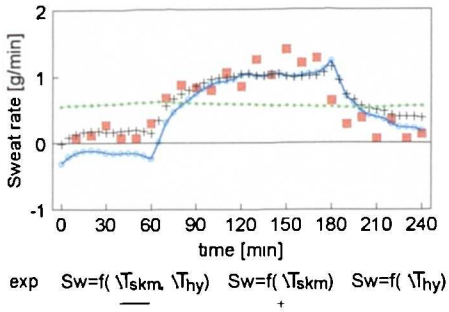

Fig.B.21 Step ch. in T_a:28-33-28°C [175]

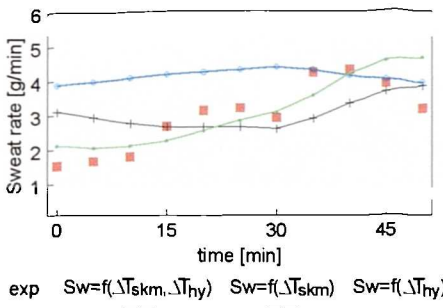

Fig.B.22 Trans. ch. in rh at T_a=36°C [59]

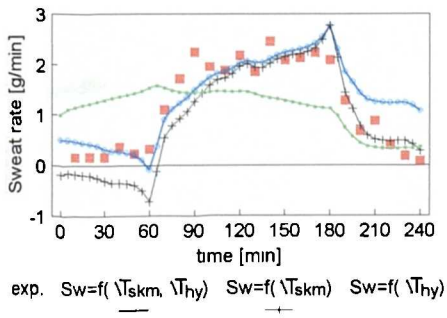

Fig.B.23 Step ch. in T_a:29-37-29°C [175]

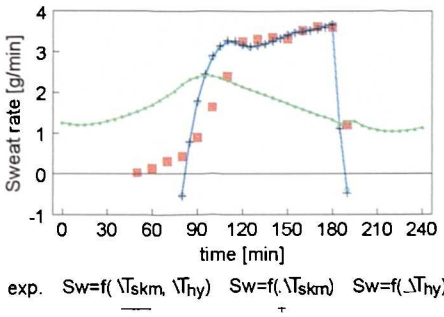

Fig.B.24 Step ch. in T_a: 18-42-18°C [75]

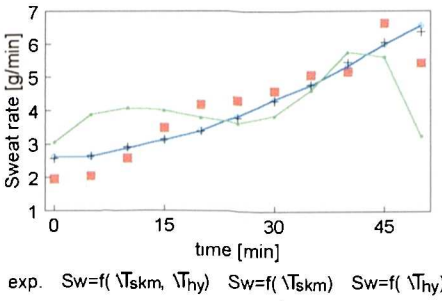

Fig.B.25 T_a- ramp: 29-44°C [59]

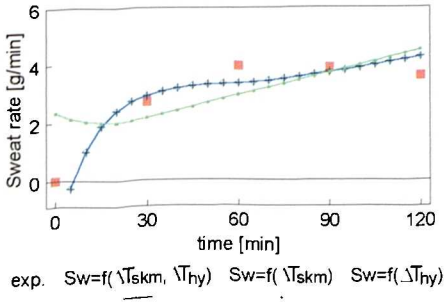

Fig.B.26 Step ch. into T_a=43°C [106]

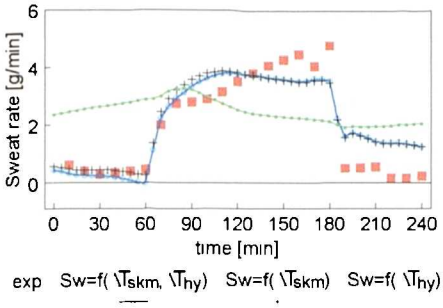

Fig.B.27 Step ch. in T_a:28-43-28 C [175]

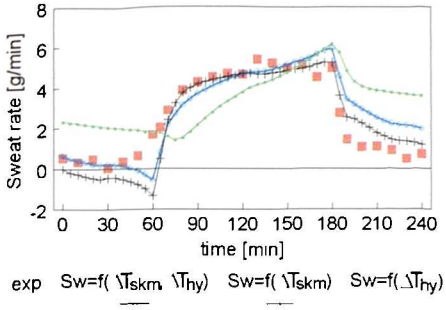

Fig.B.28 Step ch. in T_a:28-48-28°C [175]

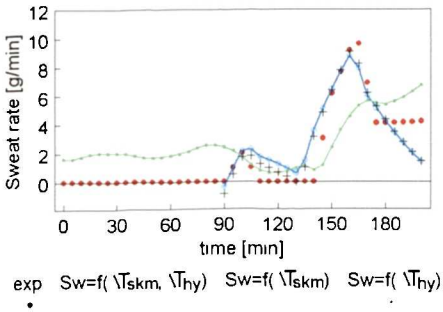

Fig.B.29 Work & rest at T_a=10°C [165]

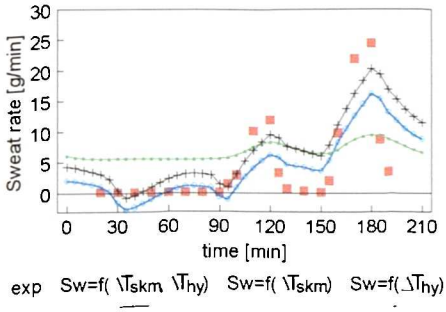

Fig.B.30 Trans. work at T_a=20°C [177]

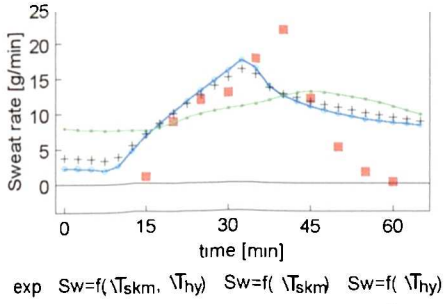

Fig.B.31 Work & rest at T_a=20°C [165]

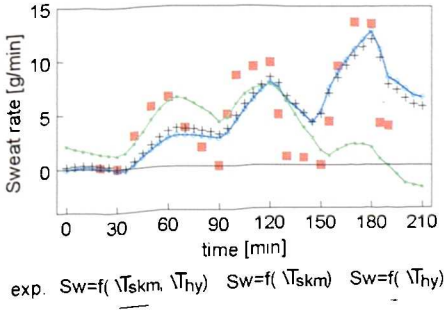

Fig.B.32 Trans. work at T_a=30°C [177]

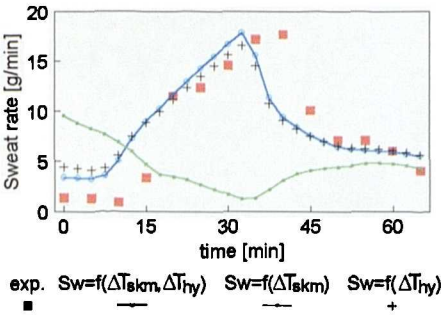

Fig.B.33 Work & rest at T_a=30°C [165]

B.2.4 Vasodilatation

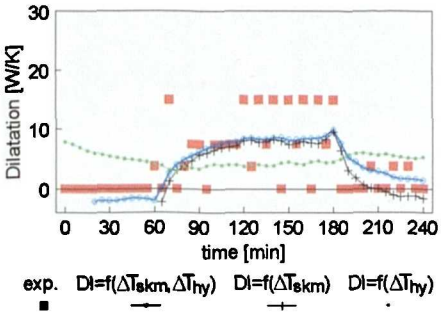

Fig.B.34 Step ch. in T_a:28-33-28°C [175]

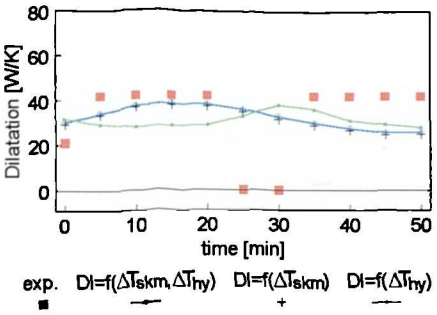

Fig.B.35 Trans. ch. in rh at T_a=36°C [59]

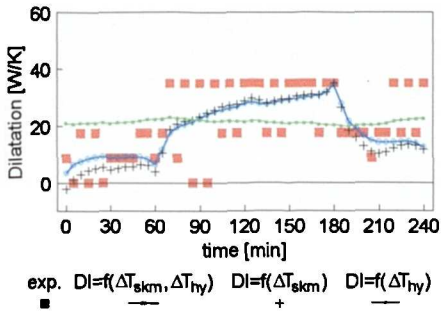

Fig.B.36 Step ch. in T_a:29-37-29°C [175]

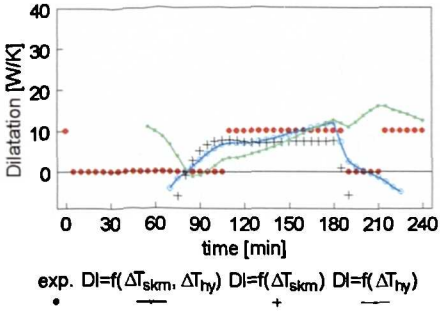

Fig.B.37 Step ch. in T_a: 18-42-18°C [75]

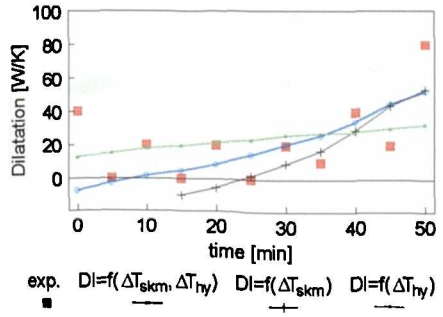

Fig.B.38 T_a- ramp: 29-44°C [59]

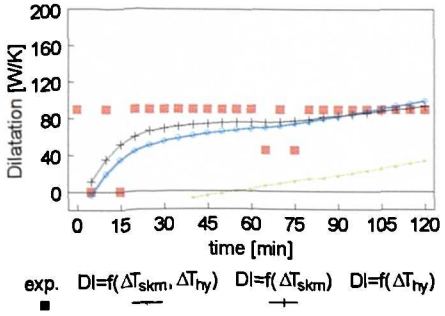

Fig.B.39 Step ch. into T_a=43°C [106]

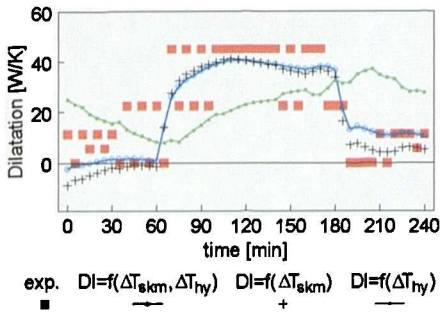

Fig.B.40 Step ch. in T_a:28-43-28°C [175]

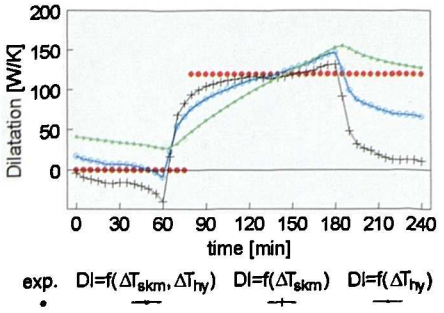

Fig.B.41 Step ch. in T_a:28-48-28°C [175]

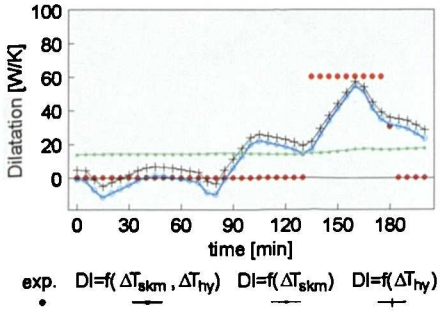

Fig.B.42 Work & rest at T_a=10°C [165]

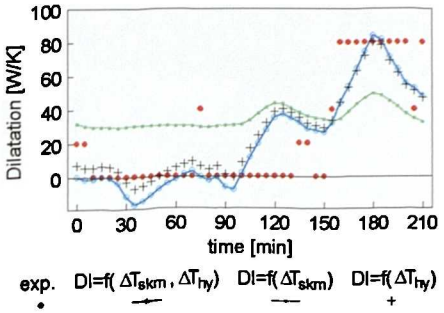

Fig.B.43 Trans. work at T_a=20°C [177]

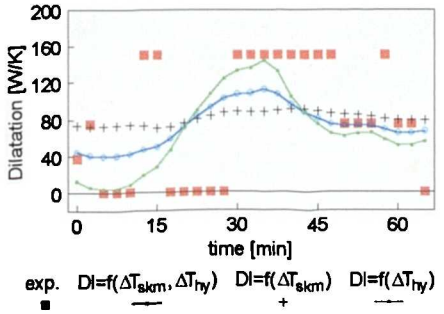

Fig.B.44 Work & rest at T_a=20°C [165]

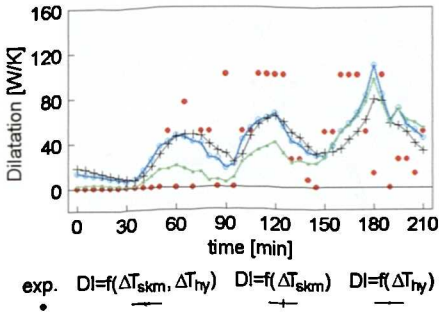

Fig.B.45 Work & rest at T_a=30°C [165]

B.3 Testing the Complete Model

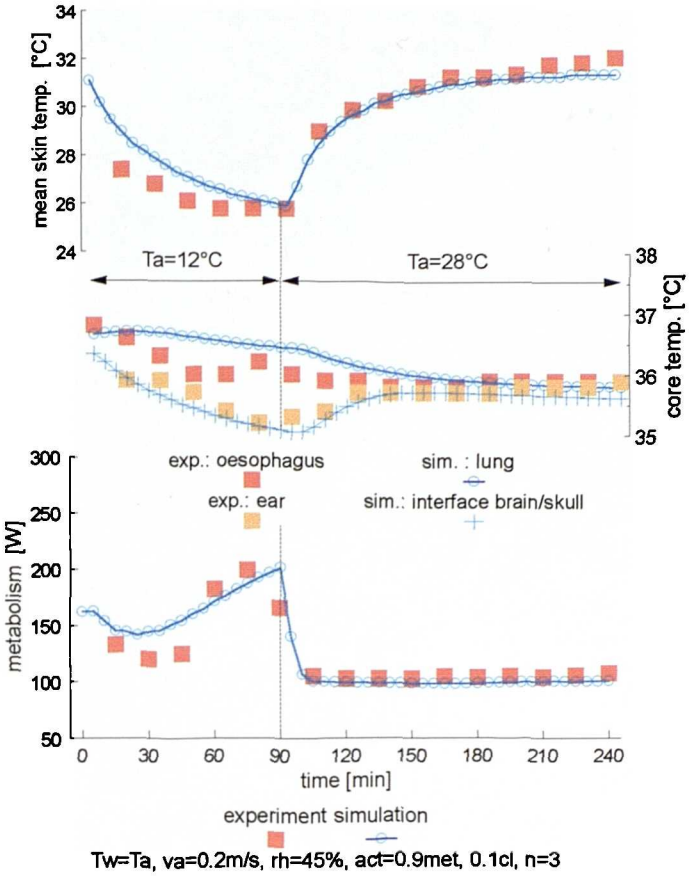

Fig.B.46

Exposure to an environment of T_a=12°C followed by a sudden change in T_a of 28°C [196].

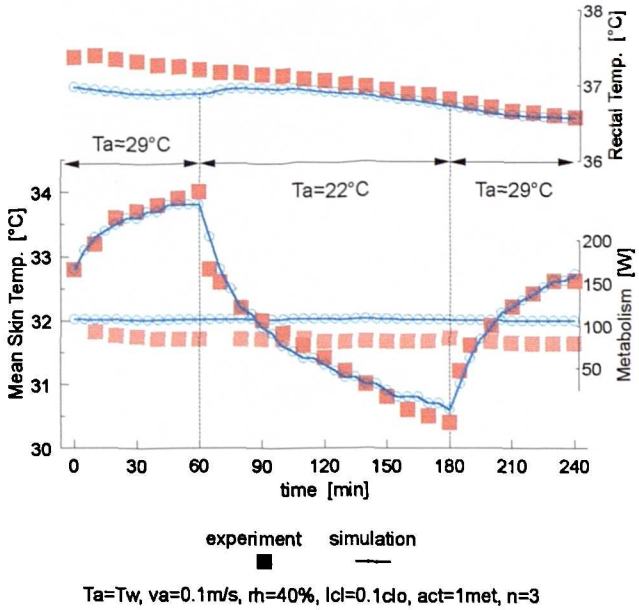

Fig.B.47

Sudden changes in ambient temperature of T_a=28-22-28°C [75].

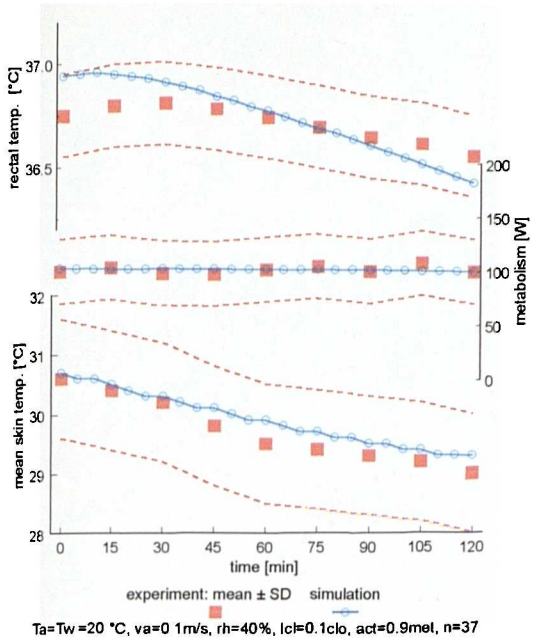

Fig.B.48

Exposure to an env. of T_a 20°C [188].

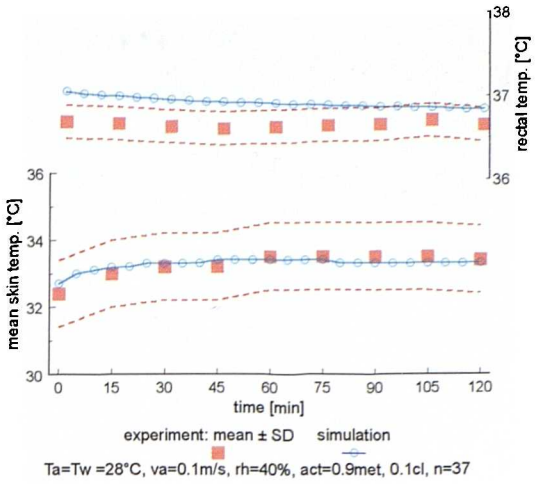

Fig.B.49

Exposure to an env. of T_a 28°C [188].

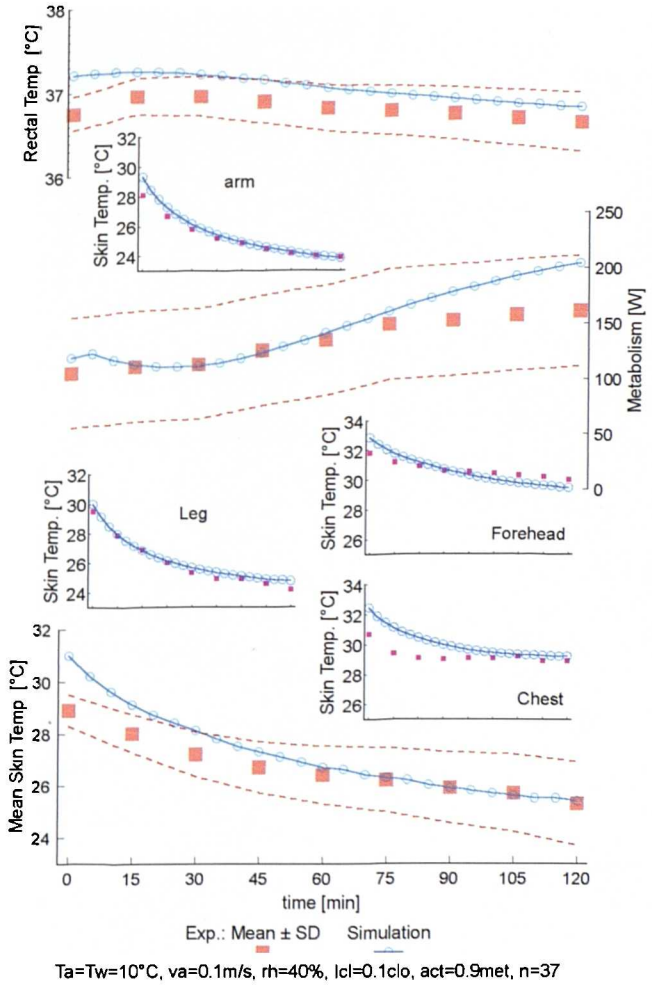

Fig.B.50

Body core temperature, skin temperatures, and metabolism during an exposure to T_a 10°C [188].

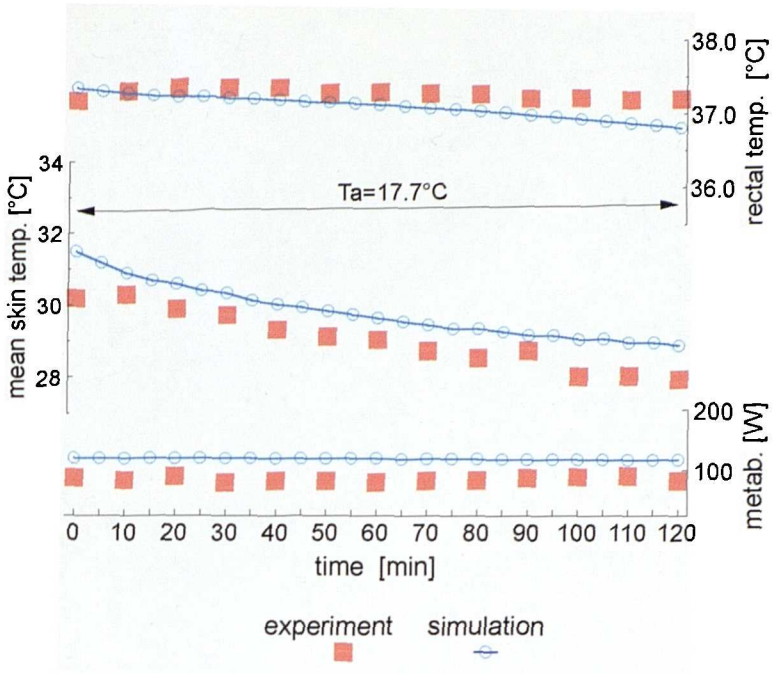

Tw=Ta, va=0.1m/s, rh=31%, Icl=0.1clo, act=1met, n=3

Fig.B.51

Exposure to an environment of T_a 17.7°C [75].

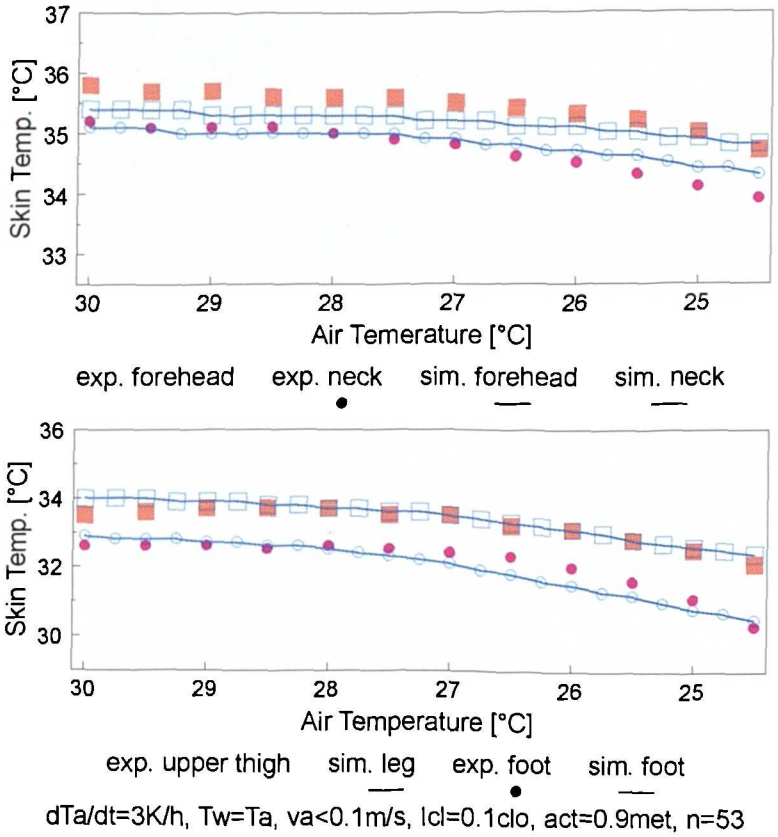

dTa/dt=3K/h, Tw=Ta, va<0.1m/s, Icl=0.1clo, act=0.9met, n=53

Fig.B.52

Gradual decrease in T_a from 30 to 25°C, dT_a dt 3K hr^{-1} [117].

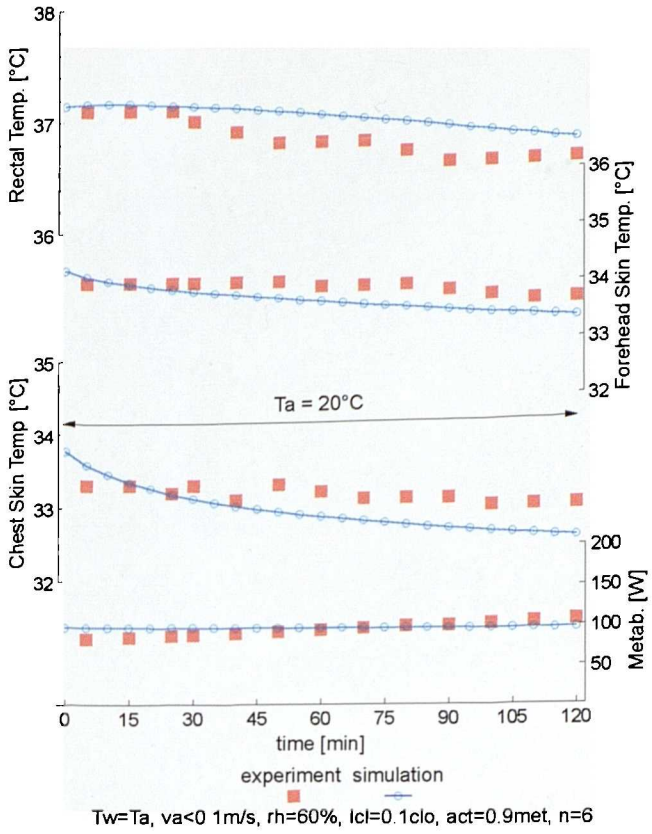

Fig.B.53

Exposure to seady environmental conditions of T_a 20°C investigated by Vogelaere et al. [187].

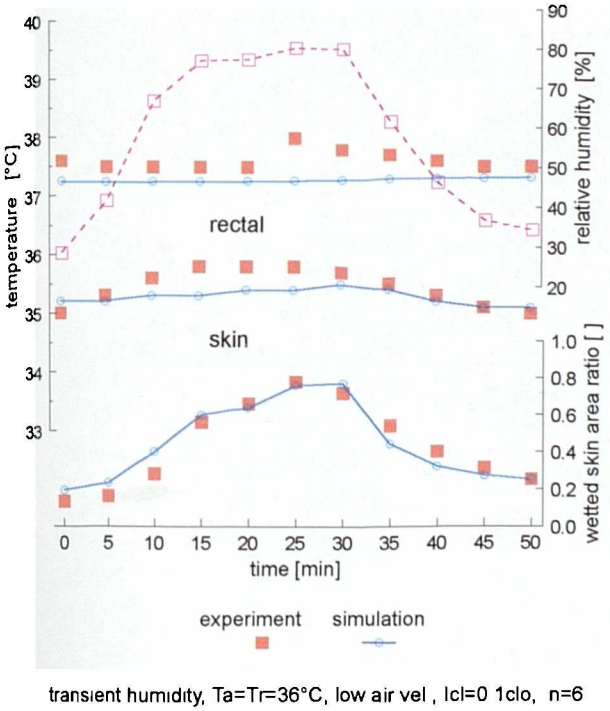

Fig.B.54

Transient changes in rh at T_a 36°C [59].

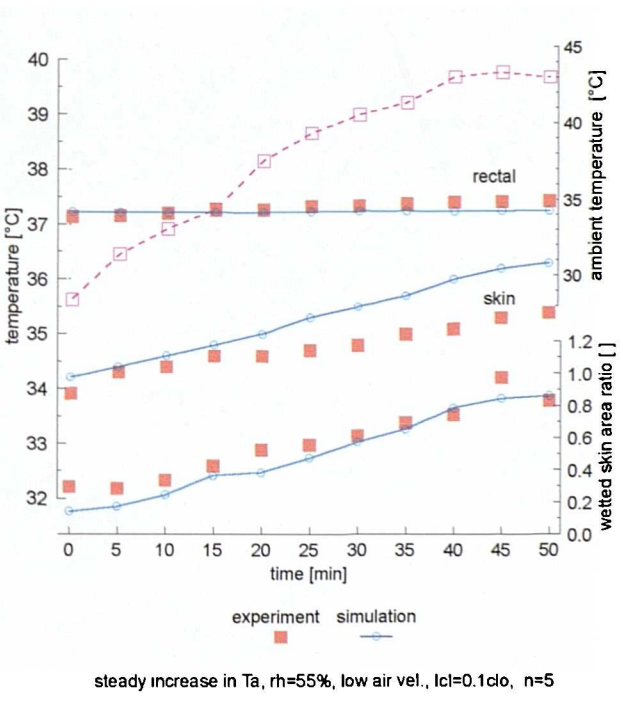

Fig.B.55

Linear increase in T_a from 29 to 44°C [59].

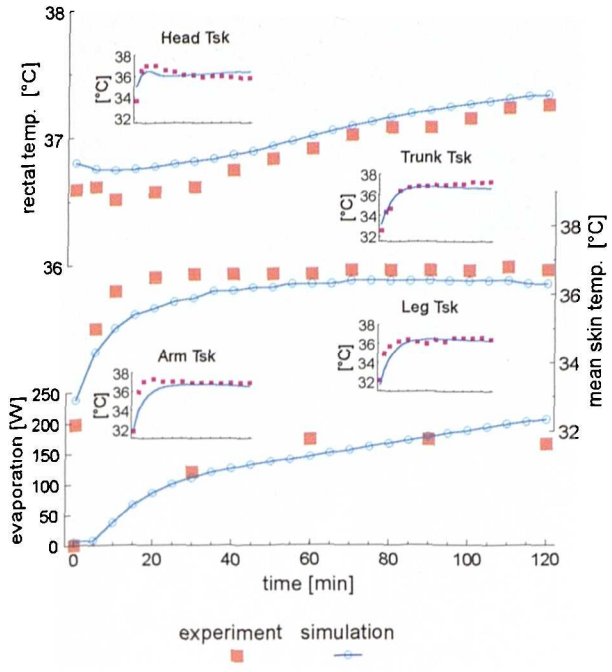

Ta=43 3 C, Tr=42 8 C, va=0 12m/s, Icl=0.1clo, act=1.2met, n=1

Fig.B.56

Step change into T_a 43°C [106].

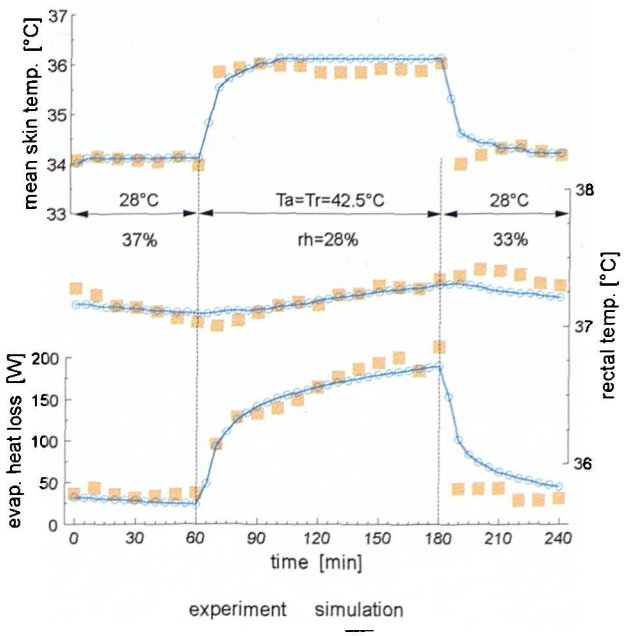

Ta=Tw, va=0.1m/s, Icl=0.1clo, act=1met, n=3

Fig.B.57

Sudden changes in T_a: 28-43-28°C [175].

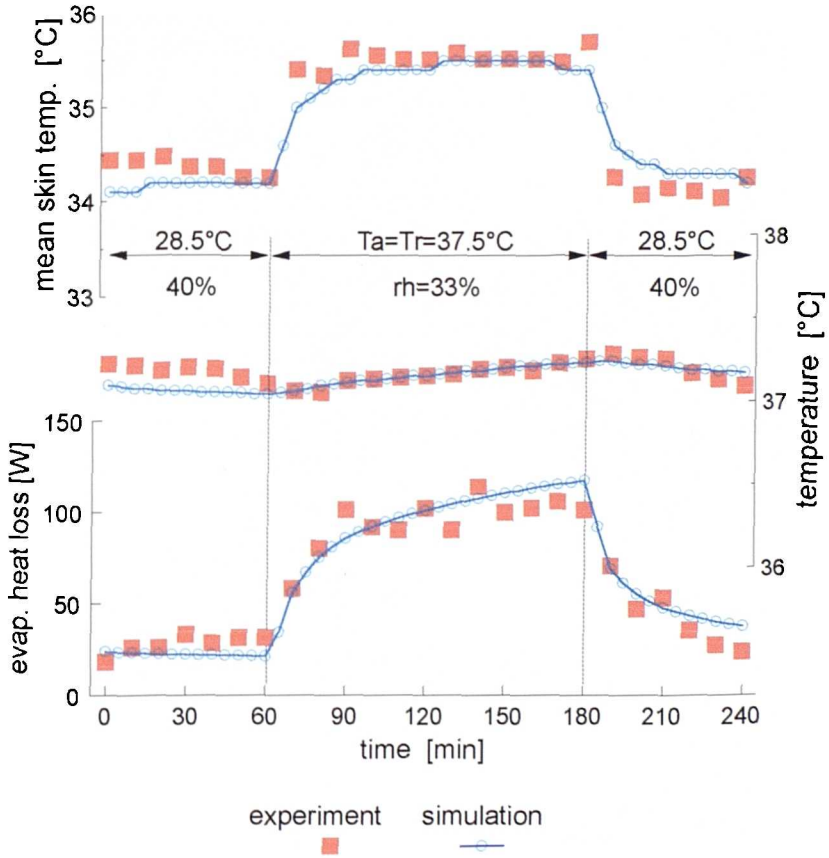

Ta=Tw, va=0.1m/s, Icl=0.1clo, act=1met, n=3

Fig.B.58

Step changes in ambient temperature of T_a 29-37-29°C [175].

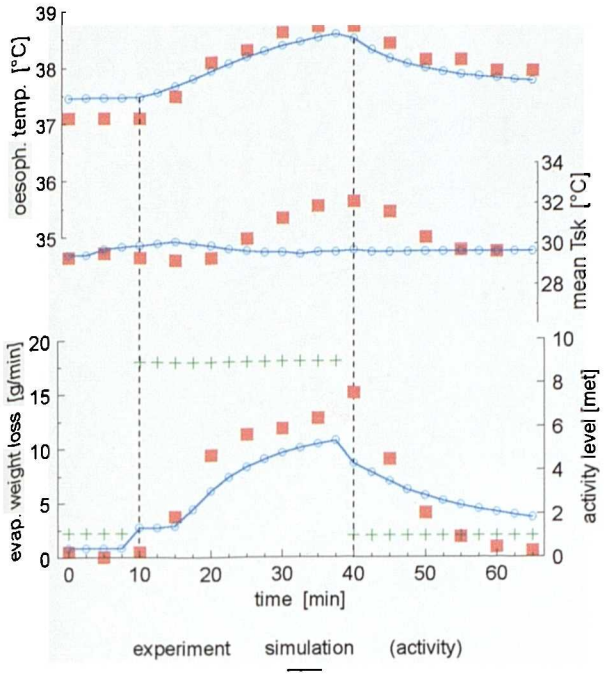

Ta=Tw=20 C, va=0 1m/s, rh=40%, Icl=0.1clo, act=9met, n=1

Fig.B.59

Work & rest at T_a 20°C [165].

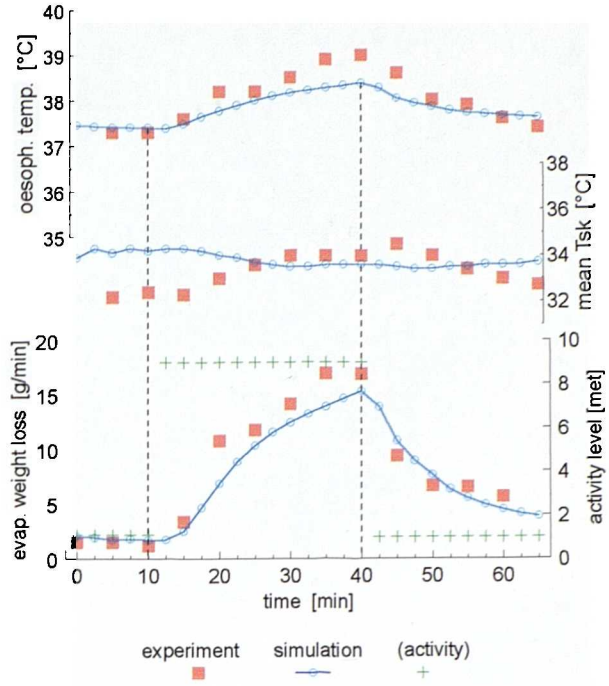

Ta=Tw=30°C, va=0.1m/s, rh=40%, Icl=0.1clo, act=8.9met, n=1

Fig.B.60

Work & rest at T_a 30°C [165].

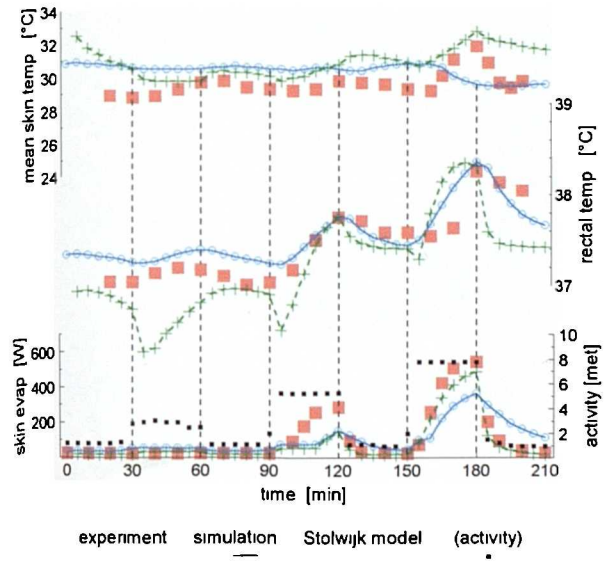

transient work at Ta=Tw=20°C, va=0.1m/s, rh=30%, Icl=0.1clo, n=3

Fig.B.62

Transient work at T_a 20°C [177].

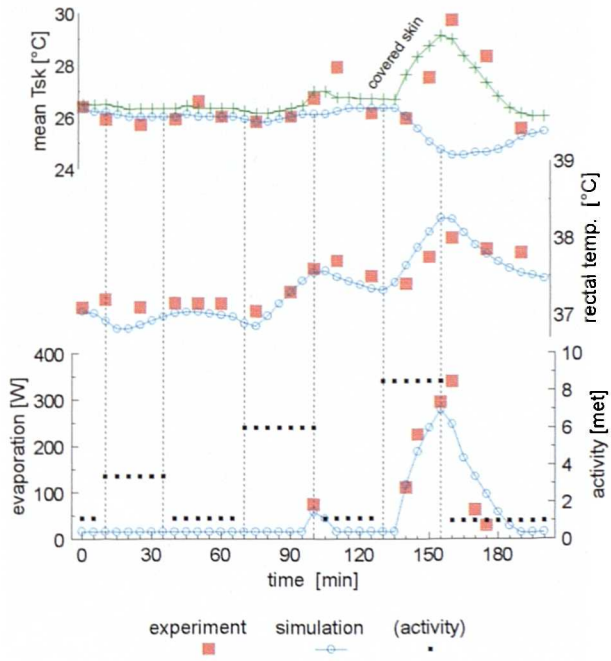

Ta=Tw=10°C, va=0.1m/s, rh=30%, Icl=0.1clo, n=1

Fig.B.61

Transient work at T_a 10°C [165].

B.4 Skin Temperature During Exercise

B.4.1 Numerical Study

A transient, model of skin covered by a small impermeable sticker (a circle with a radius of 8 mm) was developed (***Fig.B.63***) to investigate the effect of preventing local evaporation of sweat from the skin. As for the whole body model (see chap. 3), the skin was modelled as two layers. Each of these (plane) skin layers was subdivided spatially into annular cylindrical nodes to allow the simulation of two-dimensional heat transport, ie. perpendicular to, and parallel to the skin surface which would result mainly from the inhomogeneity of evaporative heat losses. The model employed heat balance equations which accounted for nodal differences in conduction, heat losses to the environment, and heat gain by blood circulation in the inner skin layer.

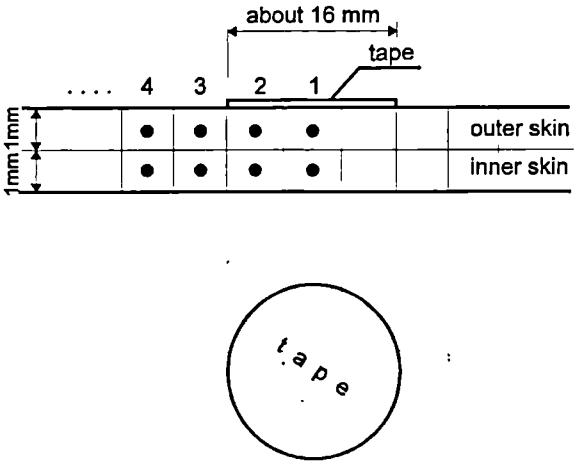

Fig.B.63

Model of skin covered by a small impermeable sticker.

The skin-model used (time-dependent) input-parameters obtained from whole-body simulations in order to prove/disprove the validity of the whole-body model for these conditions - the reason for the test. The input-variables were the overall cutaneous blood perfusion rate, the arterial blood temperature, the overall coefficients for the combined heat transfer via convection and radiation h, and the overall evaporative heat loss from the skin, E_{sk}. The evaporative heat loss from the skin surface below the tape was reduced by a factor which weighted E_{sk} by 0.1 to 0.3 to simulate the vapour resistance of the tape. Of primary interest was the effect of the local sweat suppression on the measured skin temperatures compared to the temperature of the uncovered skin. Hence, temperature differences between each

node and the node farthest from the sticker (representing undisturbed, uncovered skin) were considered. The temperature difference for node 1 was added to the skin temperature predicted by the whole body model. The result was then compared with experimental data to provide a direct measure for the effect of evaporation suppression compared to the predicted skin temperatures for the whole body model (dashed line in ***Fig.4.25*** and ***Fig.B.62***).

B.4.2 Experiment

The lack of adequate information in the literature was the reason for performing a simple experiment which directly compared the temperature of uncovered and covered skin. The covered skin temperature was measured by a thermocouple probe (copper/constantan) attached on the skin using surgical tape. The tape was made of close weare fabric which was adhesive on one side to stick down the thermocouple. It covered a skin area of about 5 cm^2. The uncovered skin temperature was measured by an optical, non-contact method using *Thermophil T 203* infrared thermoscopy device. Two subjects participated in the experimental series. Each subject, wearing only shorts, entered a cool room of static ambient conditions for at least 30 minutes. The subjects then sat on a bicycle-ergometer and the thermocouple was attached. Subsequently, the participants began pedalling at a constant level of activity for about 30 minutes. After finishing the exercise they remained seated for a further 30-60 minutes. During the entire test, the prevailing environmental parameters were measured using a *B&K Indoor Climate Analyzer type 1213*. The variations of the skin temperature were continuously measured both optically and via the thermocouple. In order to obtain comparable results, the temperature of the uncovered skin was measured close to the location where the thermocouple probe was attached.

The change in temperature of one subject's back, as measured by the two methods whilst exercising in ambient temperatures of 20°C is shown in ***Fig.B.64***. During the work-phase which is shown indicatively in the figures (the metabolic rate, ie. the oxygen consumption of the subjects, was not recorded in the experiment) the thermocouple probe measured a fairly constant skin temperature. This was in contrast to the results of Saltin et al. in ***Fig.4.25***, where measured skin temperatures were increased. Perhaps, in my experiment, the level of activity was not high enough to sufficiently elevate the blood temperature and SBF thereby

increasing the skin temperature below the tape. The lack of physical fitness did not allow the subject to work constantly at a higher activity level for the period of exercise. Nevertheless, the optical measurement indicated a decrease in the temperature of the uncovered skin when sweating began. The differences between the thermocouple and optical measurement of skin temperature reached 3 K and such a difference could explain the discrepancies observed between experimentation and the model's predictions. It should be noted that optical measurements respond slightly to changes in the surface emissivity. However, as one can estimate by calculation, and as observed by Clark et al. [32], changes in the emissivity of the skin due to the appearance of sweat liquid on the skin are too small to noticeably affect the results.

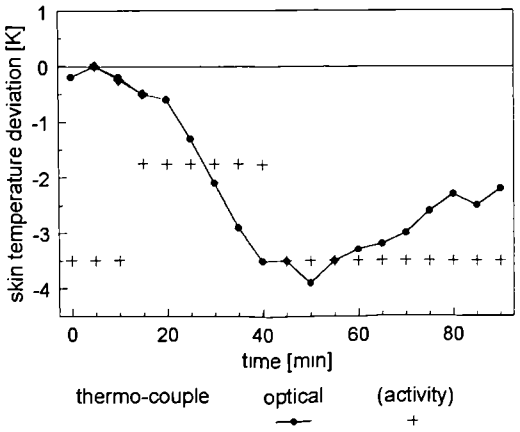

Fig.B.64

Skin temperature measured on the back during padalling at T_a 20°C using a thermocouple probe and the optical method.

An illustrative result was obtained for the forehead of the other subject when exercising in an ambient temperature of 25°C (***Fig.B.65***). In this environment the subject was sweating considerably. Beginning at the 15th minute of the work-period (25th min of the experiment) the subject reached saturation of sweat evaporation on the forehead, and sweat moisture ran off. Between 25<t<35 minutes of exposure evaporative cooling could not be increased any more (despite elevating sweat liquid production) and thus also the optical instrument recorded a rise in temperature of the skin which was warmed by *SBF*. Nevertheless, the discrepancies between the thermocouple-measurement and the optical measurement reached values of up to 3 K. Even higher differences could be achieved if the whole volume of sweat could be evaporated. A possible trend of the skin temperature which might be measured optically in conditions of a complete sweat moisture evaporation, ie. in conditions with air movement (the experiment involved still air) is also provided indicatively by a dashed line in ***Fig.B.65***.

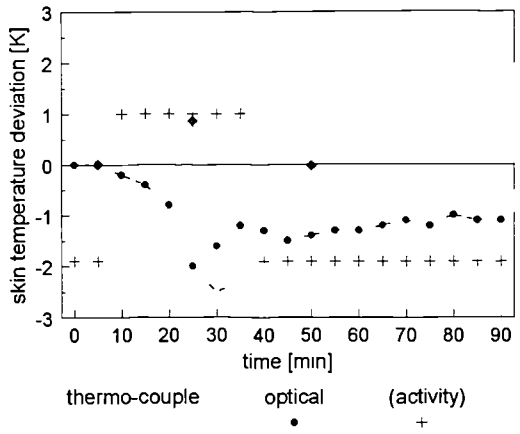

Fig.B.65

Skin temperature measured on the forehead during padalling at T_a 25°C using a thermocouple probe and the optical method.

B.5 Validation of the Complete Model

sedentary subject : activity = 1 met

	env. conditions				experiment			simulation		
Icl	Ta	MRT	v.air	rh	mTsk	Tre	EWtL	mTsk	Tre	EWtL
[clo]	[°C]	[°C]	[m/s]	[%]	[°C]	[°C]	[g/(m²h)]	[°C]	[°C]	[g/(m²h)]
0.6	24.5	24.8	< 0.1	43.3	33.7 ± 0.2*)	37.1 ± 0.1*)	26.4 ± 2.1*)	33.73	37.16	28.00
	26.7	20.0	< 0.1	50.2	33.0 ± 0.2	36.9 ± 0.1	24.3 ± 2.1	33.51	37.13	24.11
	26.4	26.4	0.80	50.1	33.1 ± 0.2	37.1 ± 0.1	23.7 ± 2.1	33.46	37.15	24.02
	26.6	21.6	0.80	49.7	32.3 ± 0.2	37.1 ± 0.1	22.2 ± 2.1	32.89	37.17	24.02
0.1	27.3	27.2	< 0.1	36.7	33.7 ± 0.2	37.3 ± 0.1	28.3 ± 2.1	33.54	37.02	27.15
	28.5	21.2	< 0.1	51.7	32.2 ± 0.2	36.9 ± 0.1	22.4 ± 2.1	32.09	36.80	20.85
	28.6	28.6	0.80	42.6	33.2 ± 0.2	37.2 ± 0.1	25.6 ± 2.1	32.46	36.89	23.80
	30.0	23.5	0.80	38.9	32.7 ± 0.2	37.3 ± 0.1	27.5 ± 2.1	32.39	36.96	24.04

EWtL = Evaporative Weight Loss *) standard deviations for one subject in two experiments

working subject : activity = 2 met

	env. conditions				experiment			simulation		
Icl	Ta	MRT	v.air	rh	mTsk	Tre	EWtL	mTsk	Tre	EWtL
[clo]	[°C]	[°C]	[m/s]	[%]	[C]	[°C]	[g/m²h]	[°C]	[°C]	[g/m²h]
0.6	16.4	17.0	< 0.1	35.7	31.1	37.5	72	31.48	37.62	91.2
	16.3	13.0	< 0.1	37.4	30.8	37.8	76	30.94	37.62	83.6
	21.5	21.6	0.81	26.0	31.2	37.6	109	31.62	37.62	97.2
	21.3	16.9	0.81	26.3	31.1	37.6	88	31.18	37.62	91.2
0.1	20.8	20.8	< 0.1	27.1	31.2	37.8	84	30.97	37.59	80.2
	23.6	16.8	< 0.1	22.9	31.1	37.6	68	30.86	37.59	78.5
	24.7	24.2	0.81	21.4	31.0	37.6	101	30.83	37.57	70.1
	25.5	19.0	0.81	20.8	31.1	37.5	80	30.48	37.56	63.9

Tab.B.2

Physiological comfort conditions (after 3hrs of exposure) at 16 combinations of activity, clothing and ambient parameters [150].

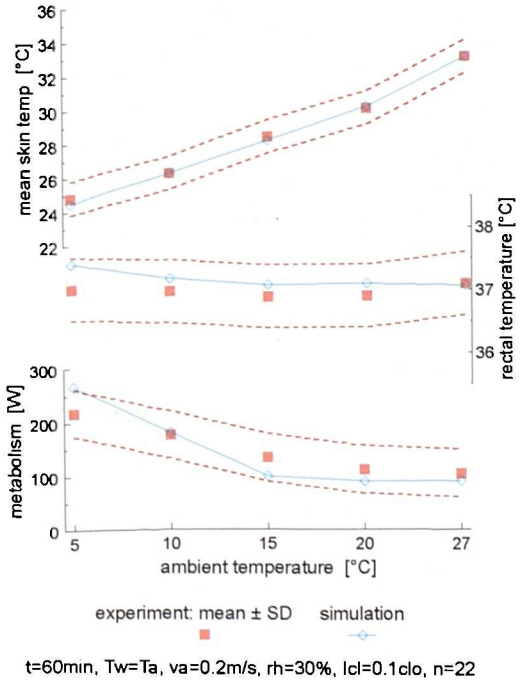

Fig.B.66

Physiological reactions of reclining subjects (after 1hr of exposure) to cold environments [204].

env. conditions				experiment			simulation		
Ta	Tr	v,air	rh	mTsk	Tre	mTcl	mTsk	Tre	mTcl
[°C]	[°C]	[m/s]	[%]	[°C]	[°C]	[°C]	[°C]	[°C]	[°C]
30.8	20.3	0.1	33.0	34.4	36.8	29.7	34.55	37.07	28.74
27.9	17.7	0.1	39.0	34.0	36.7	28.1	34.33	37.02	27.00
25.2	26.7	0.1	41.6	34.5	36.8	29.8	34.60	37.12	29.20
24.8	19.1	0.1	42.6	33.7	36.9	27.3	34.21	37.01	26.52
23.5	15.1	0.1	46.0	33.1	36.6	25.5	33.71	37.01	24.71
20.2	29.1	0.1	50.7	34.2	36.9	28.5	34.40	37.04	28.40
19.1	33.1	0.1	48.2	34.5	37.1	29.3	34.41	36.96	29.28
15.6	24.0	0.1	60.2	32.7	36.8	25.0	33.54	37.01	24.88

Tab.B.3

Body- and clothing temperatures of a seated, clothed (1.25clo) subject after 2hr-exposure to combinations of ambient conditions [143].

Skin Temperature Distribution

Temperature [°C]	experiment	simulation
mean skin	33.2	33.66
head skin	33.7	33.65
trunk skin	34.4	
thorax skin		35.07
abdomen skin		34.70
arm skin	33.3	33.98
hand skin	32.4	31.96
thigh skin	32.9	
(lower) leg skin	31.9	
leg skin		32.88
foot skin	30.4	31.33

Ta=Tr=20°C, rh=50%, v=0.1 m/s, activity=1 met, Icl=1.25 clo

Tab.B.4

Local skin temperatures of a seated, clothed (1.25clo) subject exposed for 2hr to an environment of T_a 20°C, Nielsen et al. [143].

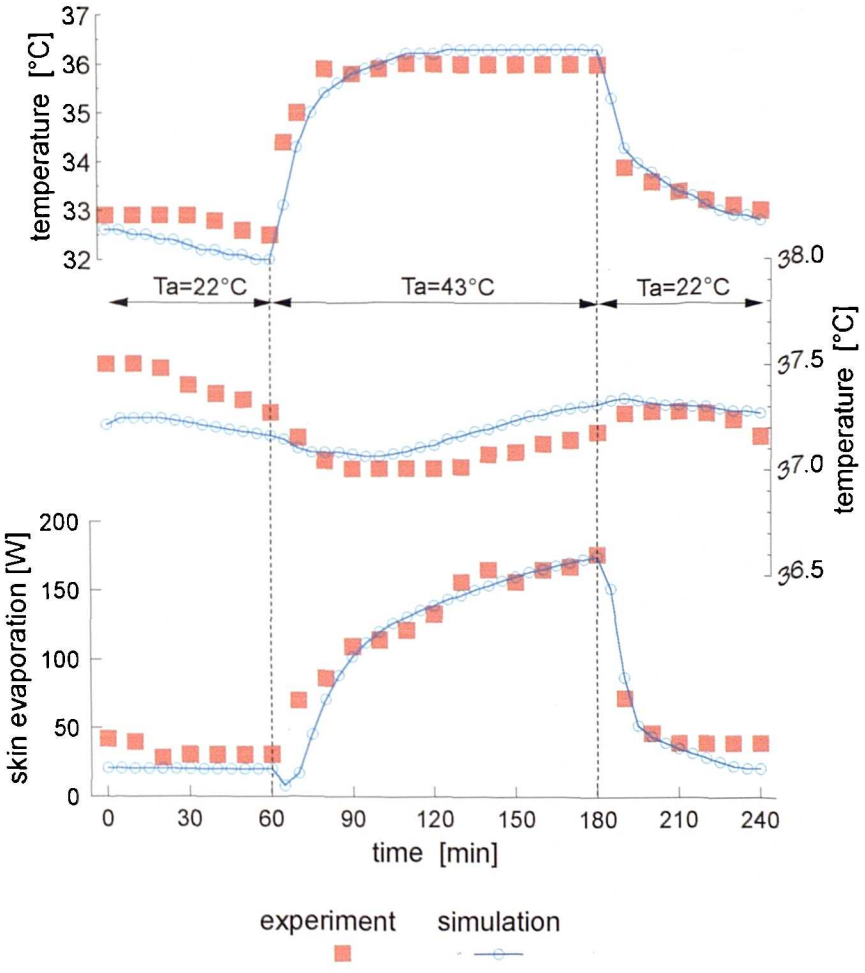

Tw=Ta, va=0.1m/s, rh=30%, Icl=0.1clo, n=3

Fig.B.67

Step changes in ambient temperature of T_a 22-43-22°C [75].

C Comfort Model

Index of Heat Stress	Physiological and Hygienic Implications of 8 hour Exposures to Various Heat Stresses
0	No thermal strain
10-30	Mild to moderate heat strain. If job involves higher intellectual functions, dexterity, or alertness, subtle to substantial decrements in performance may be expected. In performing heavy physical work, little decrement is expected unless ability of individuals to perform such work under no thermal stress is marginal.
40-60	Severe heat strain, involving a threat to health unless men are physically fit. Break-in period required for men not previously acclimatized. Some decrement in performance of physical work is to be expected. Medical selection of personnel desirable because these conditions are unsuitable for those with cardiovascular or respiratory impairment or with chronic dermatitis. These working conditions are also unsuitable for activities requiring sustained mental effort.
70-90	Very severe heat strain. Only a small percentage of the population may be expected to qualify for this work. Personnel should be selected: (a) by medical examination; and (b) by trial on the job (after acclimatization). Special measures are needed to assure adequate water and salt intake. Amelioration of working conditions by any feasible means is highly desirable, and may be expected to decrease the health hazard while increasing job efficiency. Slight "indisposition" which in most jobs would be insufficient to affect performance may render workers unfit for this exposure.
100	The maximum strain tolerated daily by fit, acclimatized young men.

Tab.C.1

Physiological and health implications of various heat stress indices defined as the ratio between the required rate of sweat evaporation and the maximum evaporative heat loss from the skin. The difference between internal heat production and the heat loss by radiation and convection termed the required sweat evaporation [10]. The HSI-index is conceptually the same as the skin wettedness w_{sk} (times 100) which is predicted by the present model of the human thermoregulatory system.